

STRESS TENSOR INVERSION FROM FOCAL MECHANISM SOLUTIONS AND
EARTHQUAKE PROBABILITY ANALYSIS OF WESTERN ANATOLIA, TURKEY

A THESIS SUBMITTED TO
THE GRADUATE SCHOOL OF NATURAL AND APPLIED SCIENCES
OF
MIDDLE EAST TECHNICAL UNIVERSITY

BY

SYED TANVIR SHAH

IN PARTIAL FULFILLMENT OF THE REQUIREMENTS
FOR
THE DEGREE OF MASTER OF SCIENCE
IN
GEOLOGICAL ENGINEERING

JANUARY 2015

Approval of the thesis:

**STRESS TENSOR INVERSION FROM FOCAL MECHANISM SOLUTIONS
AND EARTHQUAKE PROBABILITY ANALYSIS OF WESTERN ANATOLIA,
TURKEY**

submitted by **SYED TANVIR SHAH** in partial fulfillment of the requirements for the degree of **Master of Science in Geological Engineering Department, Middle East Technical University** by,

Prof. Dr. Gülbin Dural Ünver
Dean, Graduate School of **Natural and Applied Sciences**

Prof. Dr. Erdin Bozkurt
Head of Department, **Geological Engineering**

Assist. Prof. Dr. A. Arda Özacar
Supervisor, **Geological Engineering Dept., METU**

Prof. Dr. Erdin Bozkurt
Co-Supervisor, **Geological Engineering Dept., METU**

Examining Committee Members:

Prof. Dr. Nuretdin Kaymakçı
Geological Engineering Dept., METU

Assist. Prof. Dr. A. Arda Özacar
Geological Engineering Dept., METU

Prof. Dr. Erdin Bozkurt
Geological Engineering Dept., METU

Prof. Dr. M. Lütfi Süzen
Geological Engineering Dept., METU

Assoc. Prof. Dr. Zeynep Gülerce
Civil Engineering Dept., METU

Date: 23-01-2015

I hereby declare that all information in this document has been obtained and presented in accordance with academic rules and ethical conduct. I also declare that, as required by these rules and conduct, I have fully cited and referenced all material and results that are not original to this work.

Name, Last name : SYED TANVIR SHAH

Signature :

ABSTRACT

STRESS TENSOR INVERSION FROM FOCAL MECHANISM SOLUTIONS AND EARTHQUAKE PROBABILITY ANALYSIS OF WESTERN ANATOLIA, TURKEY

Shah, Syed Tanvir

M.S., Department of Geological Engineering

Supervisor: Assist. Prof. Dr. A. Arda Özacar

Co-Supervisor: Prof. Dr. Erdin Bozkurt

January 2015, 182 Pages

Western Anatolia is one of the most important tectonic elements of Turkey, and constitutes the eastern margin of Aegean Extensional Province. The area is one of the most seismically active continental margins around the globe experiencing N–S extension. Earthquake data in this study is used to analyze the active stress patterns and to estimate the earthquake probabilities for different sub-regions in western Anatolia. Various processing techniques to attain homogeneity are applied to the earthquake catalogue for the area, which is then used for investigation of spatial and temporal variations in frequency magnitude distribution. More frequently occurring smaller magnitude earthquakes represented by high b-values are associated with relatively low stress conditions. The prominent high b-value regions identified in the study area are along Bakırçay Graben and between İzmir and Manisa. Spatial distribution of high b-values correlates well with the distribution of hot springs and high heat flow anomalies. The temporal variations in b- values are associated with major earthquakes in the region.

Before the earthquake, b-values show a small scale decrease followed by an abrupt increase after the event and this variation disappears after some time. Focal mechanism solution data is used for determining the orientations and ratios of principal stress components in the area. Minimum principal stress (σ_3) is sub horizontal in the region trending in almost N–S (N15° E) direction and the region is characterized mainly by normal fault regime. The area is sub-divided into 10 sub-regions based on the variations in focal mechanism solutions and tectonic setting. The results for sub-regions showed that apart from the predominant extensional regime; Bakırçay and Gulf of Sığacık sub-regions are dominated by strike-slip, while Manisa and Soma sub-regions are dominated by extensional strike-slip regimes. These sub-regions roughly coincide with the İzmir Balıkesir Transfer Zone (IBTZ), which is characterized by mixture of normal and strike-slip faults. Computed principle stress directions shows that the area is mostly characterized by N–S extension except Gökova region marked by NW–SE extension and Dinar and Fethiye regions displaying more variable stress tensor solutions with more dominant NE-SW extension. The earthquake probabilities computed using Gutenberg-Richter relation and Gumbel extreme value method shows that the whole region has a return period of 3 and 7 years for a magnitude 6 earthquake. According to our results, Simav and Gulf of Gökova sub-regions have highest and Manisa has lowest earthquake probabilities. The fractal dimension (D_c) analysis illustrates that Gulf of Gökova and Fethiye sub-regions have highest and Dinar-Burdur, Büyük Menderes and Gulf of Sığacık have lowest levels of seismicity clustering. The comparison of results computed for sub-regions also showed that a-, b- values and stress variance are negatively correlated with D_c and stress ratio (R) while D_c correlates positively with R.

Keywords: Western Anatolia, b-value, stress tensor inversion, earthquake probability, Gumbel extreme value method, fractal dimension

ÖZ

STRES TENSÖRÜNÜN ODAK MEKANİZMALARI İLE TERS ÇÖZÜMÜ VE BATI ANADOLU, TÜRKİYE’NİN DEPREM OLASILIK ANALİZİ

Shah, Syed Tanvir

Yüksek Lisans, Jeoloji Mühendisliği Bölümü

Tez Yöneticisi: Yard. Doç. Dr. A. Arda Özacar

Ortak Tez Yöneticisi: Doç. Dr. Erdin Bozkurt

Ocak 2015, 182 sayfa

Batı Anadolu, Türkiye'nin en önemli tektonik öğelerinden birini teşkil etmekte ve Ege Genişleme Bölgesi'nin doğu sınırını oluşturmaktadır. Bölge dünyada K-G gerilimleri gözlenen sismik olarak en aktif kıta kenarlarından birisidir. Bu çalışmada aktif stres desenlerini ve farklı alt-bölgelerde ki deprem olasılıklarını keşfetmek için deprem verilerini kullandık. Bölgede homojenliğe ulaşmak adına deprem kataloğuna çeşitli işlem teknikleri uygulandı ve işlenen veri büyüklük frekans dağılımındaki mekansal ve zamansal değişiklikleri saptamak için kullanıldı. Daha sık gözlenen küçük depremlerin yüksek b-değerlerine sebep olduğu saptandı ve bu düşük stres koşulları ile ilişkilendirildi. Bu araştırmada bölgenin göze çarpan yüksek b-değerleri Bakırçay grabeni ve İzmir Manisa arasında kalan alanda yer almaktadır. Yüksek b-değerlerinin mekansal dağılımı, bölgedeki sıcak su kaynaklarının dağılımı ve yüksek ısı akısı anomalileri ile uyumludur. İncelenen bölgelerdeki saptanan zamansal b-değeri değişimleri büyük depremlerle bağlantılıdır. Depremlerin hemen öncesinde b-değerleri küçük ölçekli düşüş ve sonrasında ise yükseliş göstermekte ve bu değişim bir süre sonra kaybolmaktadır. Odak mekanizma katalogları kullanılarak ayrıca ana stres yönleri ve bileşenlerin birbirine oranları saptanmıştır. Sonuçlara göre en küçük ana stres (σ_3) yaklaşık yatay ve K-G yönelimli ($N15^\circ E$) olup, bölge normal faylanma ile karakterize

edilmektedir. Çalışma alanı, odak mekanizmalarındaki değişimlere ve tektonik yapılar göre 10 alt-bölgeye bölünmüş ve gerilme tensörü ters çözümleri bu bölgeler için bağımsız olarak gerçekleştirilmiştir. Sonuçlara göre genişleme rejiminden ayrı olarak Bakırçay grabeni ve Sığacık körfezi doğrultu atımlı rejim, Manisa ve Soma bölgeleri ise genişlemeli doğrultu atımlı rejim tarafından kontrol edilmektedir. Bu bölgeler normal ve doğrultu atımlı aktif faylar ile temsil edilen İzmir Balıkesir Transfer Zonu (IBTZ) ile çakışmaktadır. Hesaplanan ana stres yönleri bölgenin çoğunlukla K-G yönlü genişleme ile karakterize edildiğini göstermektedir. Fakat bölge genelinden farklı olarak Gökova KB-GD yönlü genişleme, Dinar-Burdur ve Fethiye ise daha değişken stres tensor sonuçları ve daha baskın KD-GB yönlü genişleme sergilemektedir. Gutenberg-Richter bağıntısı ve Gumbel uç değer methodu kullanılarak ayrı ayrı hesaplanan deprem olasılığı, bütün bölgenin büyüklüğü 6 olan depremler için 3 ila 7 yıllık dönüş periyoduna sahip olduğunu göstermektedir. Sonuçlara göre, Simav ve Gökova alt-bölgeleri en yüksek, Manisa ise en düşük deprem olasılığına sahiptir. Oransal kırılma boyutu analizine (Dc değeri) göre Gökova ve Fethiye alt-bölgeleri en yüksek ve Dinar-Burdur, Büyük Menderes ve Sığacık körfezi en düşük düzeyde sismik kümelenme göstermektedir. Alt-bölge bazlı yapılan sonuç kıyaslamaları a-, b- değerleri ve stres değişkenliğinin Dc ve stres oranı (R) ile ters orantılı, Dc'nin ise R ile doğru orantılı olduğunu göstermektedir.

Anahtar kelimeler: Batı Anadolu, b-değeri, stres tensör ters çözümü, deprem olasılığı, Gumbel uç değer methodu, oransal kırılma boyutu

To my family

ACKNOWLEDGMENTS

I would like to express my sincere gratitude to my supervisor Assist. Prof. Dr. A. Arda Özacar, for his invaluable guidance, immense knowledge, enthusiastic approach and useful critiques of this research work. His guidance helped me throughout the research and writing of this thesis. Thank you Sir for being so patient and kind to me. I could not have imagined having a better advisor than you.

Besides my supervisor, I would like to thank my Co-Supervisor Prof. Dr. Erdin Bozkurt and the committee members of my thesis; for their insightful comments and providing me with suggestions to improve my research work.

A special thanks to my beloved family. Words cannot express how grateful I am to them; especially my parents and my elder brother Mr. Said Kashif Shah. Your sacrifices and prayers for me was what sustained me thus far.

I would like to extend my heartfelt gratitude to all my friends; for their moral support, motivation and entertainment they provided me with. It would have been very hard to accomplish this study without them. I shared with them some of the fond memories of my life in this duration.

TABLE OF CONTENTS

ABSTRACT.....	v
ÖZ.....	vii
ACKNOWLEDGEMENTS.....	x
TABLE OF CONTENTS.....	xi
LIST OF TABLES.....	xv
LIST OF FIGURES.....	xvi

CHAPTERS

1. INTRODUCTION.....	1
1.1 Purpose and Scope.....	1
1.2 Previous Studies.....	2
1.3 Data and Methods.....	5
1.4 Organization of the Thesis.....	6
2. TECTONIC SETTING AND SEISMICITY.....	7
2.1 Regional Tectonic Setting.....	7
2.2 Geological Setting of Western Anatolia.....	14
2.3 Major Tectonic Structures in the Region	15
2.3.1 Central Portion	16
2.3.2 Gökova Region.....	17

2.3.3	Fethiye-Burdur Fault Zone.....	18
2.3.4	Izmir Balikesir Transfer Zone (IBTZ).....	19
2.4	Seismicity of Western Anatolia	21
3.	SPATIAL AND TEMPORAL VARIATIONS IN FREQUENCY MAGNITUDE DISTRIBUTION OF EARTHQUAKES.....	27
3.1	Earthquake Statistics.....	27
3.2	Data and Processing Techniques.....	28
3.2.1	Declustering of the Catalogue.....	33
3.2.2	Detection and Removal of Quarry Blast Events.....	33
3.3	Frequency Magnitude Distribution of Earthquakes in the Study Area.....	37
3.3.1	Spatial Variations of b-value	39
3.3.2	Temporal Variations of b-value.....	46
3.3.2.1	Temporal Variations of b-value and Seismicity Rate Changes in Simav Area.....	53
3.3.2.2	Aftershocks Decay Rate of Simav Earthquake	56
4.	STRESS ANALYSIS USING FOCAL MECHANISM SOLUTIONS.....	59
4.1	Focal Mechanism Solutions.....	59
4.1.1	Pressure and Tension (P-T) axes and Rake Distributions of the Study Area.....	63
4.2	Sub-regions Classification.....	64

4.2.1	Pressure and Tension (P-T) axes and Rake Distributions of Sub-regions.....	67
4.3	Stress Tensor Inversion.....	70
4.3.1	Stress Tensor Analysis by Slick Method.....	70
4.3.1.1	Simav Region (Sub-region 01).....	75
4.3.1.2	Alaşehir Region (Sub-region 02).....	78
4.3.1.3	Manisa Region (Sub-region 03).....	78
4.3.1.4	Dinar-Burdur Region (Sub-region 04).....	80
4.3.1.5	Büyük and Küçük Menderes Grabens (Sub- region 05).....	82
4.3.1.6	Soma Region (Sub-region 06).....	83
4.3.1.7	Bakırçay Graben (Sub-region 07).....	84
4.3.1.8	Gulf of Sığacık (Sub-region 08).....	85
4.3.1.9	Gulf of Gökova (Sub-region 09).....	85
4.3.1.10	Fethiye Region (Sub-region 10).....	89
4.3.2	Stress Tensor Analysis by Win-Tensor Program.....	91
4.5	Horizontal Stress Directions.....	94
5.	EARTHQUAKE PROBABILITIES AND FRACTAL DIMENSION OF SEISMICITY.....	97
5.1	Introduction.....	97
5.2	Gutenberg-Richter Relation.....	98
5.2.1	Data and Methods.....	98
5.2.2	Results.....	101
5.3	Gumbel's Annual Extreme Value Method.....	108

5.3.1	Data, Method and Results.....	109
5.4	Earthquake Probabilities and Return Periods.....	111
5.5	Maximum Expected Earthquake Magnitudes (Mmax).....	121
5.6	Fractal Dimensions of Recorded Seismicity.....	125
6.	DISCUSSION AND CONCLUSION.....	131
	REFERENCES.....	141

APPENDICES

	APPENDIX A: Focal Mechanism Solutions.....	165
	Table A. 1: Parameter list of earthquake focal mechanism solutions compiled in this study from various sources.....	165
	Table A. 2: P- T-, S_{Hmax} , S_{Hmin} axes and stress regimes computed from focal mechanism solutions listed in Table A. 1.....	174

LIST OF TABLES

TABLES

Table 4.1: Comparison of stress tensor inversion results for the whole region and sub-regions; using slick method (Michael, 1987) and method using right dihedron with rotational optimization in Win-Tensor program (Delvaux and Sperner, 2003). Results of slick method are given in the upper row and results of Win-Tensor program are given in the lower row for each sub-region.....	92
Table 5.1: Table showing a-value, b-value, magnitude of completeness (M_c), observation time (T_{obs}) and the earthquake probabilities (%) in the study area and within each sub-region for magnitudes 5, 6 and 7 and time periods 10, 50 and 100 years. The last column shows the calculated return periods within each category.....	112
Table 5.2: : Table showing the M_{min} , α , β and the earthquake probabilities (%) in the study area and within each sub-region for magnitudes 5, 6 and 7 and time periods 10, 50 and 100 years. The last column shows the calculated return periods within each category	117
Table 5.3: Table showing the maximum expected magnitude (M_{max}) in 100 years obtained for the sub-regions using Gutenberg-Richter (G-R) and Gumbel annual extreme methods	121
Table 5.4: Table showing the fractal dimension values (D_c) obtained for sub-regions.....	126
Table 6.1: Table showing the summary of results obtained for the selected sub-regions in the study area. N: Extensional, S: Strike-slip, NS: Extensional Strike-slip, G-R: Gutenberg-Richter relation.....	135

LIST OF FIGURES

FIGURES

- Figure 1.1:** Generalized tectonic map of Turkey (from Bozkurt, 2001). The box indicates location of the study area.....2
- Figure 2.1:** Generalized tectonic map of Turkey taken from Taymaz *et al.*, 2007. BGF: Beyşehir Gölü Fault; BMG: Büyük Menderes Graben; BuF: Burdur Fault; CTF: Cephalonia Transform Fault; DF: Deliler Fault; DSF: Dead Sea Transform Fault; EAF: East Anatolian Fault; EcF: Ecemis Fault; EF: Elbistan Fault; EPF: Ezinepazarı Fault; ErF: Erciyes Fault; G: Gökova; Ge: Gediz Graben; KFZ: Karatas-Osmaniye Fault Zone; MF: Malatya Fault; NAF: North Anatolian Fault; PTF: Paphos Transform Fault; SF: Sultandağı Fault; Si: Simav Graben; TF: Tatarlı Fault; TGF: Tuz Gölü Fault.....8
- Figure 2.2:** Map illustrating the major neotectonic provinces and related governing structures in Turkey and surrounding areas. The figure is adapted from Çiftçi (2007), modified from Koçyiğit and Özacar (2003), Woodside *et al.* (2002) and Zitter *et al.* (2005).....9
- Figure 2.3:** Simplified geological map of western Turkey, from Bozkurt (2000). Abbreviations: AG: Acıpayam Graben; BaG: Baklan Graben; BçG: Bakırçay Graben; BG: Burdur Graben; BMG: Büyük Menderes Basin; DB: Demirci Basin; DG: Denizli Graben; GB: Gördes Basin; GG: Gediz Graben; KMG: Küçük Menderes Graben; SB: Selendi Basin; SG: Simav Graben; UGB; Uşak-Güre Graben.....13
- Figure 2.4:** Active fault map of the area compiled from MTA (1992); Bozkurt (2000, 2001); Uzel and Sözbilir (2008) and Hall *et al.* (2014). The white dotted lines show the main tectonic sub-divisions proposed for the area.....16
- Figure 2.5:** Cartoon model proposed for the İzmir Balıkesir Transfer Zone (IBTZ) taken from Ocakoğlu *et al.* (2005). CLFZ: Cephalonia-Lefkada Fault Zone; EG: Edremit Gulf; I: Ikaria Island; IG: İzmir Gulf; GKG: Gökova Graben; NAFZ: North Anatolian Fault

Zone; R: Rhodes Island; S: Samos Island; SG: Saros Gulf; ZBF: Zeytindağ-Bergama Fault.	21
Figure 2.6: Map showing the distribution of seismicity with topography in the study area. The seismic catalogue is obtained from KOERI ($M \geq 3.0$) for the period of 1990-2013. The events are scaled according to their magnitude and the stars show the locations of recent major events in the area.....	23
Figure 2.7: Earthquake density map of the area.....	25
Fig. 3.1: Cumulative number of earthquakes vs time of the KOERI catalogue between 1900 and January,2014.....	29
Fig. 3.2: Cumulative number of earthquakes vs time of the KOERI catalogue between 1990 and January, 2014.....	29
Figure 3.3: Depth histogram of the earthquakes.....	30
Figure 3.4: a) South to North and b) West to East depth sections of recorded seismicity in the study area	30
Figure 3.5: Graph showing the relationship between ‘ M_d ’ and ‘ M_l ’. The scatter plot is constructed using the events that have both ‘ M_d ’ and ‘ M_l ’ available in the KOERI catalogue.....	31
Figure 3.6: Cumulative moment release vs time plot of earthquakes in the study area.....	32
Figure 3.7: Hourly histograms of the seismic events a) all recorded events; b) only $M \geq 2.0$ events; c) only $M \geq 3.0$ events.....	35
Figure 3.8: Day vs night time events ratio map of the area constructed for earthquakes with $M \leq 3.0$. The areas shown by pink color have a day/night time ratio of ≥ 1.5 and are possible sites of quarry contamination.....	35
Figure 3.9: Day vs night time events ratio map after removing the quarry blast events constructed for earthquakes with $M \leq 3.0$	37
Figure 3.10: Frequency magnitude distribution (FMD) plots of the study area (1990-January 2014). a) FMD plot of the unprocessed catalogue; b) FMD plot of the quarry free catalogue (no declustering algorithm applied); c) FMD plot after applying Reasenberg (1985) declustering algorithm and subsequently removing quarry events and d) FMD plot after applying Gardner and Knopoff (1974) declustering algorithm and	

subsequently removing quarry events.....	38
Figure 3.11: Map showing the spatial variations in b-values for the area. The map is constructed using the unprocessed catalogue downloaded from KOERI (1990-January 2014). The catalogue includes the quarry blast events and aftershock sequences associated with the major events.....	41
Figure 3.12: Map showing the spatial variations in b-values for the area. The map is constructed using the catalogue that is free of quarry blast events (1990- January 2014). The catalogue includes the foreshocks and aftershock sequences associated with the major events.....	42
Figure 3.13: Map showing the spatial variations in b-value for the study area. The map is constructed using the declustered (Reasenberg, 1985) and quarry free catalogue. The catalogue does not include any quarry blast events and or aftershock sequences associated with the major events.....	43
Figure 3.14: Map showing the spatial variations in b-value for the study area. The map is constructed using the declustered (Gardner & Knopoff, 1974) and quarry free catalogue. The catalogue does not include any quarry blast events and or aftershock sequences associated with the major events.....	44
Figure 3.15: Heat flow map of western Anatolia modified from heat flow map of Turkey (Akın <i>et al.</i> , 2014). The locations of hot springs are shown as white stars (from Yolsal <i>et al.</i> , 2005) and the location of Quaternary Kula volcanism is shown with a black triangle. The active faults in the area are also shown with black lines.....	45
Figure 3.16: b-value against time for the whole study area. a) unprocessed catalogue; b) quarry free catalogue declustered using Reasenberg (1985) and c) quarry free catalogue declustered using Gardner and Knopoff (1974)	47
Figure 3.17: a) Pre Alaşehir earthquake b-value map; b) post Alaşehir earthquake b-value map (circular area shows the rupture area characterized by aftershocks where the value is increased); c) magnitude vs time plot of Alaşehir; d) b-value vs time plot of Alaşehir and e) zoomed in section of the b-value vs time plot.....	49
Figure 3.18: a) Post Dinar earthquake b-value map; b) magnitude vs time plot; c) b-value vs time plot of Dinar area and d) zoomed in section of the b-value vs time plot.....	51

Figure 3.19: a) Post Gulf of Sığacık earthquake b-value map; b) magnitude vs time plot; c) b-value vs time plot of Gulf of Sığacık and d) zoomed in section of the b-value vs time plot	52
Figure 3.20: a) Pre Simav earthquake b-value map; b) post Simav earthquake b-value map; c) magnitude vs time plot; d) b-value vs time plot of Simav area and e) zoomed in section of the b-value vs time plot	54
Figure 3.21: a) Seismic quiescence before Simav earthquake and b) calculated rate changes for Simav area using AS(t) function (time window 1.5 years, bins = 15 days).....	55
Figure 3.22: a) Magnitude of completeness with time and b) occurrence rate of earthquake vs time for the Simav region.....	57
Figure 4.1: Available focal mechanism solutions overlaid over topography. The sizes of the solutions are scaled according to their magnitude. Note that parameters of these solutions are listed in Appendix A.....	62
Figure 4.2: a) Rake based ternary plot of faulting types; b) pressure and tension (P-T) axes plotted on lower hemisphere projection and c) contoured plot of P-T axes for all the earthquakes in the study area. Note that orientations of P-T axes are listed in Appendix A.....	64
Figure 4.3: Map showing focal mechanism solutions and sub-regions in study area that are selected for analyzing stress orientations independently	66
Figure 4.4: Stereographic projection of P-T axes and rake based ternary plots identified within each sub-region.....	67
Figure 4.5: a) Results of stress tensor inversion of all available focal mechanism solutions in the study area using Michael's method and b) the resultant histogram of stress ratio (R) vs frequency.....	72
Figure 4.6: a) Orientation bars of horizontal compression directions. Tectonic regimes are represented by different colors (NF: Normal, NS: Normal with strike-slip, SS: Strike-slip, TS: Thrust with strike-slip, TF: Thrust). b) Orientation bars of horizontal compression directions overlaid on to colored stress tensor variance map of the study area	74

Figure 4.7: A close-up map of the Simav sub-region showing topography and focal mechanism solutions. Mainshock and aftershocks of Simav earthquake are grouped in the east (except solution 12 which occurred earlier).....76

Figure 4.8: **a)** Results of stress tensor inversion and histogram of stress ratio (R) vs frequency for Simav sub-region and **b)** results of stress tensor inversion and histogram of R vs frequency for Simav sub-region excluding the Simav earthquake sequence.....77

Figure 4.9: **a)** Close-up map of the Alaşehir sub-region showing topography and focal mechanism solutions and **b)** results of stress tensor inversion and histogram of stress ratio (R) vs frequency for Alaşehir sub-region.....79

Figure 4.10: **a)** Close-up map of the Manisa sub-region showing topography and focal mechanism solutions and **b)** results of stress tensor inversion and histogram of stress ratio (R) vs frequency for Manisa sub-region.....80

Figure 4.11: **a)** Close-up map of the Dinar-Burdur sub-region showing topography and focal mechanism solutions and **b)** results of stress tensor inversion and histogram of stress ratio (R) vs frequency for Dinar-Burdur sub-region.....81

Figure 4.12: **a)** Close-up map of the Büyük and Küçük Menderes sub-region showing topography and focal mechanism solutions and **b)** results of stress tensor inversion and histogram of stress ratio (R) vs frequency for the sub-region.....82

Figure 4.13: **a)** Close-up map of the Soma sub-region showing topography and focal mechanism solutions and **b)** results of stress tensor inversion and histogram of stress ratio (R) vs frequency for Soma sub-region83

Figure 4.14: **a)** Close-up map of the Bakırçay Graben sub-region showing topography and focal mechanism solutions and **b)** results of stress tensor inversion and histogram of stress ratio (R) vs frequency for Bakırçay sub-region.....84

Figure 4.15: **a)** Map of the Gulf of Sığacık sub-region showing topography and focal mechanism solutions. The seismic cluster at the top-left is related to Gulf of Sığacık earthquake sequence; **b)** Close-up view of the Gulf of Sığacık earthquake sequence.....86

Figure 4.16: **a)** Results of stress tensor inversion and histogram of stress ratio (R) vs frequency for Gulf of Sığacık sub-region and **b)** results of stress tensor inversion and

histogram of stress ratio (R) vs frequency for the sub-region excluding the cluster related to the Gulf of Sığacık earthquake sequence.....87

Figure 4.17: **a)** Close-up map of the Gulf of Gökova sub-region showing topography and focal mechanism solutions and **b)** results of stress tensor inversion and histogram of stress ratio (R) vs frequency for Gökova sub-region.....88

Figure 4.18: **a)** Close-up map of the Fethiye sub-region showing topography and focal mechanism solutions and **b)** results of stress tensor inversion and histogram of stress ratio (R) vs frequency for Fethiye sub-region.....90

Figure 4.19: Map showing horizontal projection of principle stresses calculated using Win-Tensor program (Delvaux and Sperner, 2003) for all sub-regions (blue: σ_1 , green: σ_2 , red: σ_3).....93

Figure 4.20: Stress map displaying maximum horizontal stress axes (S_{Hmax}) associated to each focal mechanism solution used in this study. Tectonic regime is color coded. Note that the resultant S_{Hmax} and S_{Hmin} axes are listed in the Appendix A.....95

Figure 4.21: Equal area rose diagrams of maximum (S_{Hmax}) and minimum horizontal stress axes (S_{Hmin})96

Figure 4.22: Stress map displaying maximum horizontal stress axes (S_{Hmax}) within the study area listed in the World Stress Map (WSM) database (Heidbach *et al.*, 2008 and the references therein).....96

Figure 5.1: The Gutenberg-Richter (G-R) relations obtained for the entire region. **a)** Maximum likelihood estimate (MLE) using all recorded events; **b)** MLE using only earthquake with magnitude greater than or equal to 4.0; **c)** Weighted Least Square estimate (WLS) using all recorded events and **d)** WLS using only earthquake with magnitude greater than or equal to 4.0.....100

Figure 5.2: Frequency magnitude distribution (FMD) plots of the sub-regions obtained by using the Weighted Least Square (WLS) method. The magnitude of completeness (M_c) is computed automatically. No magnitude cutoff is applied.....102

Figure 5.3: Frequency magnitude distribution (FMD) plots of the sub-regions using Weighted Least Square (WLS) with a magnitude cutoff at 4.0. Note that M_c for each region is still automatically computed.....104

Figure 5.4: Map of b-values computed for sub-regions using Weighted Least Square

(WLS) with earthquake magnitude greater than or equal to 4.0. The sub regions are colored according to their b-value.....106

Figure 5.5: Map of a-values computed for sub-regions using Weighted Least Square (WLS) with earthquake magnitude greater than or equal to 4.0. The sub regions are colored according to their a-value.....107

Figure 5.6: Graphs showing the least square regression relations between ‘Magnitude’ and ‘ln (-ln G)’ for sub-regions in the study area110

Figure 5.7: The Gutenberg-Richter (G-R) relation based map showing earthquake probabilities (Pr) of sub-regions for a magnitude 6 event within 50 years. Pr values (in %) are taken from Table 5.1.....114

Fig. 5.8: The Gutenberg-Richter (G-R) relation based map showing earthquake probabilities (Pr) of sub-regions for a magnitude 7 event within 100 years. Pr values (in %) are taken from Table 5.1.....115

Figure 5.9: The Gumbel annual extreme method based map showing earthquake probabilities (Pr) of sub-regions for a magnitude 6 event within 50 years. Pr values (in %) are taken from Table 5.2.....119

Figure 5.10: The Gumbel annual extreme method based map showing earthquake probabilities (Pr) of sub-regions for a magnitude 7 event within 100 years. Pr values (in %) are taken from Table 5.2.....120

Fig. 5.11: The Gutenberg-Richter (G-R) relation based map showing maximum expected earthquake magnitudes (Mmax) within 100 years for the selected sub-regions.....122

Fig. 5.12: The Gumbel annual extreme method based map showing maximum expected earthquake magnitudes (Mmax) within 100 years for the selected sub-regions123

Figure 5.13 Fractal dimension (Dc) plots of the sub-regions. Dc is computed using the quarry free KOERI catalog between 1990 and January, 2014.....127

Figure 5.14: Map showing the spatial variation of fractal dimension values (Dc) across the selected sub-regions. Each sub-region is colored accordingly to its Dc value129

Figure 6.1: Map showing focal mechanism solutions which are colored according to the

tectonic regime classification of Zoback (1992). Red: normal, pink: transtensional, green: strike-slip, cyan: transpressional, blue: thrust and black: undefined faulting. Note that identified regimes are listed in Appendix A.....133

Figure 6.2: Stress map showing minimum horizontal stress axes (S_{Hmin}) associated to each focal mechanism solution used in this study. The resultant axes indicate the extension directions in the study area.....134

Figure 6.3: Linear correlation between a- and b- values of the sub-regions. The sub-regions are classified according to the dominant tectonic regime (N: Extensional, S: Strike-slip, NS: Extensional-Strike-slip).....136

Figure 6.4: Linear correlation between **a)** fractal dimension (D_c) and b-value and **b)** D_c and a-value of the sub-regions. The sub-regions are classified according to the dominant tectonic regime (N: Extensional, S: Strike-slip, NS: Extensional-Strike-slip).....137

Figure 6.5: Linear correlation between **a)** stress ratio and b-value; **b)** stress ratio and a-value and **c)** stress ratio and fractal dimension (D_c) of the sub-regions. The sub-regions are classified according to the dominant tectonic regime (N: Extensional, S: Strike-slip, NS: Extensional-Strike-slip). Dashed trend lines are computed by excluding the outlier Dinar-Burdur sub-region.....138

Figure 6.6: Linear correlation between **a)** stress variance and stress ratio and **b)** stress variance and fractal dimension (D_c) of the sub-regions. The sub-regions are classified according to the dominant tectonic regime (N: Extensional, S: Strike-slip, NS: Extensional-Strike-slip).....139

CHAPTER 1

INTRODUCTION

1.1 Purpose and Scope

Western Anatolia constitutes one of the important active tectonic elements of Turkey. The region forms eastern part of active Aegean extensional province and has been experiencing episodic N–S crustal extension since the latest Oligocene. Ongoing deformation in the region is controlled by northward subduction of African plate beneath the Anatolian plate and the right-lateral slip along the North Anatolian fault system. Along with N–S extension, the area is also characterized by oblique-slip and strike-slip deformations in its north-western part and Fethiye-Burdur Fault Zone which forms its eastern extremity. The region is one of the seismically active areas in Turkey and has experienced large magnitude historical earthquakes and some moderately-sized recent earthquakes. The purpose of this study is to investigate the active stress patterns and their spatial variations within the study area. The second objective of this thesis is to estimate the probabilities and return periods of earthquakes for various sub-regions in the study area. This study covers the area between the latitude and longitude intervals of 36.5–39.5° N and 26.5–30.5° E, respectively.

This study will lead us to the better understanding of active stress patterns of the region which is necessary for understanding the geodynamics of the region and will also help in finding any local variations within these stress patterns. Moreover, the seismicity analysis will help in better characterization of the active fault zones and is expected to serve as basis for evaluating the seismic hazards, which will further help us in the urban and regional planning of the nearby cities (e.g., İzmir, Denizli, Kütahya, Uşak, Manisa, Muğla, Bodrum etc.).

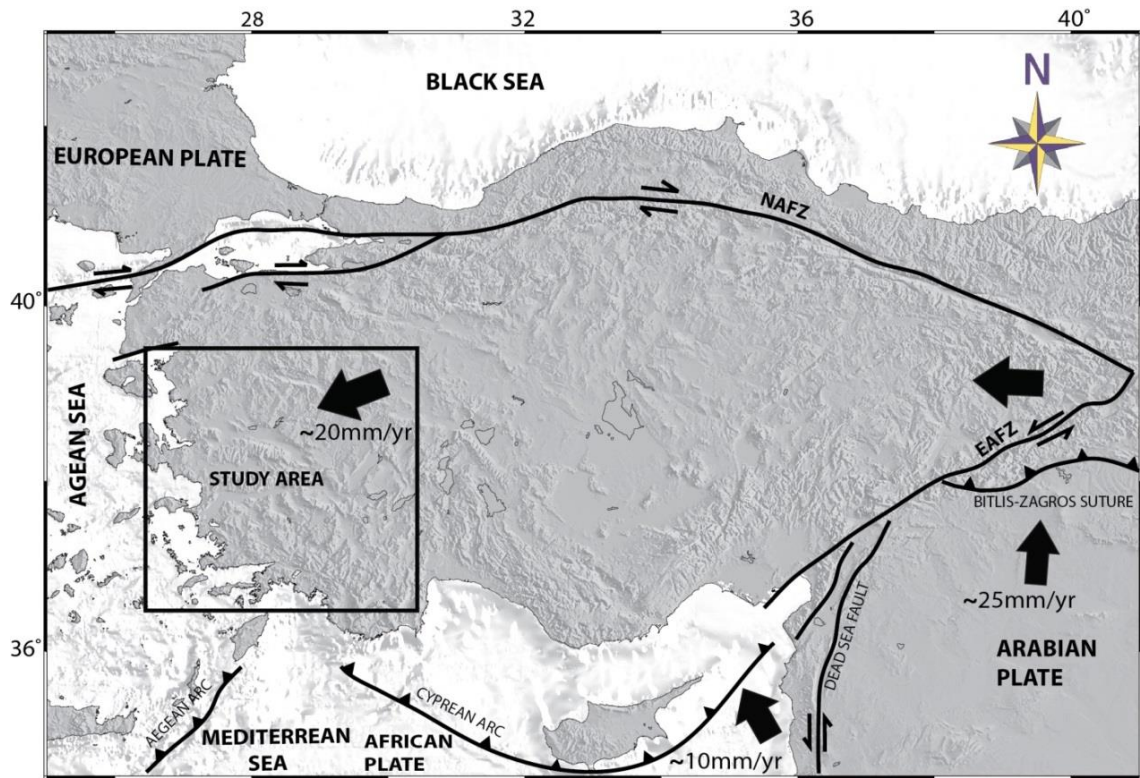


Figure 1.1: Generalized tectonic map of Turkey (from Bozkurt, 2001). The box indicates location of the study area.

1.2 Previous Studies

Western Anatolia is one of the extensively studied continental regions in the world due to its seismically active nature and its role in the geodynamics of the region. The area has been a topic of active debate for various scientists due to its tectonic complexities. A detailed review of the tectonic complexities and associated discussions regarding western Anatolia is given in Chapter 2. The area is categorized as one of the most seismically active regions of Turkey and is therefore analyzed by various researchers for earthquake probabilities related studies as well. As our study deals with stress tensor inversion from focal mechanism solutions (FMS) and seismicity analysis, therefore a brief review of the previous studies related to these topics is given here. These studies

include the focal mechanism solutions determination of earthquakes for seismotectonic investigations and the statistical processing of earthquake catalogues for hazard assessment of the area. The prominent studies related to the seismotectonics of western Turkey and surrounding regions are summarized below.

McKenzie (1972, 1978) investigated the active tectonics of Mediterranean region and Alpine-Himalayan belt including the Aegean Sea and surrounding regions on the basis of fault plane solutions of earthquakes in the region. Based on seismological techniques and surface observations, Eyidođan and Jackson (1985) studied the Demirci, Alaşehir and Gediz Earthquakes of 1969–1970 in western Turkey and their implications for the nature and geometry of deformation in the continental crust. Taymaz and Price (1992) determined the source parameters for May, 12 1972 Burdur earthquake using seismological and geological observations. Taymaz *et al.* (1991) also provided a revised account of active tectonics of the north and central Aegean Sea based on an updated focal mechanism solutions database, including previous data and FMS determined in their study. The focal mechanism solutions for Dinar earthquake were determined by Eyidođan and Barka (1996); Pınar (1998) and Wright *et al.* (1999). Papazachos *et al.* (1991, 1998) used the focal mechanism solutions to investigate the active tectonic patterns in the Aegean region. Kirtazi (2002) carried out the stress tensor inversions along the westernmost North Anatolian Fault Zone and its continuation into the North Aegean Sea using the already published focal mechanism solution catalogue. Kiratzi and Louvari (2003) developed an updated database of focal mechanisms of shallow earthquakes for a period of 1953–1999 in the Aegean Sea and the surrounding regions. Zhu *et al.* (2006) carried out the seismotectonic investigation of western Turkey using high resolution earthquake relocations and moment tensor determinations. Their results showed that the N–S extension in western Turkey is accommodated by strike-slip faulting in the region. Benetatos *et al.* (2006) and Aktar *et al.* (2007) reported the focal mechanism solutions for Gulf of Sığacık earthquake sequence and its aftershocks and reported a strike-slip fault system in the area. Irmak (2013) determined focal mechanisms for small to moderate earthquakes in Denizli area and showed that the earthquakes in the area are characterized by normal faulting mechanism associated with small strike-slip components. Tan (2013) discussed the dense micro-earthquake activity

along the boundary between the Anatolian and South Aegean micro-plates around the Karaburun Peninsula area. Çevikbilen *et al.* (2014) studied the source mechanism and rupture histories of recent earthquakes in western Turkey for the ongoing active deformation in the region and suggested a strike-slip tectonic domain associated with the dominant extensional domain in the region. Doğru *et al.* (2014) carried out geodetic and seismological investigation of crustal deformation around Izmir area. The strain related studies from GPS measurements for the region and surroundings includes: Kahle *et al.* (1998); McClusky *et al.* (2000, 2003); Reilinger *et al.* (2006); Erdoğan *et al.* (2008); Aktuğ *et al.* (2009) and Özener *et al.* (2013).

The earthquake probabilities and seismic risk related studies for western Turkey are also summarized. Altınok (1991) evaluated the seismic risk of west Anatolia by application of Semi-Markov model. Bağcı (1996) investigated seismic risk of western Anatolia using the Poisson model for earthquake data from 1930 to 1990. Sayıl and Osmañahin (2004, 2005) and Sayıl (2005) applied time- and magnitude- predictable model to west Anatolia and other regions of Turkey for long-term earthquake prediction. Sayıl and Osmañahin (2008) estimated the seismic risk and recurrence periods by using Poisson model from historical and instrumental data (1900–2006) for selected characteristic sub-regions in western Anatolia. Polat *et al.* (2008) investigated the earthquake hazard for western Aegean extensional region using the Gutenberg-Richter b- parameter, seismic quiescence (z- value) and fractal behavior using earthquake data from 1900 to 2002. Bayrak *et al.* (2008, 2009) carried out the seismicity assessment for different regions in and around Turkey using Gumbel first asymptotic distribution and G-R cumulative frequency law. Bayrak and Bayrak (2012a) evaluated, using historical and instrumental data, the seismic hazard potential for different regions in western Anatolia. Other studies for the region includes those of Papazachos, (1999); Jenny *et al.* (2004); Bayrak *et al.* (2005); Firuzan, (2008) and Çobanoğlu and Alkaya, (2011).

Bayrak and Bayrak (2012b) studied the variations and correlation of Gutenberg-Richter (a- and b- values) and fractal dimension (Dc) for various seismogenic zones in western Anatolia. Öztürk (2012) also studied the statistical correlation between these parameters for 55 tectonic zones of Turkey including western Anatolia. Other regional studies

related to fractal dimension includes those of the Öncel and Wilson, (2002); Öncel, (2004) and Ceylan, (2006).

1.3 Data and Methods

The research methodology includes acquiring a seismic catalogue for the area from KOERI (<http://www.koeri.boun.edu.tr/>). The catalogue is evaluated for its temporal and spatial homogeneity and different processing techniques (e.g., homogeneity through time; removing quarry blasts; homogeneity of magnitude scales and declustering of the catalogue) are applied to acquire a homogeneous catalogue for the region. The statistical analysis of the catalogue and b-value maps of frequency magnitude distribution (FMD) for the whole region and for some recent major events in the area is carried out using ZMAP (Wiemer, 2001) software package. For investigating the active stress patterns of the region, a focal mechanism solution (FMS) catalogue is compiled from different local and international agencies and available literature. The area is divided into sub-regions on the basis of tectonic sub-domains and variations in focal mechanism solutions. Using the FMS, stress tensor inversion has been carried out using Slick method of Michael (1984, 1987) for the whole area and principal stress directions are determined. The results are compared with the structural data and other available datasets. Stress tensor inversion is also carried out using Win-Tensor program of Delvaux and Sperner (2003) for checking the reliability of Michael's method results. After dividing the area into sub-regions, a well-established seismic source zone model is attained, which can be used for detailed seismic hazard analysis of the region. The hazard analysis is carried out for these sub-regions using Gutenberg-Richter relation and Gumbel's annual extreme value method. The fractal dimension (Dc) analysis is also carried out for sub-regions using the correlation dimension of Grassberger and Procaccia (1983).

1.4 Organization of the Thesis

This thesis is organized into six (6) chapters. In Chapter 2, an overview on the regional tectonic settings of the area and the associated discussions is given in detail. Afterwards, the major fault structures in the area are described in association with the tectonic sub-domains in the area. At the end of this chapter, the spatial distribution of the seismicity and its relation with the fault structures is discussed in detail. Chapter 3 deals with earthquake statistics. b- value maps of frequency magnitude distribution for the region and some recent events are presented in this chapter for investigation of spatial and temporal variations of b-values. Chapter 4 is related to the stress tensor inversion from focal mechanism solutions. Horizontal stress directions are also computed for the area using the focal mechanism solutions. In Chapter 5, earthquake probabilities and fractal dimension values have been calculated for all the sub-regions in the study area using different methods. The results of this thesis are then discussed and interpreted in Chapter 6.

CHAPTER 2

TECTONIC SETTING AND SEISMICITY

2.1 Regional Tectonic Setting

Turkey falls within an important sector in the western part of Alpine-Himalayan orogenic belt. Hellenides and Carpathians branches of Alpine system cross Turkey in the form of complex Tauride and Pontide blocks and connect with Bitlis-Zagros Zone to the east (Şengör and Yılmaz, 1981). This part of the Alpine-Himalayan belt is dominated by compressional, strike-slip and extensional deformations that resulted from the complicated convergence of African and Eurasian plates. The continental convergence governs the major neotectonic configuration of Turkey (Figure 2.1). The African Plate to the south is subducting beneath the Anatolian microplate and Eurasia to the north along the Aegean-Cyprian subduction zone that constitutes the southern limit of this tectonic regime. The subduction is accompanied by dextral North Anatolian Fault System (NAFS) to the North and sinistral East Anatolian Fault System (EAFS) to the East, to accommodate the movement of the overriding Anatolian wedge. These fault systems bound the Anatolian microplate and guide its westward escape from the zone of continental collision along the Bitlis-Zagros suture zone between the African and Eurasian plates (Şengör, 1979; Dewey and Şengör, 1979; Şengör *et al.*, 1985). The escape of the Anatolian microplate is accompanied by counterclockwise rotation (Rotstein, 1984). As a result of all these movements, Turkey is characterized by four different kinds of unique deformation styles and sedimentary basin formation (Figure 2.2) (Koçyiğit and Özacar, 2003).

- (1) An extensional regime dominates across southwestern parts of Turkey. The region is characterized by active continental extension and forms the eastern part of well-known Aegean Extensional Province (AEP) and extends westward into Aegean Sea and southern Balkan region. The study area falls in this neotectonic regime;
- (2) The East Anatolian compressional province;
- (3) The North Anatolian Fault Zone strike-slip province;
- (4) The Central Anatolian province.

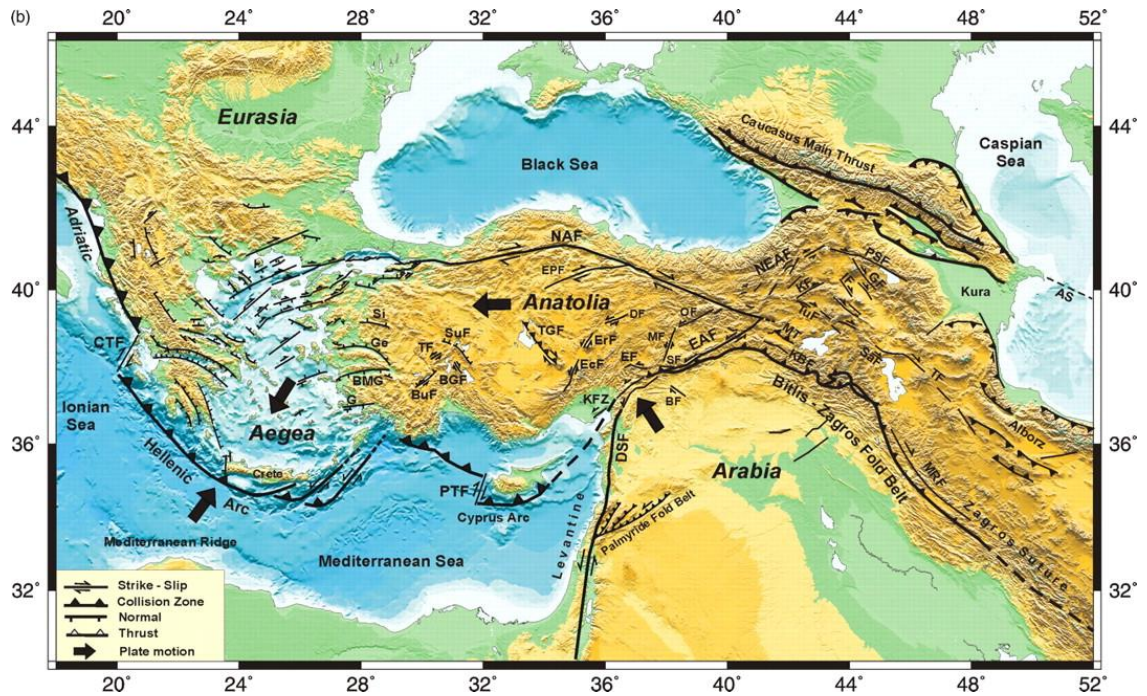


Figure 2.1: Generalized tectonic map of Turkey taken from Taymaz *et al.*, 2007. BGF: Beyşehir Gölü Fault; BMG: Büyük Menderes Graben; BuF: Burdur Fault; CTF: Cephalonia Transform Fault; DF: Deliler Fault; DSF: Dead Sea Transform Fault; EAF: East Anatolian Fault; EcF: Ecehis Fault; EF: Elbistan Fault; EPF: Ezinepazarı Fault; ErF: Erciyes Fault; G: Gökova; Ge: Gediz Graben; KFZ: Karatas-Osmaniye Fault Zone; MF: Malatya Fault; NAF: North Anatolian Fault; PTF: Paphos Transform Fault; SF: Sultandağı Fault; Si: Simav Graben; TF: Tatarlı Fault; TGF: Tuz Gölü Fault.

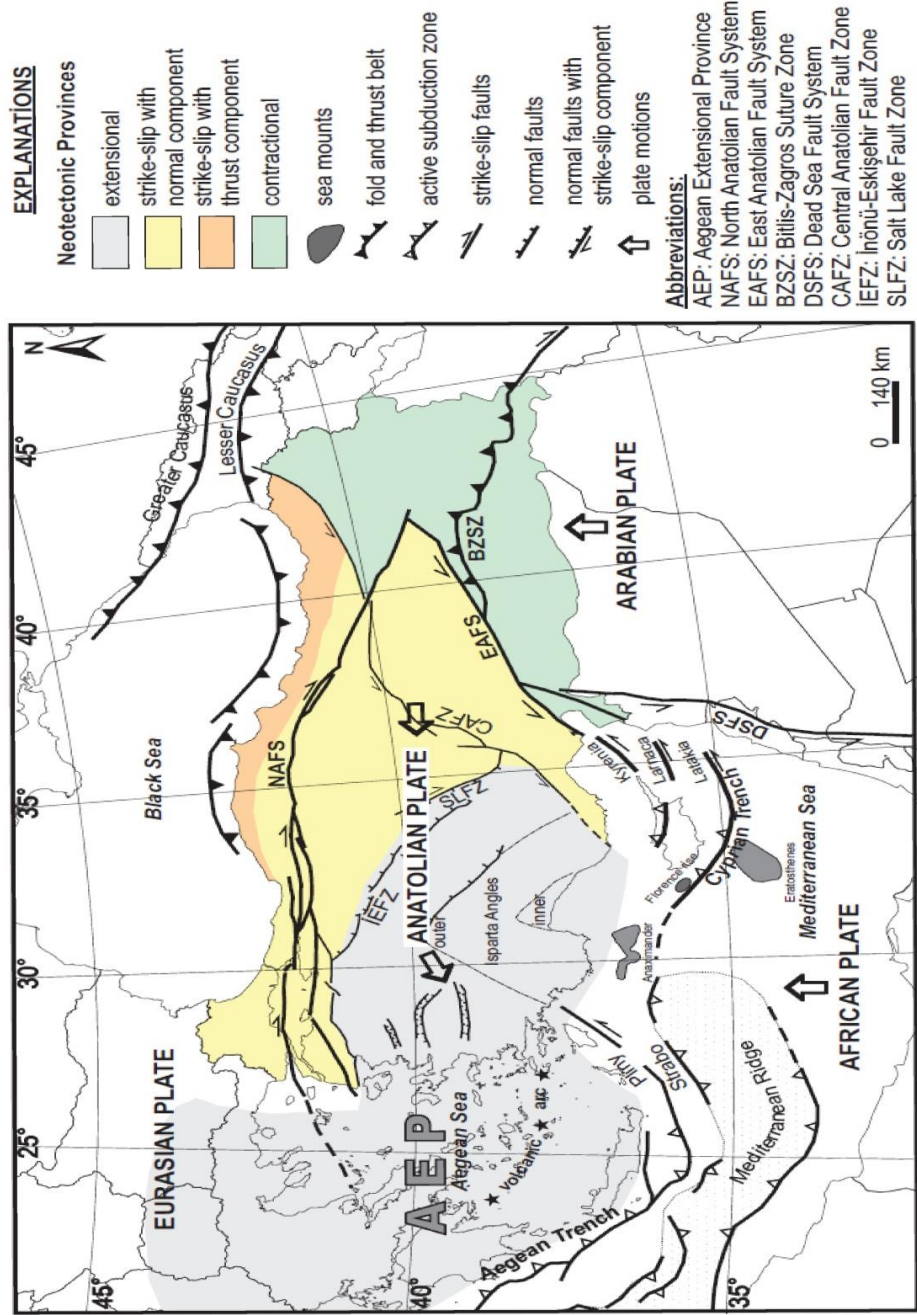


Figure 2.2: Map illustrating the major neotectonic provinces and related governing structures in Turkey and surrounding areas. The figure is adapted from Çiftçi (2007), modified from Koçyiğit and Özacar (2003), Woodside *et al.* (2002) and Zitter *et al.* (2005).

The Anatolian microplate is composed of various amalgamated continental fragments with several suture zones acting as a divide between them. These continental fragments forms basement to the neotectonic sedimentary basins of the Anatolian microplate. The continental fragments were welded against each other by means of continent-continent collisions across the northern and southern branches of Neotethys during the Early Tertiary (Şengör and Yılmaz, 1981). Deformation fabrics resulted from this collision played a major role in governing the neotectonic framework of the region. The major continental fragments of western Anatolia are bounded by two major suture zones. The Intra-Pontide suture zone separates the İstanbul Zone to the north from the Sakarya Zone to the south and the İzmir-Ankara Suture acts as divide between the southern margin of Sakarya Continent in the north and the Anatolide-Tauride Platform in the south. This platform is made up of several tectonic units bounded by major faults. These units include Tavşanlı Zone, the Bornova Flysch Zone, the Afyon Zone, the Menderes Massif and Lycian Nappes (Piper *et al.* 2002; Bozkurt and Oberhänsli, 2001 and references therein).

Western Anatolian extensional province is one of the important structural elements of Turkey constituting the eastern margin of active Aegean Extensional Province (AEP) (Figure 2.2). The region is one of the best studied region in Turkey, with most of the research focusing on the cause of extensional stress field and the time of initiation of extension (e.g., Seyitoğlu and Scott, 1991, 1992; Taymaz, 1993; Le Pichon *et al.* 1995; Reilinger *et al.* 1997; Ambrasseys and Jackson, 1998; Altunel, 1999; Koçyiğit *et al.* 1999a, b; McClusky *et al.*, 2000; Bozkurt, 2001; Bozkurt and Sözbilir, 2004; Koçyiğit, 2005; Bozkurt and Mittwede, 2005 and references therein). In essence, the region as a whole was shortened by a series of collisional events in the late Mesozoic and early Tertiary (Robertson and Dixon, 1984; Şengör *et al.*, 1984) and since latest Oligocene the area has been experiencing episodic active N–S crustal extension.

The ongoing extensional deformation in the area is controlled by the northward subduction of African Plate beneath the Anatolian Plate and the right lateral slip along North Anatolian Fault Zone. It has been well established that this region is now undergoing N–S extensional phase at a rate of 30–40 mm/yr (Oral *et al.* 1995; Le

Pichon *et al.* 1995). But the origin, time, cross cutting relationship between faults in the area, nature of folding (whether compressional or extensional) and evolution through time of the extensional phase has been a topic of debate for various scientists working on the area.

The origin of extension in this region has been attributed to (i) westward escape of the Anatolian block along the North Anatolian Transform Fault Zone (Dewey and Şengör, 1979), (ii) Roll-back along the Neogene to Recent subduction in the Aegean-Cyprean subduction zone or Back-arc spreading model (Le Pichon and Angelier 1979), and/or (iii) gravitational collapse of thickened crust following Palaeogene Alpine-Himalayan compression (Seyitoğlu and Scott, 1991).

According to the first model, AEP formed as a result of the westward motion or escape of the Anatolian microplate from the collision zone of Arabian and Eurasian plates across the Bitlis Suture, in southwestern Turkey by motion along dextral North Anatolian Fault Zone (NAFZ) and sinistral East Anatolian Fault Zone (EAFZ). The westward escape of the Anatolian wedge is being obstructed by a bend in the course of the NAFZ in southwestern part near Aegean Sea and Greece (Şengör *et al.* 1985). This obstruction resulted in E–W shortening, which was relieved in the form of N–S extension by lateral spreading in the AEP region (Şengör *et al.* 1985). The roll back model suggests that migration of the trench system in Aegean-Cyprian subduction zone to the south and southwest gave rise to extensional forces in the back-arc (Aegean) region. This process consequently led to the subsidence of Aegean Sea and the formation of present day AEP (McKenzie, 1978; Le Pichon and Angelier, 1979; Jackson and McKenzie, 1988; Meulenkamp *et al.* 1988, 1994). Nevertheless, there are still discussions about the inception date of subduction, rollback process and the consequential extension. The orogenic collapse model requires an orogenic belt with an over-thickened crust to collapse under its own weight due to exceed of body forces (resulting from isostatically compensated elevation) from the compressional tectonic forces forming the orogenic belt (Dewey, 1988). This crustal thickening, further supported by structural inhomogeneity and thermal anomaly of the lithosphere, creates an extensional stress field and promotes continental rifting. It is suggested that the

orogenic collapse and inception of the roll-back process developed simultaneously and the former has been balanced by the latter since the Middle Miocene (15 Ma). Another model proposed by Doglioni *et al.* (2002) claim that the current deformation in the AEP is a result of differential rate of convergence between the subducting African Plate and the overriding plate, with faster southwestward moving Greece as compared to Anatolian microplate. None of the afore-mentioned models can independently address the problems related with the origin and age of extensional tectonics of the graben system in western Turkey in a satisfactory manner. Therefore, recently geologists used a combination of two or more of these models in an episodic manner to address these issues.

Koçyiğit *et al.* (1999a, b) defined two distinct extensional phases, separated by a short phase of compression for the Gediz Graben on the basis of his field evidences. The first phase of extension (Early Miocene) was driven by the orogenic collapse model along the İzmir-Ankara suture zone, intercepted by an intervening short phase of N–S compression in late Miocene to early Pliocene times which was probably as a result of change in the kinematics of Eurasian and African plates. The second or current phase of extension was probably triggered by the commencement of sea-floor spreading along Red Sea in early Pliocene times. At that time the Anatolian microplate and its bounding structures, NAFZ and EAFZ, had formed and the westward escape of Anatolian microplate was initiated; this lead to the extension in the Aegean region. Further studies supported by field evidences validated the episodic two stage extension model (Bozkurt, 2000, 2001, 2003, 2004; Yılmaz *et al.* 2000; Sözbilir, 2001, 2002; Çiftçi, 2007; Çiftçi and Bozkurt, 2010; Cihan *et al.* 2003; Bozkurt and Sözbilir, 2004, 2006; Purvis and Robertson, 2004, 2005; Rojay, *et al.*, 2005; Kaya *et al.* 2004; Bozkurt and Rojay, 2005; Beccaletto and Stenier, 2005; Westaway *et al.* 2005).

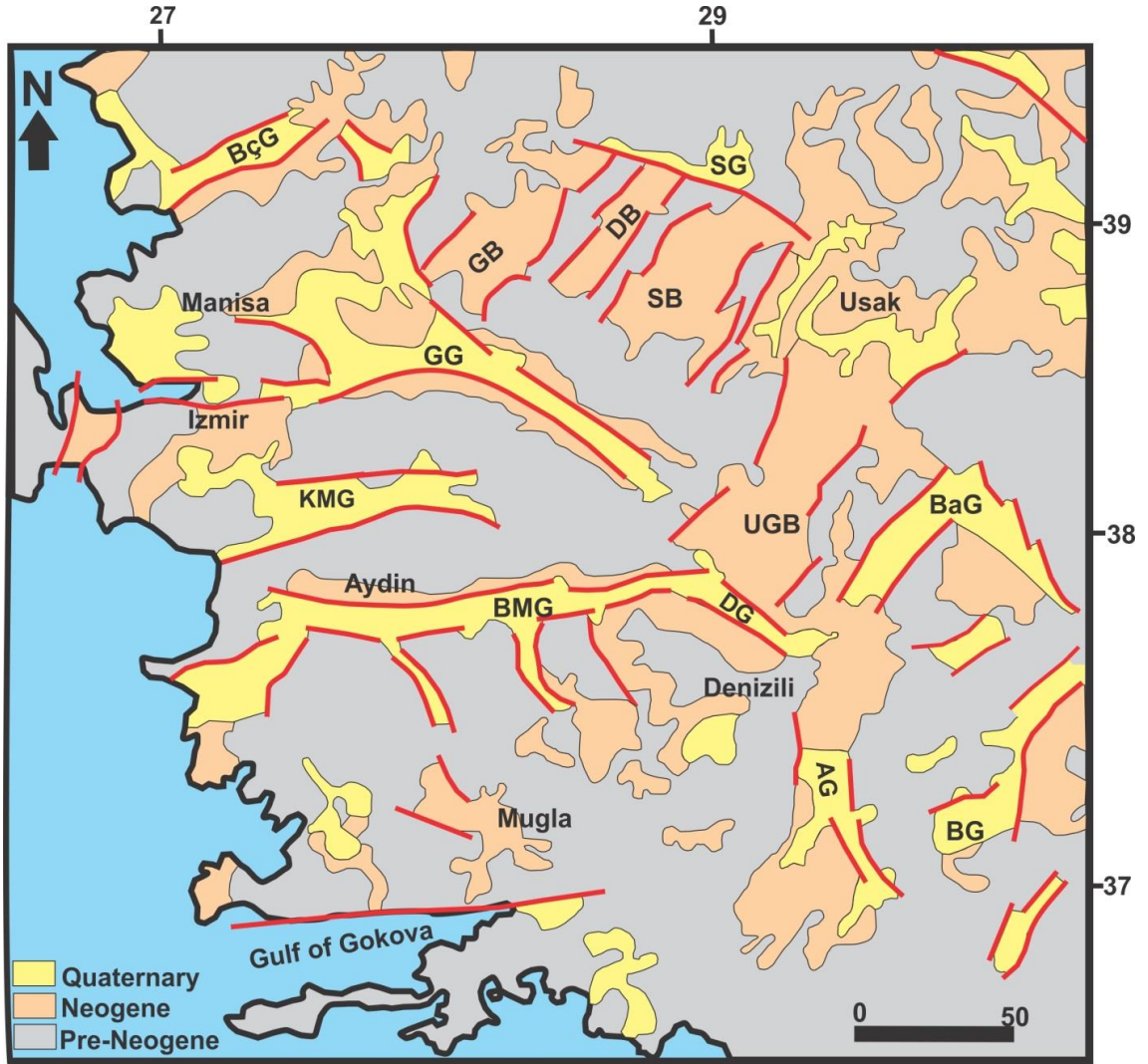


Figure 2.3: Simplified geological map of western Turkey, from Bozkurt (2000). Abbreviations: AG: Acıpayam Graben; BaG: Baklan Graben; BçG: Bakırçay Graben; BG: Burdur Graben; BMG: Büyük Menderes Basin; DB: Demirci Basin; DG: Denizili Graben; GB: Gördes Basin; GG: Gediz Graben; KMG: Küçük Menderes Graben; SB: Selendi Basin; SG: Simav Graben; UGB; Uşak-Güre Graben.

2.2 Geological Setting of Western Anatolia

Western Anatolian region is characterized by horst blocks of the Menderes Massif, which acts as a divide between the adjacent grabens. These basins include Gediz Graben, Küçük Menderes Graben, Büyük Menderes Graben and Simav Graben (Figure 2.3). The Graben basins are filled with Neogene to Recent stratas. The grabens are the sites of active continental depositions by alluvial and fluvial processes (Koçyiğit *et al.*, 1999a and b; Yılmaz *et al.*, 2000; Bozkurt, 2004; Koçyiğit, 2005). Apart from the grabens, there are NE–SW- trending basins to the North of Gediz Graben and NW–SE basins to the south of Büyük Menderes Graben; they include Gördes, Demerici, Selendi and Uşak-Güre basins (Figure 2.3). The origin of these basins is controversial. Some researchers (Şengör *et al.*, 1985; Şengör, 1987; Yılmaz *et al.*, 2000) refer them as Tibetan type graben system that formed after the closure of northern branch of Neotethys under the N–S compressional conditions prevailing at that time. Others regard them as synchronous with the E–W graben system (Seyitoğlu and Scott, 1991, 1992; Collins and Robertson, 1998) while some say that they are controlled by cross accommodation faults on hanging wall of presently low angle detachment fault bounding the southern margin of Gediz Graben (Şengör 1987, Bozkurt, 2003). The grabens in the region have an east-west- trending morphometric expression with a well-defined topography on satellite images and aerial photographs. The southern part of the region, Gökova region, is dominated by two different rift systems of different age and orientations (Görür *et al.*, 1995). It consists of a younger east–west- trending rift system that cut across the northwest-southeast trending rifts (Şengör *et al.*, 1984). The most prominent neotectonic features of this system include Gökova, Yatağan-Muğla and Milas-Ören basins. The grabens in the northwest–southeast system are separated by basement highs forming horsts. The prominent basins in Fethiye-Burdur fault zone include Burdur, Acıpayan, Eşen (ten Veen, 2004; Alçıçek, 2007) and Çameli-Göhlhisar (Alçıçek *et al.*, 2006) basins. The basins are bounded by NE–SW- trending oblique-slip faults having sinistral strike-slip components (Elitez, 2010; Elitez *et al.*, 2009; Elitez and Yaltırak, 2014). To the north, Fethiye-Burdur fault zone merges into NW–SE- trending grabens, including Dinar, Beyşehir, Akşehir-Afyon, Dombayova grabens. The

Quaternary basins included in IBSZ are bounded by NE–SW- trending strike-slip and E–W- trending normal faults that are obliquely oriented to the former, so they are categorized as rhomb or strike-slip basins (Uzel & Sözbilir 2005, 2006). The prominent basins in this zone include Bakırçay and Cumaovası basins (Figure 2.4).

2.3 Major Tectonic Structures in the Region

Most of the faults in the study area are associated with the grabens and they act as bounding structures for them. Apart from normal faults associated with the extensional tectonics of the area; the north-western part of the area is dominated by strike-slip faults associated with the İzmir Balıkesir Transfer Zone (IBTZ) (Figure 2.4). The scarps of the faults show linear segments and they can be clearly marked, as they separate the alluvial plains from the rougher terrains.

The faults in the area have been categorized into four groups based on their tectonics sub-domains, fault mechanisms and geographic locations (Figure 2.4). These groups are

- 1) Central portion of the study area, that is faults associated with Gediz, KMG, BMG, Simav grabens and the transtensional basins (Gördes, Selendi, Demerici, Uşak-Güre basins);
- 2) Gökova Region (southern margin of the study area);
- 3) Fethiye-Burdur Fault Zone;
- 4) İzmir Balıkesir Transfer Zone (IBTZ)

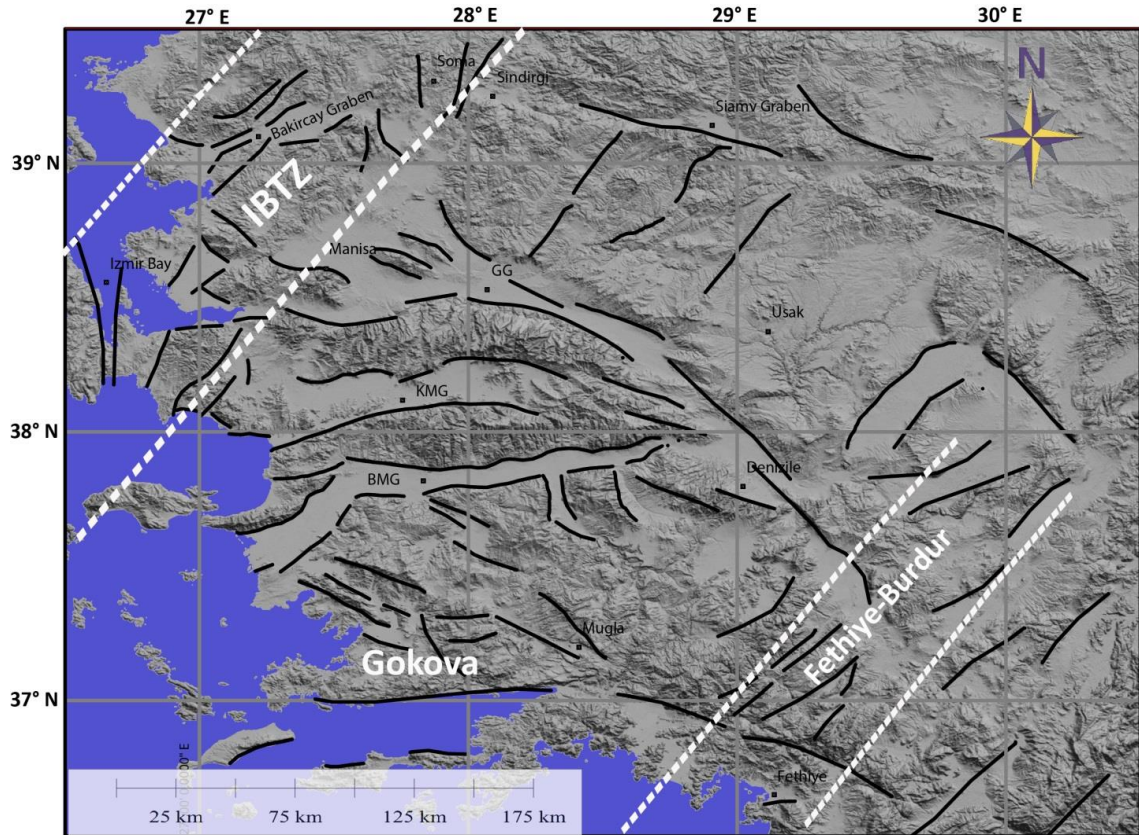


Figure 2.4: Active fault map of the area compiled from MTA (1992); Bozkurt (2000, 2001); Uzel and Sözbilir (2008) and Hall *et al.* (2014). The white dotted lines show the main tectonic sub-divisions proposed for the area.

2.3.1 Central Portion

This portion of the study area is dominated by the extensional grabens (i.e. Küçük Menderes, Büyük Menderes, Gediz and Simav grabens) and their associated bounding faults. The bounding structures of these grabens are low-angle normal faults associated with many historical and recent earthquakes (Ambraseys and Jackson, 1998; Altunel, 1999, Bozkurt, 2004; Koçyiğit, 2005). The transtensional basins (Gördes, Gördes, Demirci, Selendi and Uşak-Güre basins) are supposed to have been formed due to strike-slip faults, where the extension direction is oblique to the margins of the basins (Ersoy *et*

al., 2011). Seismicity associated with these transtensional basin bounding faults is not pronounced as compared to the graben system (McKenzie, 1978; Eydođan and Jackson, 1985).

The faults associated with Gediz Graben, range in size from large graben bounding faults extending to 100 km to small scale faults with only meters of offsets. The faults are segmented, discontinuous and comprise planar and short segments that are marked by coalesced Quaternary alluvial fans (Bozkurt and Sözbilir, 2006). Geological evidence suggests that southern margin forms the most active and intensely deformed part of the Gediz Graben. The fault pattern in Büyük Menderes Graben is similar to that of the Gediz Graben with segmented and discontinuous fault pattern. The difference is that its northern margin bounding fault is more pronounced as compared to its southern margin bounding fault. Zhu *et al.* (2006) reported; based on the moment tensor inversions, two strike-slip faults in western Anatolia that were not reported previously. One of the faults is located near Buldan area and was named Derbent fault; it is a NNW trending strike-slip fault that connects the eastern end of Gediz graben and BMG. The fault is categorized as a transfer fault that accommodates the lateral termination of the E–W-trending grabens. Simav Fault Zone bounds the southern margin of Simav half graben. The E–W- trending fault zone is interpreted as a normal with right-lateral strike-slip component (Seyitođlu, 1997). It is surrounded by other active normal faults trending in WNW–ESE directions. Simav Fault is considered as a segment of the Sındırgı-Sincanlı Fault Zone which is the structural boundary between Aegean extensional and NW Anatolia transition tectonic regimes (Dođan and Emre, 2006).

2.3.2 Gökova Region

Recent studies suggests presence of active normal faults in Gökova region associated with the east-west trending rift system (Şarođlu *et al.*, 1995; Görür *et al.*, 1995; Kurt *et al.*; 1999; Uluđ *et al.*, 1996). These faults cut across each other at some places (Şengör *et al.*, 1984). The rifts are also complicated by short faults that give rise to transversal structures within or between the grabens and work as transfer faults (Şengör, 1987). The

rift system is characterized by normal faults of various sizes, dip and throw. The prominent fault in the area is Gökova fault; which is responsible for the opening of the recent gulf system in western Turkey and forms the northern margin of Gökova Gulf. The faults on the northern margin are larger and continuous as compared to the southern margin of the Gulf which suggests a listric nature. The southern margin of the gulf is bounded by north dipping Datça fault, which is an EW- trending submarine active listric fault associated with other small antithetic faults (Kurt *et al.*, 1999). Detailed bathymetric and seismic surveys have shown a number of younger faults in the gulf region as well (Görür *et al.*, 1995).

2.3.3 Fethiye-Burdur Fault Zone

To the east of the Gökova region, in the southern part of the study area lays the Fethiye-Burdur Fault Zone. The fault zone is one of the tectonically active parts of SW Turkey. Various researchers have regarded it as the eastern extension of the Pliny-Strabo Fault zone (e.g., Woodside *et al.*, 2000; ten Veen, 2004; Hall *et al.*, 2009; Ocakoğlu, 2012; Hall *et al.*, 2014). It runs in a NE–SW direction between the Fethiye Gulf and Sultan Mountains for a length of 300 km with a width of 40 to 50 km (Hall *et al.*, 2014). The fault zone lacks a single major fault at the surface and is composed of various linear, near vertical fault segments trending in NS or NE direction with an oblique sense of normal faults and/or sinistral strike-slip faults, although there are controversies on the mechanism of the fault zone (e.g., Dumont *et al.*, 1979; Eyidoğan and Barka, 1996; Barka *et al.*, 1997; Taymaz *et al.*, 1991; Taymaz and Price, 1992; Koçyiğit *et al.*, 2000; Alçiçek *et al.*, 2006; Hall *et al.*, 2014). The notable structural element of this zone is a WNW–ESE- trending fault zone composed of numerous en-échelon normal faults transecting the basin bounding faults and is referred as Gökova-Yeşilüzümlü Fault Zone.

To the north the Fethiye-Burdur Fault Zone merges with a series of WNW–ESE grabens and their bounding faults (Westaway, 1990; Alçiçek *et al.*, 2006). Dinar Fault is one of the major fault in this zone and caused the October 1st, 1995 ($M= 6.1$) earthquake and is predominantly normal fault with minor strike-slip component (Eyidoğan and Barka,

1996). The earthquake reactivated this fault which was previously supposed to be inactive by Price and Scott (1994). The NW–SE- trending fault is about 60 km long and a 10 km rupture was produced by the 1995 earthquake with ≤ 50 cm vertical movement (Altunel *et al.*, 1999).

2.3.4 İzmir Balıkesir Transfer Zone (IBTZ)

Studies based on GPS measurements shows that the westward escape of Anatolian Plate changes its direction in western Turkey to southwest by an abrupt anticlockwise rotation over the Aegean Trench (McClusky *et al.*, 2000). The axis of this motion is approximately trending N20° E and is characterized by an intermittently active transfer zone between İzmir and Balıkesir (Sözbilir *et al.*, 2003; Erkül *et al.*, 2005) (Figure 2.4). This zone acts as a boundary between the E–W- trending grabens and the north Aegean region and accommodated N–S extension during their formation (Figure 2.5). Based on evidences from paleomagnetic data for the switching of rotation direction from clockwise to anticlockwise in western Anatolia (Kissel and Laj, 1988) and other data from field; Ring *et al.* (1999) named this zone as wrench corridor that accommodates the differential extension rates between the western Anatolia and Aegean region. The southwest Anatolia and Aegean Sea, which are at the southern part of this zone rapidly moves towards the Hellenic trench along the right lateral Tuzla Fault (eastern margin of IBTZ) and left-lateral Pliny-Strabo Fault Zone (Fethiye-Burdur Fault Zone).

The zone is considered as a deep crustal transform fault zone that formed during the late Cretaceous and later acted as a transtensional transfer fault zone during the Neogene (Okay and Siyako, 1993; Okay *et al.*, 1996; Sözbilir *et al.*, 2008, 2011; Uzel and Sözbilir, 2008; Uzel *et al.*, 2012; Özkaymak *et al.*, 2011). The western margin of the zone is characterized by NE- trending Quaternary basins such as the Cumaovası, Bakırçay and Urla basins; the development of these basins are dominated by NE- trending active strike-slip faults. The focal mechanisms of recent earthquakes that occurred in the region indicate that both E–W- trending normal and NE–SW and NW–SE- striking strike-slip faults are active in the region. On the other hand Oçakoğlu *et al.*

(2005) and Zhu *et al.* (2006) suggested a transpressional character for the strike slip faults in the region.

Apart from normal faults associated with the E–W graben systems (i.e. Gediz and BMG, Gökova, Dinar, etc.) observed in western Turkey; the strike-slip faults associated with IBTZ are also capable of generating destructive earthquakes in the area. These faults are reported at the western end of Gediz Graben and KMG in the area surrounding the Karaburun Peninsula and the areas north of it. Similar type of faulting is well documented along the Manisa Fault (Bozkurt and Sözbilir, 2006). Studies based on surface morphology and marine seismic reflection data in the İzmir region (Emre and Barka 2000; Genç *et al.*, 2001 Ocakoğlu *et al.*, 2004; Ocakoğlu *et al.*, 2005; Uzel and Sözbilir, 2005; Uzel and Sözbilir, 2008; Uzel *et al.*, 2012) shows two sets of active faults in the main land and offshore of the area. These are approximately NE–SW- trending strike-slip faults and E–W- trending normal faults. Among them, the prominent ones are the dextral strike-slip Gülbahçe Fault Zone (GFZ), dextral strike-slip Seferihisar Fault Zone (SFZ), dextral strike-slip Orhanlı Fault Zone (OFZ), Karaburun Fault (KF), Urla Fault (UF), Tuzla Fault and İzmir Fault (IF). The Tuzla strike-slip fault zone (TF) is proposed to be extended towards the İznik in the north and towards the Samos Island in the south. Focal mechanism solutions (Tan and Taymaz, 2001) from earthquakes near Doğanbey and the slip measured from the offset of river channels (Emre and Barka, 2000) show a right-lateral slip character for NE–SW- trending Tuzla fault.

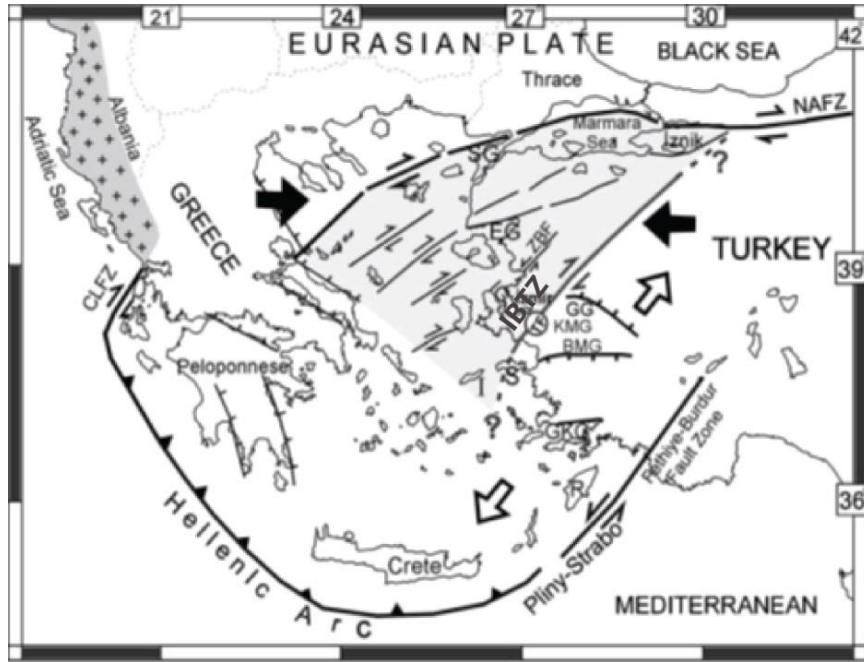


Figure 2.5: Cartoon model proposed for the İzmir Balıkesir Transfer Zone (IBTZ) taken from Ocakoğlu *et al.* (2005). CLFZ: Cephalaria-Lefkada Fault Zone; EG: Edremit Gulf; I: Ikaria Island; IG: İzmir Gulf; GKG: Gökova Graben; NAFZ: North Anatolian Fault Zone; R: Rhodes Island; S: Samos Island; SG: Saros Gulf; ZBF: Zeytindağ-Bergama Fault.

2.4 Seismicity of Western Anatolia

The spatial distribution of seismicity in a region is dependent upon the distribution of active faults. Figures 2.6 show topography, active faults and distribution of seismicity in the region. The figure illustrates that the distribution is not homogeneous throughout the region and that the seismicity being mostly concentrated around the graben bounding faults; the graben floors and horst structures are generally devoid of seismicity. The northwestern portion of the study area that falls in İzmir-Balıkesir Transfer Zone; the southern coastal areas that falls in Gökova region and Fethiye-Burdur Fault Zone are also seismically active. There are some distinct seismically active regions in the study

area that are dominated by different styles of faulting and fall in different tectonic domains. These are Simav, Gediz, Soma, north-western margin (İzmir), Gökova, and Fethiye-Burdur regions.

Simav Graben bounding fault system is located in the northern part of the study area. These faults dominantly have normal character while remaining ones are characterized by right-lateral strike-slip components. This active fault system produced the March 28th 1970 Gediz earthquake ($M_s=7.1$). The seismicity is aligned along the fault trace with a cluster located at the central portion of Simav Graben. This cluster is related to the main shock and associated aftershock sequence of the Simav earthquake of 2011. The seismicity is well pronounced along the fault, thus confirming that the fault is still active.

The eastern margin of Gediz Graben is also one of the most seismically active region in western Anatolia and its bounding fault produced the 28th March 1969 Alaşehir earthquake ($M_s=6.1$). The graben has large bounding faults and seismicity along its southern margin, manifested by earthquakes in the past century (Arpat and Bingöl, 1969; Eyidoğan and Jackson, 1985). The seismicity is further diffused towards east of the Gediz Graben. The region is the junction of faults from the Gediz and BMG Grabens and is dominated by normal faulting.

The north-western part of the study area that coincides with IBTZ is also seismically active. The seismicity in this region is diffused over a large area and the region is characterized by complex tectonics. In the north it extends to the western extent of Simav Graben bounding fault system. The seismicity is diffused over a large area between Soma and Bigadiç and extends offshore in the south to the İzmir Bay. The area is dominated by NE–SW trending strike-slip faults and E–W trending oblique-slip normal faults. The cluster at the western margin of this area (near İzmir) is related to 2005 Gulf of Sığacık earthquake sequence.

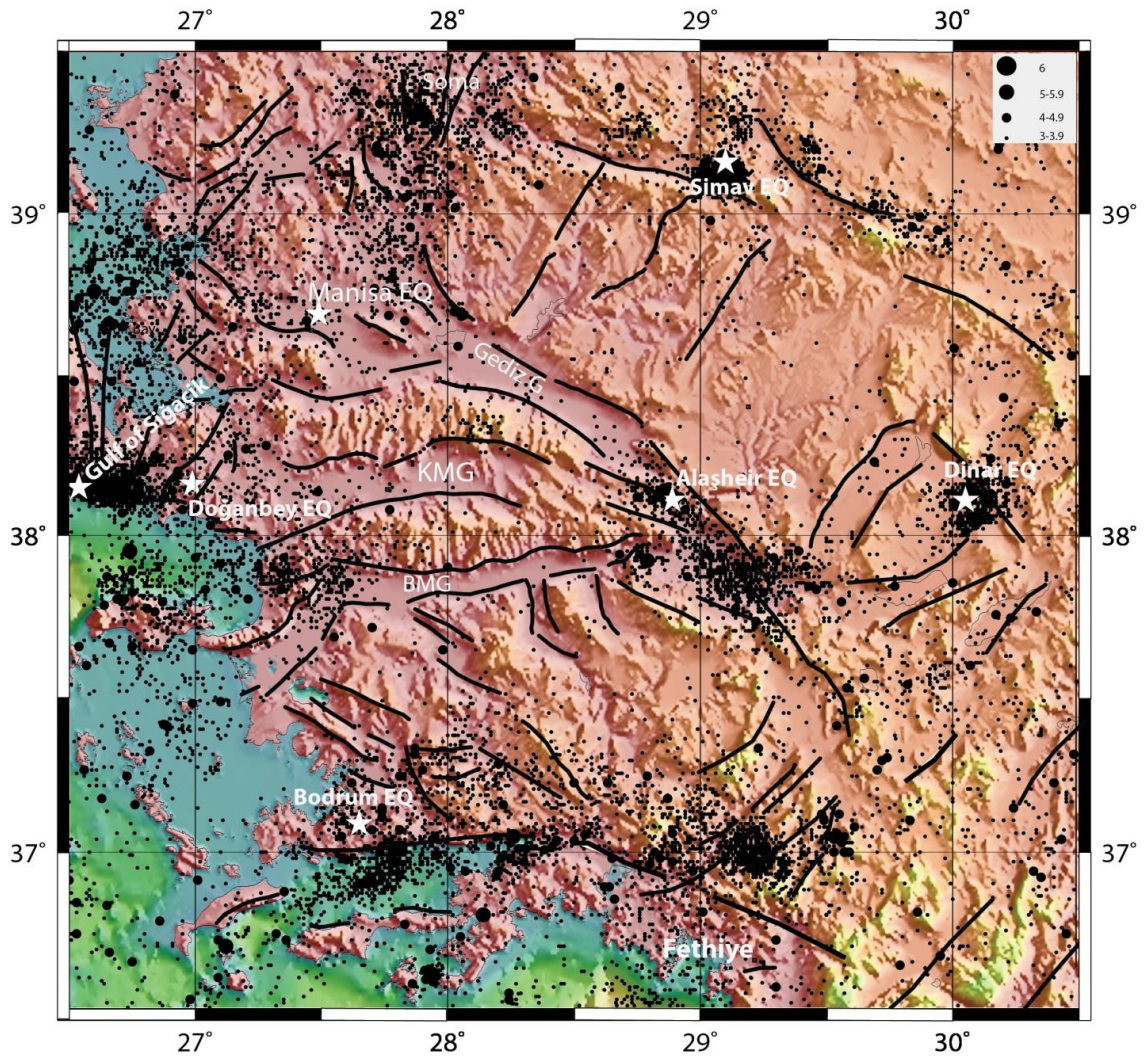


Figure 2.6: Map showing the distribution of seismicity with topography in the study area. The seismic catalogue is obtained from KOERI ($M \geq 3.0$) for the period of 1990-2013. The events are scaled according to their magnitude and the stars show the locations of recent major events in the area.

The southern part of the region is dominated by E–W and NW–SE- trending basins and associated normal faults. The Gulf of Gökova, Muğla-Yatağan and Bodrum are the seismically most active parts of the region. The gulf area is characterized by earthquake clusters that occur for a long period of time. The major events in Gökova region includes the earthquakes of 23 April, 1933 ($M_s= 6.4$), May 23, 1941 ($M_s= 6.0$) and 13 December, 1941 ($M_s= 6.5$) earthquakes.

The seismicity in the south eastern part of the study area is related to the seismically active Fethiye-Burdur Fault Zone. The zone is characterized by a combination of normal faults which have generally left lateral components and extends in NE–SW direction towards the north. The fault zone is one of the tectonically active parts of SW Turkey and is responsible for many historical earthquakes in the region as well as some major earthquakes in this century like Burdur (1914, $M=7.0$), Fethiye (1957, $M=7.1$) and Dinar (1925, $M=6.0$) earthquakes. The cluster east of the Gediz Graben (Figure 2.5) is associated with October 1995, Dinar earthquake that occurred along the NW–SE-trending Dinar Fault.

The earthquake density map (Figure 2.7) shows the pattern of distribution of recent seismicity in the area which is consistent with the geographic distribution of active faults in the region.

The most recent moderate-sized earthquakes that occurred in the area after 1990 are as follows (Figure 2.6). Alaşehir earthquake occurred on July 26, 2003 ($M_l=5.4$, $M_w=5.1$) at east of the Gediz Graben and was preceded by another $M_l=5.2$ event (on 23rd July). Simav earthquake occurred on May 19, 2011, with $M_l=5.9$ near Simav along a normal fault segment of Simav Graben bounding fault system. The earthquake was followed by aftershocks that lasted for months. The epicenter was 40 km west of the epicenter of the magnitude 6.9, 1970, Gediz earthquake. The focal mechanism solution reported for the earthquake and associated aftershocks by KOERI showed a normal fault mechanism for this event. The Gulf of Sığacık earthquake sequence started on 17th October, 2005, with three main events. First event ($M_w=5.4$) occurred on 17 October 2005 (05:45 UTC) at the western end of Gulf of Sığacık, and was followed (09:46 UTC) by an M_w 5.8 event.

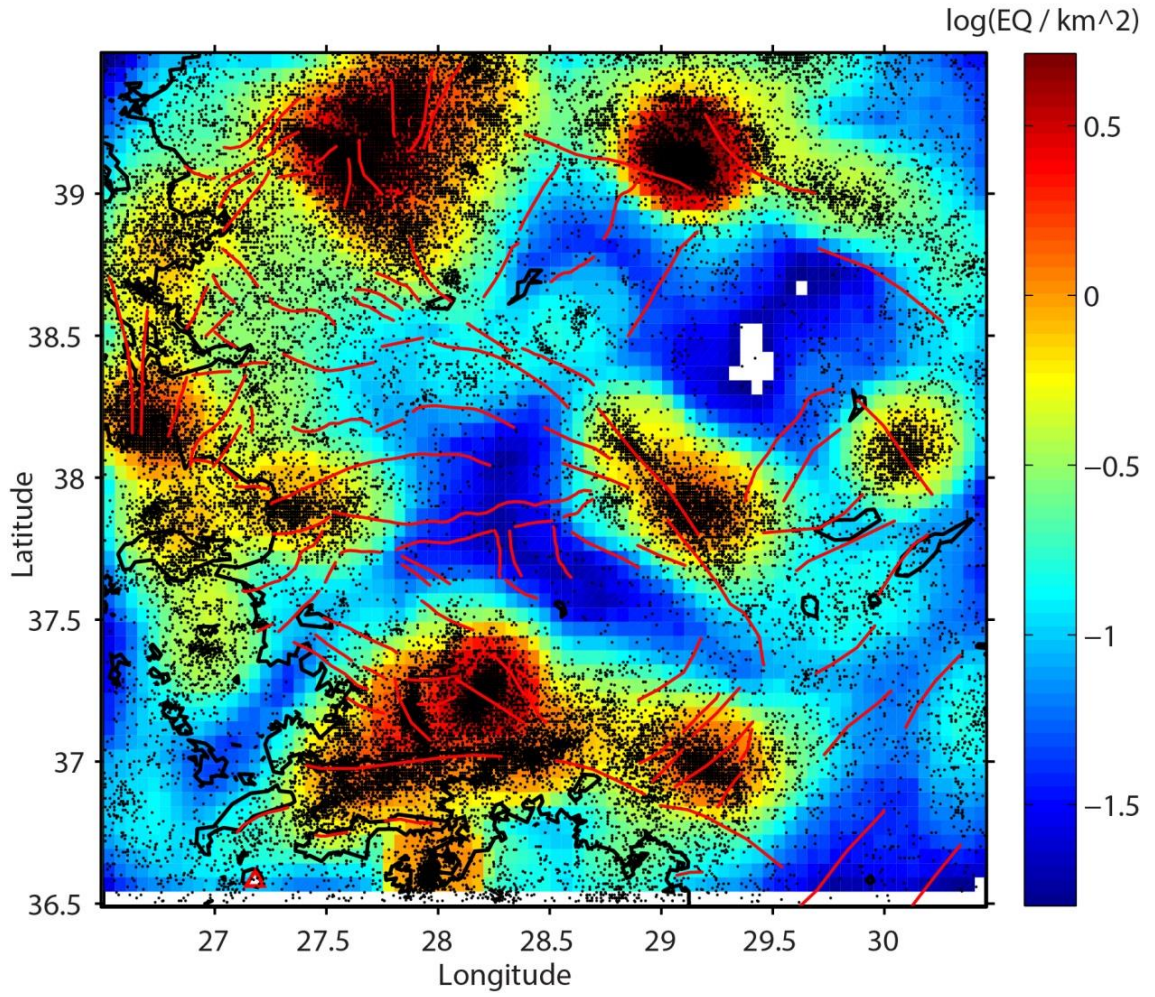


Figure 2.7: Earthquake density map of the area.

Three days later, on 20th October another, M_w 5.8 event occurred along the central part of Sığacık Gulf. A total of 839 earthquakes ($M > 2.4$) were reported from October 17 to 31 by KOERI, with most of them concentrated along the southern part of the Gülbahçe Fault (KOERI, 2005). The focal mechanism solution for the main shocks and associated aftershocks showed a strike-slip mechanism for the sequence (Benetatos *et al.*, 2006). Bodrum Earthquake sequence started on August 2, 2004 with a series of moderate magnitude earthquakes in the Gulf of Gökova. The main event occurred on August 4, 2004 ($M_w = 5.5$). The largest aftershocks occurred on the same day with magnitudes 4.8 and 5.0 and the activity continued for several months. The focal mechanism solution for Bodrum earthquake and its aftershocks showed a normal character for the sequence (Yolsal-Çevikbilen., *et al.*, 2014). Dinar earthquake ($M_s = 6.0$) on 1st of October 1995 along Dinar Fault and had a predominant normal fault mechanism with minor strike slip components (Eyidoğan and Barka, 1996). The earthquake reactivated the fault which was previously supposed to be inactive (Price and Scott, 1994). The NW–SE trending fault is about 60 km long and a 10 km rupture was produced by the 1995 earthquake with ≤ 50 cm vertical movement (Altunel *et al.*, 1999). November 6, 1992 Doğanbey (İzmir) Earthquake ($M_l = 5.7$, $M_s = 6.0$) occurred east of İzmir and showed a strike-slip fault mechanism (Harvard CMT). Manisa earthquake ($M_s = 5.1$) occurred on January 28, 1994 in the western part of Gediz Graben and the focal mechanism solution reported for the main shock is normal fault with a minor strike slip component (Tan and Taymaz, 2003).

CHAPTER 3

SPATIAL AND TEMPORAL VARIATIONS IN FREQUENCY MAGNITUDE DISTRIBUTION OF EARTHQUAKES

3.1 Earthquake Statistics

In any seismic region, at any time, the number of small earthquakes is many folds greater than the larger earthquakes. The logarithmic form of this law was quantified by Gutenberg and Richter in 1944 and is also known as the Frequency Magnitude Distribution (FMD)

$$\text{Log}_{10} N = a - bM$$

where N is the cumulative number of earthquakes greater than or equal to magnitude M, 'b' is the proportion of small earthquakes to large earthquakes and can be calculated from slope of the line and 'a' is the intercept that defines the seismic productivity. The distribution of magnitudes in a region follows this law with some deviations for very small or large earthquakes. For a large area and a long interval of time, the deviations are generally due to incomplete catalogues at both the ends of M. The b-value ranges from 0.6–1.4 and is generally near 1.0 for active regions and in the earth crust. High values show that the region is characterized by a large number of small magnitude earthquakes as compared to large magnitude earthquakes. Variations of b-value from one region to another depend upon the changes in the mechanical characteristics of the region. High b-value shows high heterogeneity, low stress condition, high thermal gradients and vice versa for low values. Seismic swarms characterized by the lack of real main shock due to high heterogeneity in the region, also have a high b-value. Therefore, spatial mapping of b-values also provides a rich source of information on the

seismotectonic framework of an area. But the degree of significance of using this tool alone has been questioned. Normally there is a slow buildup of high stress conditions before major earthquakes in a region with the passage of time. Therefore, changes in b-value through the span of time for the same region can be used as a predicting tool for high magnitude earthquakes. The detection of temporal changes in b-values is difficult to observe as compared to the spatial variations (Wiemer and Wyss, 2002). Magnitude of completeness or 'Mc' is defined as the magnitude above which 100% of all earthquakes can be detected (Stein and Wysession, 2003).

3.2 Data and Processing Techniques

A catalogue downloaded from the KOERI (Kandilli Observatory and Earthquake Research Institute, available at <http://www.koeri.boun.edu.tr/>) is used in this study for the characterization of different seismicity parameters of the study area, which covers the latitude-longitude interval of 36.5–39.5° N and 26.5–30.5° E, respectively. The catalogue covers a time span from 1900 to January, 2014 and has events ranging from magnitude of 0.9 to 7.7. In order to get reliable results, the homogeneity of the catalogue with time and space should be checked. To check the temporal homogeneity of the catalogue, the time histogram and the cumulative number curve of the catalogue is shown in Figure 3.1. It is obvious from the figures that the distribution of the earthquakes is not constant with time. The reason may be because of the lack of the coverage of the area by the seismic networks before 1980s. After 1980 the cumulative number of earthquakes graph is constant with small variations until 1990, this may be probably because of the improved seismic network and computation software used in the recording stations in the area. To avoid any uncertainties in the catalogue, a cut in time is applied to the catalogue at 1990, leaving 53669 events in the catalogue. The cumulative number curve and the time histogram for the catalogue after applying the time cut-off are shown in Figure 3.2. The stars in the cumulative number of earthquake graph and the increase in number of earthquakes in time histogram shows Dinar, Gulf of Sığacık and Simav earthquakes. The depth histogram of the catalogue (Figure 3.3) shows that most of the events are restricted to the upper 40 km of the earth crust. Figure

3.4 shows two representative cross sections (south–north and west–east) of the seismicity of the region. As the data is primarily restricted to the upper crust seismicity, the results obtained from the data will only be applicable to upper crust. For this reason the deeper events are eliminated and the catalogue is restricted to the upper 50 km depth, leaving behind 52642 events in the catalogue.

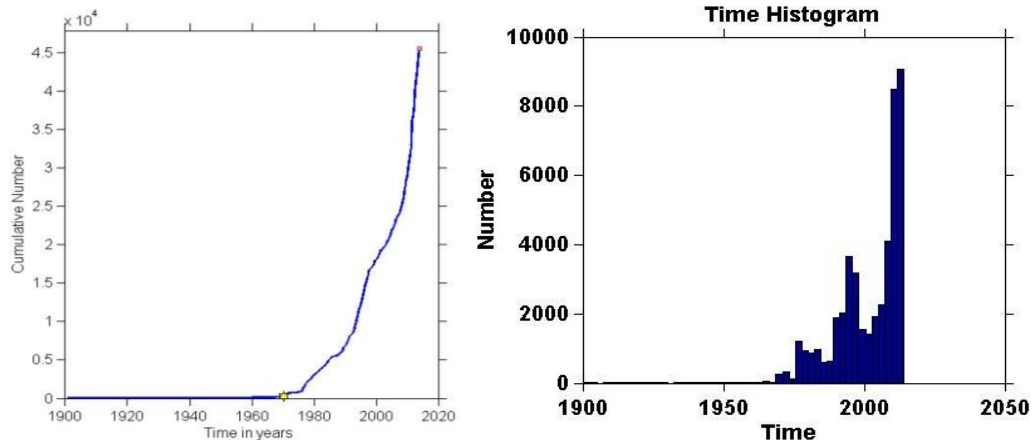


Figure 3.1: Cumulative number of earthquakes vs time of the KOERI catalogue between 1900 and January,2014.

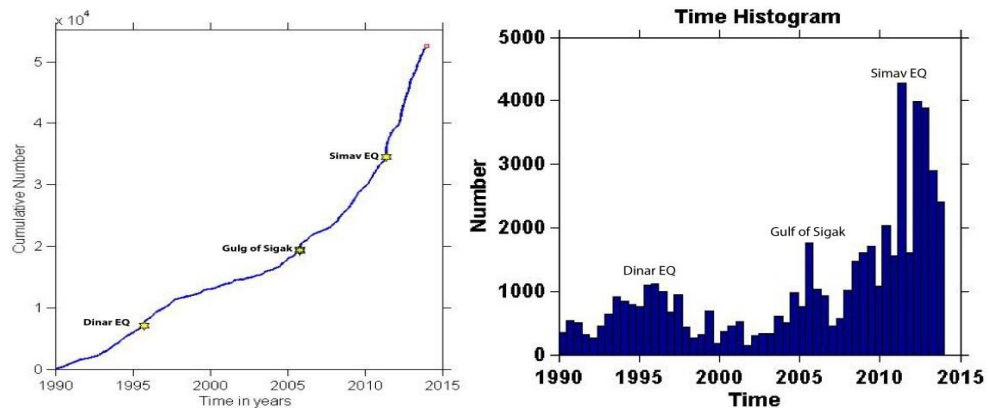


Figure 3.2: Cumulative number of earthquakes vs time of the KOERI catalogue between 1990 and January, 2014.

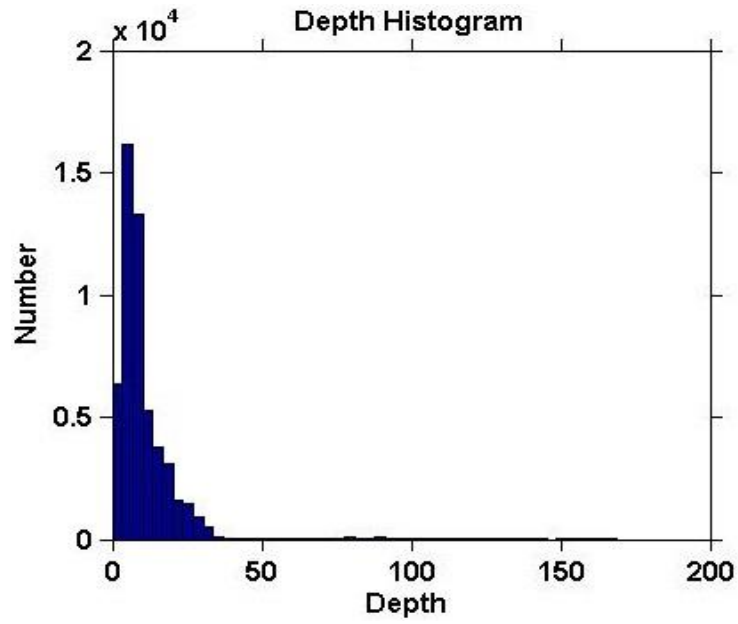


Figure 3.3: Depth histogram of the earthquakes.

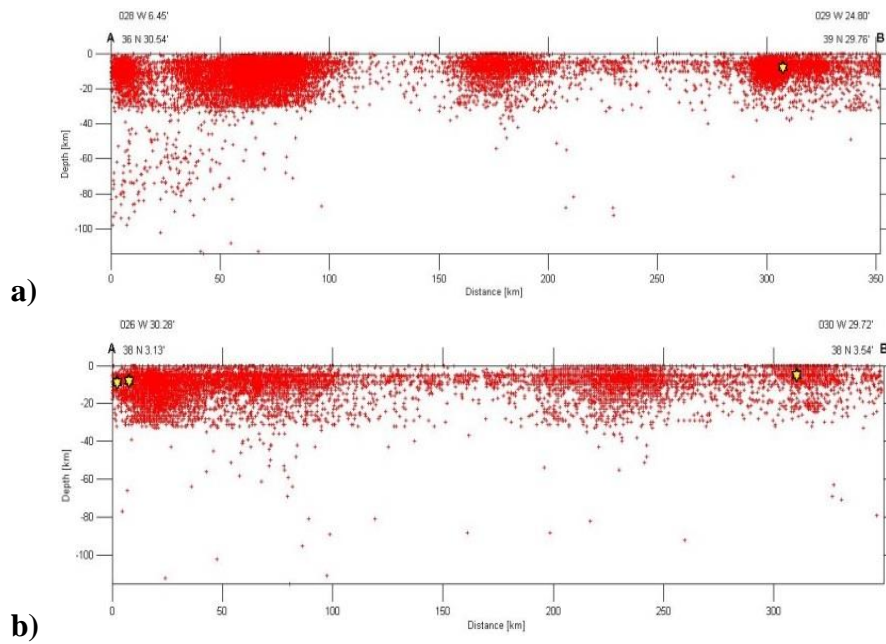


Figure 3.4: a) South to North and b) West to East depth sections of recorded seismicity in the study area.

KOERI provides catalogue with different magnitude ‘M’ scales (i.e. M_d , M_l , M_s , M_b) and provides a M_{max} that can be any of the aforementioned ‘M’ types. The variations in the magnitude scales can cause artifacts in the b-values, so the catalogue should be checked for magnitude homogeneity. For a catalogue to be homogenous it should have a single magnitude type, or if different magnitude scales are used, the magnitudes should be calibrated with each other. A single magnitude type catalogue is not possible in our case because all the events do not have every type of magnitude available for them. The catalogue is checked for the most frequently available ‘M’ type. The catalogue has ‘ M_d ’ for the earlier parts and ‘ M_l ’ is the most frequent type of ‘M’ available after the mid of 2011. So ‘ M_d ’ is used as a primary magnitude type followed by ‘ M_l ’ and for the events that don’t have ‘ M_d ’ or ‘ M_l ’ available, ‘ M_b ’ is used. The catalogue that is used in this study has 71.05% of the events with M_d , 28.88% events with M_l , 35 events (that do not have either M_d or M_l) with ‘ M_b ’ and 1 event has ‘ M_s ’ magnitude. The relationship between ‘ M_d ’ and ‘ M_l ’ is checked for the events that have both ‘ M_d ’ and ‘ M_l ’ available (Figure 3.5).

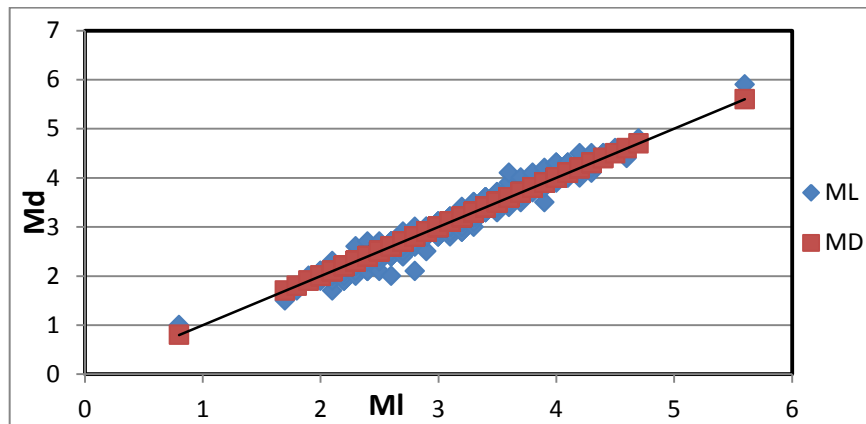


Figure 3.5: Graph showing the relationship between ‘ M_d ’ and ‘ M_l ’. The scatter plot is constructed using the events that have both ‘ M_d ’ and ‘ M_l ’ available in the KOERI catalogue.

The graph shows a linear trend for both the ‘M’ types, so ‘ M_d ’ and ‘ M_l ’ can be used in combination. Figure 3.6 shows the cumulative moment release vs. time curve for the earthquakes in the region. The earthquakes associated with the abrupt changes in the cumulative moment curve are shown in the graph. The most significant changes are associated with the May, 19, 2011 Simav earthquake ($M_w=5.7$) and October 17, 2005 Gulf of Siğacık earthquake sequence ($M_l=5.9$ on 17 and $M_l=5.9$ on 20th of October). Other significant changes are associated with October 1st 1995, Dinar earthquake ($M_s=6.0$) east of the Gediz Graben; 6 November, 1992 Doğanbey (İzmir) earthquake ($M_l=5.7$) in the west of Gediz Graben; January 28, 1994 Manisa earthquake ($M_s=5.1$) in the north western part of the region; July 23 and 26, 2003, Alaşehir earthquakes ($M_l=5.1$ and 5.5) and August 4, 2004 Bodrum (Muğla) earthquake in the southern extremity of the region.

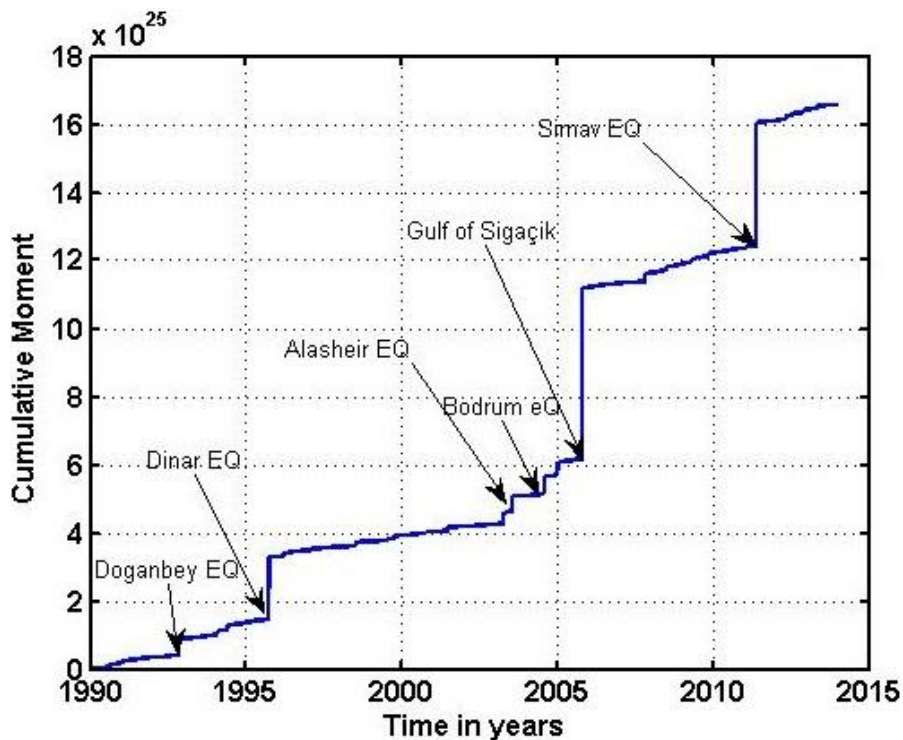


Figure 3.6: Cumulative moment release vs time plot of earthquakes in the study area.

3.2.1 Declustering of the Catalogue

Seismicity declustering is the process of separating the earthquakes into foreshocks, main shock and aftershock sequences or the process of separating the seismicity into independent and dependent seismicity. The process is applied to get the background seismicity of the regions and is widely used for the seismic hazard assessment and in earthquake prediction models. There are many algorithms and methods proposed for the declustering, but the most often used ones include Gardner and Knopoff (1974) and Reasenber (1985) because of their simplicity and availability of their source codes. Gardner and Knopoff (1974) algorithm identifies the foreshocks and aftershocks on the basis of simple space and time window. The space and time window varies according to the magnitude of earthquake. Reasenber (1985) creates an interaction zone to identify the foreshocks and aftershocks. The interaction zone is modeled by spatial and temporal parameters. The spatial parameter is based on physical fault models while the temporal parameter is modeled using a heterogeneous Poisson process with the decay rate of aftershocks determined; using Omori law. These two algorithms (Gardner and Knopoff, 1974; Reasenber, 1985) are applied in this study to the catalogue using ZMAP software package. Reasenber (1985) algorithm identified 2115 clusters in the catalogue, comprising 19198 events, leaving behind 35601 events out of 53609 events. Gardner and Knopoff (1974) algorithm identified 5045 clusters, classifying a total of 41913 events as aftershocks out of 53609 events, leaving 11405 events in the catalogue.

3.2.2 Detection and Removal of Quarry Blast Events

Most of the catalogues are contaminated by quarry blasts and mine explosions. Quarry blasts locations usually shows a high b-value ($b > 1.5$), because they are frequently occurring small events mostly of similar size (Wiemer and Wyss, 2002). Therefore quarry blasts should be mapped and removed from the catalogues, because they are potential source of errors and they falsify the results in statistical studies like b-value and frequency magnitude distribution (e.g., Wiemer and Wyss, 1997). Habermann (1987) proposed that a lower magnitude cutoff can be a solution to explosions removal as they

are associated with low energy. Another solution can be the limitation of the catalogue to only night time events as quarry and mine blasts are usually performed during daytime (e.g., Wiemer and Wyss, 1997). The problem with these solutions is that they lead to loss of a considerable amount of useful tectonic events.

Statistical analysis shows that explosions are generally performed exclusively during the daytime hours (e.g., Rydylek and Sacks, 1989, 1992). Therefore a histogram showing the number of events as a function of hour of the day will have a peak during daytime hours in a region where quarries blasts exist. The detection threshold is generally lower in regions devoid of quarries during the daytime due to the higher ambient noise, so these regions will show an opposite trend (low record during the daytime).

Based on this statistical fact, Wiemer and Baer (2000) proposed an algorithm that identifies and remove the areas with higher (>1.5) day/night time ratios. The software (ZMAP) computes a map of day/night ratio for eight different sample sizes 'N' and consequently converts each value into probability of occurrence. If the value of most significant node exceeds the 99% confidence level, all the daytime events at that node are removed. The method is repeated until no volume with anomalous ratio (>1.5) is left in the catalogue. The removal of all events from that specific volume represents a limit to this procedure because it removes tectonic events too. In order to reduce the number of tectonic events removed by the algorithm, Gaulia (2010) proposed two changes to it: (1) Cutting of the catalogue at an upper magnitude threshold and restricting the quarry removing procedure to that magnitude threshold. (2) Removal of the aftershock sequences using Reasenberg (1985). The criteria used by Wiemer and Bear (2000) to eliminate the aftershock sequence is that no more than 20% of the daytime events occur on one day.

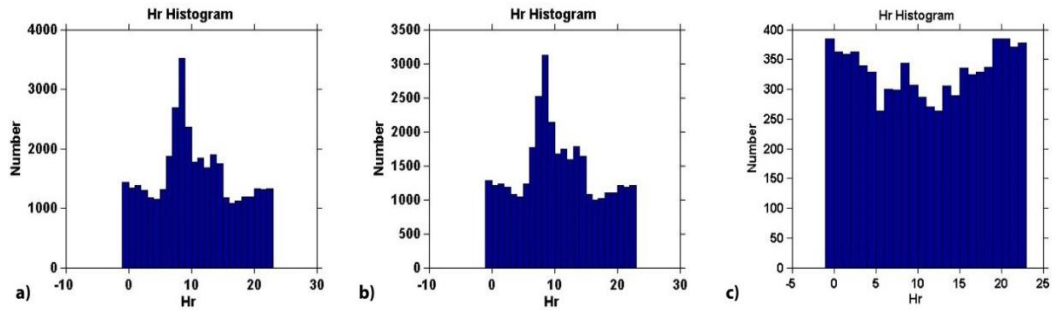


Figure 3.7: Hourly histograms of the seismic events **a)** all recorded events; **b)** only $M \geq 2.0$ events; **c)** only $M \geq 3.0$ events.

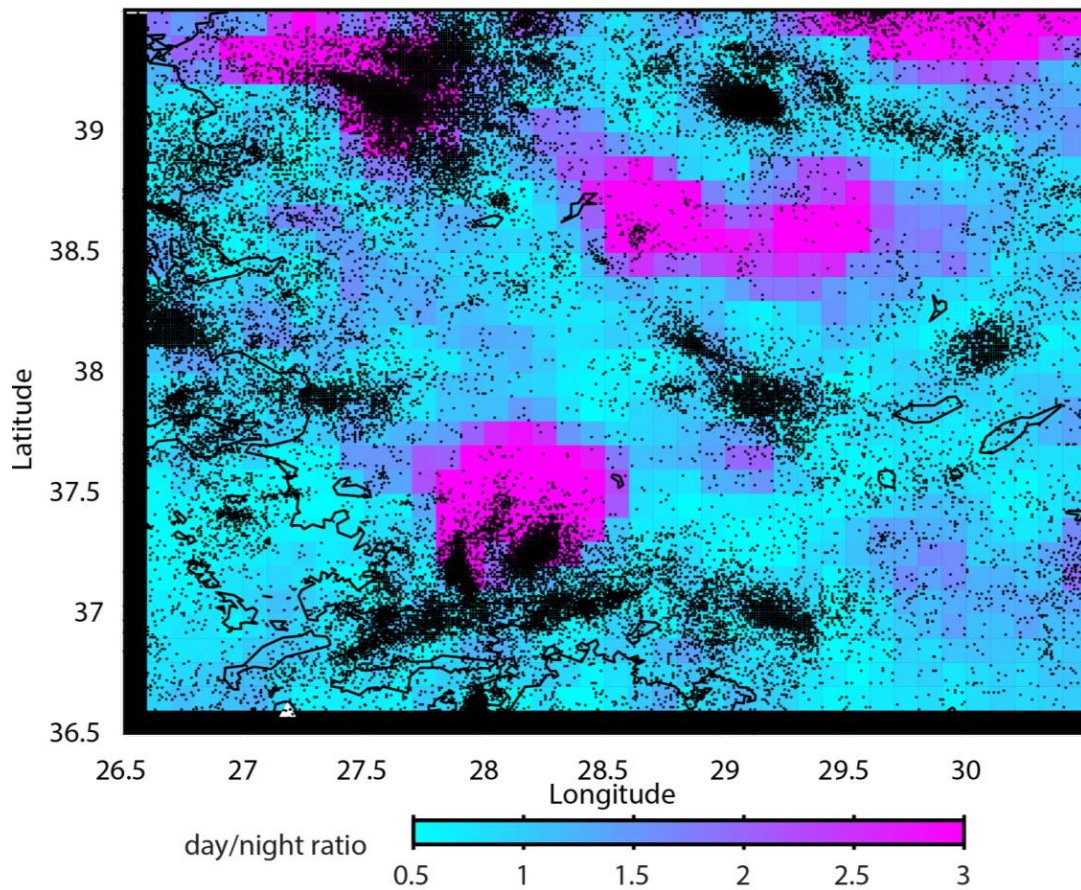


Figure 3.8: Day vs night time events ratio map of the area constructed for earthquakes with $M \leq 3.0$. The areas shown by pink color have a day/night time ratio of ≥ 1.5 and are possible sites of quarry contamination.

The declustered catalogues obtained in the previous section are used to identify quarry locations and their blast events are removed using ZMAP software. The number of events as function of their occurrence hour for the catalogue shows a strong peak during the working hours (7–16hrs), so the data may be contaminated by quarry blast events. The catalogue is checked for the upper magnitude threshold (Figure 3.7). The histograms show that the high ratio (peak in day time) is restricted to the magnitude 3.0; for magnitudes greater than 3.0 the histogram does not follow any trend. It implies that the quarry blast events are restricted to a magnitude threshold of 3.0 in the region. So the catalogue is cut at magnitude 3.0 and a map is produced to identify the possible quarry sites. The map is produced using 100 nearest events to each node and a grid spaced by $0.1^{\circ} \times 0.1^{\circ}$ (Figure 3.8). Four possible sites of quarries are identified in the area. These regions are checked, if they coincide with any mining or quarry locations. The sites identified in the map are

1. North-western part of study area, Soma region: lignite mines
2. North eastern corner of the region, Emet: Boron open pit mines
3. Uşak, central portion: White Onyx quarries
4. Bozdoğan, west of Denizli: marble quarries.

As the sites identified by the map coincide with the quarries and mine locations in the area so the data at these sites is contaminated with quarry blasts. In order to eliminate quarry events from the catalogue, events with magnitude less than or equal to 3.0 in these specified quarry areas are analyzed using algorithm of Wiemer and Baer (2000) to remove day time events. The process is repeated several times and the day vs. night time histogram and ratio map are checked iteratively until the histogram changed to a low number of day time events vs. night time and the ratio map changed to a maximum ratio of 1.5 (Figure 3.9). After removing the quarry blast events, 9105 (out of 11405) are left in the catalogue that was declustered using the Gardner and Knopoff (1974) algorithm and 25623 events (out of 35601) are left in the catalogue that was declustered using Reasenberg (1985) algorithm.

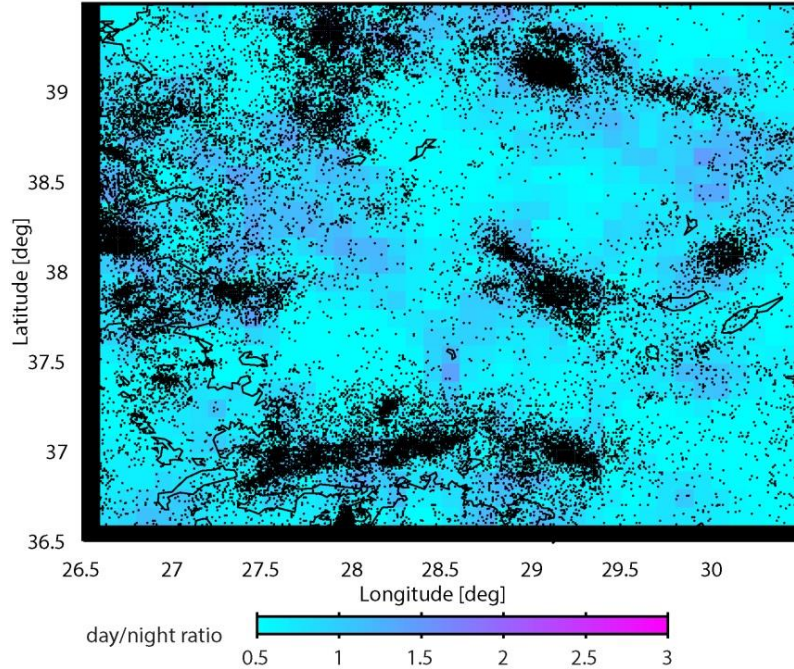


Figure 3.9: Day vs night time events ratio map after removing the quarry blast events constructed for earthquakes with $M \leq 3.0$.

3.3 Frequency Magnitude Distribution of Earthquakes in the Study Area

After applying all the aforementioned processing techniques (i.e. cut in time and depth, magnitude homogeneity, declustering and removing of quarry blast events), a nearly homogeneous catalogue is obtained for the area. The catalogue can be used for assessing the frequency magnitude distribution (FMD) relation and for analyzing the spatial and temporal variations of b-values in the area.

The FMD plots for the area are obtained using the processed and unprocessed (original) catalogues using ZMAP software (Figure 3.10) to check whether the processing techniques has any impact on the results. These plots are computed using the Maximum Likelihood Estimate (MLE) method. The b- and a- value obtained for the whole region using the unprocessed catalogue are 1.35 and 8.15 respectively, while for the catalogue from which the quarry events are removed these values are 1.45 and 8.45 respectively.

The b- and a- values obtained for the whole region, after applying Reasenberg (1985) algorithm to the catalogue and subsequently removing the quarry blast events, are 1.39 and 8.16 respectively. On the other hand the catalogue obtained after applying Gardner and Knopoff (1974) algorithm and quarry removal technique, gives b- and a- values; 1.26 and 7.42 respectively.

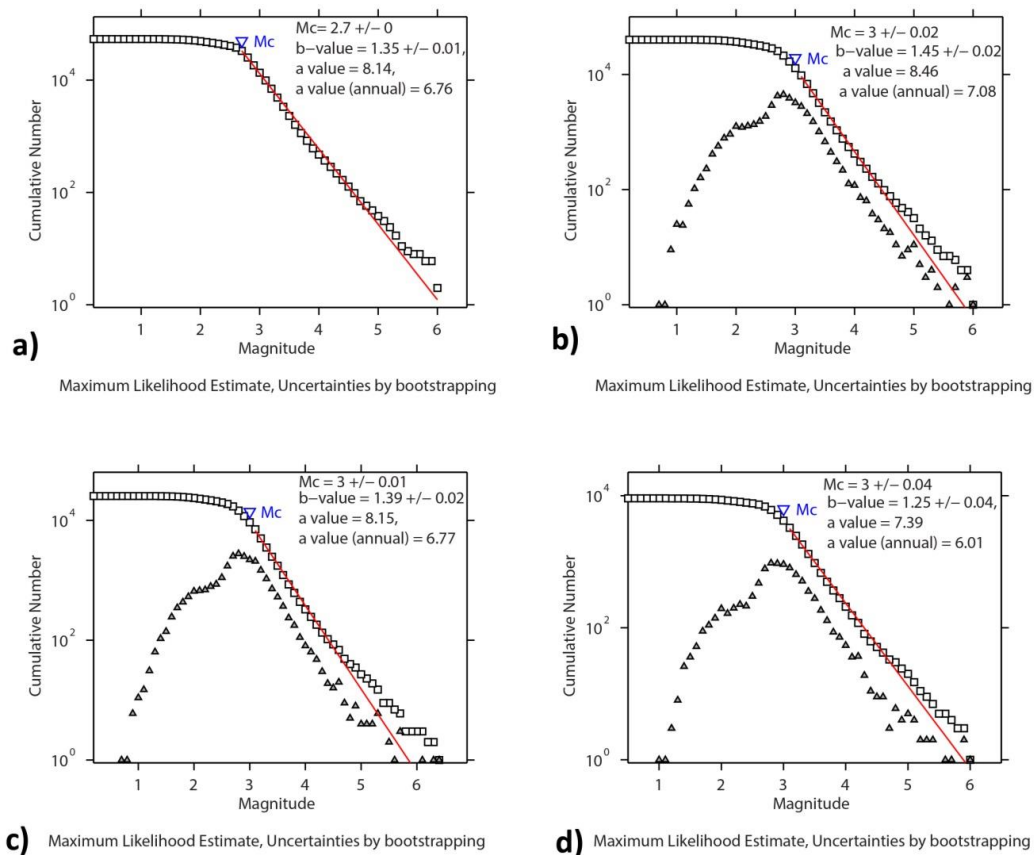


Figure 3.10: Frequency magnitude distribution (FMD) plots of the study area (1990-January 2014). **a)** FMD plot of the unprocessed catalogue; **b)** FMD plot of the quarry free catalogue (no declustering algorithm applied); **c)** FMD plot after applying Reasenberg (1985) declustering algorithm and subsequently removing quarry events and **d)** FMD plot after applying Gardner and Knopoff (1974) declustering algorithm and subsequently removing quarry events.

3.3.1 Spatial Variations of b-value

The b-value of frequency magnitude distribution gives a relative measure of small earthquakes to large earthquakes within a specified region and time, and hence provides a depictive image of seismicity, seismotectonics, stress conditions and seismic hazard potential of an area. Researchers believe that b-value exhibits significant temporal and spatial variations. On local scale, b-value has been reported to show considerable variations on a range of 0.3 to 2.5 or more (e.g., Scholz, 1968; Wiemer *et al.*, 1998; Jaume and Sykes, 1999 and many others). In order to get an idea of the spatial variation of b-value and their associations with local conditions in our study area, the b-value maps of the region are constructed in this study.

The maps are constructed using ZMAP software package (Wiemer, 2001). The software estimates the b-value at each node of densely spaced grid using either the 'N' number of earthquakes or a constant radius 'R'. The sampling volumes are vertically oriented cylinders which overlap and their sizes are inversely proportional to the density of earthquakes enclosed in them. The b-value calculated at each node is converted into a color code and plotted on the map. The maps in this study are constructed using maximum likelihood estimate (MLE) method and magnitude of completeness (M_c) is computed using Best Combination Method (M_{c95} - M_{c90} -Maximumcurvature). Earthquakes epicenters are selected using a radius 'R' of 20 km and the grid spacing is 0.05° (~ 5 km) and the minimum number of earthquakes that should be greater than M_c is 20.

b-value maps are constructed using the original (unprocessed catalogue including the quarry blast events and aftershock sequences) and the processed (quarry blast events and aftershock sequences removed) catalogues. The purpose of constructing the b-value maps with the unprocessed catalogue and processed catalogue is to check whether the spatial variations of b-value are related to tectonic complexities in the region or are associated with the artifacts in the catalogue (i.e. quarry events or aftershocks). Figure 3.11 show the map constructed using the original (unprocessed) catalogue. The b-values in this map are relatively higher and have anomalous regions; whose b-values are above 2.5. These anomalous regions coincide with the quarry contamination sites identified in

the area. These regions show comparatively low b-value after removing the quarry blast events from the catalogue (Figure 3.12). The maps obtained from the de-quarried and de-clustered catalogue (Figures 3.13 and 3.14) gives more realistic b- values for the seismically active parts of the region. The areas that are devoid of minimum number of earthquakes (i.e. 100 events) are not assigned by any b-values. These blank regions generally coincide with the grabens and basins, which display lack of seismicity. The greater the number of events in a grid, the more reliable will be the b-value results and vice versa. Some grids are characterized by high b-values (>2.0), which may be due to small number of events leading to erroneous interpretations.

According to the resultant b-value maps (Figures 3.13 and 3.14), Samos Island and NE-SW- trending area between Marmaris and Köyceğiz have the lowest b-values indicating that stress is efficiently stored in the regions. The most prominent high b-value regions identified in the study area are along Bakırçay Graben and between İzmir and Manisa. High b- values shows that stress is being released more frequently in the form of small earthquakes in these regions. The reason for high b-values in these regions may be due to low local stress conditions and high geothermal gradients. Temperature distribution within the upper crust has considerable impacts on the seismicity distribution of a region. Areas characterized by high geothermal gradients, volcanic activities and hot springs have elevated b-values (Wiemer and Wyss, 2002; Wyss, 1997; Warren and Latham, 1970 and many others). Due to crustal stretching in western Anatolian region caused by the graben system; the region is characterized by comparatively high thermal gradients and constitutes one of the most important geothermal region of Turkey. The heat flow map of western Turkey and the hot springs locations within the study area are shown in Figure 3.15 (taken from Akin *et al.*, 2014). The comparison of b-value and heat flow maps indicates that the high b-value areas identified in the region are roughly coinciding with the locations characterized by high heat flow; thus confirming the observation that areas marked by high geothermal gradients are characterized by elevated b-values.

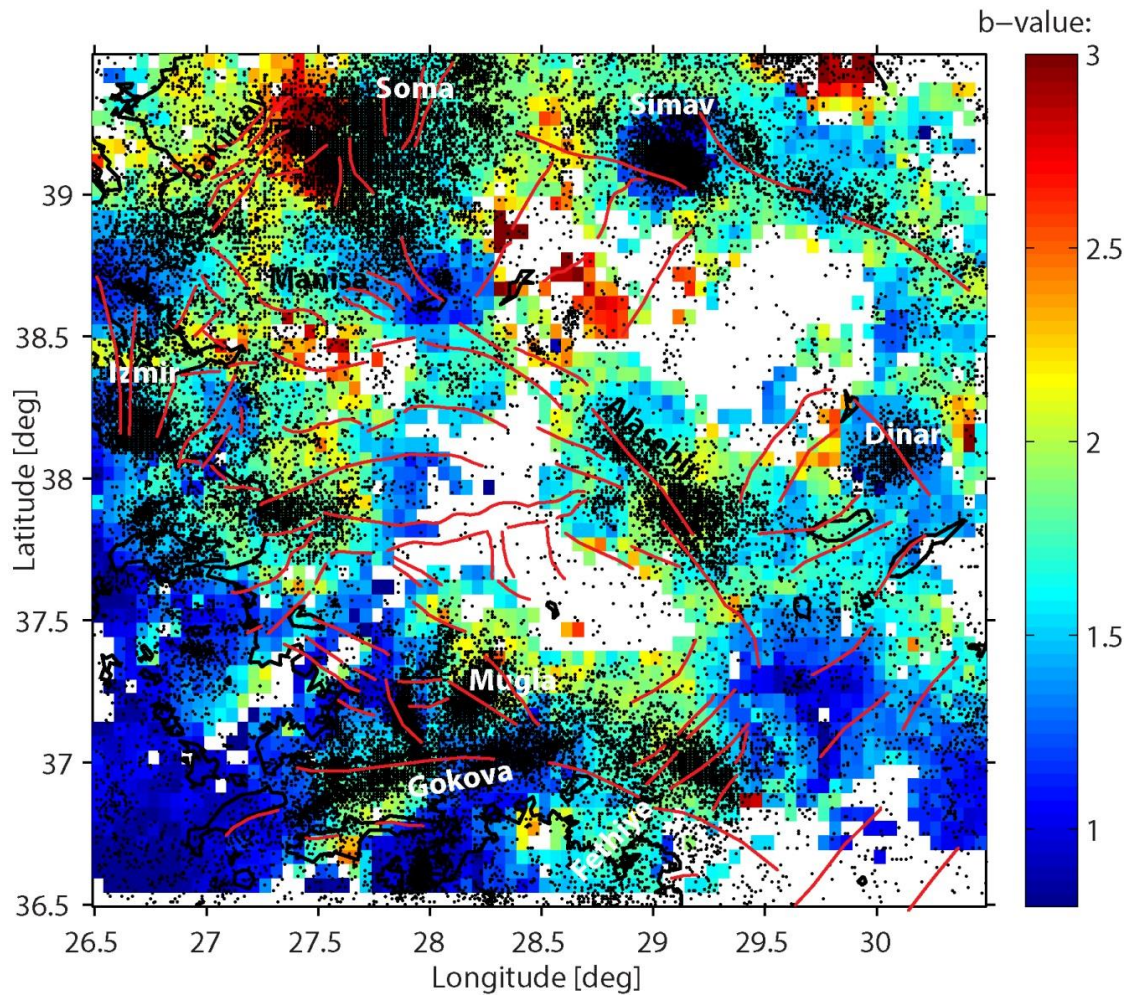


Figure 3.11: Map showing the spatial variations in b-values for the area. The map is constructed using the unprocessed catalogue downloaded from KOERI (1990-January 2014). The catalogue includes the quarry blast events and aftershock sequences associated with the major events.

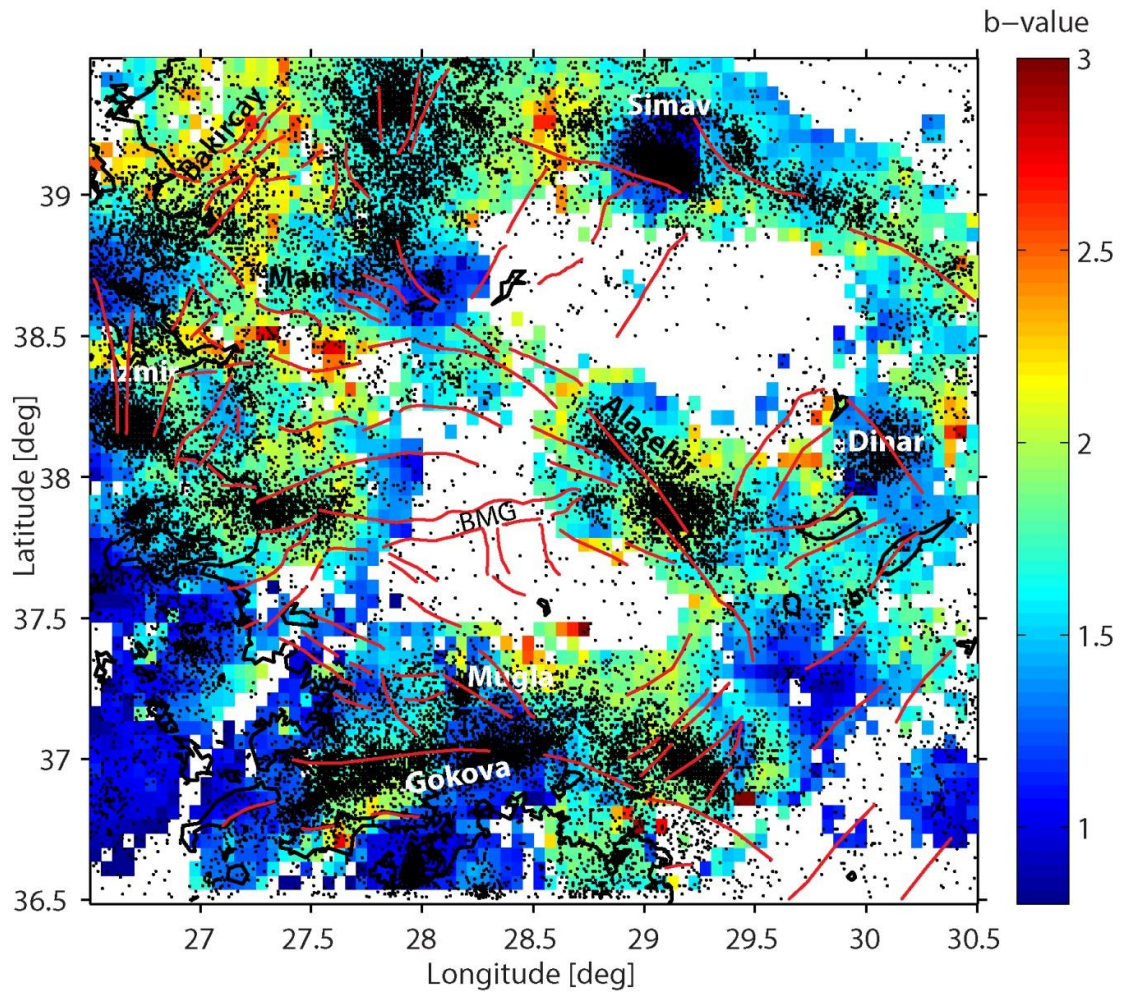


Figure 3.12: Map showing the spatial variations in b-values for the area. The map is constructed using the catalogue that is free of quarry blast events (1990- January 2014). The catalogue includes the foreshocks and aftershock sequences associated with the major events.

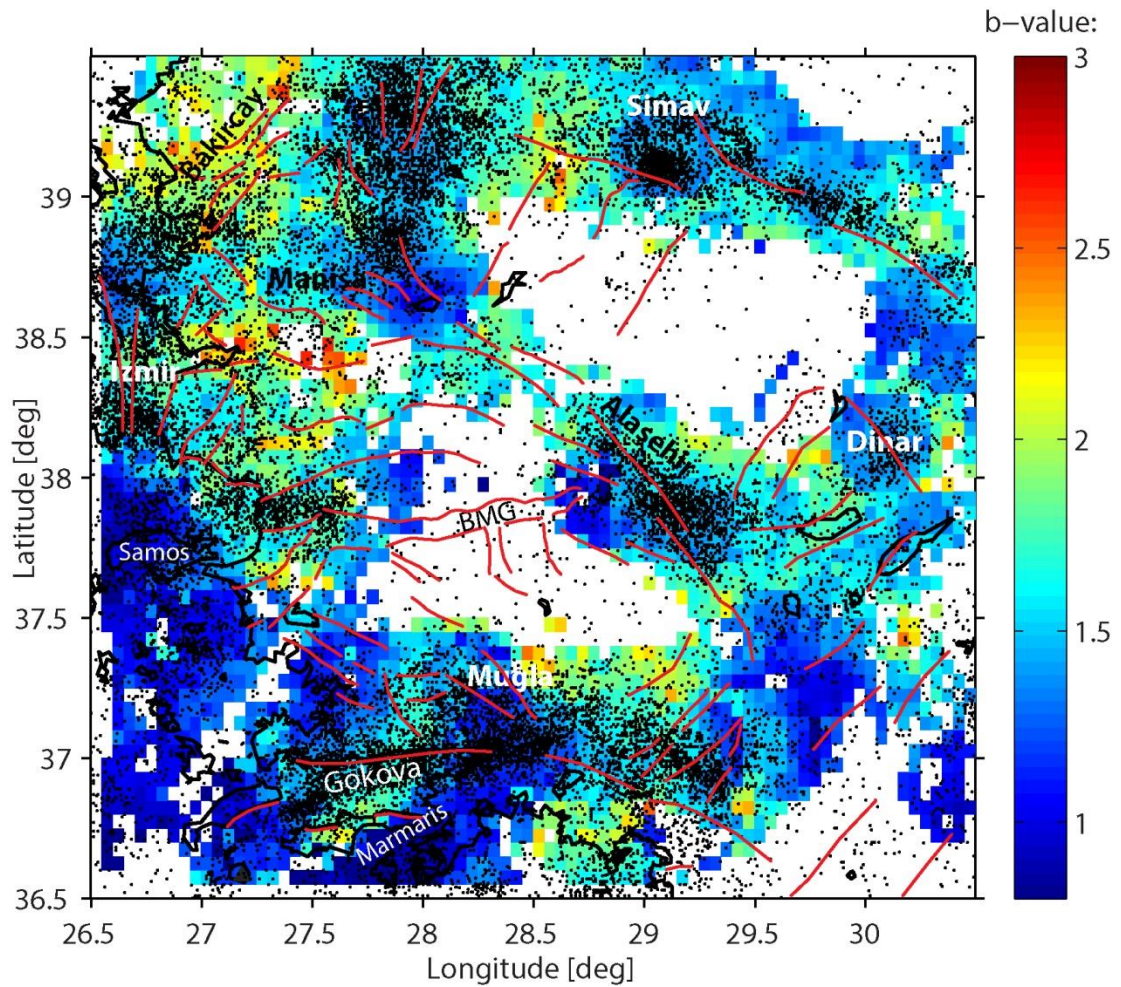


Figure 3.13: Map showing the spatial variations in b-value for the study area. The map is constructed using the declustered (Reasenberg, 1985) and quarry free catalogue. The catalogue does not include any quarry blast events and or aftershock sequences associated with the major events.

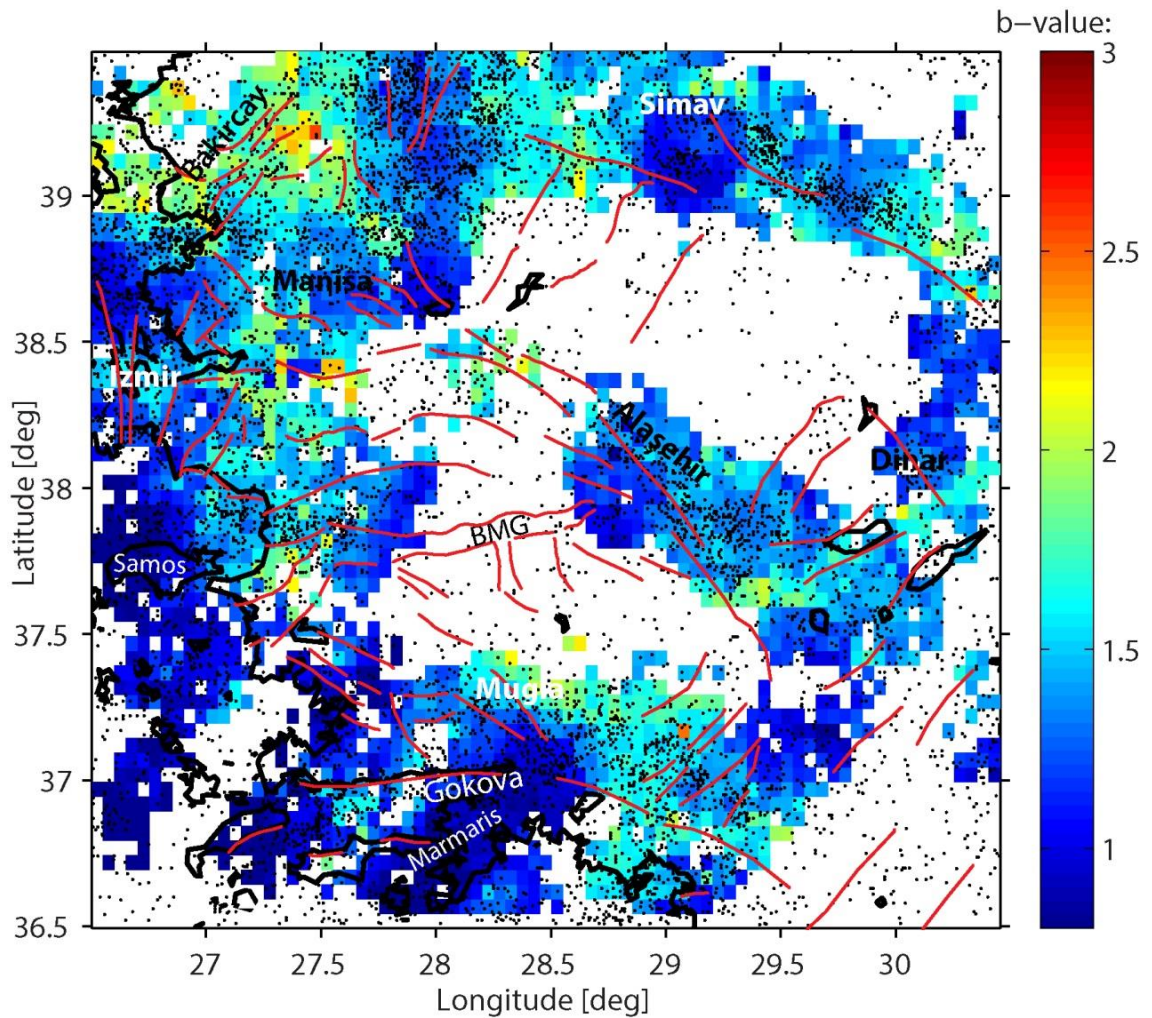


Figure 3.14: Map showing the spatial variations in b-value for the study area. The map is constructed using the declustered (Gardner & Knopoff, 1974) and quarry free catalogue. The catalogue does not include any quarry blast events and or aftershock sequences associated with the major events.

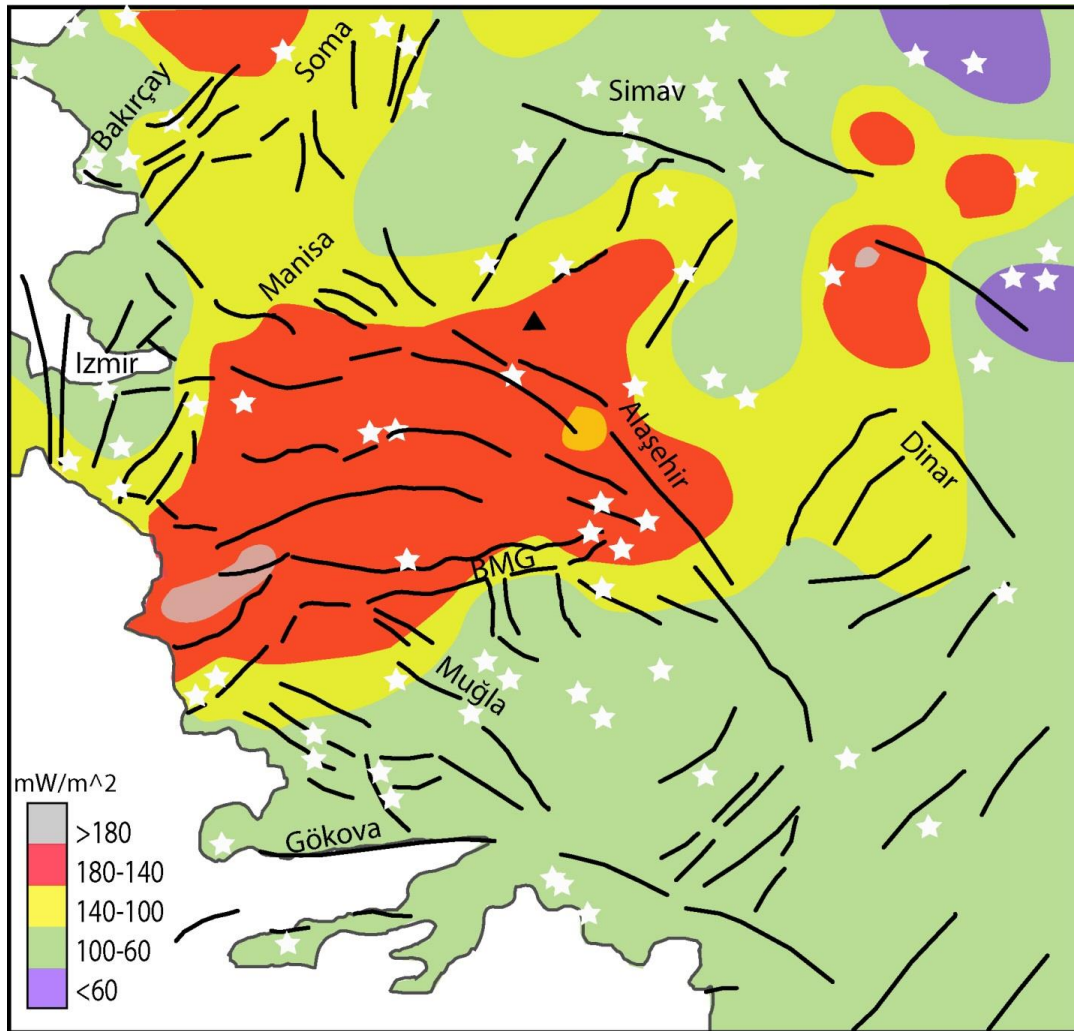


Figure 3.15: Heat flow map of western Anatolia modified from heat flow map of Turkey (Akm *et al.*, 2014). The locations of hot springs are shown as white stars (from Yolsal *et al.*, 2005) and the location of Quaternary Kula volcanism is shown with a black triangle. The active faults in the area are also shown with black lines.

3.3.2 Temporal Variations of b-value

As mentioned earlier that b-value shows temporal variations with time on local scale within an area and specified time, so an attempt is made here to detect any changes in b-value associated with major earthquakes. Temporal variations in b-values show the variations in stress conditions within a region through time. Studies suggest that temporal variations are of second order compared to the spatial variations and are generally more difficult to observe as compared to the spatial variations and the results should be interpreted with caution (e.g., Wiemer and Wyss, 1997, 2002; Wiemer *et al.*, 1998).

The b-value versus time graph has been checked for the whole region using the original (unprocessed) and the processed catalogues (quarry free and declustered) to observe changes in b-values with time. ZMAP software computes the variation of b-values through time, using a sliding time window approach. The size of window depends on the number of events in the catalogue. The number of events selected in sample window for unprocessed catalogue is 700 events. For the catalogues declustered by Reasenberg (1985) and Gardner & Knopoff (1974) algorithms; this number is 600 and 400, respectively. The results obtained are shown in Figure 3.16.

The original (unprocessed) catalogue has aftershocks events, so the plot shows many abrupt changes in b-value with time associated to recent major earthquakes. The catalogue declustered using Reasenberg algorithm has more events (25623 events) as compared to the Gardner and Knopoff (9105 events); therefore the latter gives a relatively smooth plot. The high frequency changes in the plots are related to the stress changes associated with the major events (Doğanbey, Gulf of Sığacık, Dinar and Simav earthquakes) occurred in the study area. There is also a remarkable decreasing trend in b-value between 2011 and 2013 which may be related to the changes in seismic network configuration and recording procedures.

In order to further investigate the temporal and spatial changes associated with major earthquakes in the region, the b-value maps have been checked for the pre- and post-event scenario of some recent major events. The events that are analyzed include;

Alaşehir (Denizli) earthquake, Dinar earthquake, Gulf of Sığacık earthquake sequence and Simav earthquake. For this purpose the quarry free catalogue including aftershocks and foreshock events (no declustering applied) is used.

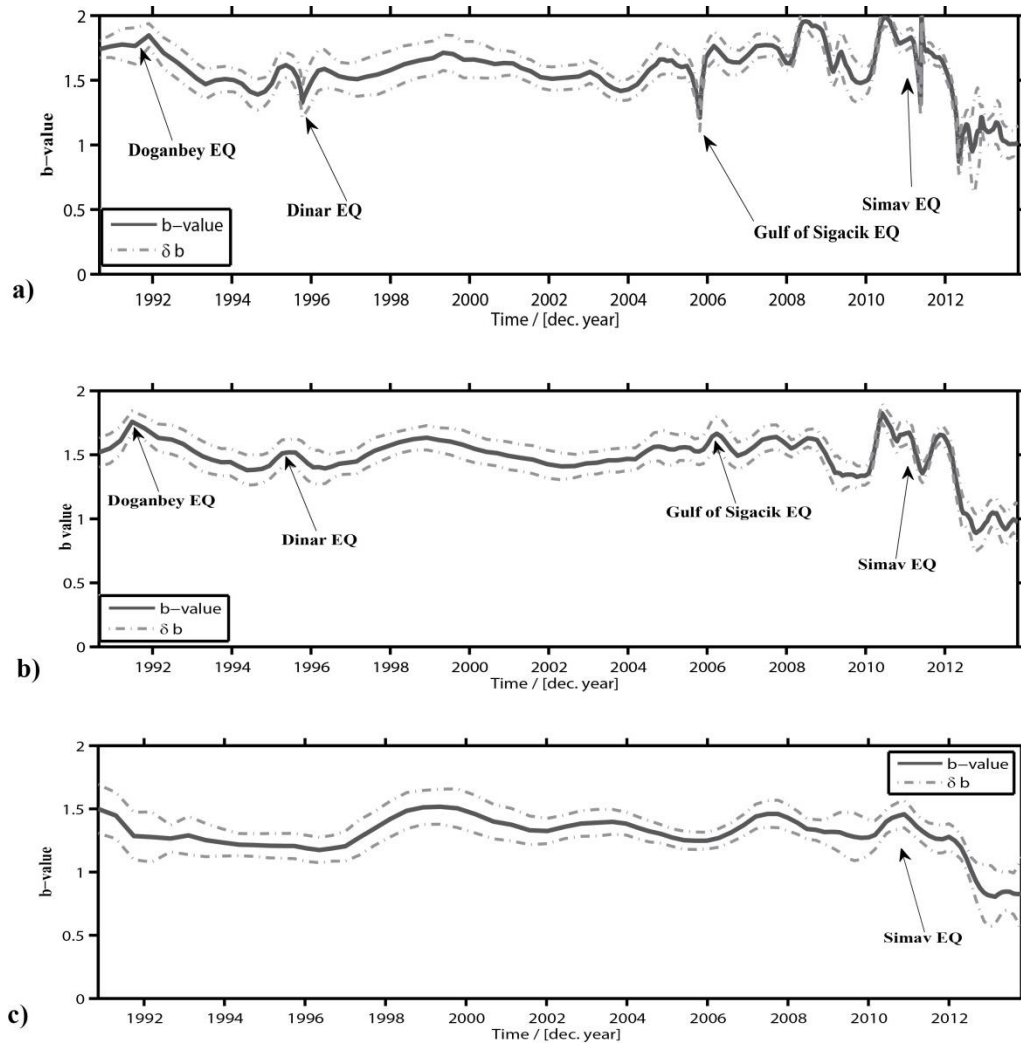


Figure 3.16: b-value against time for the whole study area. **a)** unprocessed catalogue; **b)** quarry free catalogue declustered using Reasenberg (1985) and **c)** quarry free catalogue declustered using Gardner and Knopoff (1974).

For constructing the b-value maps, the catalogue has been separated for the events using a polygon around the occurrence site of main-shocks. The catalogue is then divided into pre- and post- earthquake time domains, by cutting the catalogue at the time of main event. The b-value maps have been computed using the Best Combination Method (Mc95-Mc90-Maximum curvature) in ZMAP software. The maps are computed using a radius of 10 km and the grid has been spaced by $0.02^\circ \times 0.02^\circ$. The minimum number of events, greater than the magnitude of completeness (M_c), is taken as 10. The earthquake magnitude and b-value versus time plots for each event is also shown to correlate the time distribution of magnitude and b-value changes.

The pre- and post- Alaşehir (Denizli) earthquake b-value map is shown in Figures 3.17a and 3.17b, respectively. The Figure illustrates that the b-value around the location of the Alaşehir earthquake was 1.0–1.3 before the main shock that changed to a higher value of 1.3–1.7 after the event. Elevated b-values around the epicenter support the effective release of stress during this earthquake. The changes in b-values in other parts of the mapped area are related to small events ($M < 5.0$) occurred within used time periods. The magnitude time plot (Figure 3.17c) shows that the magnitude mostly varies between 3.0 and 4.0 through time, except for Alaşehir earthquake and another event with magnitude 5.0 that occurred in 2010. For b-value with time plot (Figure 3.17d); 30 events per window are selected. The plot shows that b-value has varied throughout the time span. b-value is decreased in the region just before the occurrence of main-shock, indicating a build-up of stress in the region before the earthquake which is followed by a characteristic increase in b-value after the mainshock associated to the released tectonic stresses (Figure 3.17e)

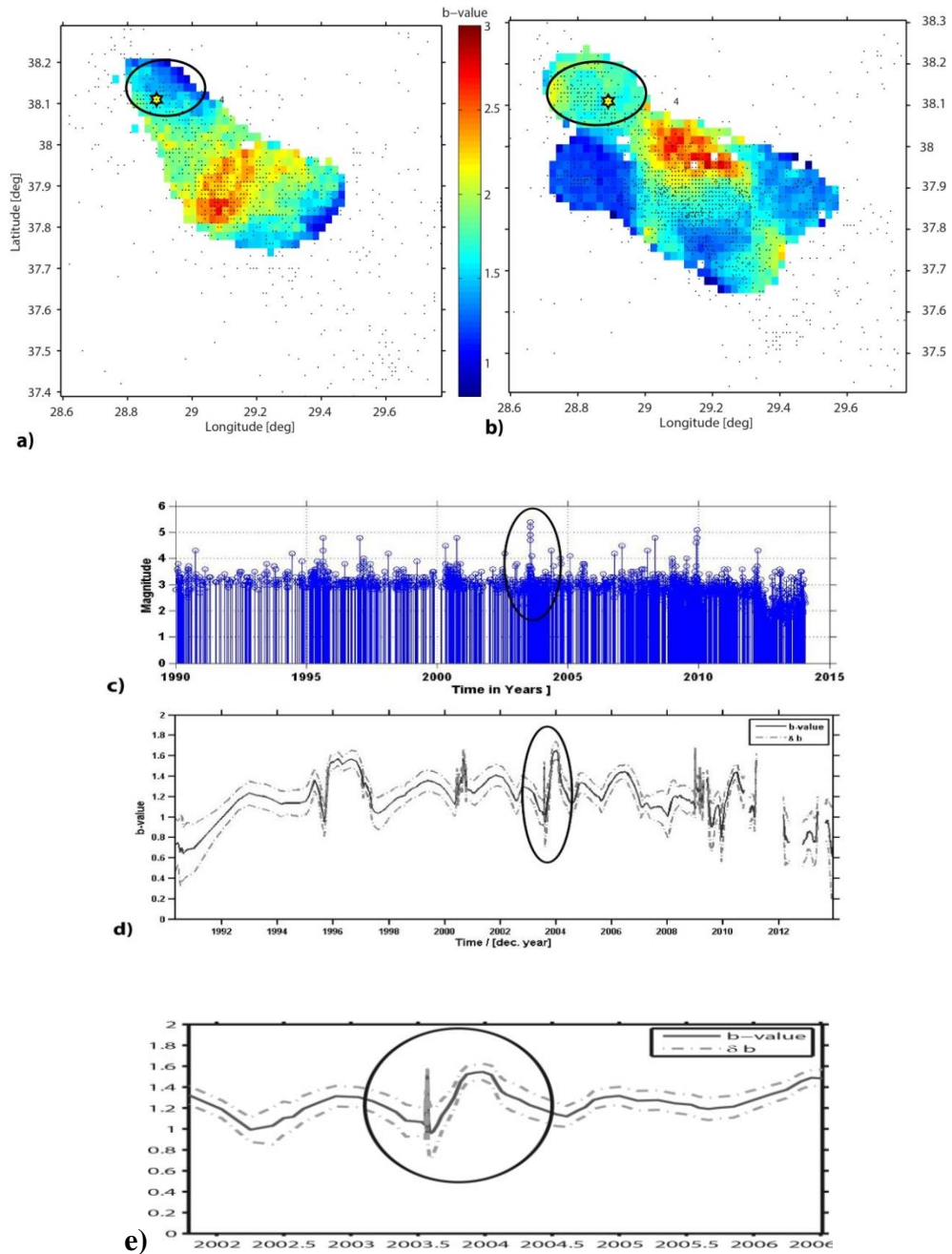


Figure 3.17: **a)** Pre Alaşehir earthquake b-value map; **b)** post Alaşehir earthquake b-value map (circular area shows the rupture area characterized by aftershocks where the value is increased); **c)** magnitude vs time plot of Alaşehir; **d)** b-value vs time plot of Alaşehir and **e)** zoomed in section of the b-value vs time plot.

Due to lack of recorded seismicity before Dinar and Gulf of Sığacık earthquakes, only post mainshock b-value maps are constructed. The b-value around the epicenter of Dinar earthquake is ~ 1.3 – 1.7 (Figure 3.18a), while the Gulf of Sığacık earthquake sequence has a b-value range of ~ 1.0 – 1.7 (Figure 3.19a). Both the events show high b-values around the epicenter of main event, because of the release of stresses. The b-value at the epicenter location (shown by star) of Gulf of Sığacık is a bit low ~ 1.1 as compared to Dinar earthquake epicenter. The magnitude time plot for both the events shows a small duration increase in the number of events after the mainshocks (Figures 3.18b and 3.19b). The b-value with time plot for both the events has been constructed using 15 and 25 events per window respectively. Both the plots show an abrupt change in b-value at the time of main shocks (Figures 3.18c and 3.19c). The pattern of b-value variations is almost the same in both the events i.e. a small scale decrease before the main event, followed by an abrupt increase at the time of main event and the return to its normal value after a short period of time (Figures 3.18d and 3.19d).

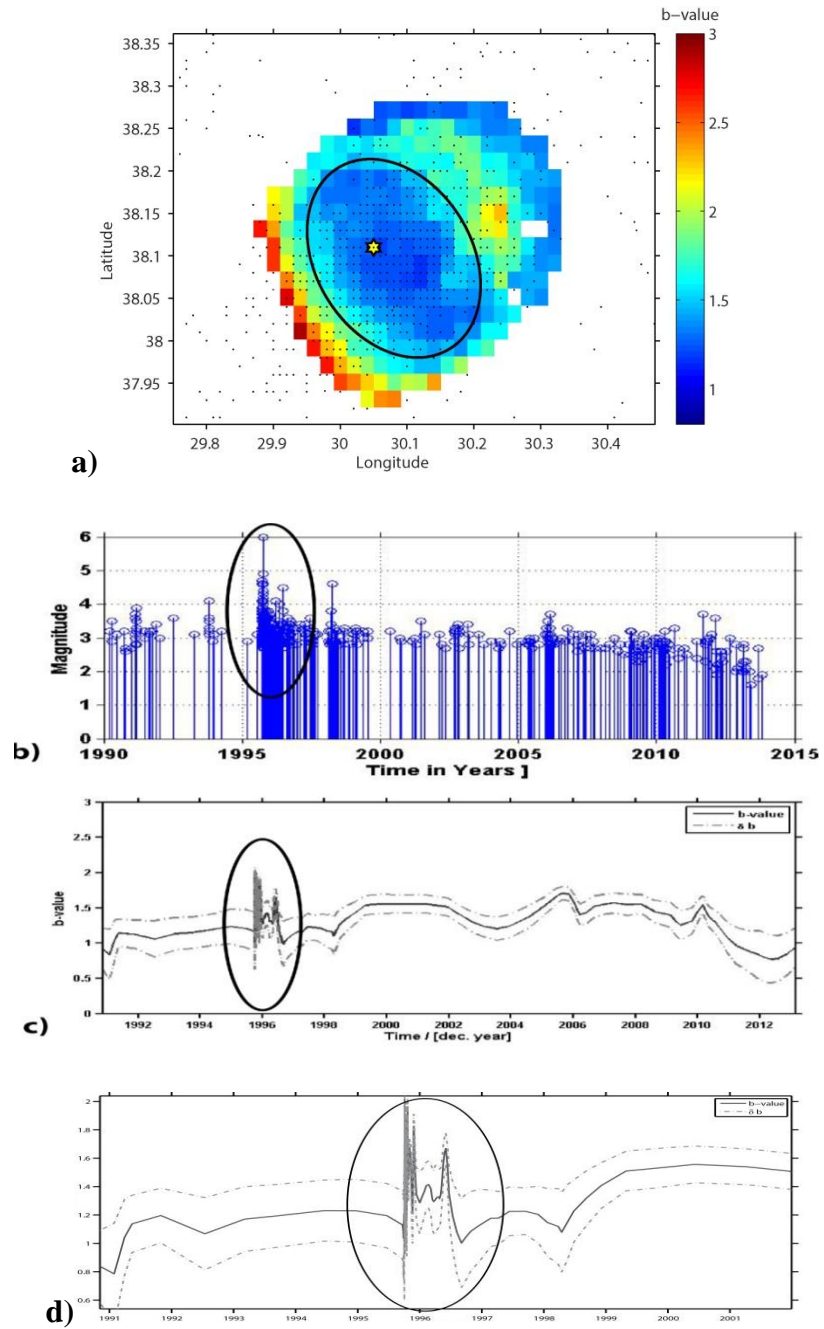


Figure 3.18: a) Post Dinar earthquake b-value map; b) magnitude vs time plot; c) b-value vs time plot of Dinar area and d) zoomed in section of the b-value vs time plot

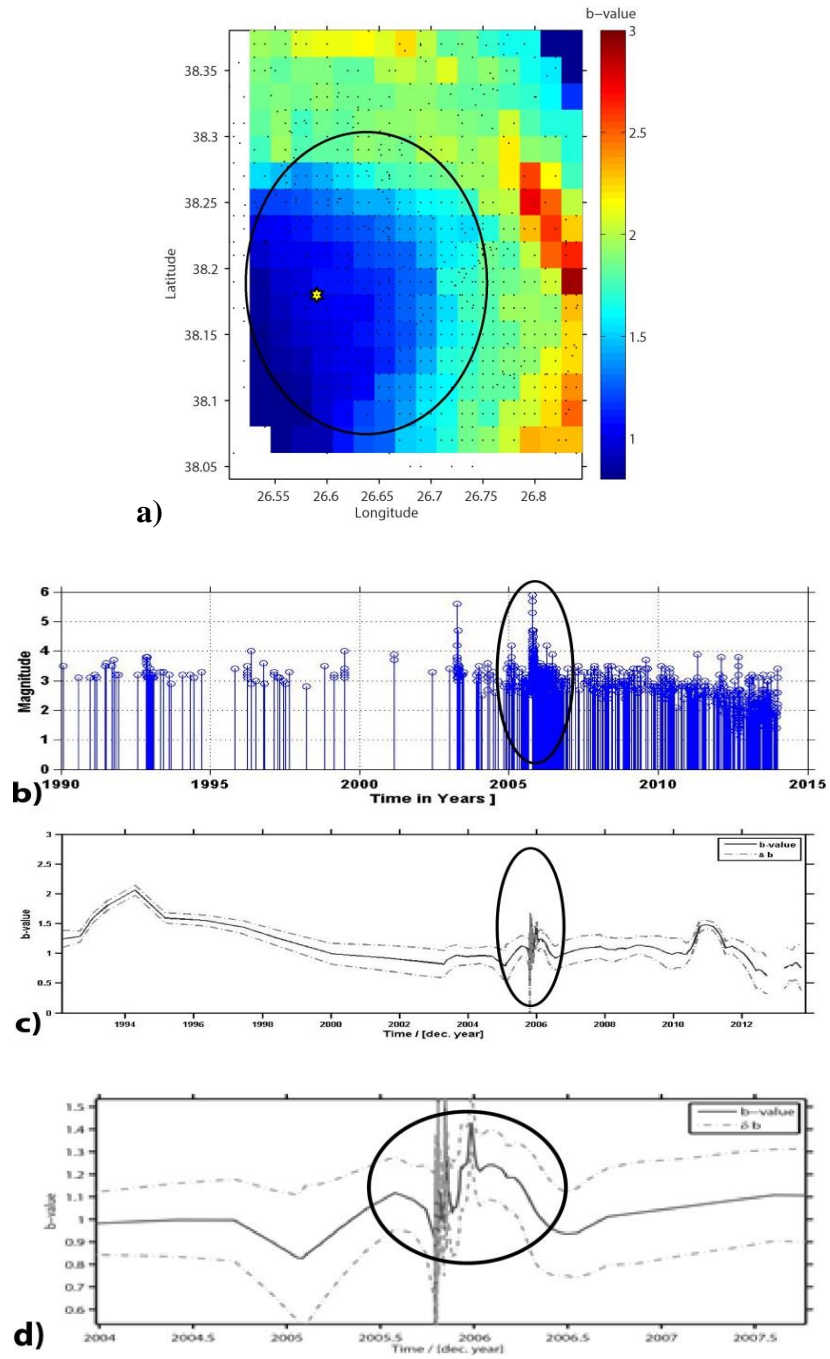


Figure 3.19: a) Post Gulf of Sığacık earthquake b-value map; b) magnitude vs time plot; c) b-value vs time plot of Gulf of Sığacık and d) zoomed in section of the b-value vs time plot.

3.3.2.1 Temporal Variations of b-value and Seismicity Rate Changes in Simav Area

The pre- and post- Simav earthquake b-value maps have been computed using the Best Combination Method (Mc95-Mc90-Maximum curvature) using ZMAP software (Figure 3.20 a and b). The maps are computed using a radius of 10 km and the grid has been spaced by $0.02^\circ \times 0.02^\circ$. The minimum number of events, greater than the magnitude of completeness (Mc) is taken as 10. The b-value around the epicenter location and on other segments of Simav fault zone shows significant variations. The b-value before Simav earthquake sequence was 1.5–1.7 around the epicenter area (Figure 3.20a), which has dropped to 1.0–1.3 after the event (Figure 3.20b). The magnitude time plot shows that there was a decrease in number of ($M = 3.0\text{--}4.0$) events after 1995 in the area (Figure 3.20c). Before Simav earthquake, in 2009 there was a magnitude 5.0 event in the area which caused an increase in the number of small magnitude events. For b-value against time plot, 350 events are selected per window. The b-value time graph (Figure 3.20d) of Simav area shows that the b-value was constant (~ 1.5) for the region between 1990 and 2010 (Figure 3.20d). Before Simav earthquake, the b-value started decreasing (after 2010.5); which is followed by an abrupt increase in b- value (~ 2.0) at the time of main event (2011.38) and then the b-value returned to its normal value (~ 1.5) (until 2012.3) (Figure 3.20e). The temporal variations in b-value from 2010.5 to ~ 2012.3 in can be related to Simav earthquake; but it cannot be confirmed that the drop in b-value after this duration is either related to Simav Earthquake or other factors. Decrease in b-value after earthquakes have been identified in several studies (El-Isa and Eaton, 2014; Smith, 1981, 1986). The permanent decrease in b-value (from 1.5 to ~ 1.0) may be due to an increase in the stress conditions in the region. One possible explanation for this decrease can be that the earthquake may have caused readjustment on the segments of fault in such a manner; that lead to more efficient storing of stresses after the earthquake. On the other hand, the decrease in b-value can also be due to changes in network configuration, changes in recording procedures and/or the increase in the number of recording stations in the area after the earthquake. Increased number of detected earthquakes in the region after 2011 also supports the improved seismic coverage.

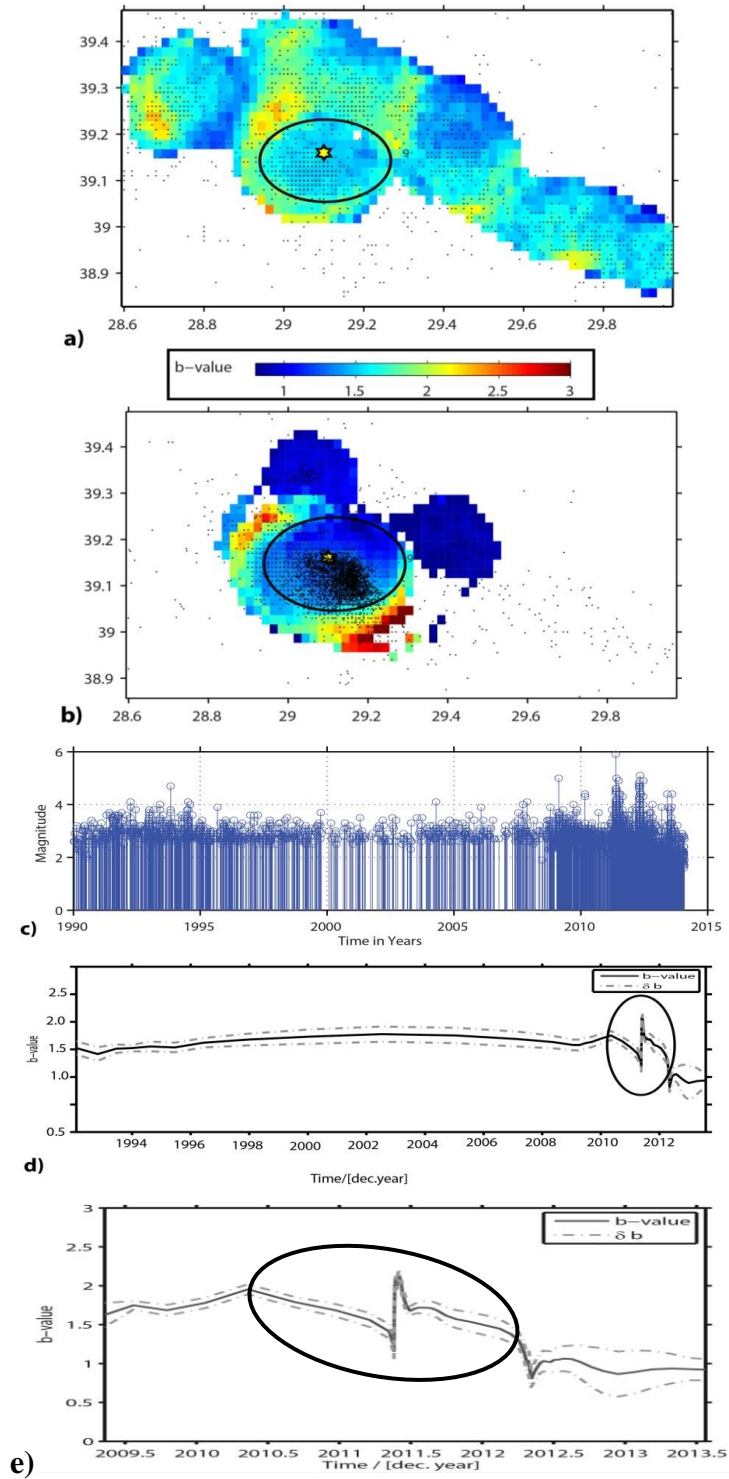


Figure 3.20: **a)** Pre Simav earthquake b-value map; **b)** post Simav earthquake b-value map; **c)** magnitude vs time plot; **d)** b-value vs time plot of Simav area and **e)** zoomed in section of the b-value vs time plot.

Simav area is characterized by sufficient amount of recorded earthquakes for a long period of time. Therefore, the area is selected for observing the seismicity rate changes. According to the time histogram (Figure 3.21a), there was a decrease in the cumulative number of earthquakes before Simav earthquake (May, 2011) that can be regarded as a seismic quiescence in the area before the earthquake. The seismicity rate changes in an area can be determined using z-value test. z-value is a statistical test that can quantify a relative decrease or increase in seismicity rate (Haberman, 1981, 1983). The rate change for the area has been computed using the AS (t) function (Haberman, 1983, 1987). AS (t) function defines where in time is the most significant rate change occurring. The catalogue used for detecting rate changes should be declustered. The z-max for the area was at 1994.6 (Figure 3.21b), and since then the z-value starts dropping until 2009, which shows a decrease in the rate of seismicity in the area. The z-value started to increase 2 years before (in 2009) Simav earthquake. This increase is also evident in the time histogram which shows largest peaks after the earthquake (Figure 3.21a).

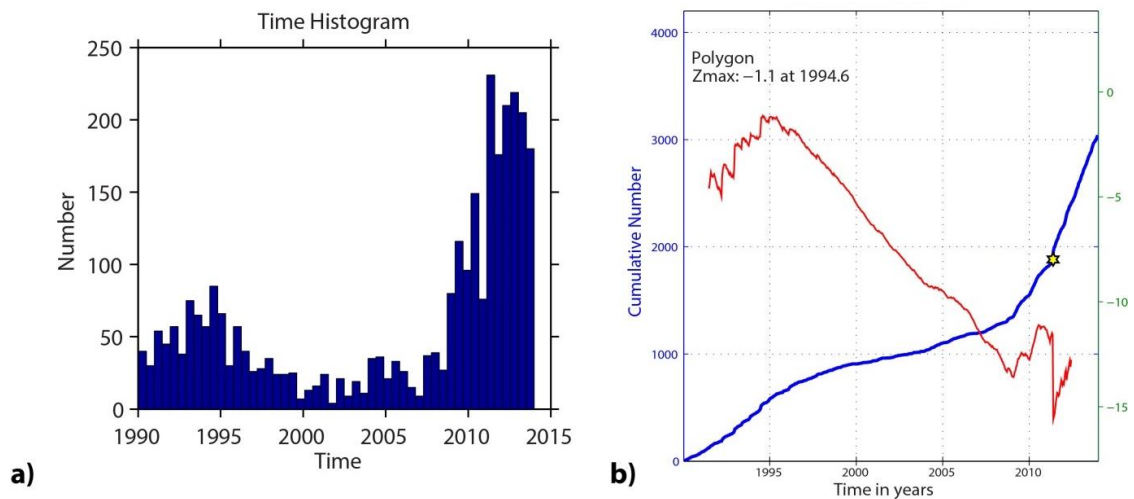


Figure 3.21: a) Seismic quiescence before Simav earthquake and b) calculated rate changes for Simav area using AS(t) function (time window 1.5 years, bins= 15 days).

3.3.2.2 Aftershocks Decay Rate of Simav Earthquake

The occurrence rate of aftershock sequences in time is empirically well described by the modified Omori law (Utsu *et al.*, 1995): $n(t) = K/(t+c)^p$, where $n(t)$ is the frequency of earthquakes per unit time, at time 't' after the main shock, and K, c, p are constants. The characteristic parameter p, which is a measure of the decay rate of aftershocks, ranges from 0.9 to 1.5 and its variability may be related to the structural heterogeneity, stress and temperature in the crust (Mogi, 1962; Kisslinger and Jones, 1991; Utsu *et al.*, 1995). Simav event is characterized by a well recorded aftershock sequence. Therefore, the event is selected for observing the p-values for Simav earthquake. The catalogue selected for the p-value analysis of Simav earthquake covers a time span from the time of occurrence of the main shock; i.e. May, 11, 2011 to February, 2012. The catalogue contains 3208 events. For computing magnitude of completeness (M_c), moving time window approach is used; using 150 events in each window. The M_c at start is 2.8 but it changes with time, the lowest M_c been 2.2, 120 days after the main shock (Figure 3.22a). For P-value plot (Figure 3.22b), completeness in the catalogue is important, thus M_{min} is selected as 2.8. The best fitting Omori parameters are then calculated and represented in Figure 3.22b. The p-value obtained is 1.2, which is a bit high and shows structural heterogeneity around the location of earthquake sequence.

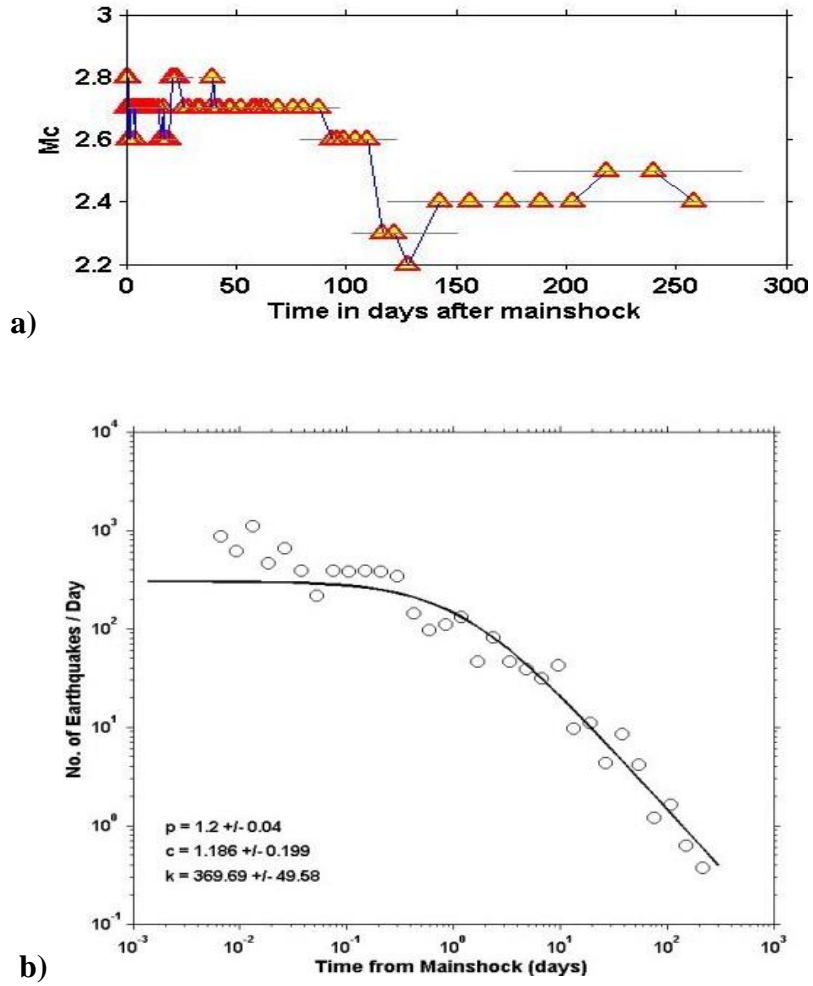


Figure 3.22: a) Magnitude of completeness with time and b) occurrence rate of earthquake vs time for the Simav region.

CHAPTER 4

STRESS ANALYSIS USING FOCAL MECHANISM SOLUTIONS

4.1 Focal Mechanism Solutions

Focal mechanism solutions (FMS) describe the geometry and mechanisms of faulting during earthquakes. FMS can be constructed from waveforms generated by an earthquake travelling in every direction and recorded by a number of seismograms at various distances and azimuths from the epicenter. The radiation pattern of these waveforms depends on the fault geometry and this fact acts as basic rule for determining the focal mechanism solution (Stein and Wysession, 2003). The methods used for determining FMS includes: P-waves first motion, moment tensor inversion (e.g., Stein and Wysession, 2003), analysis of P/S amplitude ratios (e.g., Kisslinger *et al.*, 1981) and polarization and amplitude of S waves (e.g., Khattri, 1973). These methods use the radiation pattern of seismic waves that expresses the orientation of the fault and the slip direction that takes place during the earthquake. The FMS obtained are then in turn used in various active tectonic related studies like stress tensor inversions, tectonic regimes assignment, maximum horizontal stress orientations, seismotectonics, etc. Recently, due to the large amount of earthquake focal mechanisms available from literature and the steadily increasing number of solutions made available to public on routine basis by agencies (e.g., Global CMT, RCMT etc.), these studies are done more frequently.

In this study a total of 480 Focal Mechanism Solutions have been assembled from Harvard CMT (Dziewonski *et al.*, 1987a and b), European-Mediterranean Regional Centroid Moment Tensor Catalog (RCMT) (Pondrelli *et al.*, 2002, 2004, 2007), EMMA (Vannucci and Gasperini, 2004), Swiss Regional Moment Tensor catalogue (SRMT) (Bernardi, *et al.*, 2004; Braunmiller *et al.*, 2002), GFZ (available at <http://geofon.gfz-potsdam.de>), AFAD (available at www.deprem.gov.tr) and from published research

articles for the study area for the period of 1909 to 2013. The latitude and longitude intervals covered by these solutions are 36.5–39.5° N and 26.5–30.5° E, respectively. The magnitude range for the events gathered is 3.0 to 7.7. Most of the events gathered in this study occurred at shallow crustal depth within the upper 50 km and very few occurred at high depths (up to 170 km); these are confined to the southern margin of the study area. For some major events, FMS are available from multiple sources and different literature studies. These solutions are checked and the most reliable ones are selected. After removing the multiple sources for the same events, solutions for 330 events are left in the catalogue.

The geographical distribution of focal mechanism solutions in the area is related to the distribution of active faults and these mechanisms are consistent with the overall sense of movements along these faults. As the study area is characterized by extensional tectonics and a transfer zone in its north-western margin, the area as a whole is dominated by normal fault solutions and the north-western part is dominated by strike slip solutions. Some normal solutions also have minor strike-slip components involved, while some of them have a predominant strike- slip component.

The spatial distribution of FMS is the same as seismicity discussed in Chapter 2, with most of them related to the seismically active parts of the region. These regions include Simav, Alaşehir, Gökova, Soma, Fethiye-Burdur Fault Zone and north-western margin of the study area (Figure 4.1). Simav region is characterized by normal faults having left lateral strike slip component in some segments of Simav Graben bounding fault system, so the area is dominated by normal earthquake mechanisms. The cluster in the area is related to the Simav earthquake and its aftershock sequence. Majority of the focal mechanism solutions for Simav earthquake shows normal fault mechanism having minor strike-slip components involved, while a few of the solutions have a predominant strike-slip components. Other solutions that are aligned along the Simav fault zone are also predominantly normal faults and some of them have minor strike-slip component involved. Soma region is characterized by complex tectonics and falls in the vicinity of İzmir-Balıkesir Transfer Zone (IBTZ). Due to its complex tectonic nature the area is characterized by a mixture of normal and strike-slip FMS. Alaşehir region is

characterized by normal faults bounding the graben. The area is dominated by normal solutions with some of them having minor oblique components and a few strike-slip solutions that can be related to the transfer zones in the area. The north-western part of the area is dominated by both strike-slip and normal faults, therefore earthquake solutions show a predominance of strike-slip mechanisms over normal mechanisms. The cluster in the area is related to the Gulf of Sığacık earthquake sequence and its aftershocks. The cluster consists of mainly strike-slip mechanisms with some of them having small normal components. Gökova region is characterized by normal faults bounding the grabens and the rift systems in the region. Therefore, the area is dominated by pure normal fault solutions with associated oblique-slip and strike-slip solutions. Fethiye-Burdur Fault Zone is characterized by complex earthquake solutions. The area shows normal, strike-slip and a few thrust fault solutions as well in its offshore region that can be related to Pliny-Strabo zone.

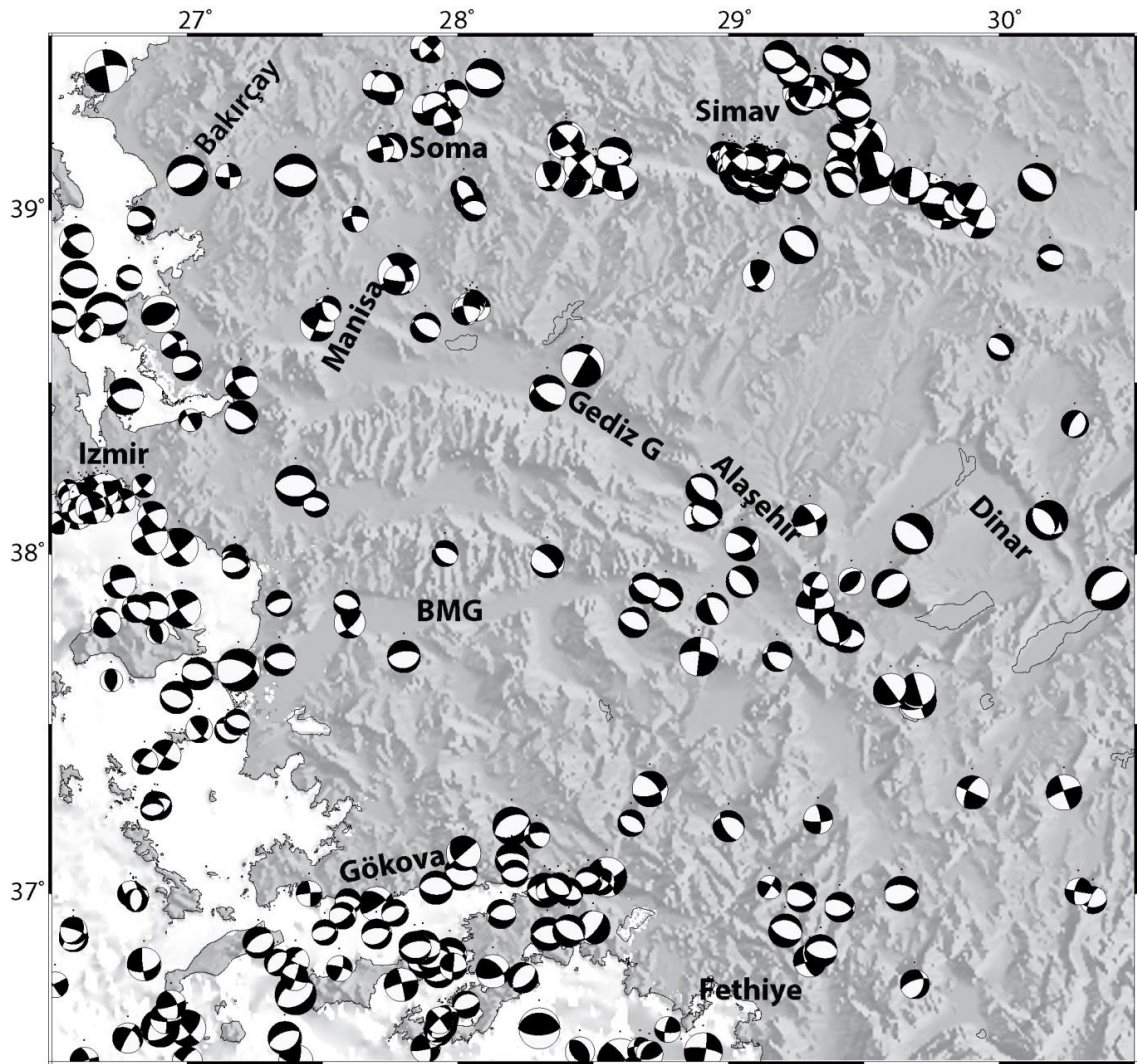


Figure 4.1: Available focal mechanism solutions overlaid over topography. The sizes of the solutions are scaled according to their magnitude. Note that parameters of these solutions are listed in Appendix A.

4.1.1 Pressure and Tension (P-T) axes and Rake Distributions of the Study Area

The rake-based ternary diagram (Figure 4.2a) of all the events shows that majority of earthquakes in the area have normal solutions which is consistent with the fact that most of the graben-bounding structures in the area are normal faults. Apart from normal faults, the area contains considerable number of strike-slip solutions which are concentrated in the north-western part of the study area where strike-slip faults are predominant. There are a few thrust solutions also present in the southern offshore area near Gökova. These solutions can be related to ongoing subduction along Aegean Arc. The pressure and tension (P-T) axes (Appendix A) shows that the area as a whole is experiencing almost N-S (more specifically NNE–SSW) extension and almost vertical compression (Figure 4.2b). The P-T axis density plot shows that T-axis is sub-horizontal and P-axis is vertical (vertical to sub-vertical) in the region (Figure 4.2c).

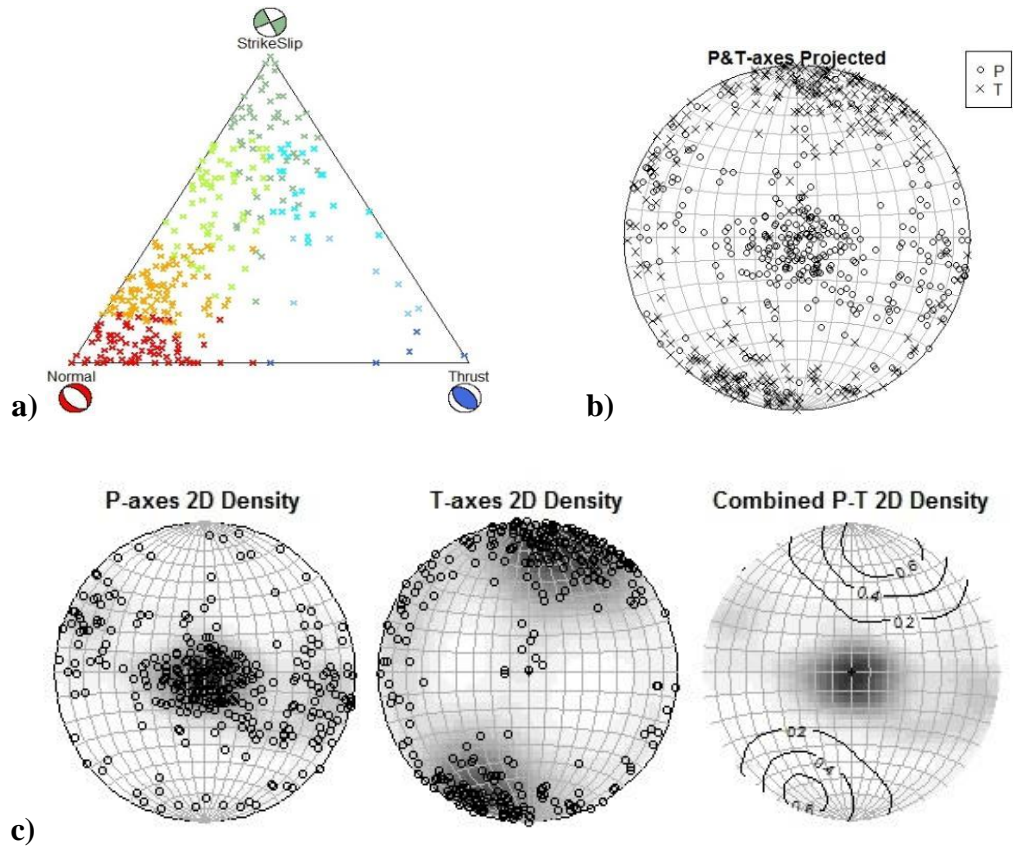


Figure 4.2: **a)** Rake based ternary plot of faulting types; **b)** pressure and tension (P-T) axes plotted on lower hemisphere projection and **c)** contoured plot of P-T axes for all the earthquakes in the study area. Note that orientations of P-T axes are listed in Appendix A.

4.2 Sub-regions Classification

It is evident from the focal mechanism solution distribution and the complex tectonic nature of the area that analyzing the area as a whole will lead us to over simplification of results. Therefore, the study area is divided into sub-regions on the basis of variations in types of focal mechanism solutions, tectonic settings, geographical proximity, faulting type and changes in trends of faulting. This approach will allow us to study the stress parameters in detail and detect local scale changes in these parameters. The whole

region is subdivided into ten (10) sub-regions as shown in Figure 4.3: **(1)** *Simav region* is predominantly characterized by normal focal mechanism solutions with some of them having minor oblique slip component and a few strike slip solutions. The cluster in the region is related to the Simav earthquake and its aftershocks; **(2)** *Alaşehir region* is also dominated by normal fault solutions with some of them having minor oblique slip components and two events have strike slip solutions; **(3)** *Manisa region* falls at the western extremity of Gediz Graben and consists of normal and some strike-slip solutions. The area is separated from Alaşehir region (sub-region 2) due to observed changes in fault trends; **(4)** *Dinar-Burdur region* is also dominated by normal solutions but the orientations of faults are orthogonal to each other; **(5)** this sub-region coincides with *Büyük Menderes (BMG) and Küçük Menderes (KMG) grabens* and is dominated by normal faulting; **(6)** *Soma region* consists of a mixture of normal and strike-slip solutions. It falls in the junction of Simav Graben bounding fault system and the north-western margin of the study area. Western portion of the study area consist predominantly strike slip solutions and some normal solutions and is further subdivided into two sub-regions; **(7)** this sub-region is in the north-western corner of the study area and coincides with *Bakırçay Graben* region. The area is characterized by a mixture of strike-slip and normal fault mechanisms; **(8)** the *Gulf of Sığacık region*, is situated in the middle portion of the western margin and lies west of KMG and BMG. The area is characterized by strike-slip solutions with a few normal fault solutions also being present in the area. The cluster in the subset is related to the Gulf of Sığacık earthquake sequence and all the solutions are strike-slip in this cluster; **(9)** *Gulf of Gökova region* has predominantly normal fault solutions and few strike-slip solutions; **(10)** *Fethiye region* is characterized by complex pattern of faulting and consists of a mixture of normal and strike-slip solutions. There are few thrust solutions (events no. 23 and 105, see Appendix A) in its offshore zone, which coincides with ongoing subduction along the Aegean arc. Thus, these thrust solutions are not included in this sub-region.

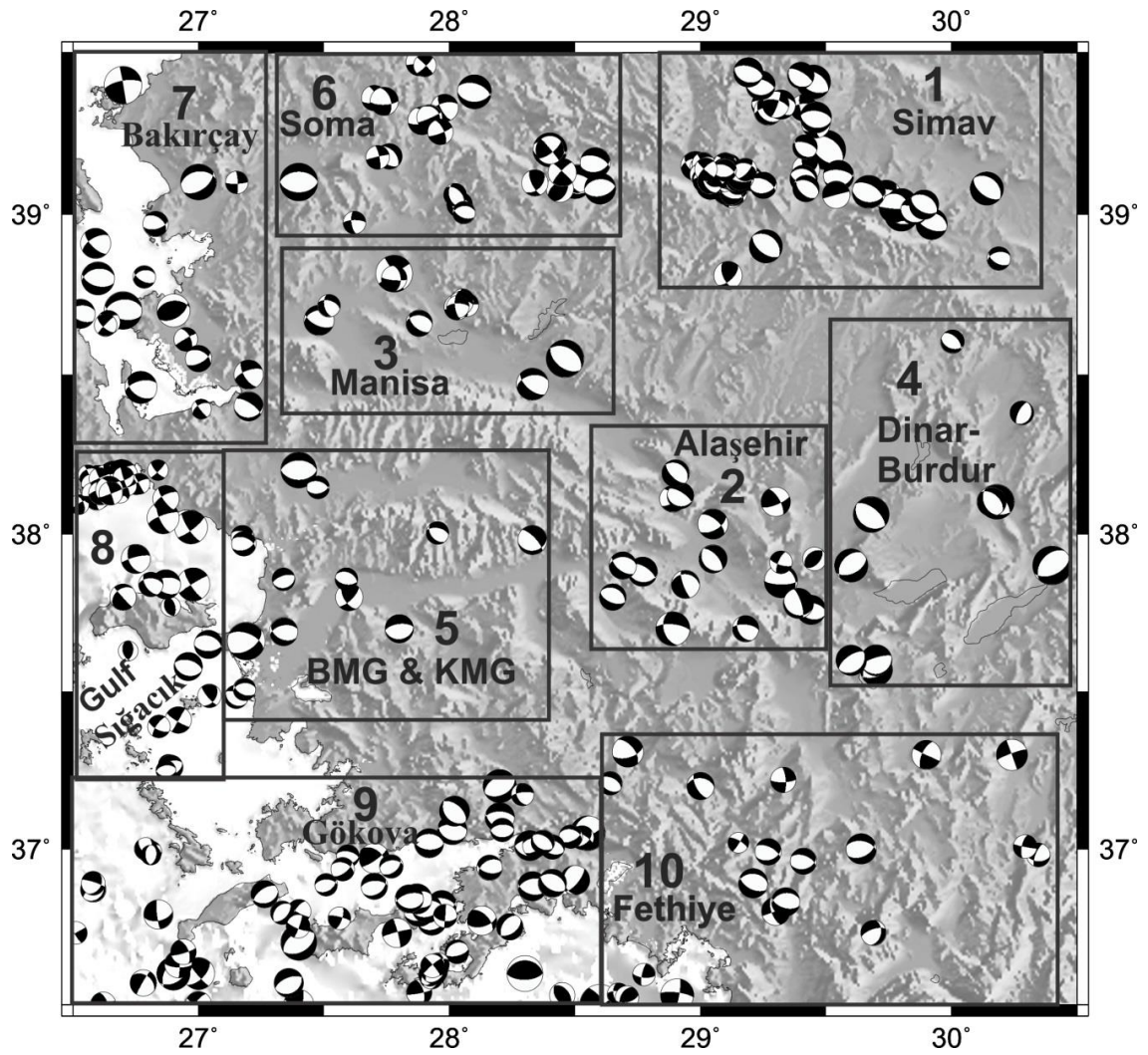


Figure 4.3: Map showing focal mechanism solutions and sub-regions in study area that are selected for analyzing stress orientations independently.

4.2.1 Pressure and Tension (P-T) axes and Rake Distributions of Sub-regions

Pressure and tension axes (P-T axes) density diagrams and ternary plots have been constructed for each subset region to get an idea of variations among the sub-regions (Fig. 4.4). The P-T axes and ternary plots for sub-regions 1, 2, 4 and 5 (Simav, Alaşehir, Dinar-Burdur and BMG-KMG region) shows that these sub-regions regions are dominated by extensional character having vertical P- axes orientations. All these regions have sub-horizontal T- axes, but in region 2, 4 and 5 the axes are diffused over a large area of the density net. The ternary plots of sub-regions 3 and 6 (Manisa and Soma) have a mixture of normal and strike-slip events. T-axis is sub horizontal in these regions while P- axis is sub-horizontal to vertical. Regions 7 and 8 have predominantly strike-slip solutions. The majority of strike-slip events in region 8 are related to gulf of Sığacık earthquake sequence. The P- and T- axes in both areas are sub horizontally oriented. Region 9 (Gulf of Gökova) is again dominated by normal events with some strike-slip events as well but both the P- and T- axis are diffused over a large area as compared to other normal fault dominated regions. Region 10 (Fethiye) is characterized by both strike-slip and normal events with a thrust event as well. P- axis is sub-vertical in the region. Both P- and T- axes are diffused in the region, which shows the heterogeneity of stress field in the region.

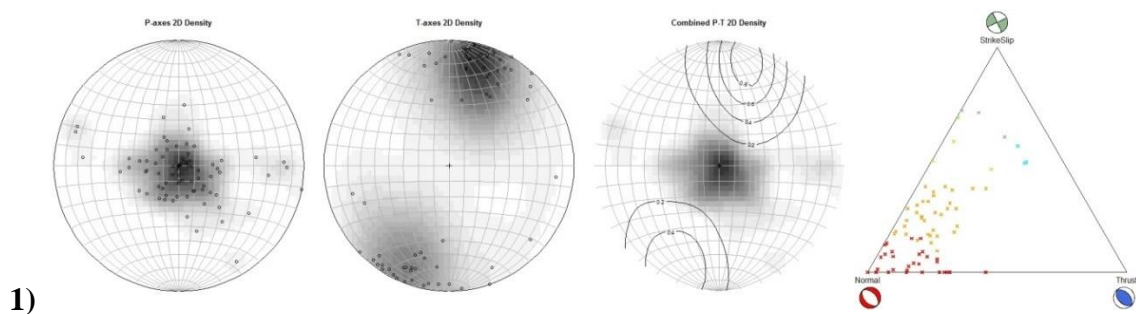


Figure 4.4: Stereographic projection of P-T axes and rake based ternary plots identified within each sub-region.

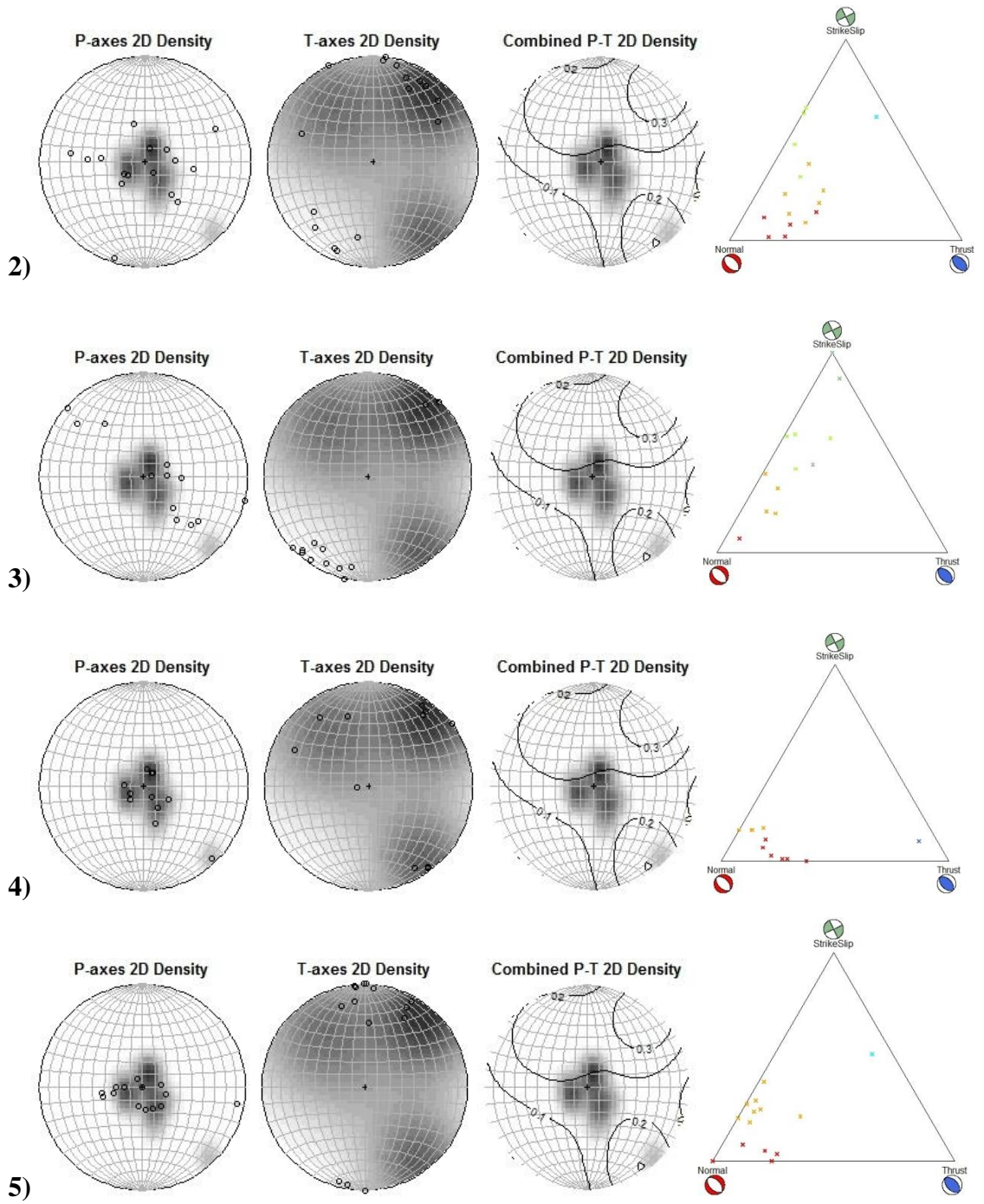


Figure 4.4: (continued)

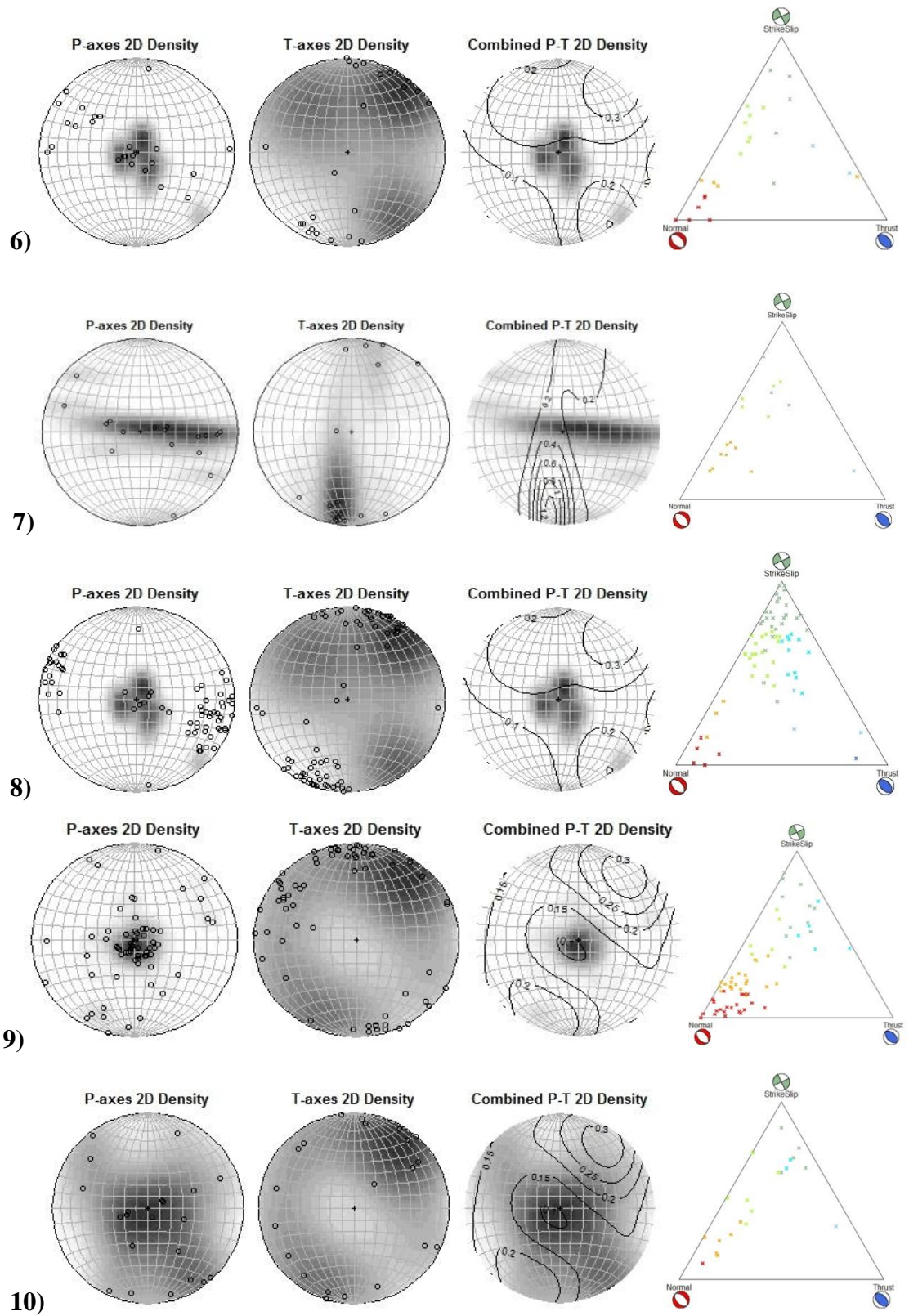


Figure 4.4: (continued)

4.3 Stress Tensor Inversion

Many stress inversion techniques have been devised for the determination of stress field orientations from focal mechanism solutions (Angelier, 1979, 1984, 2002; Gephart and Forsyth, 1984; Michael, 1984, 1987; Gephart, 1990; Rivera and Cisternas, 1990; Delvaux and Sperner, 2003). These techniques are capable of solving for the orientations of three principle stress axes and the relative magnitudes of the stress axes $R = (\sigma_2 - \sigma_3) / (\sigma_1 - \sigma_3)$, where σ_1 , σ_2 , σ_3 indicates maximum, intermediate and minimum principal compressive stresses respectively. However, these inversions are not capable of determining stress magnitudes. The aim of these methods is to determine the stress which minimizes the discrepancy between the resolved shear stress direction and the slip direction for all data set. The major difference between all these methods is the technique they use to handle the fault plane ambiguity. Stress inversion was first used for slickenside field data in which the fault plane was already known, therefore some algorithms needed the fault plane to be determined a priori which is not possible in most cases. Gephart and Forsyth (1984) primarily treats all the nodal planes as fault planes and then removes the poor fitted auxiliary planes in the next step leaving behind the planes that are best fitted by a uniform stress field. Michael's (1987) approach applies a bootstrap routine that randomly picks fault planes from the original data. Angelier (2002) provided a method free of choice, in which the fault plane is chosen automatically. Arnold and Townend (2007) requires a priori information on the stress field into a probabilistic stress analysis of FMS that accounts for the fault plane ambiguity by calculating probability density functions for the orientations of the principal stress axes.

4.3.1 Stress Tensor Analysis by Slick Method

In slick method of Michael (1984, 1987) the stress tensor is calculated using a linear least-square inversion technique. It uses the statistical method of bootstrap resampling for determining the orientation of three principle axes and stress magnitude by finding the best fitting stress tensor to the observed focal mechanisms (Görgün *et al.*, 2010).

Variance quantifies the heterogeneity of a stress field and is defined as the squared summed solution misfit, which is the angle between the individual focal mechanism and the assumed tensor (Wiemer *et al.*, 2002). The value of variance should be less than 0.2 for a spatially uniform stress field. Higher values indicate poor fitting stress orientation and hence stress field remains heterogeneous within the analyzed volume (Wiemer *et al.*, 2002). The basic assumptions for the models are that (1) the stress in the selected volume is uniform and invariant in space and time, and (2) that the earthquake slip follows the direction of maximum shear stress; Wallace-Bott hypothesis, 1951 (Delvaux and Barth, 2010).

Maximum compressive stress may have an orientation anywhere in the dilatational quadrant of the focal mechanism and the pressure and tension axes from a single solution may vary significantly from the principal stress directions depending on the orientation and strength of the faults (McKenzie, 1969). Therefore, a single focal mechanism or many mechanisms with similar orientations will lead to poorly constrained principal stresses. However, a large number of solutions with a variety of orientations within a uniform stress region will lead to a good quality determination of principal stress directions.

In this study Michael's (1987) linearized stress inversion method is used in ZMAP software package (Wiemer, 2001). Using the FMS, the stress tensor inversion for the entire study area has been carried out using Michael's slick method (Figure 4.5). The inversion results shows that the maximum principal stress (σ_1) is oriented in the vertical direction, minimum stress axes (σ_3) is sub-horizontal striking in NNE–SSW direction and the intermediate principal stress (σ_2) is trending in NW-SE direction (Figure 4.5a). Variance in the area that defines the homogeneity of stress directions is 0.16, which is within the range (variance should not be greater than 0.2). Phi ratio (or stress ratio, R), which defines the type of faulting is 0.59 and suggests a normal faulting style for the area (Figure 4.5b).

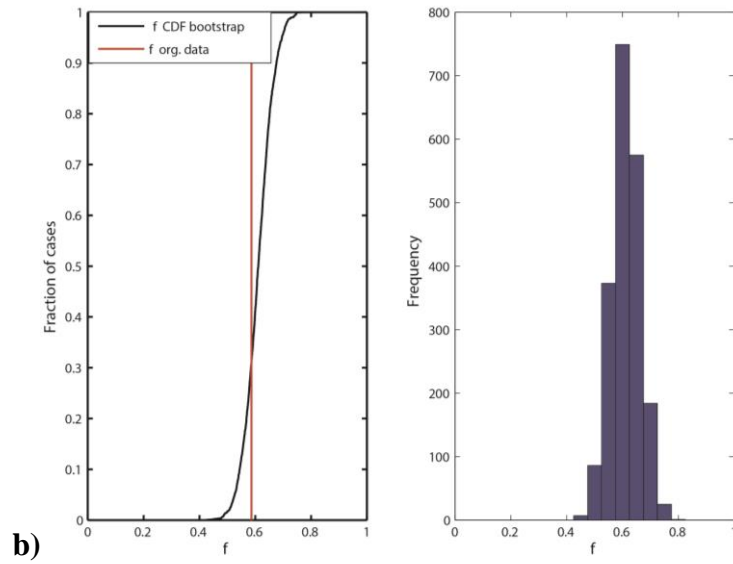
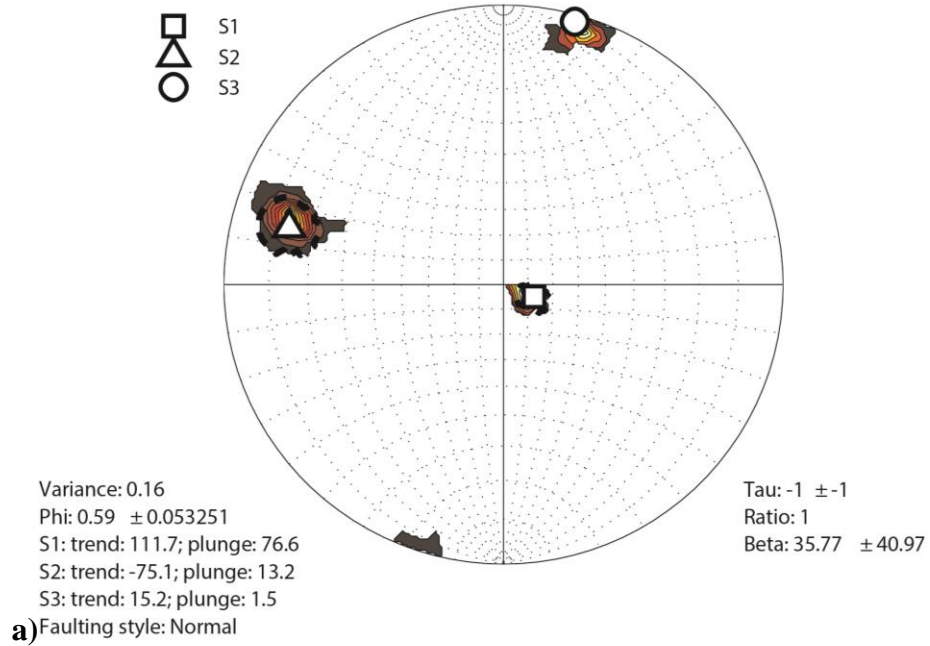


Figure 4.5: a) Results of stress tensor inversion of all available focal mechanism solutions in the study area using Michael's method and b) the resultant histogram of stress ratio (R) vs frequency.

The earthquake spatial distribution in the area shows that the data has enough resolution to measure the stress regime and variance throughout the study area. Maps of stress regime and variance are constructed using 5 events at each node and $0.1^{\circ} \times 0.1^{\circ}$ grid spacing. Figure 4.6a shows colored bars indicating horizontal compression directions and associated tectonic regime. It shows that the area is dominated by normal faulting except for the western margin of the study area, where strike-slip faulting is predominant. Apart from normal faults there are some regions which have a mixture of normal and strike slip faults, for example Soma, Manisa regions and some parts of southern margin of the study area. Stress variances greater than 0.2 indicate a heterogeneous stress field or a poor resolution of data. The overall stress variance for the area is well within this range except for a few locations in the study area (Figure 4.6b). Except locations marked with high stress variance, stress inversion results are accounted as reliable.

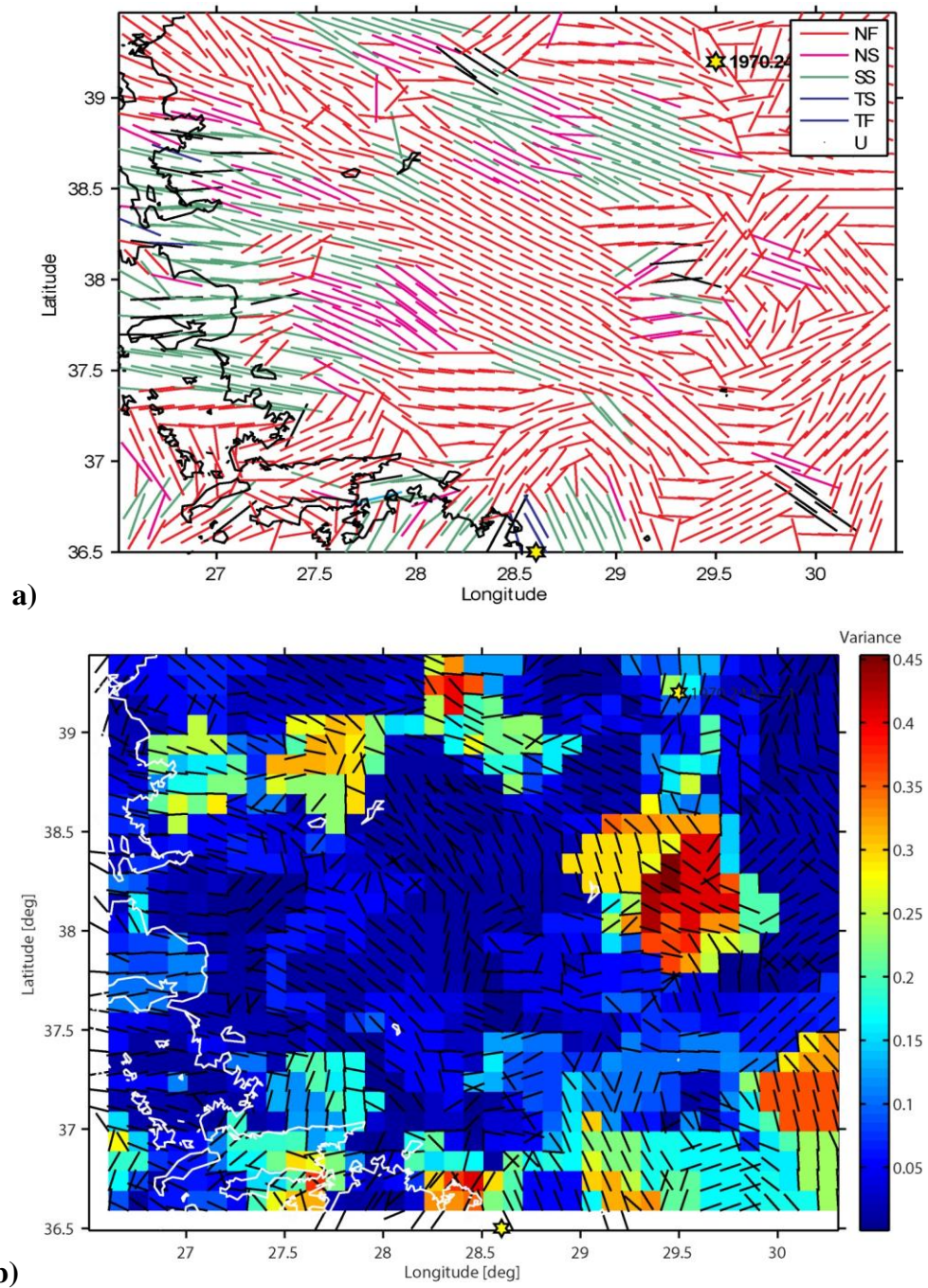


Figure 4.6: **a)** Orientation bars of horizontal compression directions. Tectonic regimes are represented by different colors (NF: Normal, NS: Normal with strike-slip, SS: Strike-slip, TS: Thrust with strike-slip, TF: Thrust). **b)** Orientation bars of horizontal compression directions overlaid on to colored stress tensor variance map of the study area.

The stress tensor inversion has also been carried out independently for the 10 sub-regions devised in the previous section of this Chapter (Section 4.2) in order to investigate the changes in orientations of principal stress components, faulting types and variances.

4.3.1.1 Simav Region (Sub-region 01)

The catalogue for Simav region consists of 76 focal mechanism solutions, with 46 solutions related to Simav earthquake cluster. The detailed view of the focal mechanism solutions distribution is shown in Figure 4.7. The map shows that most of the earthquakes in the area have normal focal mechanism solutions. The Simav earthquake sequence is dominated by normal solutions with most of them having minor strike-slip components involved. The stress tensor inversion for Simav region shows that σ_1 is oriented vertically in the region with σ_3 being sub-horizontal trending in NNE–SSW direction and σ_2 trends in NW–SE (Figure 4.8a). The variance value for the sub-region is 0.061 which is quite low and suggests a homogeneous stress field in the area. Stress ratio (Phi) is 0.59 and tectonic regime is governed by normal faulting. There is a cluster of earthquakes related to Simav earthquake sequence in the area. The stress tensor inversion has also been carried out for the area excluding this cluster. The reason is that sometimes clusters may affect the results for the region because of their greater statistical impact on the data. The results show that the orientations for the σ_2 and σ_3 remain almost same while the trend of σ_1 has changed from 115° to 165° (Figure 4.8b). The variance has increased (0.061 and 0.079) due to small number of events and Phi value does not show any significant changes (0.59 and 0.61).

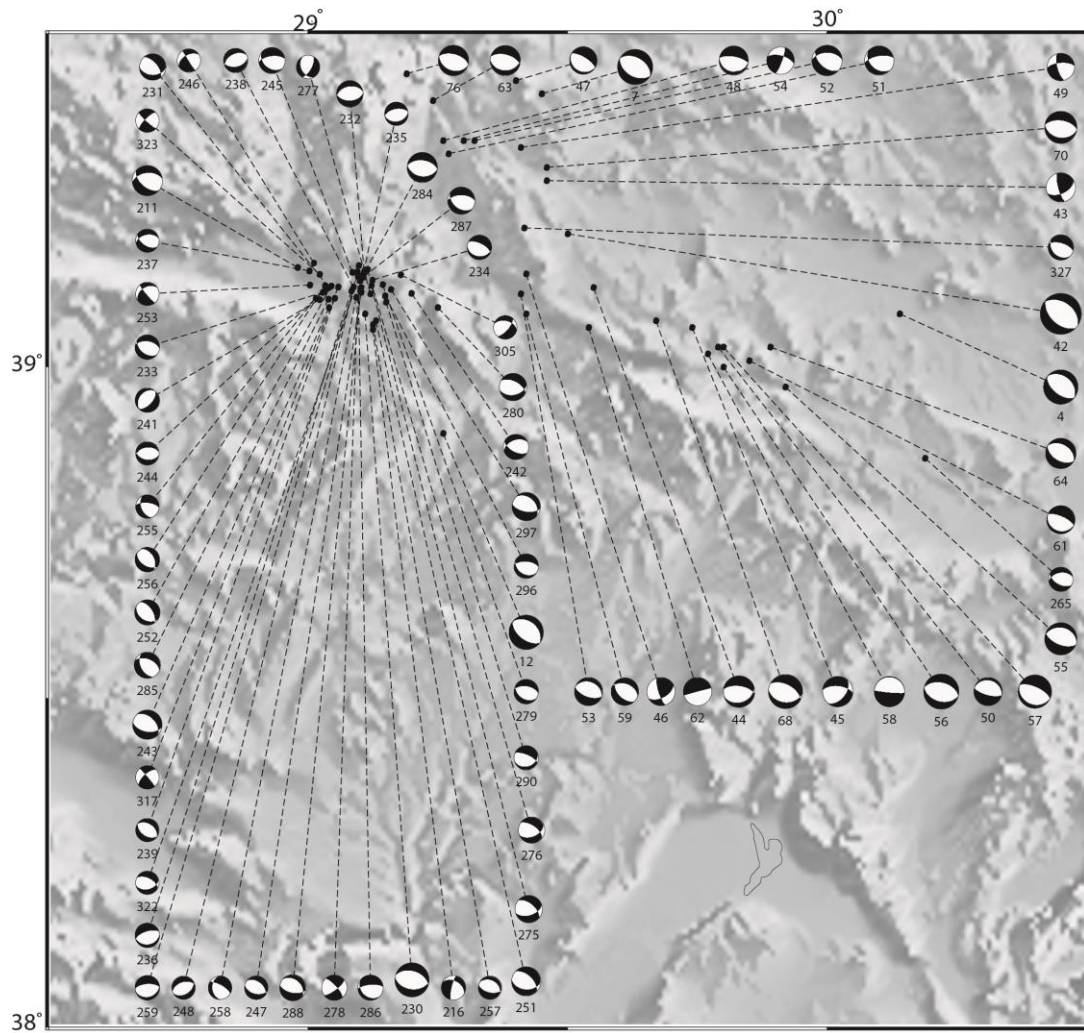


Figure 4.7: A close-up map of the Simav sub-region showing topography and focal mechanism solutions. Mainshock and aftershocks of Simav earthquake are grouped in the east (except solution 12 which occurred earlier).

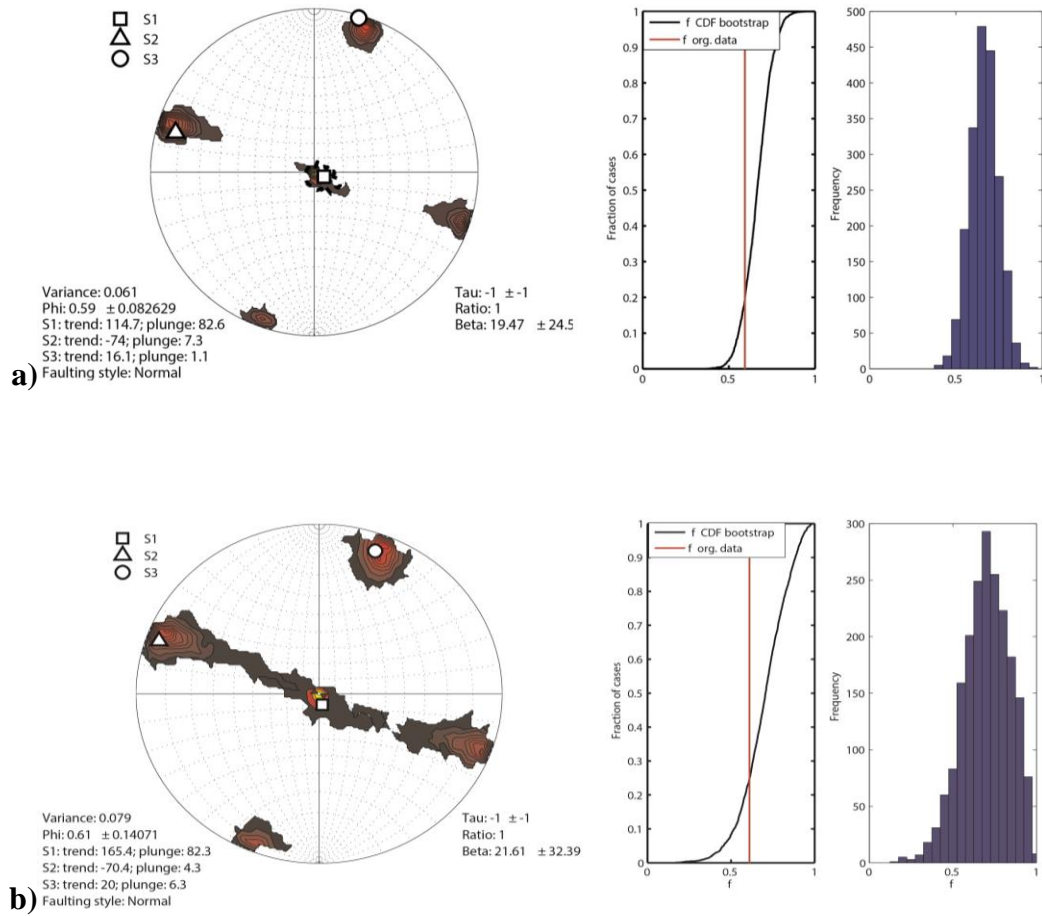


Figure 4.8: a) Results of stress tensor inversion and histogram of stress ratio (R) vs frequency for Simav sub-region and b) results of stress tensor inversion and histogram of R vs frequency for Simav sub-region excluding the Simav earthquake sequence.

4.3.1.2 Alaşehir Region (Sub-region 02)

The catalogue for Alaşehir sub-region consists of 16 solutions and their distribution is shown in Figure 4.9a. This area is located at the junction of Gediz and Büyük Menderes grabens. According to the available focal mechanisms, this sub-region is dominated by normal solutions but there are also some strike-slip solutions present in the area. The stress tensor inversion results for Alaşehir region shows that orientation of σ_1 is vertical in the area; σ_3 is sub-horizontal trending in NE–SW direction and σ_2 trends in NW–SE direction (Figure 4.9b). Variance in the area is 0.13, which is a bit high as compared to Simav region, but is still in the permissible range. The reason may be due to the complex faulting style in the area, due to the fact that eastern ends of Gediz and BMG join at this location. Stress ratio is 0.41 and the sub-region is characterized by normal faulting. Overall the trend and plunge of the principal axes are same as Simav region with minor differences but the variance value at Alaşehir region is a bit higher.

4.3.1.3 Manisa Region (Sub-region 03)

Manisa region constitutes the western end of Gediz graben and is dealt separately from the Alaşehir sub-region (sub-region 2) because of dominance of strike-slip solutions and the trend of faulting in the area. The catalogue for this region consists of 12 solutions (Figure 4.10a). The stress tensor inversion results show that σ_1 and σ_2 are sub-horizontally oriented in the region and σ_3 is almost horizontal, trending in SW–NE direction (Figure 4.10b). Variance in the area is low (0.02) and shows a homogeneous stress field in the area. Stress ratio is 0.92 indicating that σ_1 and σ_2 are close in magnitude. The sub-region is characterized by extensional strike-slip regime.

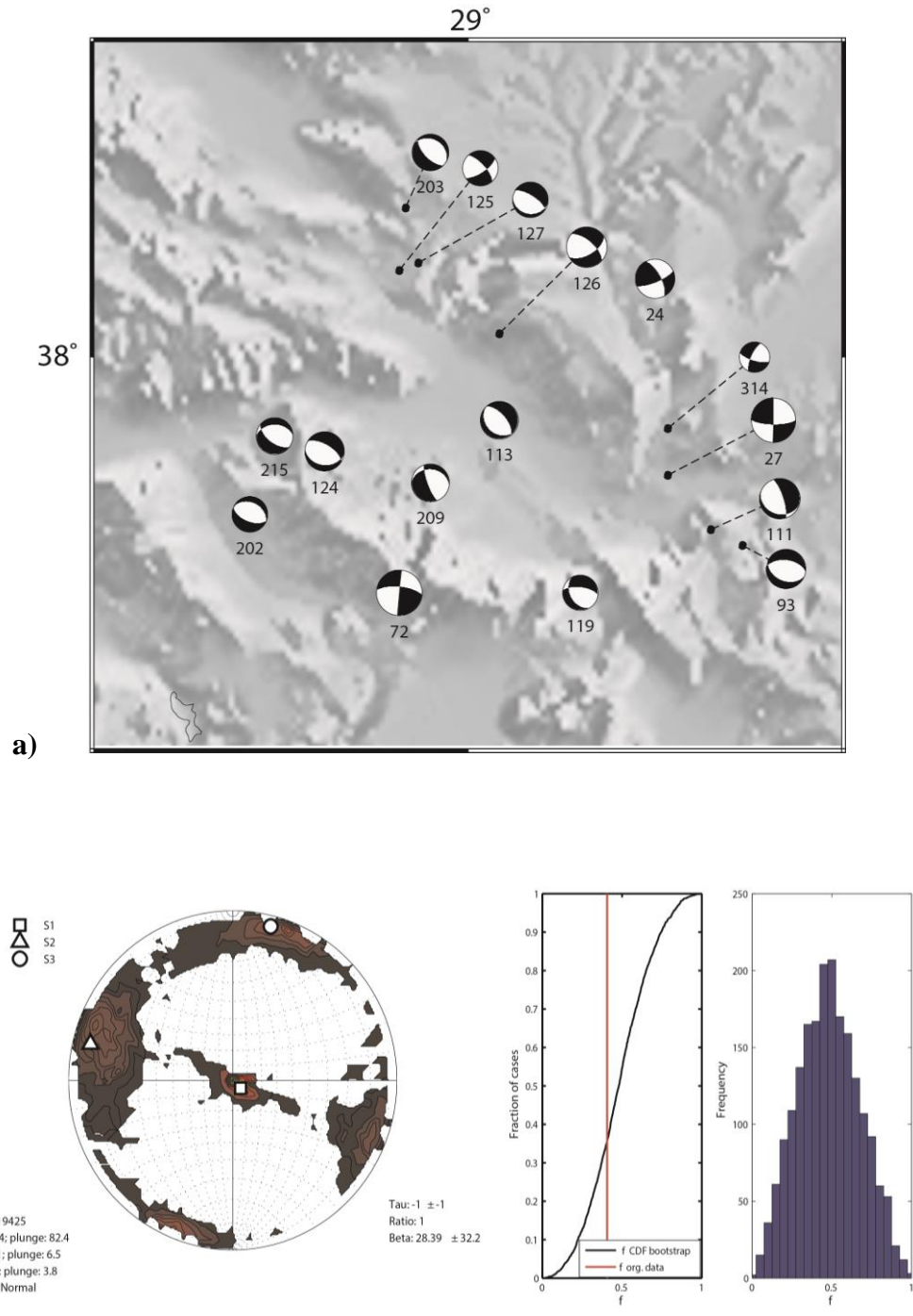


Figure 4.9: a) Close-up map of the Alaşehir sub-region showing topography and focal mechanism solutions and b) results of stress tensor inversion and histogram of stress ratio (R) vs frequency for Alaşehir sub-region.

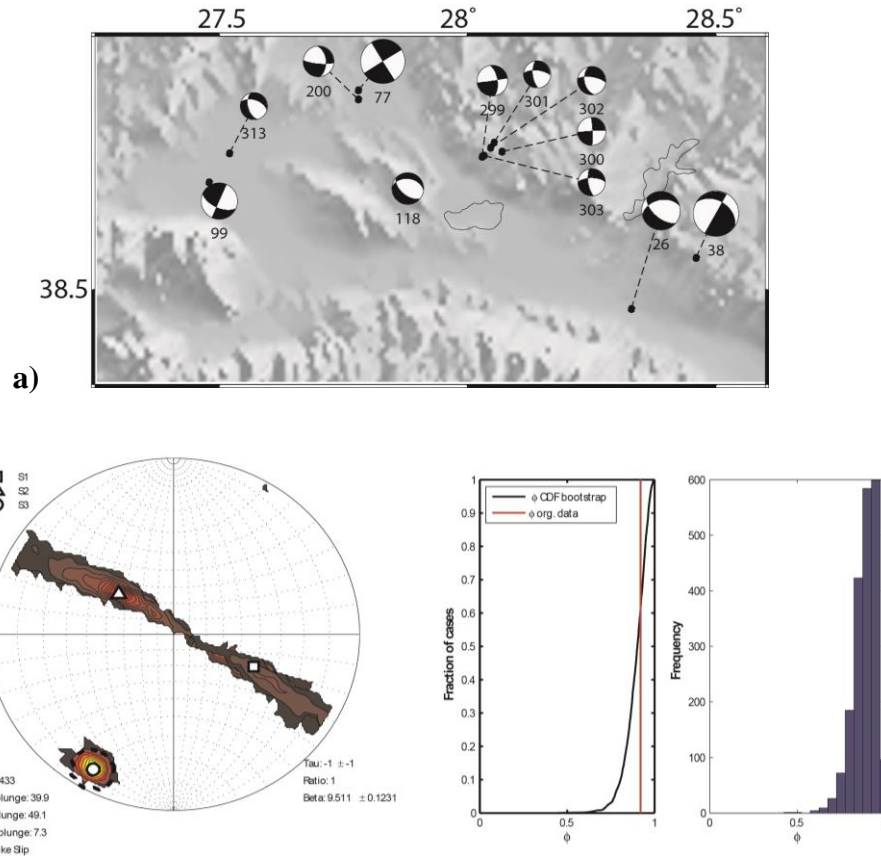


Figure 4.10: a) Close-up map of the Manisa sub-region showing topography and focal mechanism solutions and b) results of stress tensor inversion and histogram of stress ratio (R) vs frequency for Manisa sub-region.

4.3.1.4 Dinar-Burdur Region (Sub-region 04)

This sub-domain is situated to the East of Gediz Graben, and Fethiye-Burdur Fault Zone merges into this region in its northward extension. The orientations of the faults are predominantly NE–SW in this region as opposed to the general, almost E–W (or NW–SE) trend in western Anatolia. The sub-catalogue for the region consists of 11 solutions and is dominated by normal earthquake mechanisms (Figure 4.11a). The stress tensor inversions results (Figure 4.11b) show that σ_1 is vertically oriented; σ_3 is

sub-horizontal and trends in NE–SW direction, which is consistent with the trend of faulting in the area. Variance in the area is 0.13, which is a bit high and may be due to a heterogeneous stress field and active orthogonal faulting. Stress ratio is 0.33 indicating that σ_2 and σ_3 are close in magnitude in agreement with multi-directional extension. The sub-region is characterized by normal faulting regime.

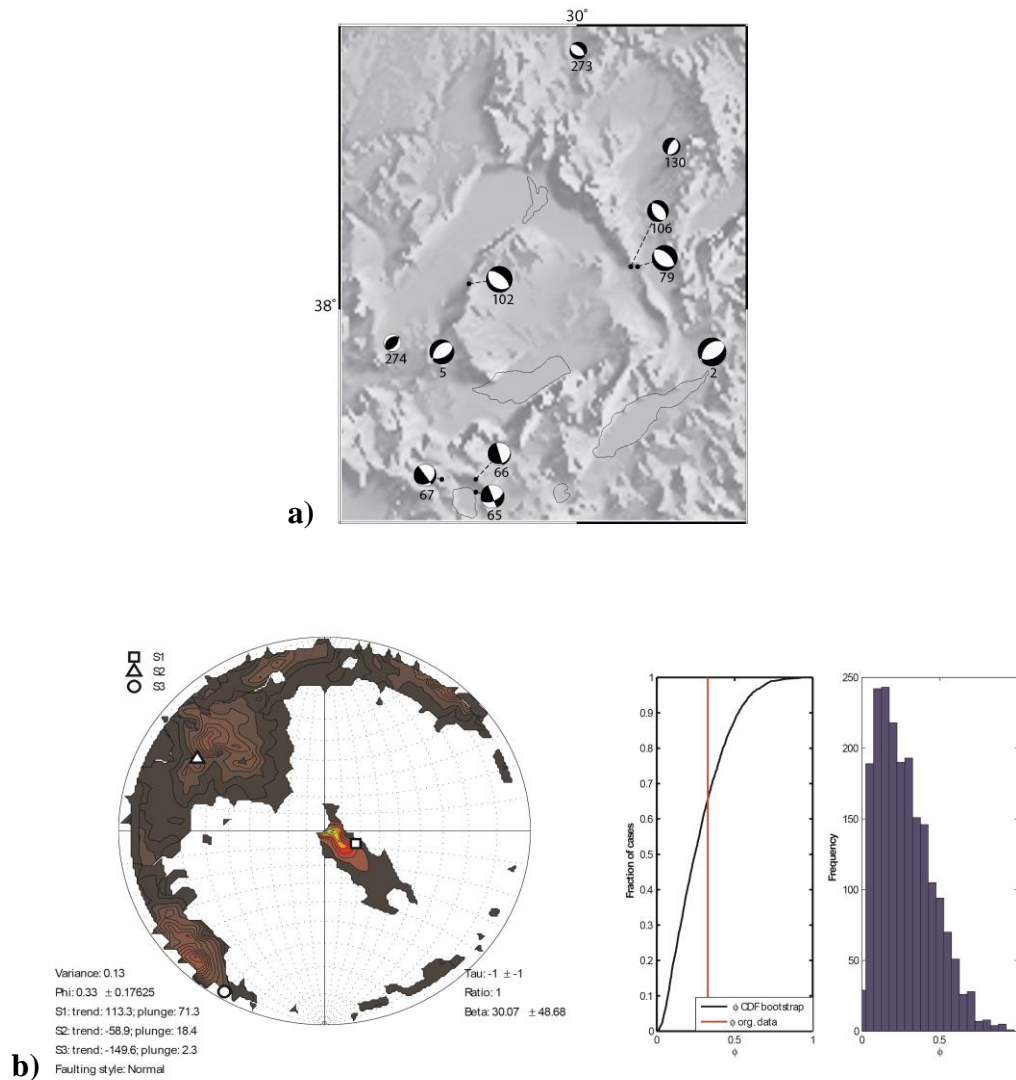


Figure 4.11: a) Close-up map of the Dinar-Burdur sub-region showing topography and focal mechanism solutions and b) results of stress tensor inversion and histogram of stress ratio (R) vs frequency for Dinar-Burdur sub-region

4.3.1.5 Büyük and Küçük Menderes Grabens (Sub-region 05)

The sub-region consists of the western parts of Büyük and Küçük Menderes grabens (BMG-KMG). The catalogue for the area has 14 earthquake events and is dominated by normal earthquakes (Figure 4.12a). The results for the area show that σ_1 is vertically oriented; σ_2 is sub-horizontal and σ_3 trends in almost N–S direction in the region (Figure 4.12b). These results are consistent with the trend of faulting in the area. Variance value (0.05) suggests a homogeneous stress pattern for the region. Stress ratio is 0.71 and the sub-region is characterized by normal faulting regime.

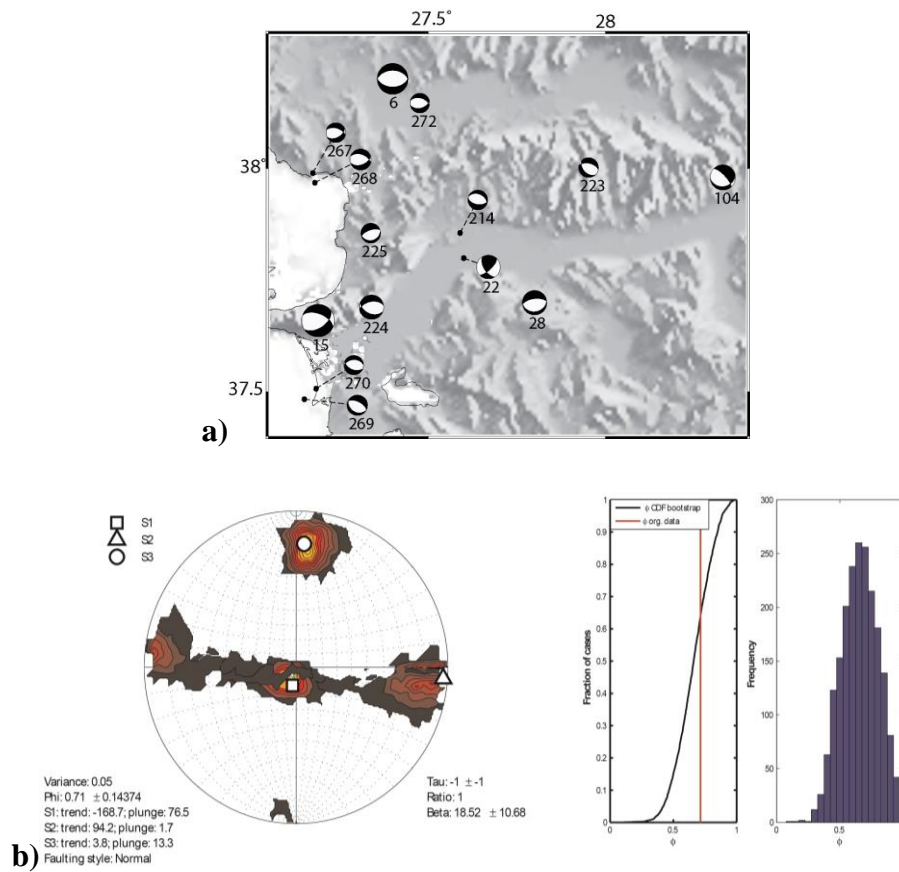


Figure 4.12: a) Close-up map of the Büyük and Küçük Menderes sub-region showing topography and focal mechanism solutions and b) results of stress tensor inversion and histogram of stress ratio (R) vs frequency for the sub-region.

4.3.1.6 Soma Region (Sub-region 06)

Soma region is characterized by a mixture of normal and strike-slip earthquake mechanisms (Figure 4.13a). The catalogue for the area consists of 25 earthquakes. The results for the region show that both σ_1 and σ_2 are in a vertical to sub-vertical orientation in the region (Figure 4.13b). σ_3 is sub-horizontal and trends in SW–NE direction. Stress ratio is 0.77, and the style of faulting obtained for the area is normal to strike slip fault. Stress variance in the area is 0.12. The area falls in a geographical location which coincides with the IBTZ location. This may be the reason for mixed faulting pattern in the region.

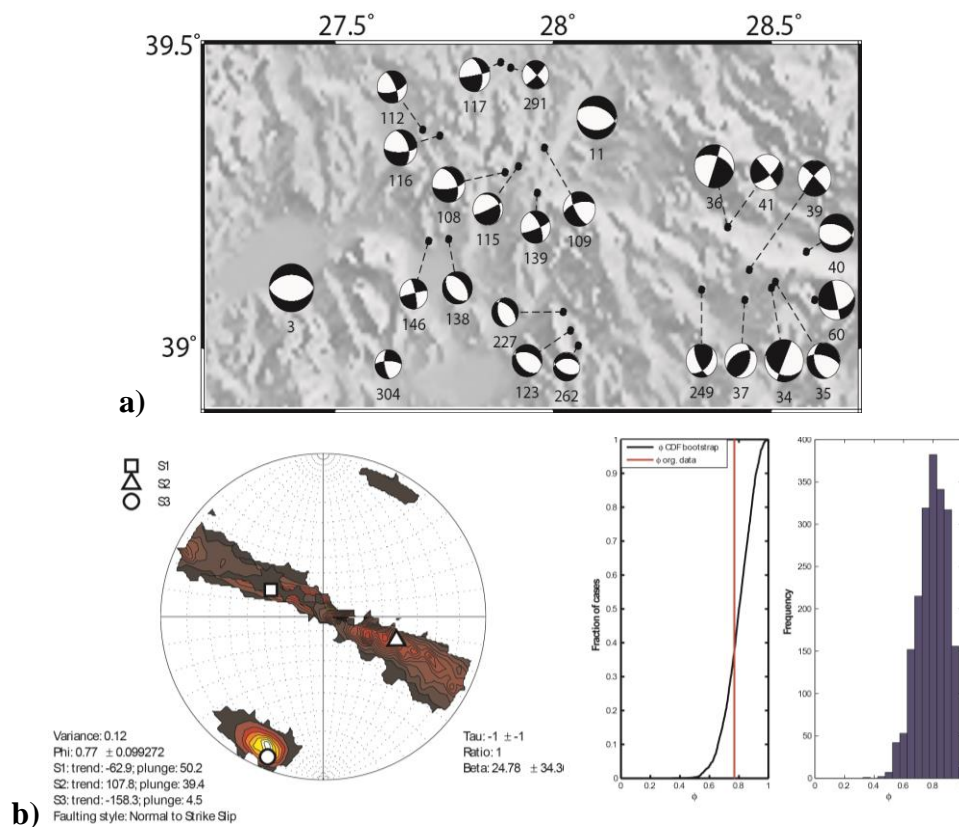


Figure 4.13: a) Close-up map of the Soma sub-region showing topography and focal mechanism solutions and b) results of stress tensor inversion and histogram of stress ratio (R) vs frequency for Soma sub-region.

4.3.1.7 Bakırçay Graben (Sub-region 07)

This sub-domain is situated at the north-western margin of the study area adjacent to the Soma region and coincides with Bakırçay Graben area. The region is characterized by strike-slip and normal earthquake solutions (Figure 4.14a). The stress tensor inversion for the area shows that σ_2 is vertically oriented in the region (Figure 4.14b). σ_1 is sub horizontal in the region and σ_3 trends in SW-NE direction. The orientations are consistent with the trends of faulting in the area. Stress ratio is 0.96 indicating that σ_1 and σ_2 are close in magnitude. The sub-region is characterized by strike-slip regime.

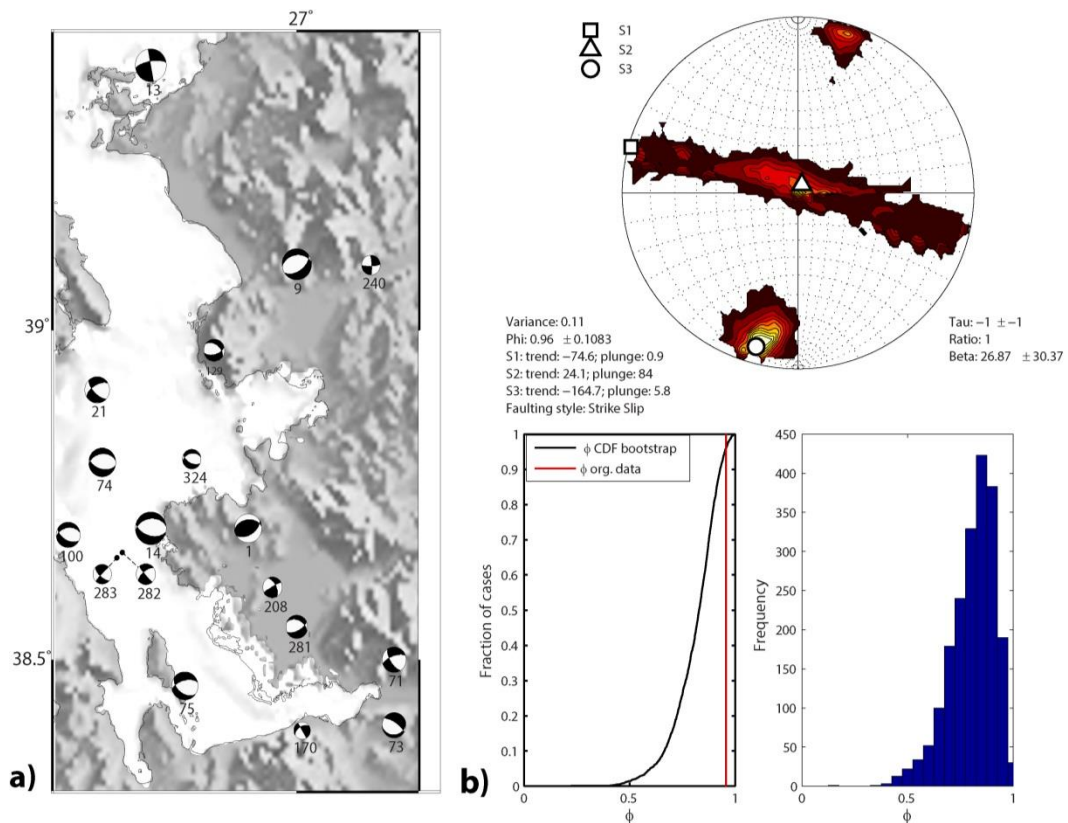


Figure 4.14: a) Close-up map of the Bakırçay Graben sub-region showing topography and focal mechanism solutions and b) results of stress tensor inversion and histogram of stress ratio (R) vs frequency for Bakırçay sub-region.

4.3.1.8 Gulf of Sığacık (Sub-region 08)

The earthquake catalogue for the area is comprised of 67 earthquakes with 49 events related to the Gulf of Sığacık earthquake sequence of 2005 (Figure 4.15a). The area is dominated by strike-slip earthquakes with some normal earthquake events. The solutions of Gulf of Sığacık earthquake sequence indicate that the sequence was characterized by strike-slip events. The stress tensor inversion results for this area show that σ_2 is directed vertically in the region; σ_3 is sub-horizontal striking in SW–NE direction and σ_1 strikes in SE–NW direction (Figure 4.16a). The Variance value (0.098) is lower and suggests a homogenous stress field for the area. Stress ratio is 0.78, and the sub-region is characterized by strike-slip faulting. The trend of σ_1 is predominantly E–W and is consistent with the regional trend. The stress tensor inversion for the area has also been carried out excluding the focal mechanism solutions of Gulf of Sığacık earthquake sequence. The results are shown in Figure 4.16b, which indicates that the results are almost the same with minor changes in the orientations of principal stress axes. Stress ratio (0.78 and 0.68) and variance (0.098 and 0.067) also show minor difference.

4.3.1.9: Gulf of Gökova (Sub-region 09)

The catalogue for the area consists of 67 earthquakes and is dominated by normal events with few strike-slip events at its western margin (Figure 4.17a). The inversion results for region shows that σ_1 is oriented vertically with σ_2 striking in NW–SE. σ_3 trends in SE–NW direction (Figure 4.17b), which is consistent with the trend of faulting in the area. The variance here is 0.15, which is a bit higher but is still within the acceptable range (0.2). The reason may be due complex fault orientations in the region which leads to the development of heterogeneous stress fields. Stress ratio is 0.39 and the sub-region is characterized by normal faulting.

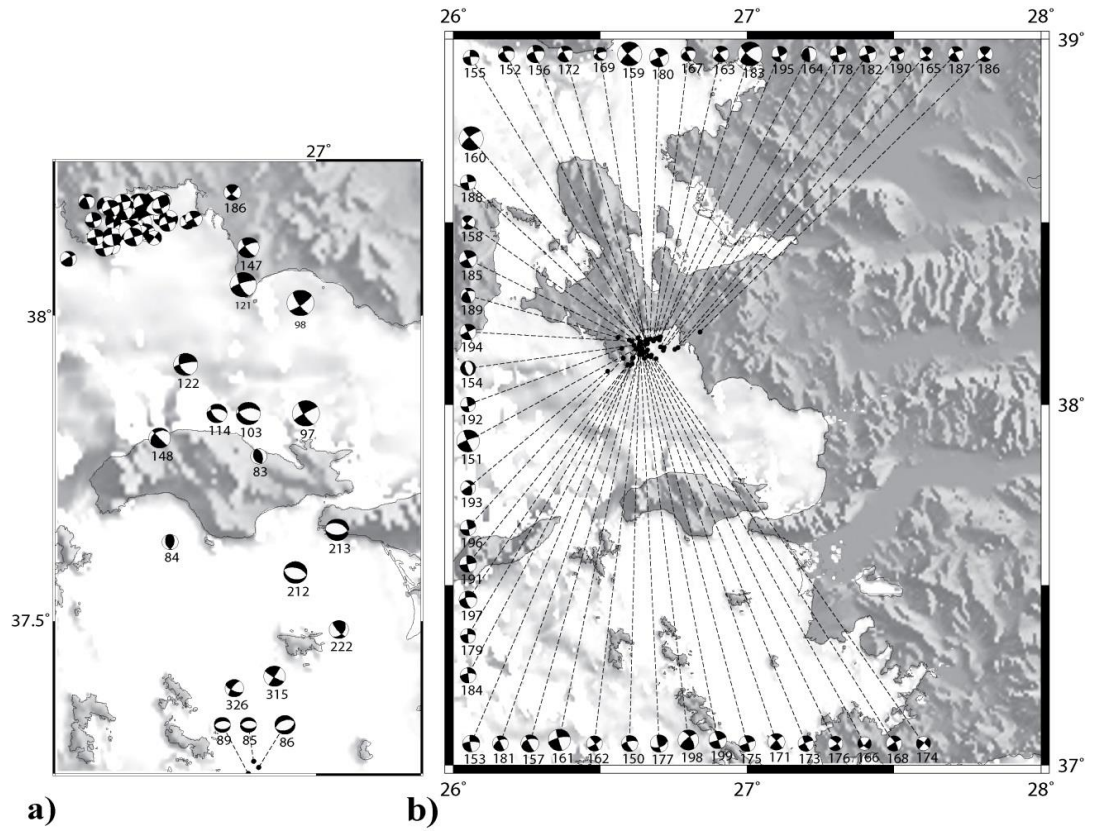


Figure 4.15: a) Map of the gulf of Sığacık sub-region showing topography and focal mechanism solutions. The seismic cluster at the top-left is related to Gulf of Sığacık earthquake sequence; b) Close-up view of the Gulf of Sığacık earthquake sequence.

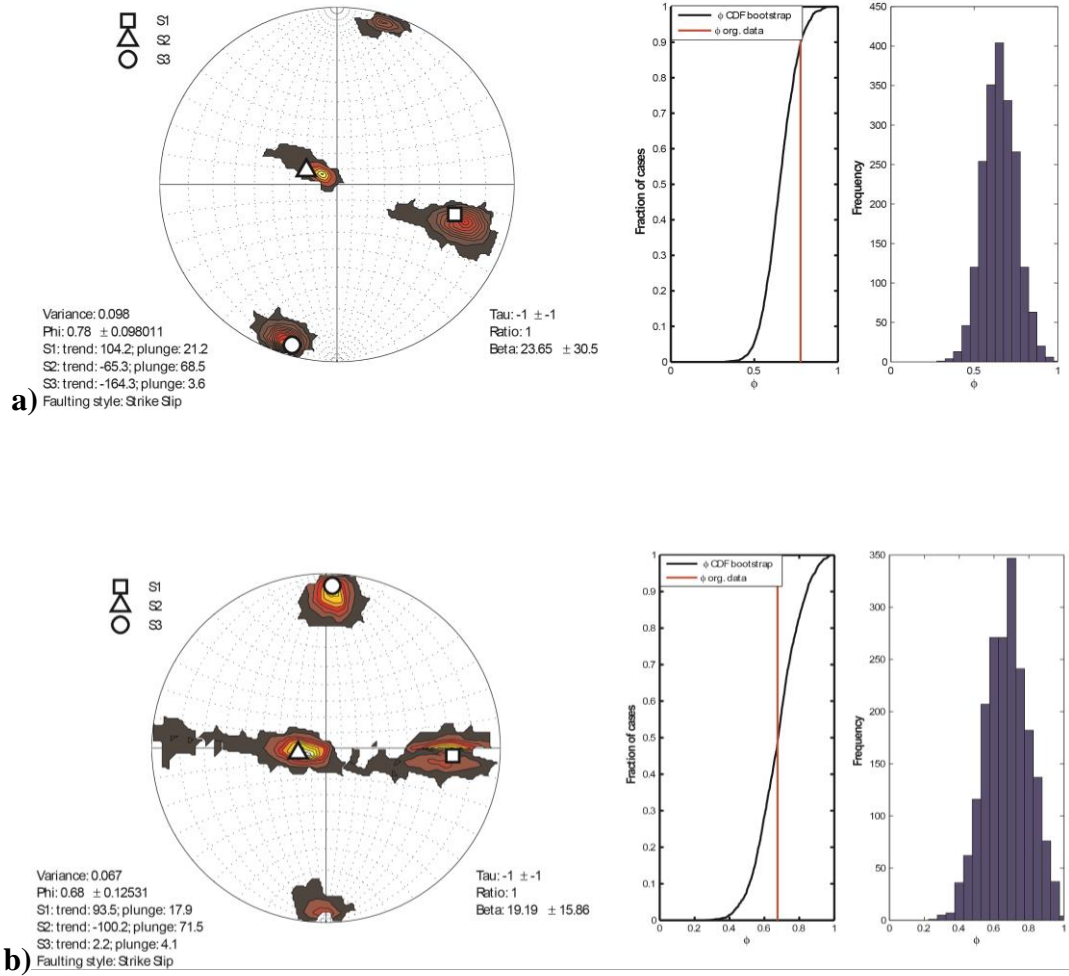


Figure 4.16: **a)** Results of stress tensor inversion and histogram of stress ratio (R) vs frequency for Gulf of Sığacık sub-region and **b)** results of stress tensor inversion and histogram of stress ratio (R) vs frequency for the sub-region excluding the cluster related to the Gulf of Sığacık earthquake sequence.

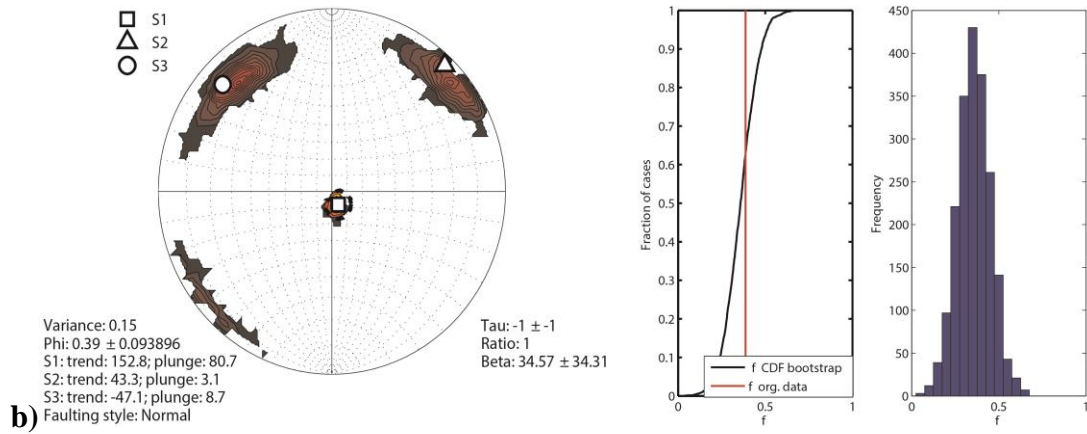
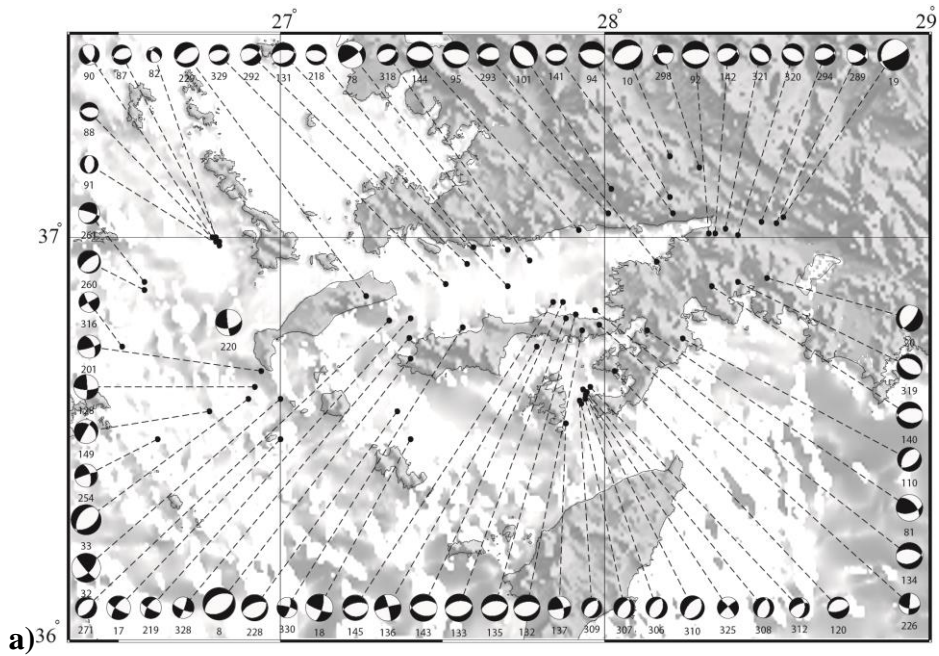
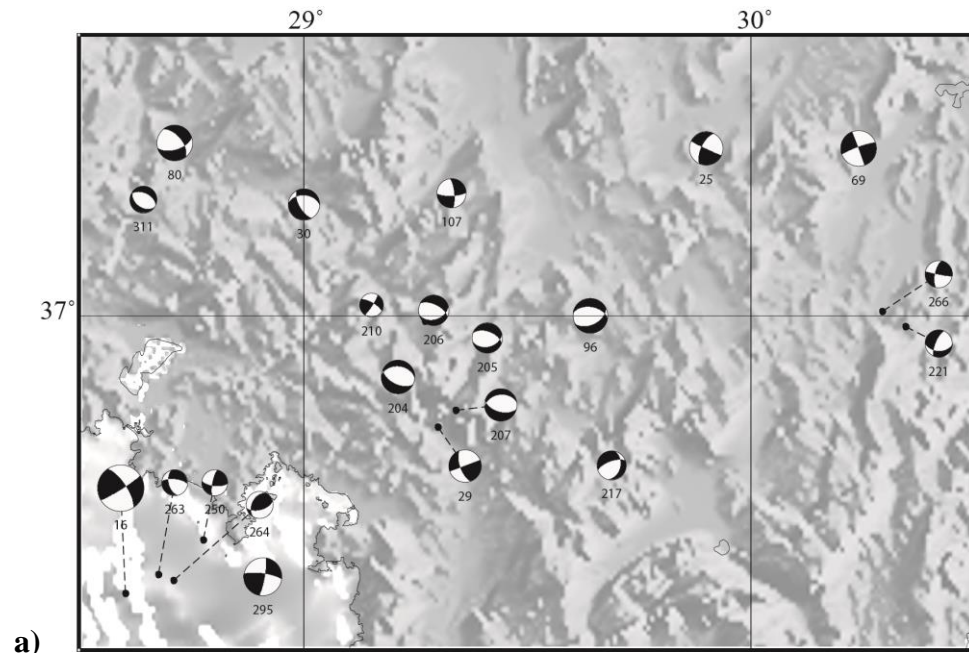


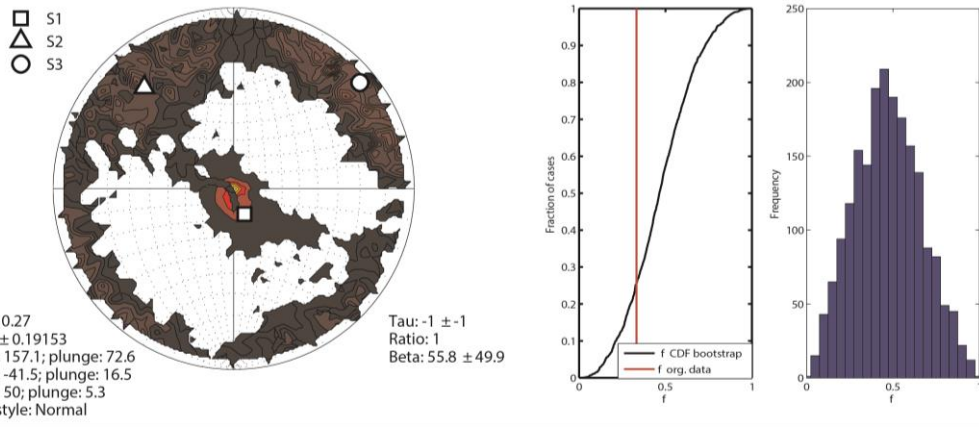
Figure 4.17: a) Close-up map of the Gulf of Gökova sub-region showing topography and focal mechanism solutions and b) results of stress tensor inversion and histogram of stress ratio (R) vs frequency for Gökova sub-region.

4.3.1.10 Fethiye Region (Sub-region 10)

Fethiye region is characterized by complex faulting pattern. The separation of focal mechanism solutions for Fethiye (sub-region 10) from Gulf of Gökova sub-region is difficult in the offshore. The region is characterized by normal, strike-slip and few thrust fault mechanisms (Figure 4.18a). The thrust events (events no. 264, 23 and 105; the latter two events are omitted) are present in the offshore region, which correlates with subduction along Aegean Arc. The stress inversion result in this area shows a complex stress pattern. σ_1 is vertical (to sub-vertical) in this region; σ_3 is sub-horizontal trending in NE–SW direction but is diffused (Figure 4.18b). Stress ratio is 0.33 indicating that σ_2 and σ_3 are close in magnitude in agreement with multi-directional extension. The sub-region is characterized by normal faulting regime. Variance value in the area is high (0.27) and is above the permissible range (0.2). The reason may be due to heterogeneous stress field which can be explained by the complex faulting pattern in the area. Other reason may be due to small number of events present in the area as compared to the scale of the area.



a)



b)

Figure 4.18: a) Close-up map of the Fethiye sub-region showing topography and focal mechanism solutions and b) results of stress tensor inversion and histogram of stress ratio (R) vs frequency for Fethiye sub-region.

4.3.2 Stress Tensor Analysis by Win-Tensor Program

TENSOR program uses an interactive process of stress tensor calculation and data separation for obtaining good quality tensor solutions (Delvaux and Sperner, 2003). In Win-Tensor (windows version of TENSOR) interactive graphical “Right Dihedron method” is used for the determination of possible range of orientations σ_1 and σ_3 . These results are used as a starting point for iterative grid-search “Rotational Optimization” technique. The misfit function in “Rotational Optimization” allows minimizing the angular deviation between the observed and theoretical slip directions and maximizes the shear stress magnitude on the focal planes. The results of stress tensor inversion using Slick method (Michael, 1984, 1987) and Win-Tensor program (Delvaux and Sperner, 2003) are compared in Table 4.1. The results obtained by both these methods are similar with minor differences except for sub-region 4 (Dinar-Burdur). In sub-region 04, the resultant orientations of σ_2 and σ_3 which are sub-horizontal deviate up to 45° between both methods. The results obtained for this region also shows very low stress ratio (0.14 and 0.33), which implies that the difference between the magnitudes of σ_2 and σ_3 is small in this region that will in turn suggest multi-directed extension. The region is characterized by orthogonal fault patterns, which may be associated to multi-directed extension.

Figure 4.19 illustrates the principal stress axes calculated by Win-Tensor program for each sub-region. The arrows indicate relative horizontal stresses while vertical stresses are shown by a circle between the arrows. Outward red arrows show extensional stresses (σ_3) while inward blue (σ_3) and green (σ_2) arrows show compressional stresses. The resultant stress distribution indicates that σ_3 is sub-horizontal in all the subsets and is oriented mostly in NNE-SSW direction except sub-regions 4, 9 and 10. Sub-region 4 (Dinar-Burdur) and 10 (Fethiye) which are located in south eastern part of the study area coinciding with the Fethiye-Burdur fault zone; display a clockwise shift leading to dominant NE-SW directed extension. On the other hand, Gökova (sub-region 9), display an anticlockwise shift where extension direction is oriented NW-SE. In sub-regions 6, 7 and 8, σ_1 is oriented in WNW-ESE direction and more sub-horizontal indicating stress

conditions suitable for strike-slip regime. In other sub-regions, σ_1 is oriented close to vertical in agreement with normal faulting.

Table 4.1 Comparison of stress tensor inversion results for the whole region and sub-regions; using slick method (Michael, 1987) and method using right dihedron with rotational optimization in Win-Tensor program (Delvaux and Sperner, 2003). Results of slick method are given in the upper row and results of Win-Tensor program are given in the lower row for each sub-region.

Region	σ_1 (tr)	σ_1 (pl)	σ_2 (tr)	σ_2 (pl)	σ_3 (tr)	σ_3 (pl)	Phi (R)	Variance	Faulting	Beta
Whole	112	77	285	13	15	2	0.59±0.05	0.16	N	36±41
	117	80	286	10	16	2	0.51		N	37±36
1	115	83	286	7	16	1	0.59±.08	0.061	N	19±25
	206	89	105	0	15	1	0.48		N	23±22
2	134	82	284	7	14	4	0.41±0.19	0.13	N	28±32
	122	80	272	8	3	5	0.25		N	36±30
3	113	40	308	49	209	7	0.92±0.06	0.02	S	9.5±0.
	104	46	309	41	207	13	0.7		NS	8±5.8
4	113	71	301	18	210	2	0.33±0.17	0.13	N	30±49
	10	75	164	13	255	6	0.14		N	19±41
5	191	77	94	2	4	13	0.71±0.14	0.05	N	19±11
	233	60	105	19	7	21	0.64		N	14±11
6	297	50	108	39	202	5	0.77±0.09	0.12	N to S	25±34
	298	36	98	52	201	9	0.99		SS	28±34
7	285	1	24	84	195	6	0.96±0.11	0.11	S	26±30
	284	2	68	88	194	1	0.92		S	27±29
8	104	21	295	69	196	4	0.78±0.09	0.098	S	24±30
	98	13	272	77	8	1	0.36		S	23±30
9	153	81	43	3	313	9	0.39±0.09	0.15	N	34±34
	169	78	33	9	302	8	0.38		N	29±33
10	157	73	318	17	50	5	0.33±0.19	0.27	N	56±50
	161	60	341	30	251	0	0.29		N	56±37

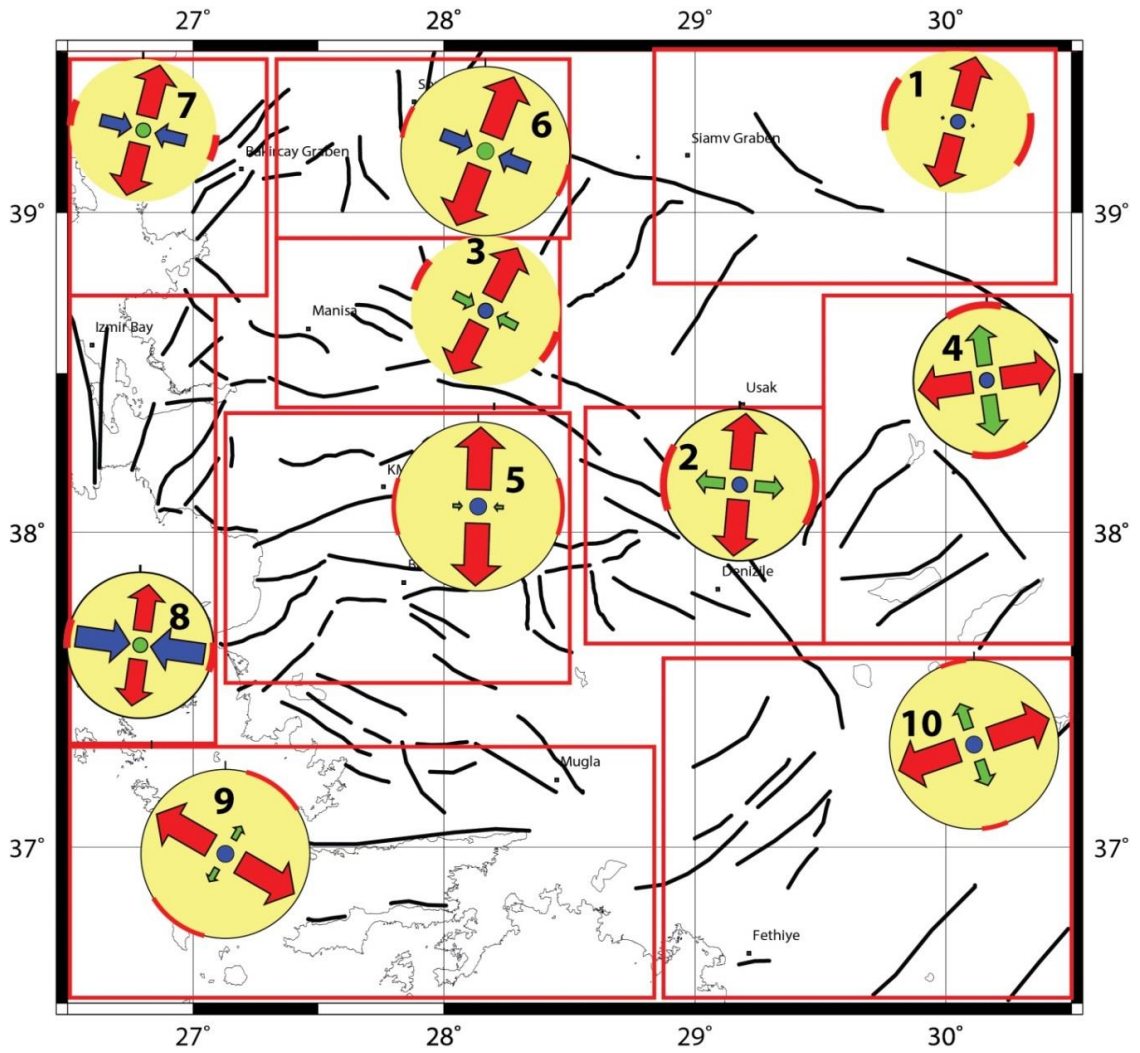


Figure 4.19: Map showing horizontal projection of principle stresses calculated using Win-Tensor program (Delvaux and Sperner, 2003) for all sub-regions (blue: σ_1 , green: σ_2 , red: σ_3).

4.4 Horizontal Stress Directions

Tectonic stress field is expressed generally in terms of maximum horizontal stress direction (S_{Hmax}). For this purpose S_{Hmax} of the individual focal mechanisms used in this study are calculated according to Lund and Townend (2007) within Win-Tensor program (Appendix A). In order to compare with tectonic structures, S_{Hmax} orientations along with regime types are plotted using the World Stress Map's (WSM) web-based source program CASMO (available at www.world-stress-map.org) following the World Stress Map Project guidelines (Figure 4.20). Overall, the revealed S_{Hmax} directions are parallel or sub-parallel to the mapped fault trends. The central portion of the study area including Alaşehir, BMG-KMG, Manisa and Soma sub-regions show NW–SE oriented S_{Hmax} directions, while the north-western parts of the study area and Simav region display dominantly E-W orientations. The orientations of S_{Hmax} are complex in Gulf of Gökova region (sub-region 09) and changes significantly within short distances. In the southeast, where Fethiye and Dinar-Burdur sub-regions are located, S_{Hmax} is commonly oriented in perpendicular directions suggesting active orthogonal faulting possibly due to multi-directed extension. The rose diagrams of S_{Hmax} and S_{Hmin} constructed using the entire database shows that the dominant direction of S_{Hmax} and S_{Hmin} are WNW–ESE and NNE–SSW respectively (Figure 4.21). A similar S_{Hmax} map of the study area is also constructed using the available database of World Stress Map Project (Heidbach, *et al.*, 2008 and the references therein) which is given in Figure 4.22. Since our database is recently updated, it includes more focal mechanism solutions leading to more complete stress map of the study area.

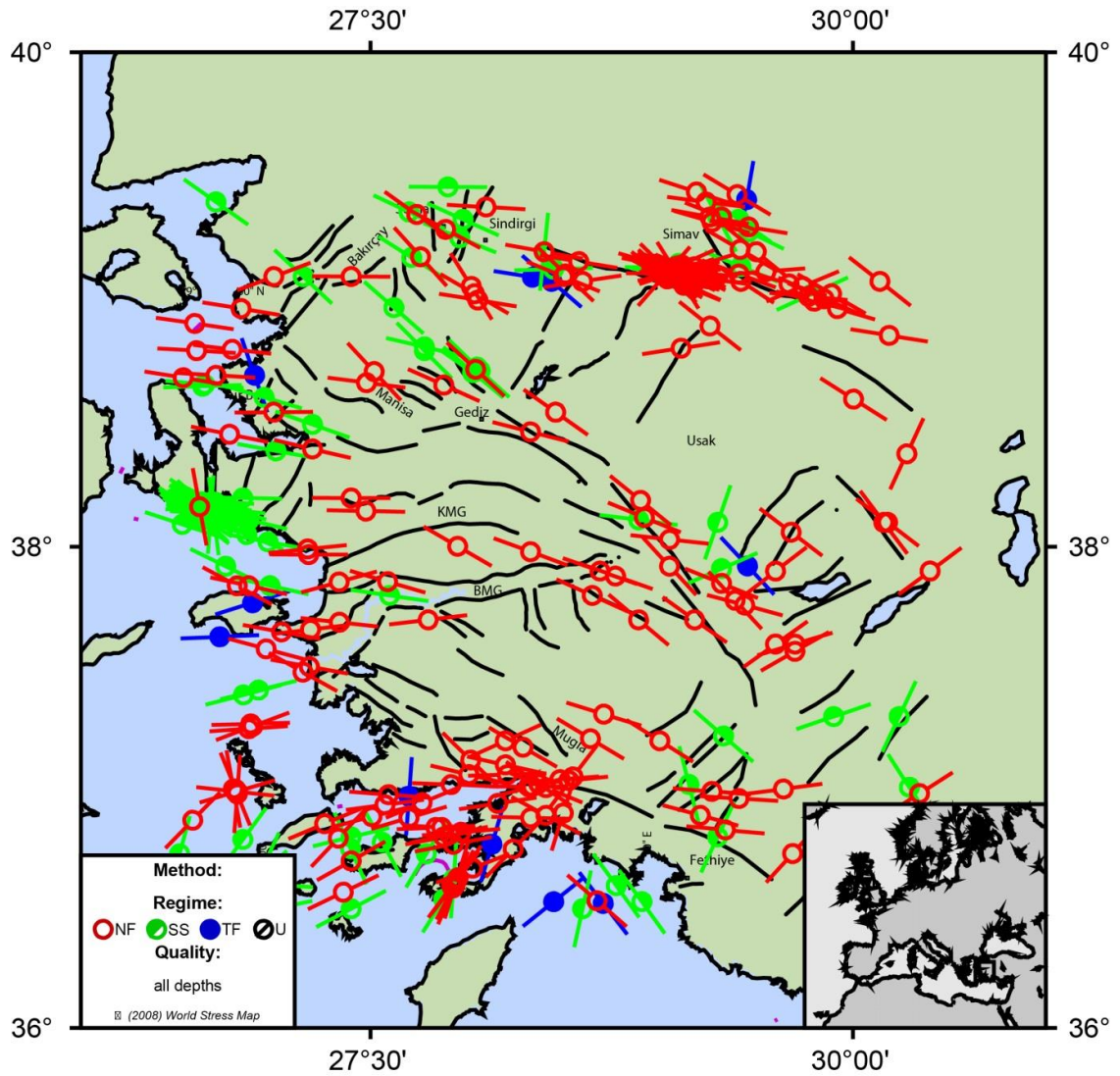


Figure 4.20: Stress map displaying maximum horizontal stress axes (S_{Hmax}) associated to each focal mechanism solution used in this study. Tectonic regime is color coded. Note that the resultant S_{Hmax} and S_{Hmin} axes are listed in the Appendix A.

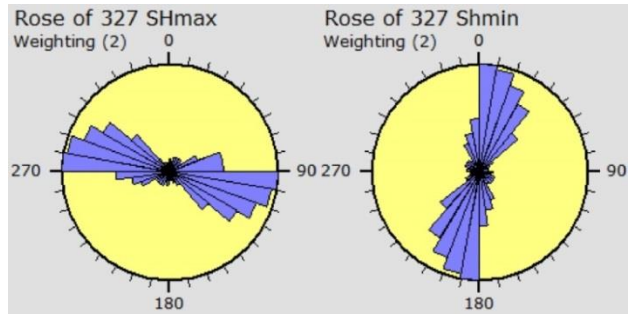


Figure 4.21: Equal area rose diagrams of maximum (S_{Hmax}) and minimum horizontal stress axes (S_{Hmin}).

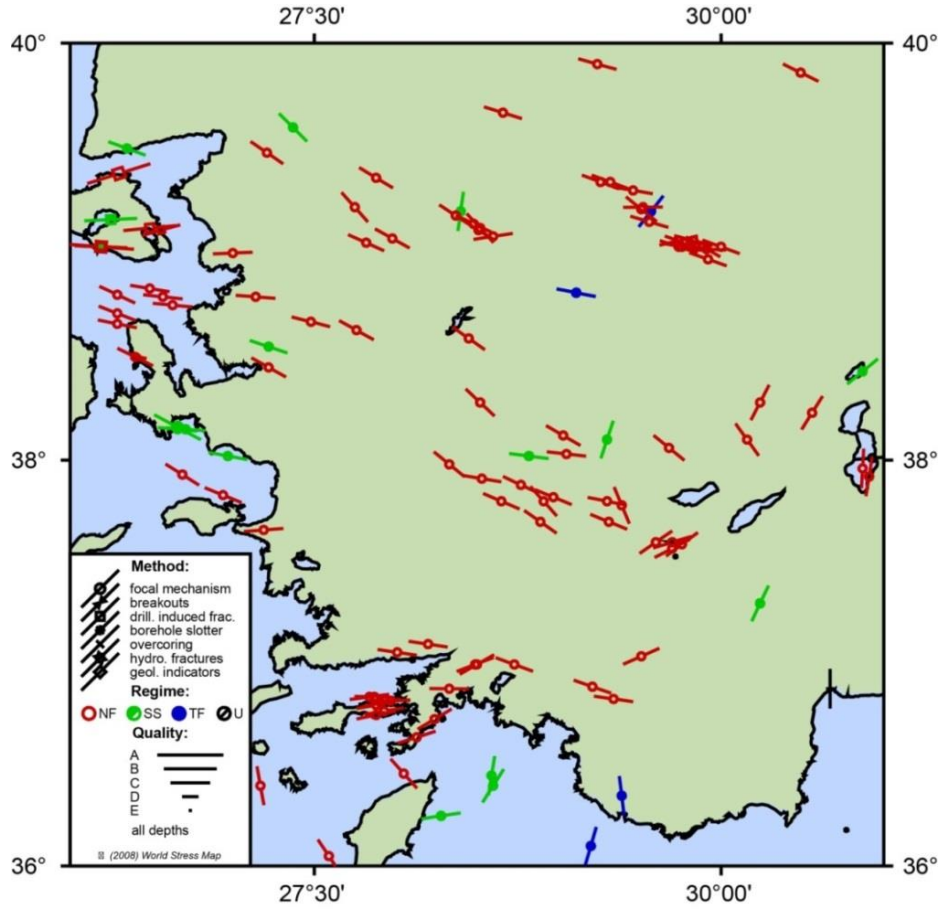


Figure 4.22: Stress map displaying maximum horizontal stress axes (S_{Hmax}) within the study area listed in the World Stress Map (WSM) database (Heidbach *et al.*, 2008 and the references therein).

CHAPTER 5

EARTHQUAKE PROBABILITIES AND FRACTAL DIMENSION OF SEISMICITY

5.1 Introduction

Western Anatolia is one of the most seismically active regions of Turkey and has produced many devastating earthquakes in historical as well as in instrumental period. Therefore, seismic hazard investigation is crucial for the area. The area has been investigated for hazard studies in the past by many researchers using statistical processing of instrumental data. The most recent studies includes Bayrak and Bayrak, 2012b; Çobanoğlu and Alkaya, 2011; Bayrak, *et al.*, 2009, Polat, *et al.*, 2009; Sayil and Osmañahin, 2008; Firuzan, 2008. In this chapter an effort is made to estimate the seismic hazard potential for various sub-regions in western Anatolia using different approaches. The most commonly used approaches for calculating the earthquake hazard parameters includes the Gutenberg-Richter (G-R) relation of earthquake frequency magnitude distribution (Gutenberg and Richter, 1944) and Gumbel annual extreme values analysis (Gumbel 1935, 1958). In this chapter both the methods are used in order to estimate the statistical parameters for sub-regions devised in the previous chapter. The parameters obtained are then used to estimate the probabilities and return periods of earthquakes. In addition, the fractal dimension values (D_c) of each sub-region which will give us an idea about the heterogeneity of seismic activity, are computed using the equations defined by Grassberger and Procaccia (1983).

5.2 Gutenberg-Richter Relation

The empirical relation, Gutenberg-Richter (G-R), between the frequency of earthquakes and their magnitudes in a region is given by the equation:

$$\text{Log (N)} = a - b (M)$$

where ‘N’ is the number of earthquakes with magnitude greater than or equal to ‘M’, ‘a’ is the activity level of seismicity and ‘b’ is the slope of the frequency magnitude distribution. a- and b- values are known as the seismicity parameters and they show significant variations from region to region. For detailed seismic hazard characterization of an area; zonation of the area on the basis of tectonics, geology, spatial variation of a- and b-value parameters and neotectonic properties is very important. In Chapter 3, we observed the spatial variations of a- and b-value parameters for different regions in the study area; therefore a detailed seismic hazard assessment will require subdivision of the area that accommodates these variations. In Chapter 4, we observed that the stress parameters are not constant throughout the area and different regions in the area are characterized by different types of focal mechanism solutions. The area was subdivided into ten (10) sub-regions on the basis of these variations. Therefore, the seismic hazard studies in this chapter are carried out using the same sub-regions as used in the previous chapter.

5.2.1: Data and Methods

The catalogue used for this study is downloaded from KOERI (<http://www.koeri.boun.edu.tr/>) and covers a time interval from 1900–2013. The catalogue used in Chapter 3 is not used in this study because it covers a short time span (1990–2013) and does not have large number of high magnitude earthquakes. The results obtained from that catalogue were checked and they showed high a- and b-values, which in turn will lead to very long return periods and very low earthquake probabilities. Seismic hazard studies are carried out for large magnitude earthquakes, therefore a catalogue that covers a long time interval and having maximum number of

large magnitude earthquakes should be used (i.e. 1900–2013). The same procedures used in Chapter 3, for quarry events removal and declustering are also applied to attain a homogenous catalogue for the area. For declustering only Reasenberg (1984) algorithm is applied; Gardner and Knopoff (1974) algorithm is not used here because it removes a large amount of data (78% of the data). After applying the quarry removal and declustering techniques, 33759 events are left in the catalogue. The catalogue is then subdivided into sub-catalogues on the basis of the geographical proximities of the sub-regions used in Chapter 4.

For computing a- and b- value parameters, the empirical relationship of Gutenberg-Richter (G-R) is used. These parameters depend on the level of seismic activity, the period of observation, the length of the area considered and the sizes of the earthquakes. The analysis is done in ZMAP software package (Wiemer, 2001). The G-R relation is first analyzed using both the automatic Maximum Likelihood Estimate method (MLE) and Weighted Least Square method (WLS). The Gutenberg-Richter relation plots for the whole region using MLE and WLS approaches are shown in Figure 5.1. The plots show that the M_c , a- and b-values for the whole region are 3.4, 6.35 and 0.8 using MLE and 2.8, 6.86 and 0.919 using WLS method respectively (Figures 5.1a and 5.1c). The plots are also obtained for the whole region using events greater than or equal to magnitude 4.0, which gives low a- and b- value for both methods (Figure 5.1b and Figure 5.1d). The plots illustrates that MLE is more dependent on the weight of small magnitude earthquakes, so it may over-estimate the hazard parameters, while WLS uses a weighted approach and the plots are well constrained to large magnitude earthquakes. The trend lines in WLS method are fitting well with the frequency magnitude distribution (FMD). The same observation was confirmed by analyzing the G-R relationships for the sub-regions. Therefore, the parameters estimated by WLS method are used for further analysis in this chapter.

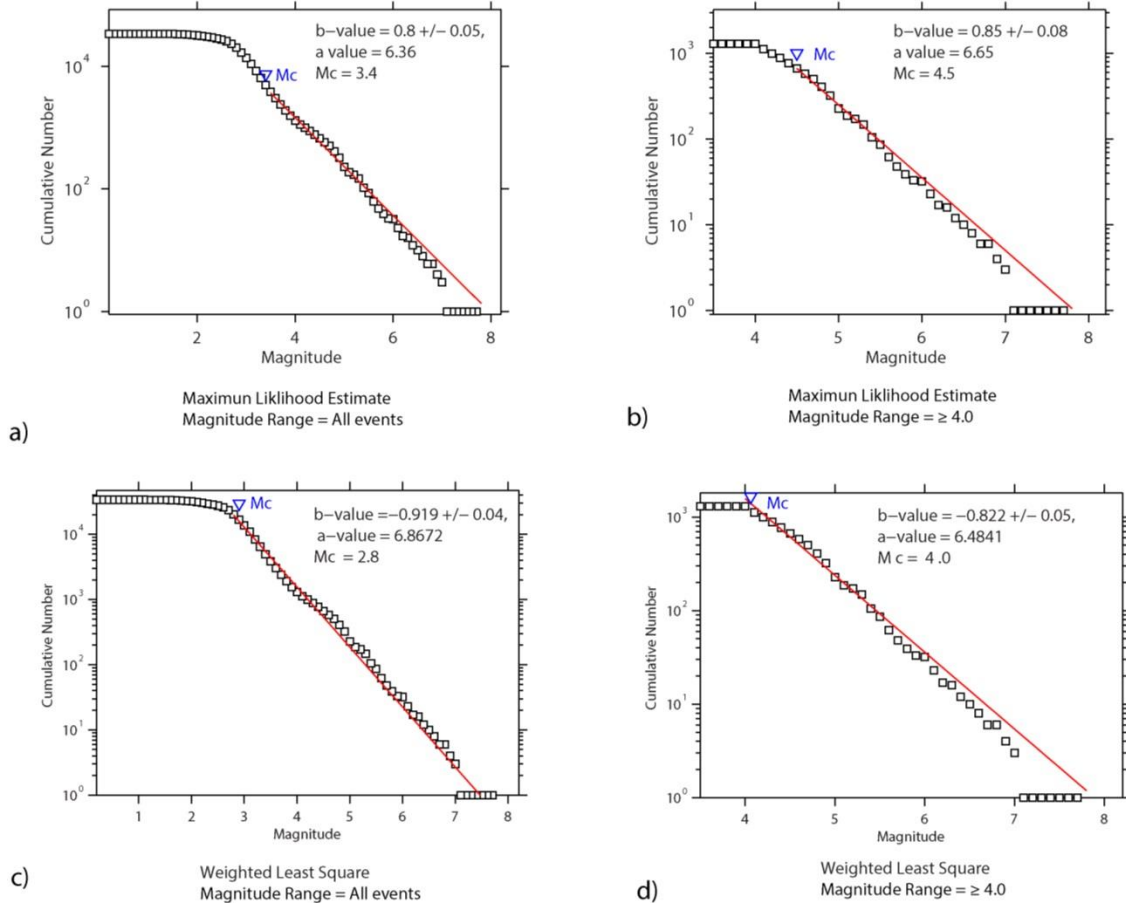


Figure 5.1: The Gutenberg-Richter (G-R) relations obtained for the entire region. **a)** Maximum likelihood estimate (MLE) using all recorded events; **b)** MLE using only earthquake with magnitude greater than or equal to 4.0; **c)** Weighted Least Square estimate (WLS) using all recorded events and **d)** WLS using only earthquake with magnitude greater than or equal to 4.0.

5.2.2 Results

The frequency magnitude distribution (FMD) plots obtained for each sub-region using WLS method are shown in Figure 5.2. Due to large number of small magnitude events in the database, the resultant trend line in FMD plots fits the distribution of smaller magnitude events more effectively than the larger magnitude events (i.e. $M \geq 4.0$). This may lead to the under estimation of earthquake probabilities for those regions. These regions include sub-regions 3, 4, 5, 6, 7 and 8. For sub- regions 1 and 2, the FMD distribution is well fitted by the trend line, while for sub-region 10 the trend of line may overestimate the seismicity parameters. In order to get an idea of the variability of the parameters with higher magnitude cutoffs, the catalogue for each sub-region is cut at magnitude 4.0. The FMD plots for each sub-region are then obtained using weighted least square (WLS) method. After applying the magnitude cutoff ($M \geq 4.0$), the computed a- and b- values showed significant differences from the analysis conducted without any magnitude cutoff. The FMD plots show that the fit of the resultant trend lines are improved for larger magnitude earthquakes (except for sub-regions 4 and 10). Thus, magnitude 4.0 is used as a minimum magnitude cutoff for all the sub-regions. The plots obtained are shown in Figure 5.3.

For both sub-region 4 and 10, automatically computed magnitude of completeness (M_c) is 4.9, which minimized the amount of used earthquake data in the analysis. The higher M_c value obtained for these sub-regions is due to the fact that the earthquake magnitude distribution is not uniform; i.e. some part of magnitude range is missing in these sub-regions. There is a significant change in a- and b- value estimates identified by applying the analysis with and without magnitude cut-off. Thus, the a- and b- values calculated for sub-regions 4 and 10 is counted as less reliable relative to other sub-regions.

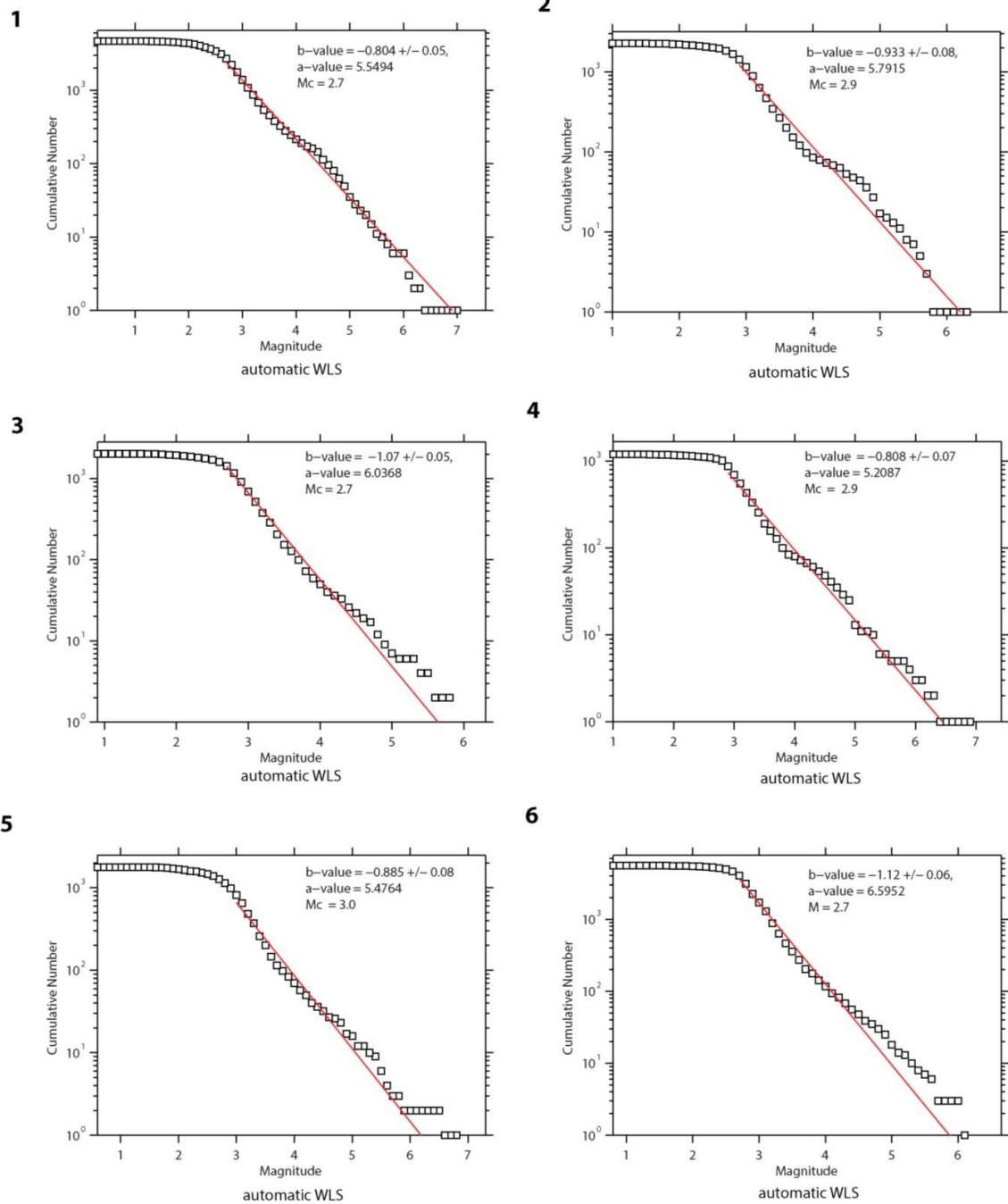
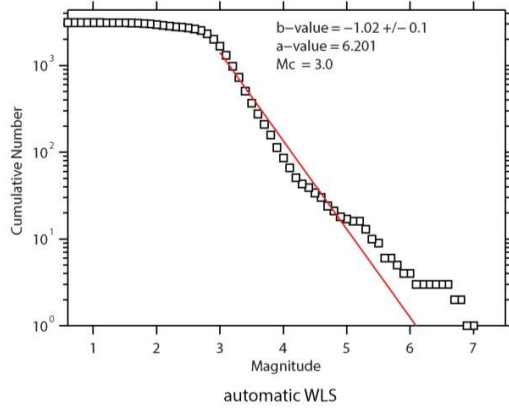
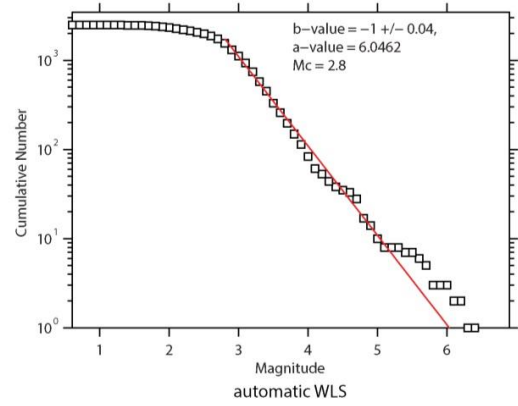


Figure 5.2: Frequency magnitude distribution (FMD) plots of the sub-regions obtained by using the Weighted Least Square (WLS) method. The magnitude of completeness (M_c) is computed automatically. No magnitude cutoff is applied.

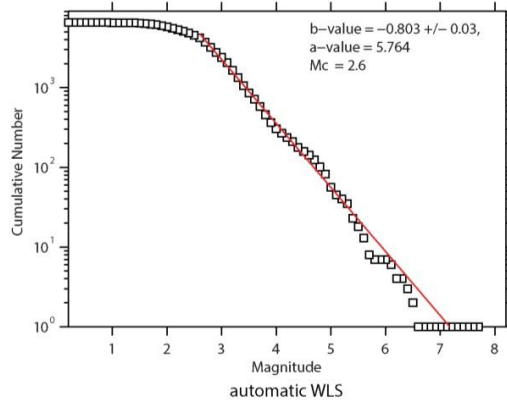
7



8



9



10

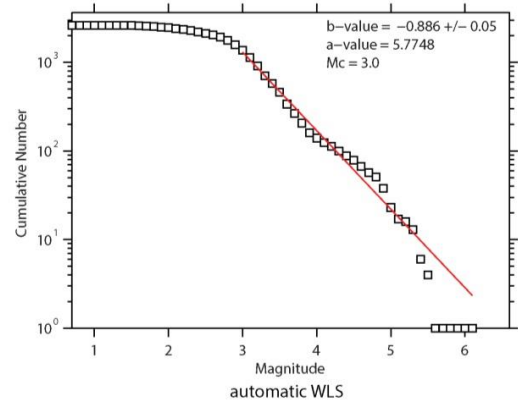


Figure 5.2 (continued)

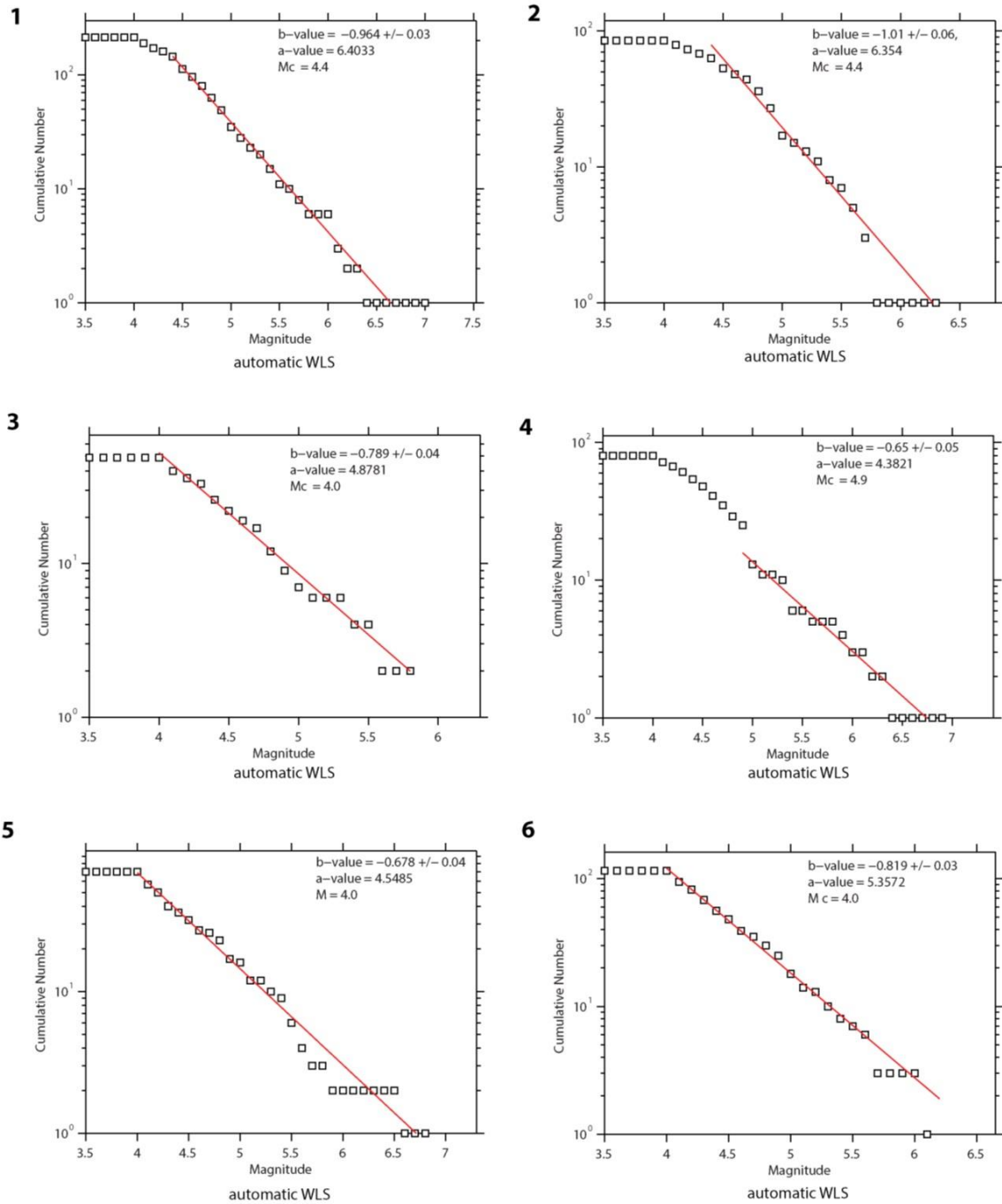


Figure 5.3: Frequency magnitude distribution (FMD) plots of the sub-regions using Weighted Least Square (WLS) with a magnitude cutoff at 4.0. Note that Mc for each region is still automatically computed.

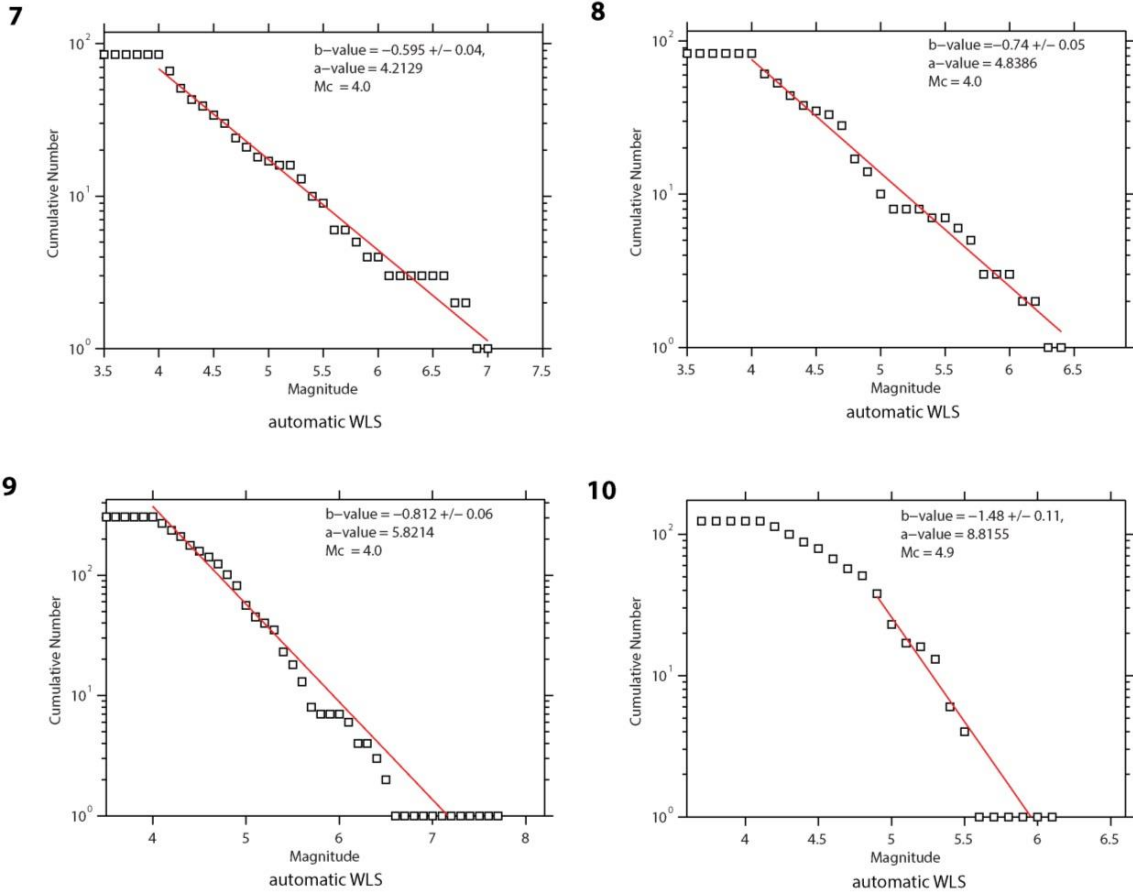


Figure 5.3 (continued)

The computed a- and b- values of each sub-region are categorized and then plotted with color coding for interpretation (Figure 5.4 and 5.5). According to our results sub-regions 4, 5 and 7 (Dinar-Burdur, BMG-KMG and Bakırçay) have the lowest; 1, 2 and 10 (Simav, Alaşehir and Fethiye) have the highest b- values. Low b- values imply high stress conditions where large earthquakes are more frequent and vice versa. The a-value pattern in the area is almost the same as the b-value; i.e. low stress regions (high b- values) characterized by high seismic productivity (high a- values) and vice versa.

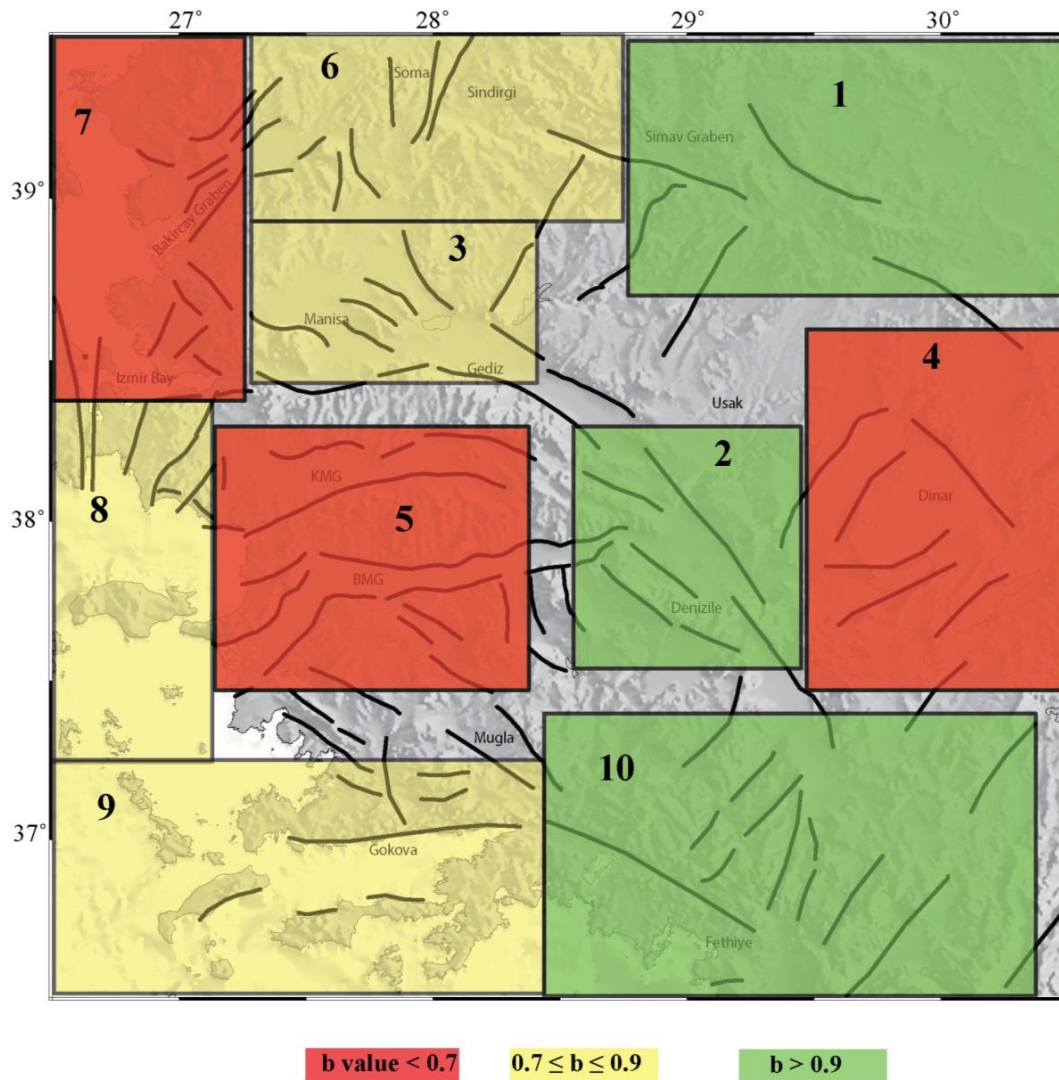


Figure 5.4: Map of b-values computed for sub-regions using Weighted Least Square (WLS) with earthquake magnitude greater than or equal to 4.0. The sub regions are colored according to their b-value.

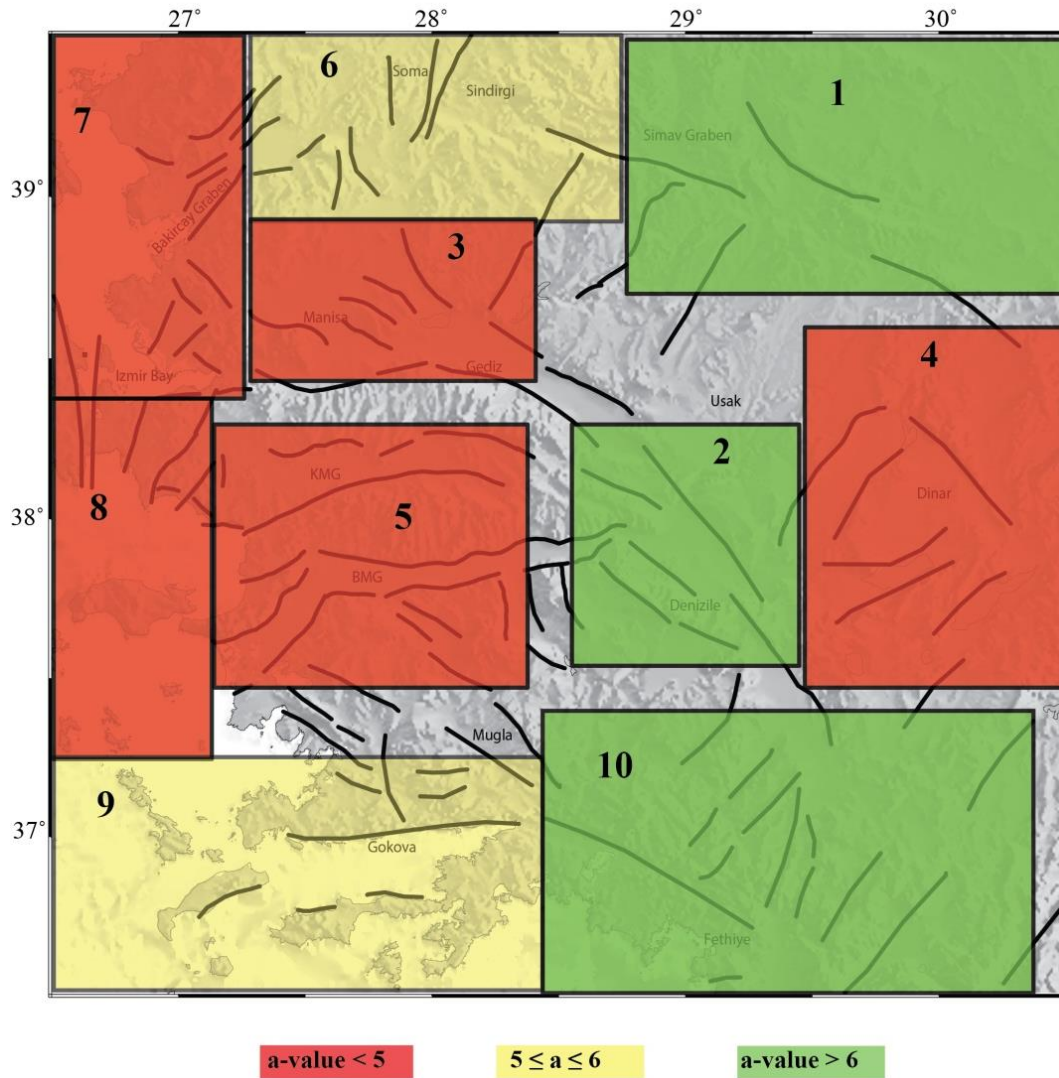


Figure 5.5: Map of a-values computed for sub-regions using Weighted Least Square (WLS) with earthquake magnitude greater than or equal to 4.0. The sub regions are colored according to their a-value.

5.3: Gumbel's Annual Extreme Value Method

Apart from Maximum Likelihood Estimate (MLE) and Weighted Least Square (WLS) method for G-R relation, Gumbel's annual extreme value method (Gumbel 1935, 1958) is also applied in this study to get an idea of changes in the hazard parameters using different approaches. Gumbel's method does not use the entire data, instead it uses only the extreme annual values for the sequence of earthquakes constructed from the largest values of magnitude over a set of predetermined time interval. The distribution of earthquakes in this method is based on the assumptions that: **(a)** the prevailing conditions must be almost the same in the future and **(b)** the observed values are independent of each other. The advantage of this method is that it considers only the extreme values and does not use the whole distribution; which is not complete in time in most of the cases. Another advantage of this method is that it uses large magnitudes which are more accurately determined as compared to the small magnitudes. According to the theory, the distribution of annual maximum earthquakes in a region is given by the equation

$$G(M) = \exp^{-\alpha e^{-\beta M}}$$

where $G(M)$ is the probability of an earthquake within a year which has a magnitude M or smaller than M . Multiplying the equation by natural log (\ln) on both sides, it takes the form

$$\ln [-\ln G(M)] = \ln \alpha - \beta M$$

This is the same form of the Gutenberg-Richter relation. The ' α ' and ' β ' parameters can be estimated from the co-efficient of least square regression. These parameters are related to the ' a ' and ' b ' parameters of Gutenberg- Richter relation by the equations

$$a = \ln \alpha / \ln 10 \text{ and } b = \beta / \ln 10$$

5.3.1 Data, Method and Results

The catalogue used in this method is the same as used for Gutenberg-Richter relation. The catalogue for each sub-region is arranged in a descending order and the maximum magnitude for each year is obtained. The catalogue for each sub-region now contains only the annual maximum magnitudes. There are two approaches for calculating the regression co-efficient: (1) using all the annual maximum magnitudes and assigning a lower magnitude value to the missing years (Tezcan, 1996); (2) using only the events from the period in which we have earthquake records (i.e. continuous record) proposed by Shanker, *et al.*, 2007 and Yadav, *et al.*, (2007). The datasets are checked for both the methods and the results are cross-checked with the G-R method. The second method (using a continuous earthquake record) gives more reliable results as compared to the first method; therefore this method is used for further analysis. The catalogue was arranged in a chronological order, and the time period for each sub-region from where we have a continuous record (no missing years) of earthquakes, was selected. The occurrence probability of earthquakes can be determined by using the equation $G = i / (N+1)$ where 'i' varies from 1 to N (Gumbel, 1958) and 'N' is the total number of observations. The co-efficient ' α ' and ' β ' are then calculated by using linear regression relation between $\ln(-\ln G)$ and the magnitude (M). The results obtained for each sub-region obtained by Gumbel's method are shown in Figure 5.6.

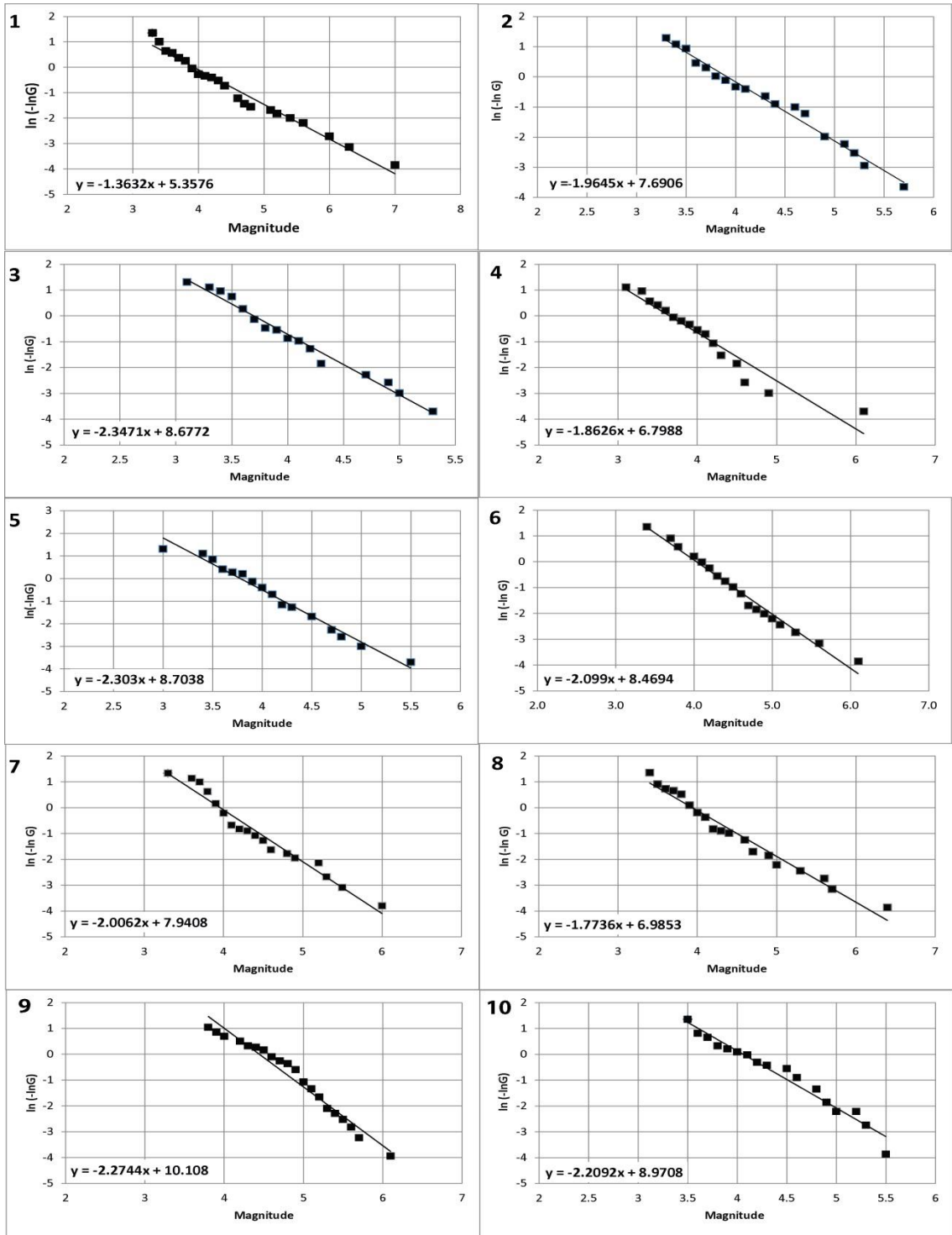


Figure 5.6: Graphs showing the least square regression relations between ‘Magnitude’ and ‘ln (-ln G)’ for sub-regions in the study area. (Adobe)

5.4 Earthquake Probabilities and Return Periods

The a- and b- values obtained from the Gutenberg-Richter relation can be used to estimate the probabilities and return periods for different magnitude earthquakes in a region. The most widely used model for calculating the earthquake probabilities in a region is the Poisson model. This model assumes that the earthquake events in a region are independent of each other in terms of location, time and size. Then the probability or occurrence risk of an earthquake in a region can be estimated by using the below equation

$$P(M) = 1 - e^{-N(M) \times T}$$

where $N(M)$ is the annual mean number of earthquakes with magnitude greater than or equal to Magnitude 'M' occurring in a region in a specific time interval 'T'.

$N(M)$ is obtained from Gutenberg-Richter relation and can be calculated by using the below equation

$$N(M) = 10^{a-bM-\log T_{obs}}$$

where a- and b- values are obtained from the frequency magnitude distribution of Gutenberg-Richter relation and ' T_{obs} ' is the observation interval for each region.

Thus the return period of an earthquake can be calculated using the below equation

$$T_m = 1/N(M)$$

Using derived G-R relations and above equations, probabilities of earthquakes with different magnitudes ($M=5.0$, $M=6.0$, $M=7.0$) for different time intervals (10, 50 and 100 years) are calculated along with the return periods for each sub-region. The results are presented in Table 5.1.

Table 5.1: Table showing a-value, b-value, magnitude of completeness (Mc), observation time (T_{obs}) and the earthquake probabilities (%) in the study area and within each sub-region for magnitudes 5, 6 and 7 and time periods 10, 50 and 100 years. The last column shows the calculated return periods within each category.

Region	b-value	a-value	Mc	T(obs)	M	N(M)	10yrs	50 yrs	100yrs	Tm
Whole	0.822	6.48	4	114	5	2.056341	99.99	99.9	99.9	0.49
				114	6	0.3098	95.49	99.99	99.99	3.23
				114	7	0.046676	37.30	90.31	99.06	21.42
1	0.96	6.4	4.4	70	5	0.568725	99.66	99.90	99.99	1.76
				70	6	0.062359	46.40	95.58	99.80	16.04
				70	7	0.006838	6.61	28.96	49.53	146.2
2	1.01	6.35	4.4	114	5	0.175023	82.63	99.98	99.99	5.71
				114	6	0.017104	15.72	57.48	81.92	58.47
				114	7	0.001671	1.66	8.02	15.39	598.2
3	0.789	4.87	4	88	5	0.095613	61.56	99.16	99.99	10.46
				88	6	0.015542	14.39	54.03	78.86	64.34
				88	7	0.002526	2.49	11.87	22.33	395.8
4	0.65	4.38	4.9	100	5	0.134896	74.05	99.88	99.99	7.41
				100	6	0.0302	26.07	77.91	95.12	33.11
				100	7	0.006761	6.54	28.68	49.14	147.9
5	0.678	4.54	4	101	5	0.139855	75.30	99.91	99.99	7.15
				101	6	0.029355	25.44	76.96	94.69	34.07
				101	7	0.006161	5.98	26.51	46.00	162.3
6	0.81	5.35	4	111	5	0.179753	83.43	99.99	99.99	5.56
				111	6	0.02784	24.30	75.14	93.82	35.92
				111	7	0.004312	4.22	19.39	35.03	231.9
7	0.59	4.21	4	110	5	0.165427	80.88	99.97	99.99	6.04
				110	6	0.042521	34.64	88.07	98.58	23.52
				110	7	0.01093	10.35	42.10	66.48	91.49
8	0.74	4.83	4	110	5	0.122633	70.66	99.78	99.99	8.15
				110	6	0.022316	20	67.23	89.26	44.81
				110	7	0.004061	3.98	18.38	33.37	246.2
9	0.81	5.82	4	95	5	0.619835	99.8	99.99	99.99	1.61
				95	6	0.096001	61.71	99.18	99.99	10.42
				95	7	0.014869	13.82	52.45	77.39	67.25
10	1.48	8.81	4.9	87	5	0.295448	94.79	99.99	99.99	3.38
				87	6	0.009783	9.32	38.69	62.41	102.2
				87	7	0.000324	0.32	1.61	3.19	3086.

The computed earthquake probabilities using G-R relation in each sub-region (Table 5.1) are categorized and plotted with color coding for interpretation. Figures 5.7 and 5.8 illustrate the probability for $M=6.0$ earthquake in 50 years and $M=7.0$ earthquake in 100 years respectively.

According to our estimates, for $M=6.0$ earthquake in 50 years, sub-regions 1, 7 and 9 (Simav, Bakırçay, Gulf of Gökova) have the highest; 2, 3 and 10 (Alaşehir, Manisa and Fethiye) have the lowest; while sub-regions 4, 5, 6 and 8 (Dinar-Burdur, BMG-KMG, Soma and Gulf of Sığacık) have intermediate probabilities (Figure 5.7). For $M=7.0$ earthquake in 100 years, sub-regions 7 and 9 (Bakırçay and Gulf of Gökova) have the highest; 2, 3, 6, 8 and 10 (Alaşehir, Manisa, Soma, Gulf of Sığacık and Fethiye) have the lowest; while sub-regions 1, 4, 5 (Simav, Dinar-Burdur, BMG-KMG) have intermediate probabilities (Figure 5.8).

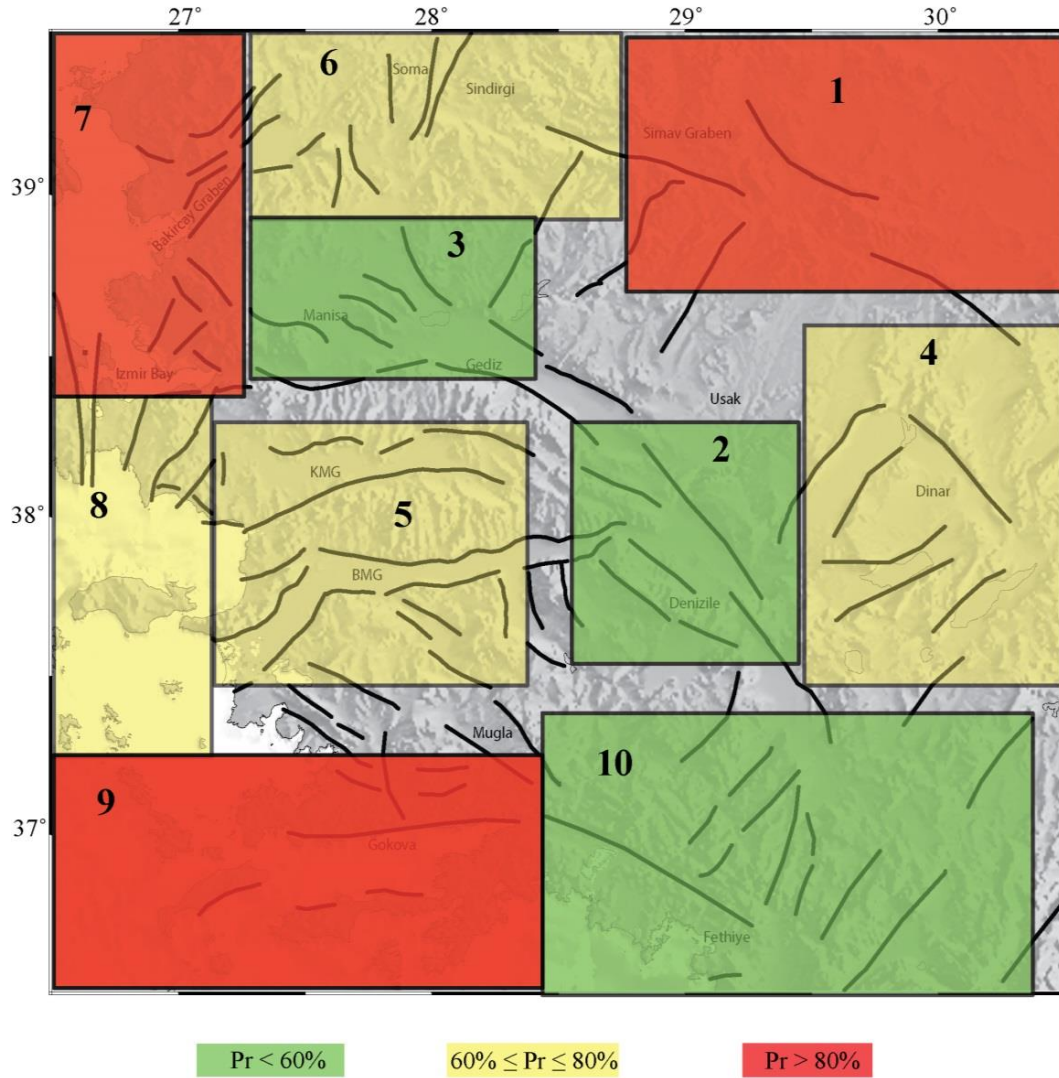


Figure 5.7: The Gutenberg-Richter (G-R) relation based map showing earthquake probabilities (Pr) of sub-regions for a magnitude 6 event within 50 years. Pr values (in %) are taken from Table 5.1.

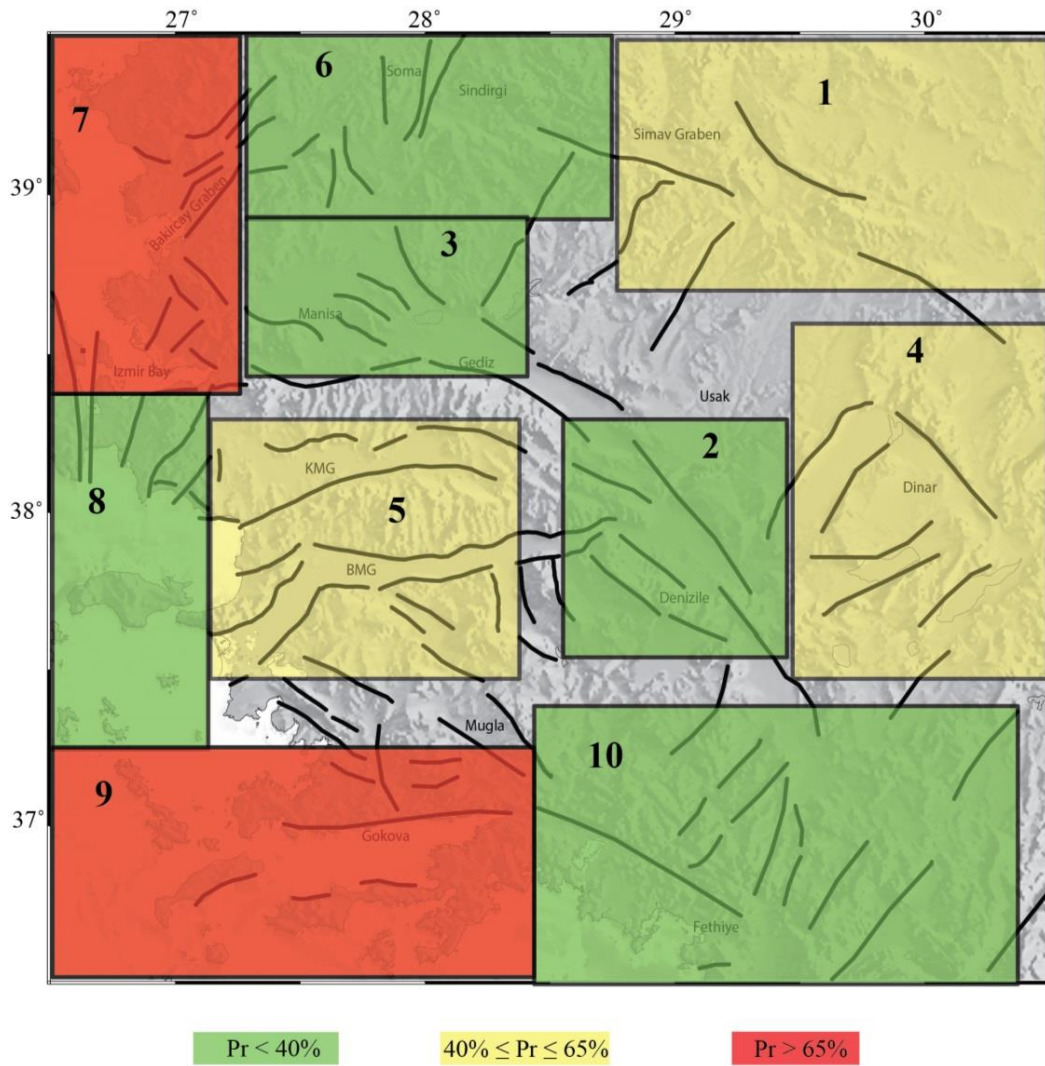


Fig. 5.8: The Gutenberg-Richter (G-R) relation based map showing earthquake probabilities (Pr) of sub-regions for a magnitude 7 event within 100 years. Pr values (in %) are taken from Table 5.1.

For Gumbel method the return periods and probabilities of earthquakes in specific time interval in a region can be calculated using the formulas given below. The ‘ α ’ and ‘ β ’ values are obtained from the regression co-efficient of the Gumbel extreme distribution for each sub-region shown in Figure 5.6.

$$N (M) = \alpha / e^{\beta M}$$

$$T_m = 1/N (M) = e^{\beta M} / \alpha$$

$$P (M) = 1 - e^{-N (M) \times T}$$

where ‘ $N (M)$ ’ is the annual mean seismicity rate, ‘ T_m ’ is the return period and ‘ $P (M)$ ’ is the probability of magnitude ‘ M ’ in certain years ‘ T ’. The earthquake probabilities and return periods obtained from Gumbel method are presented in Table 5.2.

From comparison of the results of both methods (Table 5.1 and Table 5.2), it can be noted that Gumbel method gives relatively long return periods and low probability values as compared to G-R method. The reason is due to the fact that ‘ $\ln\alpha$ ’ parameter, calculated from the intercept of Gumbel distribution, has small values. ‘ $\ln\alpha$ ’ can be in turn used to calculate the a- value of G-R relation ($a = \ln \alpha / \ln 10$). The comparison shows that the a-values obtained from Gumbel method are very low as compared to the a-values obtained from the G-R method for all the sub-regions. The short observation times for Gumbel method as compared to the G-R method can be another reason for obtaining lower probabilities. Previous studies also suggests that Gumbel method gives low a- values as compared to G-R method which will in turn lead to low probabilities and long return periods (Bayrak *et al.*, 2008; Özmen, 2014).

Table 5.2: Table showing the M_{min} , α , β and the earthquake probabilities (%) in the study area and within each sub-region for magnitudes 5, 6 and 7 and time periods 10, 50 and 100 years. The last column shows the calculated return periods within each category.

Region	Tobs	Mmin	β	$\ln\alpha$	α	M	N(M)	10yrs	50yrs	100yrs	Tm
Whole	51	4.3	2.09	10.656	42446.51	5	1.228753204	99.9	99.9	99.9	0.81
						6	0.151980964	78.1	99.9	99.9	6.58
						7	0.01879809	17.1	60.9	84.73	53.2
1	46	3.3	1.36	5.35	210.6083	5	0.234570288	90.4	99.9	99.99	4.26
						6	0.060204992	45.2	95.1	99.75	16.61
						7	0.01545226	14.3	53.8	78.67	64.7
2	38	3.3	1.96	7.69	2186.375	5	0.121237966	70.2	99.7	99.99	8.25
						6	0.017077389	15.6	57.4	81.87	58.56
						7	0.002405494	2.37	11.3	21.38	415.7
3	40	3.1	2.34	8.67	5825.499	5	0.048315638	38.3	91.1	99.2	20.7
						6	0.004654131	4.54	20.7	37.21	214.8
						7	0.000448321	0.44	2.21	4.38	2230
4	40	3.1	1.86	6.79	888.9136	5	0.08126823	55.6	98.2	99.97	12.30
						6	0.01265124	11.8	46.8	71.77	79.04
						7	0.00196945	1.95	9.37	17.87	507.7
5	40	3	2.3	8.7	6002.912	5	0.060810063	45.5	95.2	99.77	16.44
						6	0.006096747	5.91	26.2	45.64	164
						7	0.000611253	0.6	3.01	5.92	1635
6	47	3.4	2.09	8.46	4722.058	5	0.136695425	74.5	99.8	99.99	7.32
						6	0.016907466	15.5	57.1	81.56	59.15
						7	0.002091236	2.06	9.92	18.87	478.1
7	44	3.3	2.00	7.94	2807.361	5	0.123687136	70.9	99.7	99.99	8.08
						6	0.016639099	15.3	56.4	81.06	60.10
						7	0.002238386	2.21	10.5	20.05	446.7
8	47	3.4	1.77	6.98	1074.918	5	0.154123662	78.5	99.9	99.9	6.49
						6	0.026252344	23.0	73.1	92.75	38.09
						7	0.00447164	4.37	20	36.05	223.6
9	51	3.8	2.27	10.1	24343.01	5	0.286504797	94.3	99.9	99.9	3.49
						6	0.029599435	25.6	77.2	94.81	33.78
						7	0.003057982	3.01	14.1	26.34	327
10	47	3.5	2.20	8.97	7863.602	5	0.125556427	71.5	99.8	99.99	7.96
						6	0.013787402	12.8	49.8	74.81	72.53
						7	0.001514	1.5	7.29	14.04	660.5

The computed earthquake probabilities using Gumbel annual extreme method in each sub-region (Table 5.2) are categorized and plotted with color coding for interpretation. Figures 5.9 and 5.10 illustrate the probability for $M=6.0$ earthquake in 50 years and $M=7.0$ earthquake in 100 years respectively.

According to our estimates for $M=6.0$ earthquake in 50 years, sub-regions 1, 8 and 9 (Simav, Gulf of Sığacık and Gulf of Gökova) have the highest; 3 and 5 (Manisa and BMG-KMG) have the lowest; while others have intermediate probabilities (Figure 5.9). For $M=7.0$ earthquake in 100 years, sub-region 1 (Simav) have the highest; 3, 4, 5, 6 and 10 (Manisa, Dinar-Burdur, BMG-KMG, Soma and Fethiye) have the lowest; while others have intermediate probabilities (Figure 5.10).



Figure 5.9: The Gumbel annual extreme method based map showing earthquake probabilities (Pr) of sub-regions for a magnitude 6 event within 50 years. Pr values (in %) are taken from Table 5.2.

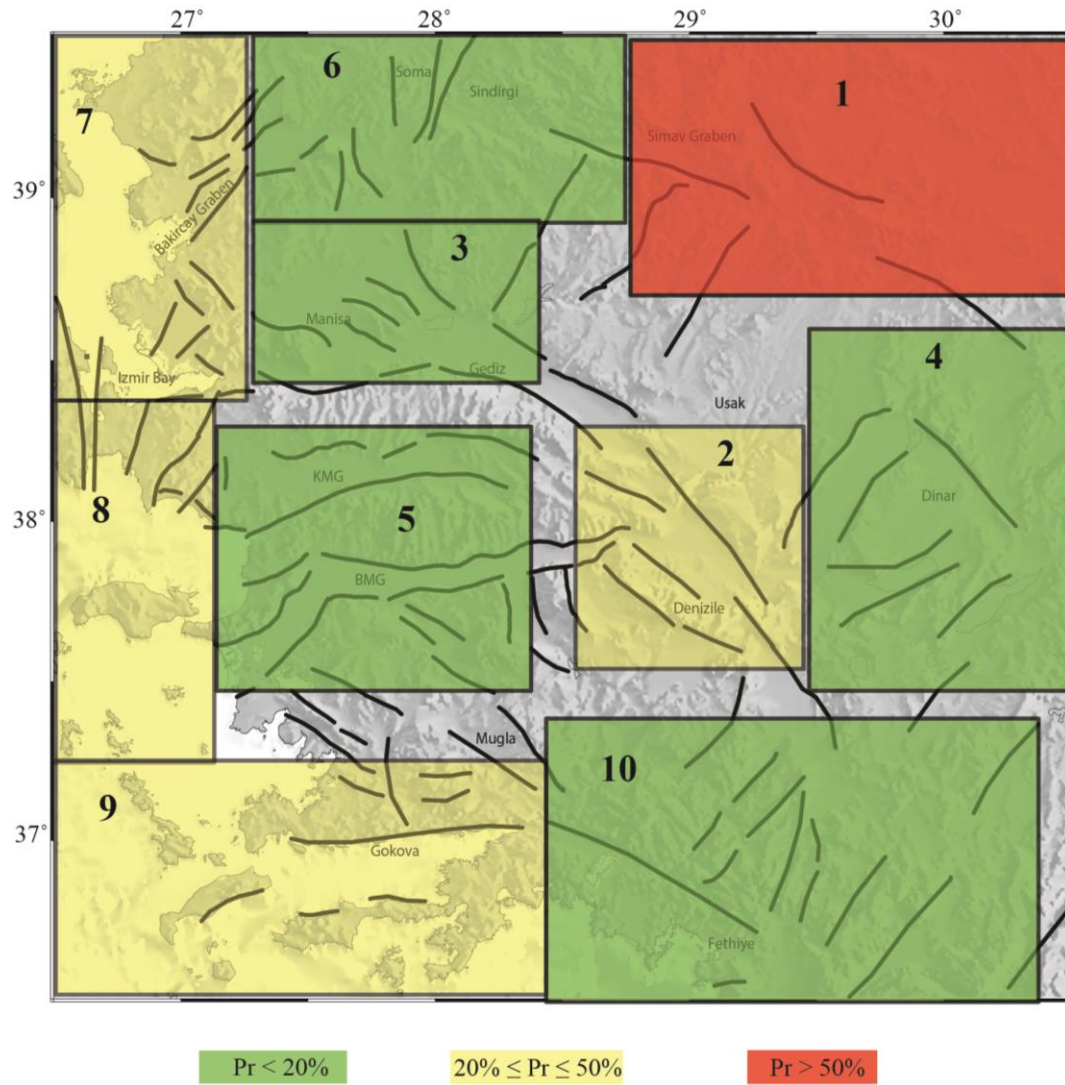


Figure 5.10: The Gumbel annual extreme method based map showing earthquake probabilities (Pr) of sub-regions for a magnitude 7 event within 100 years. Pr values (in %) are taken from Table 5.2.

5.5 Maximum Expected Earthquake Magnitudes (Mmax)

The expected maximum magnitude (Mmax) earthquake for a region in a certain time period can be calculated from the relationship between return periods and magnitude of earthquakes. The Mmax for sub-regions in 100 years are calculated using both the Gutenberg-Richter (G-R) and Gumbel methods (Table 5.3).

The results obtained from G-R method are shown in Figure 5.11. According to these results; sub-regions 1, 7 and 9 have the largest and 2, 3 and 10 have the smallest expected magnitude for an earthquake in 100 years. The results obtained from Gumbel method are given in Figure 5.12. According to these results; sub-regions 1, 9 and 8 have the largest and 3, 5 have the smallest expected magnitude for an earthquake in 100 years.

Table 5.3: Table showing the maximum expected magnitude (Mmax) in 100 years obtained for the sub-regions using Gutenberg-Richter (G-R) and Gumbel annual extreme methods.

Maximum Magnitude (Mmax) within 100 years			Recorded Mmax since 1900	Date
Sub-region	G-R	Gumbel		
1	6.8	7.3	Ms=7.0; Mw=6.2	28/3/1970
2	6.2	6.3	MD=6.3	16/3/1926
3	6.2	5.7	Ms,Mw=5.8	13/1/1926
4	6.7	6.1	Ms=6.9; Mw=6.6	3/10/1914
5	6.7	5.8	Ms=6.8; Mw=6.5	16/7/1955
6	6.6	6.3	Ms=6.5; Mw=6.1	28/3/1969
7	7.1	6.3	Ms=7.0; Mw=6.7	18/11/1919
8	6.5	6.6	Ms=5.7; Mw=5.8	17/10/2005
9	7.2	6.5	Ms=7.7; Mw=7.2	26/6/1926
10	6.0	6.2	Ms=6.1; Mw=6.0	1/3/1926

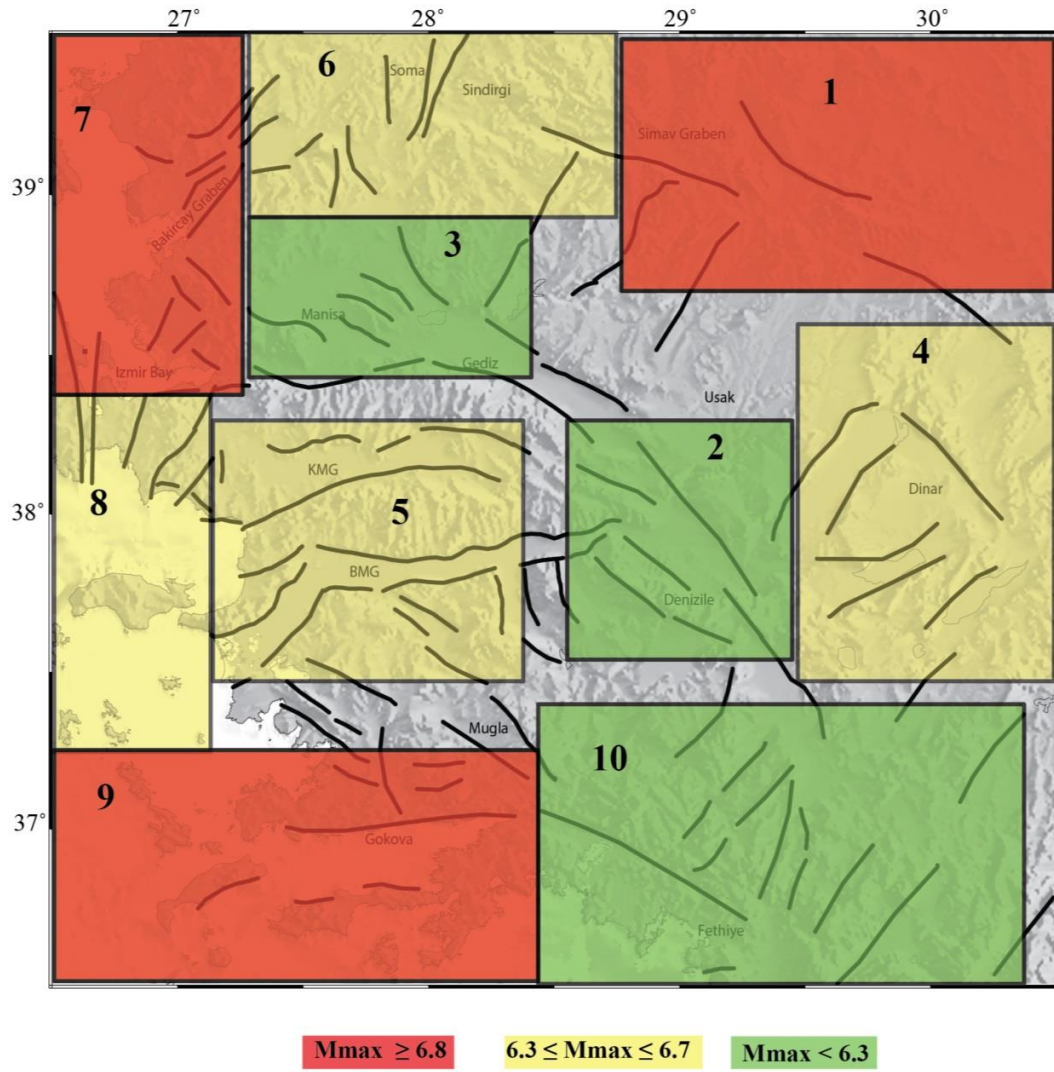


Fig. 5.11: The Gutenberg-Richter (G-R) relation based map showing maximum expected earthquake magnitudes (M_{max}) within 100 years for the selected sub-regions.

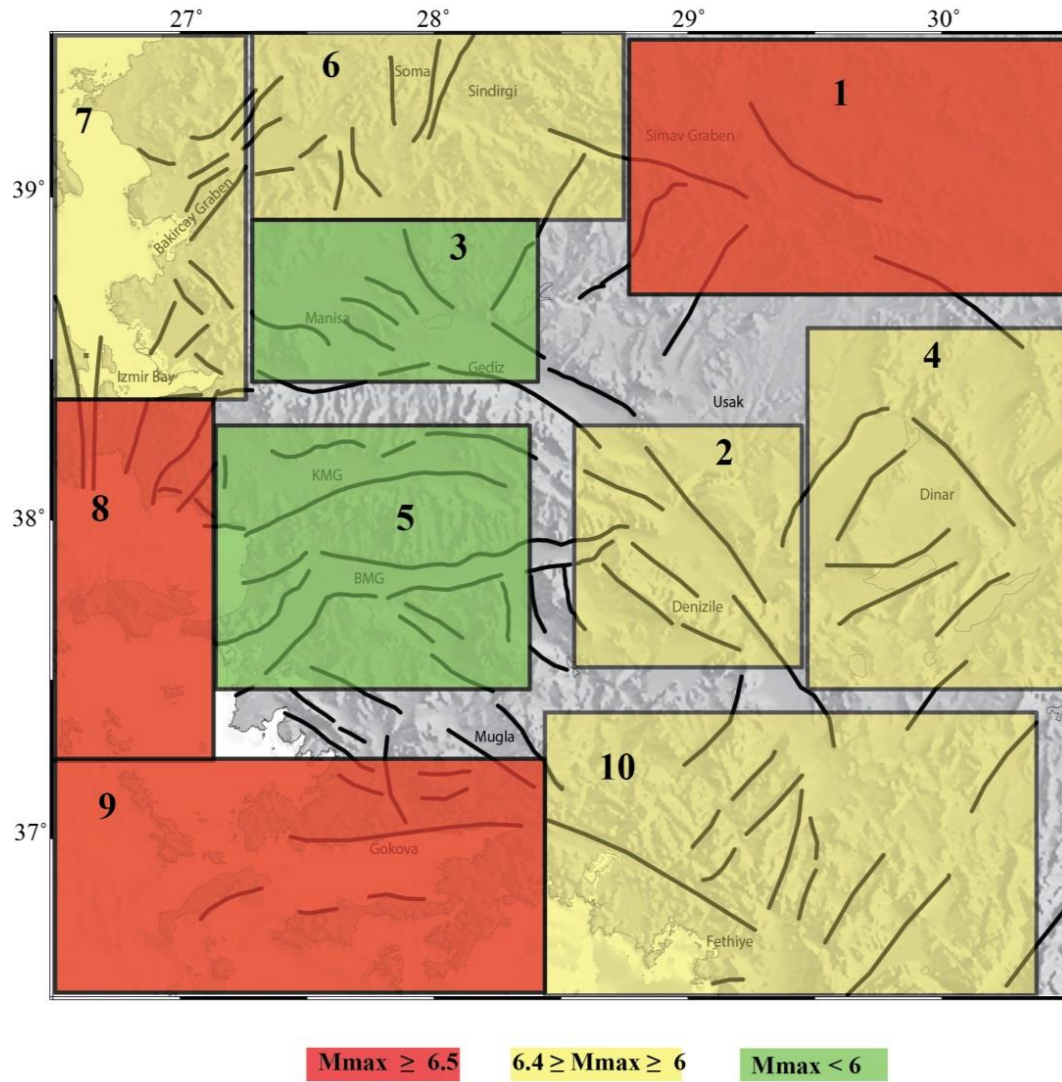


Fig. 5.12: The Gumbel annual extreme method based map showing maximum expected earthquake magnitudes (M_{max}) within 100 years for the selected sub-regions.

According to results based on G-R method; sub-regions 1, 7 and 9 (Simav, Bakırçay and Gulf of Gökova) have the largest; based on Gumbel method sub-regions 1, 8 and 9 (Simav Gulf of Sığacık and Gulf of Gökova) have the largest M_{max} values for an earthquake in 100 years.

Maximum expected magnitude for an earthquake in a given region within a certain time period (e.g., 100 years) also depends on recorded M_{max} . If the region is struck by an earthquake of comparable size to maximum expected magnitude, the probability of having a large earthquake in the near future diminishes. Thus, we list the recorded M_{max} values within each sub-region next to the expected M_{max} estimates (Table 5.3). In Simav (sub-region 1), the maximum recorded magnitude for the region is $M_s=7.0$ (1970) and apart from this event, it was recently struck by $M_l=5.9$ event (May, 2011), thus reducing the risk in this region. The Gulf of Gökova (sub-region 9) has the recorded M_{max} of $M_w=7.2$ ($M_s=7.7$) in the year 1926; well above the expected M_{max} . This event is likely related to ongoing subduction along Aegean Arc and our study area does not cover the full extent of this tectonic domain. The second recorded M_{max} in the region is an $M_s = 6.5$ event (13/12/1941) which is well within the range of our study area and can be taken as the recorded M_{max} for this sub-region. The sub-region also had an $M_w = 5.5$ event (August, 2004) which would have released some stress in the region. Sub-region 3 and 7 (Bakırçay and Manisa) on the other hand has not been struck by any significant magnitude earthquake in the near past (1919 and 1926), but the b- value map (Figure 3.13) shows that these regions are currently characterized by high b-values, which implies that energy in this region is currently releasing in the form of more frequently occurring small magnitude earthquakes. Gulf of Sığacık (sub-region 8) was struck by two $M_w=5.8$ (October, 2005) earthquakes in recent times. This implies that a considerable amount of stresses in this region have been released recently in the form of these moderately sized earthquakes. Dinar-Burdur (sub-region 4), which gives moderate M_{max} in both methods was also struck by $M_s = 6.0$ earthquake (October, 1995). Sub-regions 2 and 10 (Alaşehir and Fethiye) have not experienced large earthquakes since 1926 which lead to increased seismic risk for the near future. It is also worth to note that

in 1955 and 1969, large earthquakes also occurred within sub-regions 5 and 6 (BMG-KMG and Soma) with magnitudes similar to expected M_{max} calculated in this study.

5.6 Fractal Dimensions of Recorded Seismicity

The clustering of earthquakes in space and time, regardless of the scale of observation, is a fundamental feature of Earth's seismicity. Therefore, earthquake's spatial and temporal distributions are regarded as a scale invariant phenomenon. Scale invariant phenomena follow fractal statistics, and therefore can be characterized by fractal dimensions. The spatial distribution of earthquakes epicenter are demonstrated to be fractal by many researchers (e.g., Kagan and Knopoff, 1980; Sadovsky, *et al.*, 1984). The correlation dimension measures the spacing or clustering properties of a set of points and can be used to characterize the distribution of earthquake epicenters (Kagan and Knopoff, 1980; Hirata, 1989). The fractal dimension (D_c) is estimated using the two-point correlation dimension. Grassberger and Procaccia (1983) defined the correlation function $C(r)$ and fractal dimension D_c as:

$$C(r) = 2 N(R < r) / N (N - 1)$$

$$D_c = \lim [\log C(r) / \log r]$$

where 'r' is the distance between two epicenters and 'N' is the number of pairs of events separated by a distance $R < r$. Distance 'r' between two epicenters is calculated by the relation

$$r = \cos^{-1}(\cos \Theta_i \cos \Theta_j + \sin \Theta_i \sin \Theta_j \cos (\phi_i - \phi_j))$$

where (Θ_i, ϕ_i) and (Θ_j, ϕ_j) are the latitudes and longitudes of the i^{th} and j^{th} events respectively. Fractal dimension value (D_c) can be obtained from the slope of the graph of $C(r)$ against 'r' on a double logarithmic plot.

The fractal dimension value decreases with the degree of clustering of earthquake epicenters (Öncel and Wilson, 2002). Fractal dimension can be used as a quantitative measure of the degree heterogeneity of seismic activity in a fault system, which is in

turn controlled by the heterogeneity of stress field and preexisting geological and structural heterogeneity in that region (Öncel *et al.*, 1996). Therefore, variations in fractal dimension values in an area can be used as quantitative measure of variations of stress heterogeneity in that area. High Dc values shows that the events are spaced apart, while low Dc values shows that the seismic activity is clustered in that region. Fractal dimensions can also be used to identify possible unbroken sites, and these sites can be regarded as seismic gaps waiting to break in future.

In order to get an idea of the degree of heterogeneity of seismic activity in the region, fractal dimension (Dc) values are calculated for each sub-region in the study area. The analysis for Dc values is done in ZMAP software package (Wiemer, 2001). The results are presented in Table 5.4 and the logarithmic plots, from which Dc values are calculated, are shown in Figure 5.13. The catalogue used in this analysis is unprocessed (clustered) and covers a time span from 1990-January, 2013. The results shows that sub-region 9, and 10 are characterized by low Dc values that shows heterogeneity of seismic activity in these areas, which can be due to geological and structural complexity or heterogeneous stress conditions in these domains. On the other hand sub-regions 1, 2, 3, 6 and 7 have intermediate Dc values. Sub-regions 4, 5 and 8 have highest Dc values, which suggest that these areas are characterized by low geological and structural heterogeneity. Figure 5.14 show each sub-region with color coding as a function of its Dc value.

Table 5.4: Table showing the fractal dimension values (Dc) obtained for sub-regions

Sub-region	1	2	3	4	5	6	7	8	9	10
Dc value	2.31	2.23	2.2	2.46	2.47	2.27	2.29	2.53	1.99	2.06

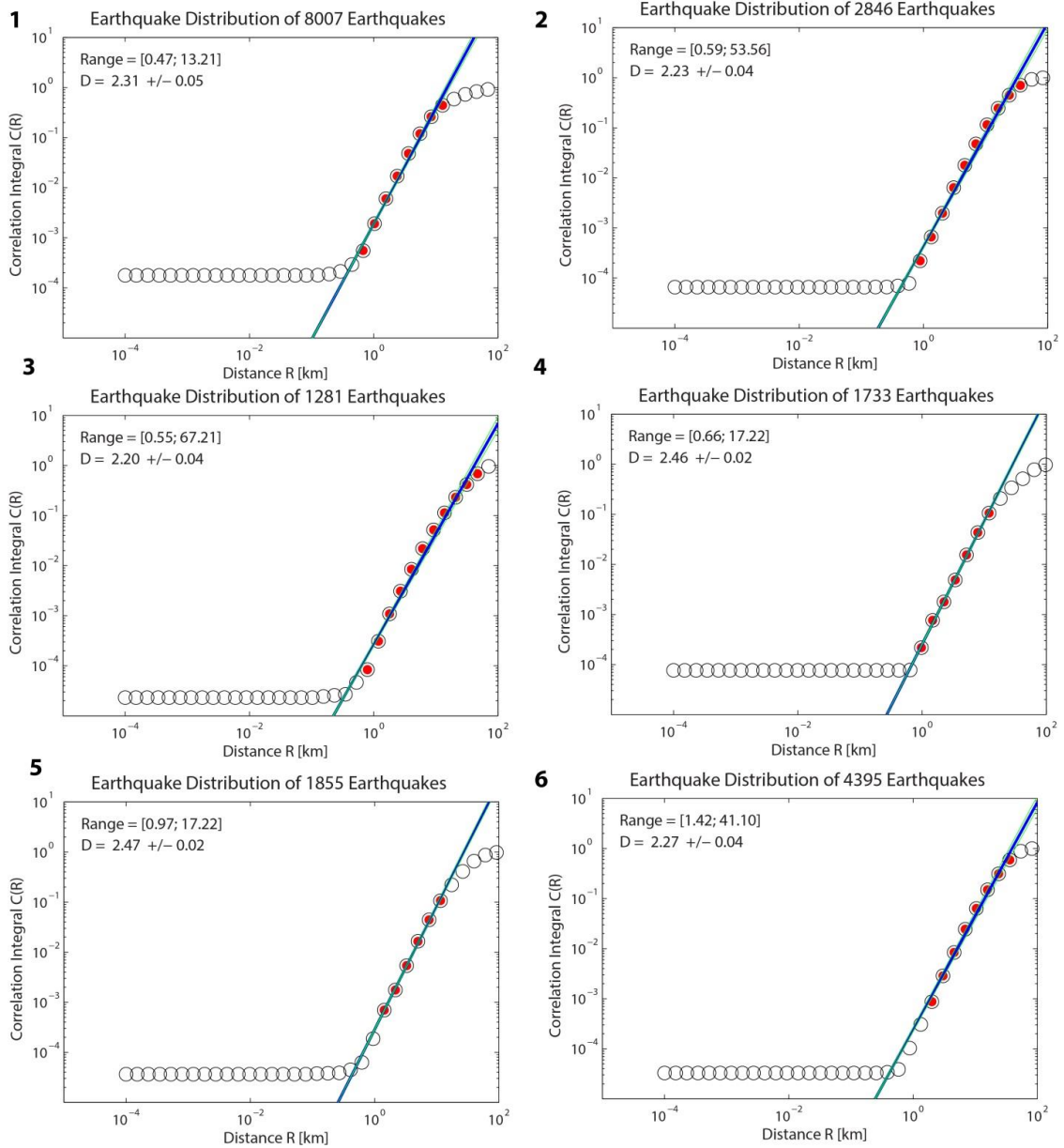


Figure 5.13: Fractal dimension (D_c) plots of the sub-regions. D_c is computed using the quarry free KOERI catalog between 1990 and January, 2014.

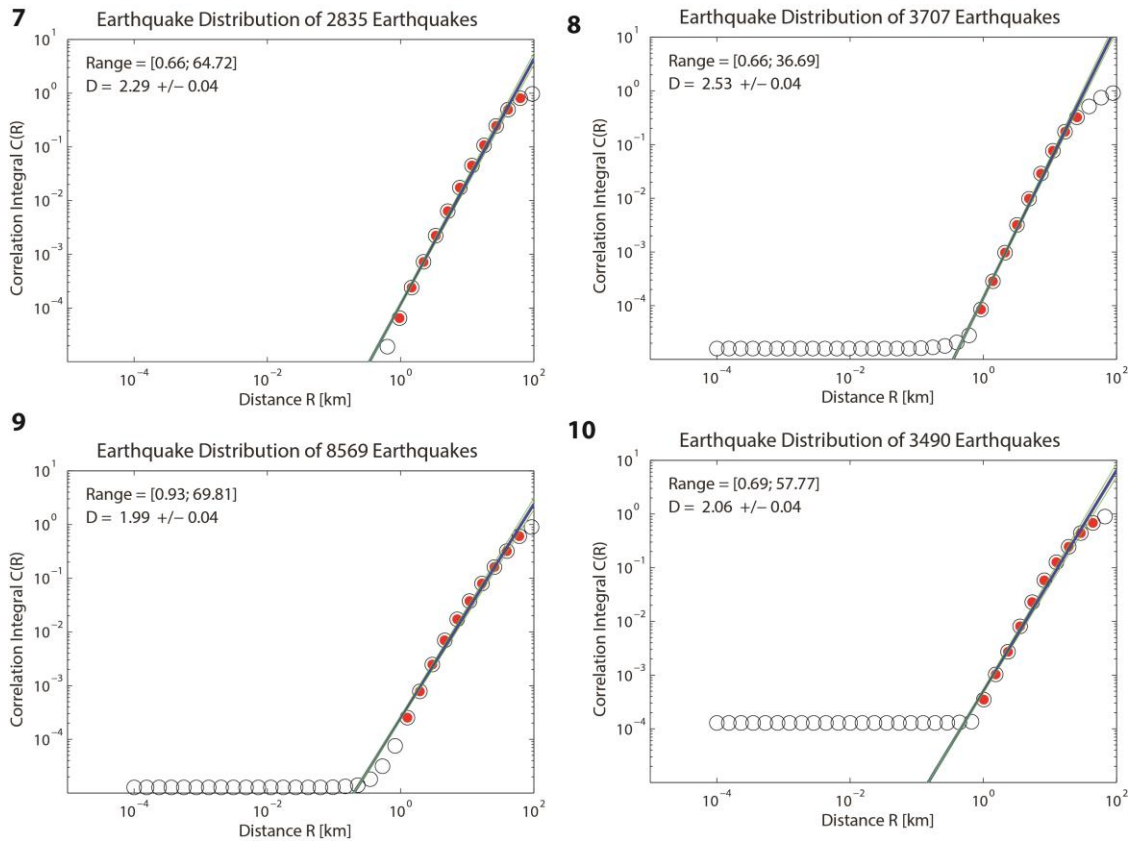


Figure 5.13: (continued)



Figure 5.14: Map showing the spatial variation of fractal dimension values (Dc) across the selected sub-regions. Each sub-region is colored accordingly to its Dc value.

CHAPTER 6

DISCUSSION AND CONCLUSION

We have analyzed earthquake data in this thesis to study the active stress conditions and to estimate the seismic hazard potential of different sub-regions in western Anatolia. In Chapter 3, the spatial and temporal variations in b-value are investigated. The spatial variations in b-value are associated with variations in local stress conditions, which are dependent on complexities in geological and structural heterogeneities in an area. The areas characterized by high b-values are associated with relatively low stress conditions where smaller magnitude earthquakes are most abundant. The results showed that Bakırçay Graben and the area between İzmir and Manisa are characterized by high b-values as compared to other regions in the study area (Figure 3.13). Spatial distribution of high b-values correlates well with the distribution of hot springs and high heat flow anomalies. The temporal variations in b-values, associated with major earthquakes in the region, shows that the events are either associated with an increase or decrease in b-value before or after the main event. All the earthquake sequences in the region show a small scale decrease prior to an abrupt increase in b-value at the time of main event, and are followed by return of b-value to its normal value after a short period of time. The increase in b-value after an earthquake is result of low stress conditions formed by the release of major tectonic stress during the main event.

In Chapter 4, the stress tensor inversion has been carried out in the study area using all the focal mechanism solutions published for the area. The stress tensor inversion for the whole region shows that σ_3 is horizontally oriented with σ_1 in a vertical orientation (Figure 4.5), and the region is characterized by NNE–SSW (almost N–S) extensional regime. The variance map shows that the areas showing high variance values

(anomalous stress fields) roughly coincide with the regions showing high b-values (Figures 4.6b; 3.13; 3.14). The results for sub-regions shows that the stress patterns are not uniform throughout the area and are marked by small scale variations in the directions of principle stress orientations. The tectonic stress regimes obtained for the sub-regions also show variations within the study area; for instance the north-western part (sub-region 3, 6, 7 and 8) is dominated by strike-slip tectonic mechanisms (Figure 6.1). This region coincides with the İzmir-Balıkesir transfer zone (IBTZ), which is characterized by both strike-slip and normal faults (Figure 2.4). The region is regarded as a transfer zone of weakness between western Anatolia (extensional) and north Aegean region (strike-slip). Our results show that sub-regions 3 and 6 are characterized by extensional strike-slip regimes while sub-regions 7 and 8 are characterized by strike-slip tectonic regimes. Overall, the central part of the study area is characterized by almost N-S extension; the area coinciding with the KMG, BMG and Simav graben area (Figure 6.2). Gökova region is marked by an anticlockwise rotation in orientation of stress directions from N-S to NW-SE. Fethiye-Burdur Fault Zone is also characterized by complex stress orientations. The maximum horizontal stress directions (S_{Hmax}) in the area are also concordant with the orientations of faults in the area (Figure 4.20).

In Chapter 5, earthquake probability analysis is carried out for the area using both the Weighted Least Square (WLS) analysis of Gutenberg-Richter relations (G-R) and Gumbel annual extreme value method. The results obtained by both methods are comparable but Gumbel method gives comparatively low probabilities and long return periods for some sub-regions (Table 6.1). The results obtained for the whole region show a return period of 3 years from G-R method and 7 years from Gumbel method for magnitude 6 earthquake (Probability of occurrence is 99.99 % in 50 years for both methods). Among the sub-regions, for magnitude $M=6.0$ in 50 years, sub-regions 1 and 9 (Simav and Gulf of Gökova) have high earthquake probabilities; sub-regions 4 and 6 (Dinar-Burdur and Soma) have moderate while Manisa (sub-region 3) has low earthquake probabilities in both methods. Sub-region 8 (Gulf of Sığacık) shows high earthquake probability in Gumbel method and moderate earthquake probability in G-R method. Sub-regions 2 and 10 (Alaşehir and Fethiye) have low and moderate; sub-region 05 (BMG-KMG) has moderate and low while sub-region 7 (Bakırçay) has high and

moderate earthquake probabilities in G-R and Gumbel method respectively for magnitude 6 earthquake in 50 years.

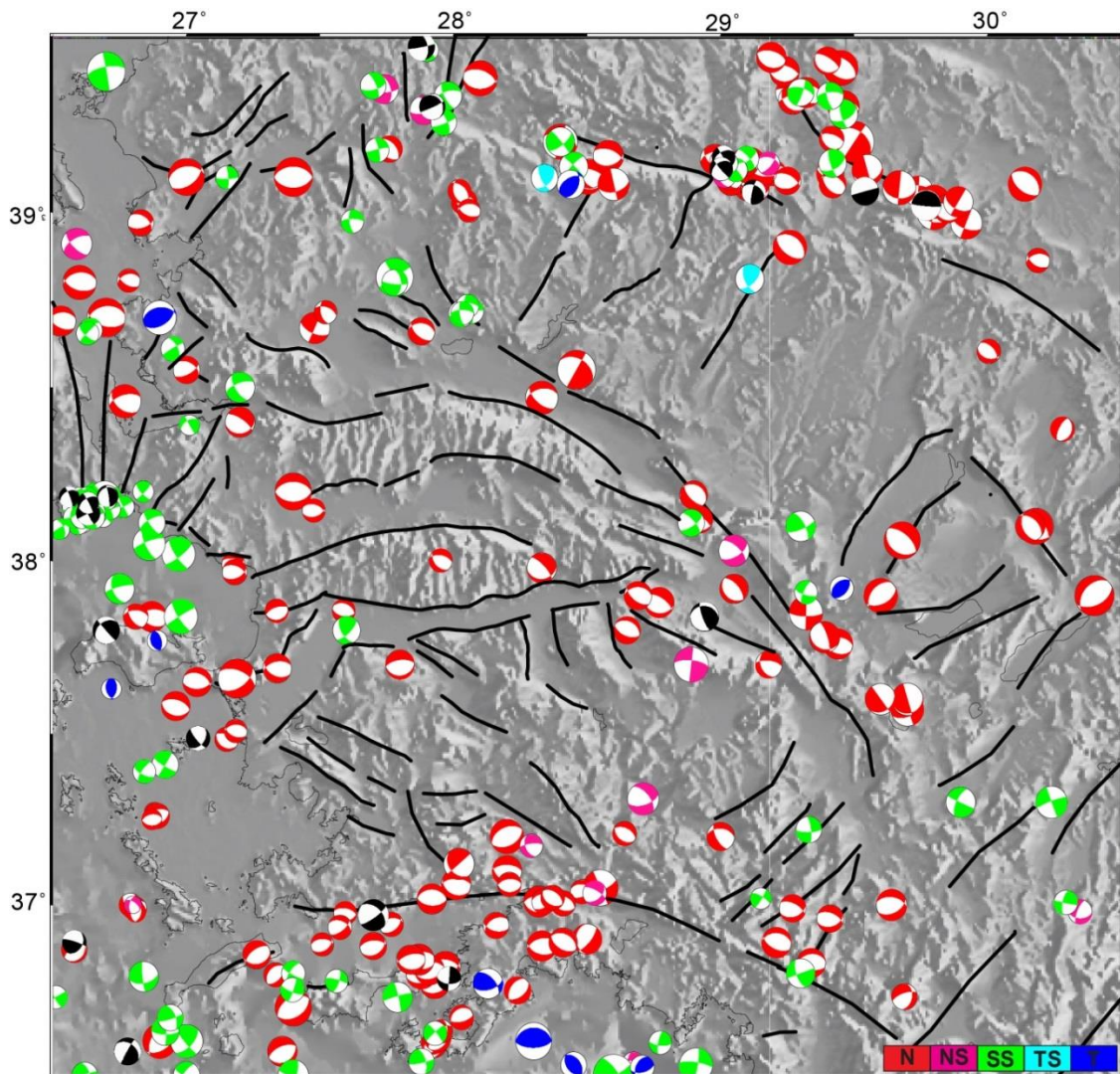


Figure 6.1: Map showing focal mechanism solutions which are colored according to the tectonic regime classification of Zoback (1992). Red: normal, pink: transtensional, green: strike-slip, cyan: transpressional, blue: thrust and black: undefined faulting. Note that identified regimes are listed in Appendix A.

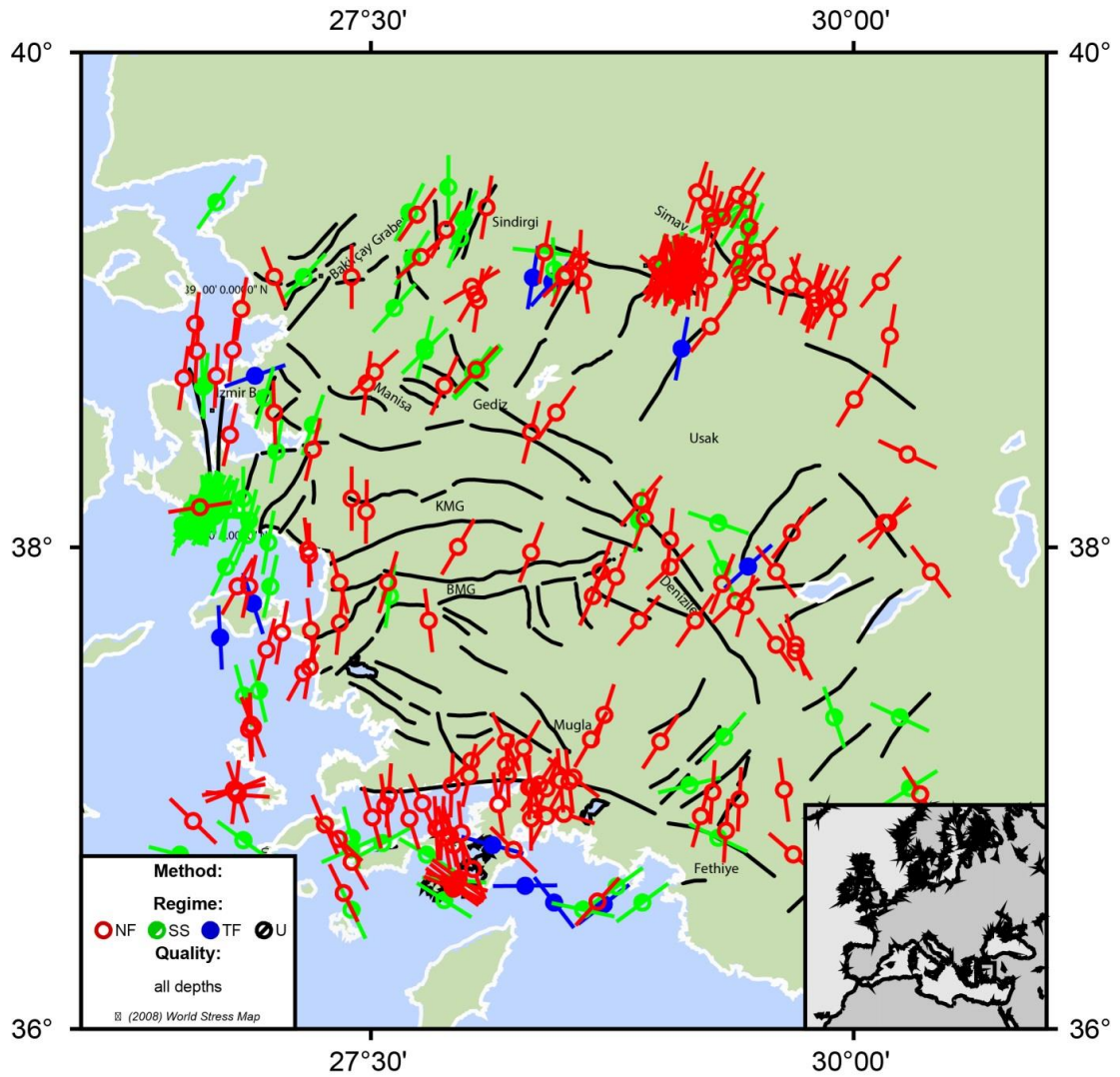


Figure 6.2: Stress map showing minimum horizontal stress axes (S_{Hmin}) associated to each focal mechanism solution used in this study. The resultant axes indicate the extension directions in the study area.

The results for maximum expected magnitude earthquake in 100 years obtained for sub-regions illustrates that Simav and Gulf of Gökova are characterized by largest expected magnitude earthquakes in both methods. Fractal dimension (Dc) values analysis shows that Fethiye and Gulf of Gökova sub-regions of study area are characterized by low Dc values which can be explained by the complex faulting pattern in these regions.

Table 6.1 gives a summary of the results obtained for the sub-regions. These parameters are cross correlated to check relationships between different parameters. The parameters that are compared; includes the b-value, a-value, Dc (fractal dimension), stress ratio (R), and stress variance.

Table 6.1: Table showing the summary of results obtained for the selected sub-regions in the study area. N: Extensional, S: Strike-slip, NS: Extensional Strike-slip, G-R: Gutenberg-Richter relation.

Sub-regions	b-value	a-value	β	$\ln\alpha$	Return period (yr) of M=6 Earthquake		Dc (fractal dimension)	R (Stress Ratio)	stress variance	Regime
					G-R	Gumbel				
1	0.96	6.40	1.36	5.35	16	16	2.31	0.59	0.06	N
2	1.01	6.35	1.96	7.69	58	59	2.23	0.41	0.13	N
3	0.79	4.87	2.34	8.67	64	214	2.20	0.92	0.02	NS
4	0.65	4.38	1.86	6.79	33	79	2.46	0.33	0.13	N
5	0.68	4.54	2.30	8.70	34	164	2.47	0.71	0.05	N
6	0.81	5.35	2.09	8.46	36	59	2.27	0.77	0.12	NS
7	0.59	4.21	2.01	7.94	23	60	2.29	0.96	0.11	S
8	0.74	4.83	1.77	6.98	44	38	2.53	0.78	0.10	S
9	0.81	5.82	2.27	10.10	10	33	1.99	0.39	0.15	N
10	1.48	8.81	2.21	8.97	102	73	2.06	0.27	0.27	N

The tectonic behavior of a region correlates well with a- and b- values obtained from G-R relation as compared to parameters ($a = \ln\alpha / \ln 10$ and $b = \beta / \ln 10$) obtained from Gumbel relation (Bayrak *et al.*, 2008), therefore we have used a- and b- values from G-R relation for correlation. High b-values show that stress is being continuously released in the form of small earthquakes and it gives a measure of stress in a region. The areas characterized by low b- values correlate with epicenters of large magnitude earthquakes and show that stress is being stored efficiently by the active faults. Large a-values indicate that the earthquake productivity of the area is relatively high. As expected a- and b- values display a strong positive linear correlation with correlation coefficient (R^2) as high as 0.97. This indicates that earthquake productivity is higher at region where stress is frequently released by smaller earthquakes (Figure 6.3).

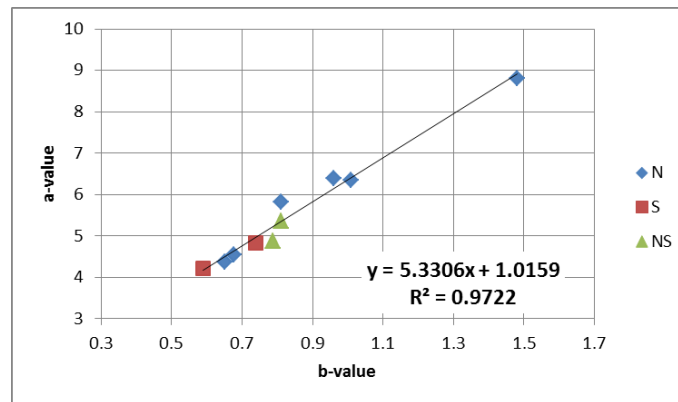


Figure 6.3: Linear correlation between a- and b- values of the sub-regions. The sub-regions are classified according to the dominant tectonic regime (N: Extensional, S: Strike-slip, NS: Extensional-Strike-slip).

Dc value measures the clustering properties of earthquakes in the region and expected to be low when events are more clustered. The previous studies suggested a negative correlation (Bayrak and Bayrak, 2012b; Öncel and Wilson, 2002 and Öztürk, 2012). Our

results also show a weak negative correlation between b- and Dc values ($R^2 = 0.31$) indicating that seismicity is more clustered (low Dc value) when the proportion of small earthquakes are larger (high b- value). This relation possibly suggests that low local stress conditions and higher level of seismic heterogeneity are coupled mostly likely due to geological and structural complexity in these sub-regions (Figure 6.4a). Clustered distribution (low Dc value) also correlates ($R^2 = 0.39$) with increased earthquake productivity (high a- value) (Figure 6.4b).

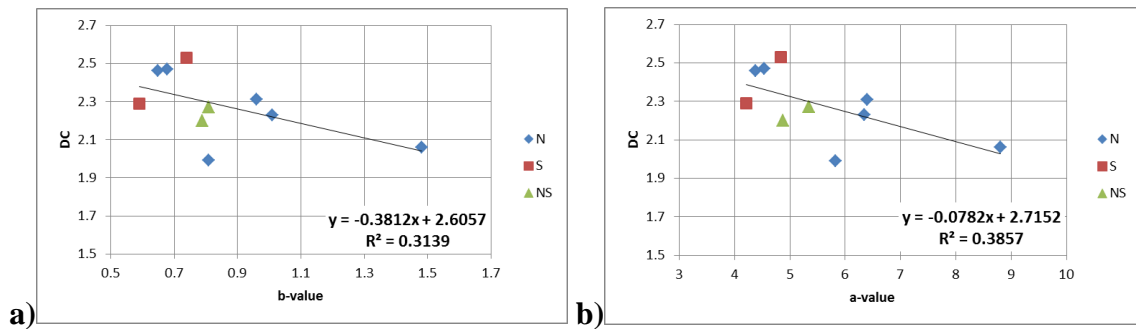


Figure 6.4: Linear correlation between **a)** fractal dimension (Dc) and b-value and **b)** Dc and a-value of the sub-regions. The sub-regions are classified according to the dominant tectonic regime (N: Extensional, S: Strike-slip, NS: Extensional-Strike-slip).

Stress ratio ($R = (\sigma_2 - \sigma_3) / (\sigma_1 - \sigma_3)$) provides a measurement for relative magnitude of principle stresses ($\sigma_1, \sigma_2, \sigma_3$). The stress ratio is low when magnitude difference between σ_2 and σ_3 is small which provides a suitable condition to have multi-directed extension. According to our results, tectonic domains characterized by strike-slip faulting or normal faulting with strike-slip components display the highest stress ratios (R) unlike pure extensional domains which have low stress ratios (Table 6.1). Moreover, there is a weak negative correlation ($R^2 = 0.34$) between stress ratios (R) and b-values, suggesting that low stress regions (high b-value) are more prone to multi-directed extension (low stress

ratio) (Figure 6.5a). Similar negative correlation ($R^2 = 0.39$) is also present between stress ratios (R) and a-values implying that the earthquake productivity increases when σ_2 and σ_3 have similar magnitudes (Figure 6.5b). In contrast, there is a weak positive correlation ($R^2 = 0.12$) between Dc value and stress ratio and suggests more clustered and heterogeneous seismicity at multidirectional stress regimes (Figure 6.5c). It is worth to note that correlation coefficients of these relations are significantly higher when sub-region 4 (Dinar-Burdur) is excluded (R vs b, $R^2 = 0.61$; R vs a, $R^2 = 0.72$; R vs Dc, $R^2 = 0.33$).

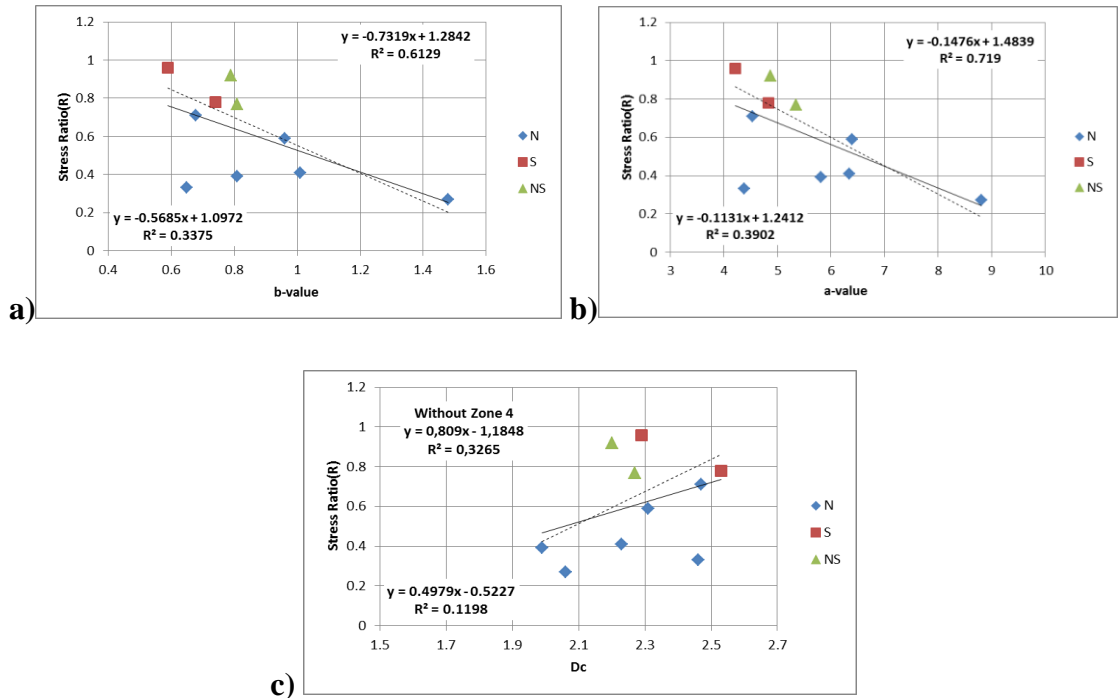


Figure 6.5: Linear correlation between **a)** stress ratio and b-value; **b)** stress ratio and a-value and **c)** stress ratio and fractal dimension (Dc) of the sub-regions. The sub-regions are classified according to the dominant tectonic regime (N: Extensional, S: Strike-slip, NS: Extensional-Strike-slip). Dashed trend lines are computed by excluding the outlier Dinar-Burdur sub-region.

Anomalous stress fields are characterized by high stress variances; therefore it can be used as a tool to quantify the degree of heterogeneity of stress field in a region. Our results show a negative correlation between stress variance and stress ratio (R), represented by rather large correlation coefficient ($R^2 = 0.47$) (Figure 6.6a). The relationship shows that sub-regions characterized by low stress ratios (σ_2 and σ_3 have similar magnitudes) display high stress variances supporting elevated level of tectonic complexity. The comparison between Dc and stress variance also gives a negative correlation ($R^2 = 0.24$) supporting more earthquake clustering at the presence of stress field complexity (Figure 6.6b).

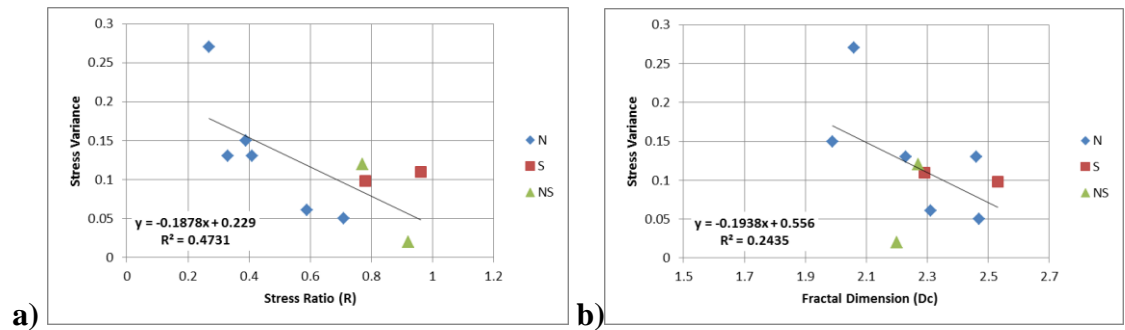


Figure 6.6: Linear correlation between **a)** stress variance and stress ratio and **b)** stress variance and fractal dimension (Dc) of the sub-regions. The sub-regions are classified according to the dominant tectonic regime (N: Extensional, S: Strike-slip, NS: Extensional-Strike-slip).

In the literature, parameters related to distribution of seismicity (b-, a- and Dc values) have been correlated with each other extensively. Unlike previous works, this study included also parameters obtained by stress tensor inversion (stress ratio, variance and regime) to identify possible relationships between stress tensor properties and seismicity. Although, all the observed correlations drawn here imply viable relations in terms of

rock physics, mechanics and geology, the error ranges of the used parameters are highly variable and rather large. Since, this study includes only limited amount of data collected from a particular region, the identified correlations must be treated with caution and should be tested using more global data sets.

REFERENCES

- AFAD: Afet ve Acil Durum Yönetimi Başkanlığı, Turkey. <http://www.deprem.gov.tr/>. Last accessed February 2014.
- Akin, U., Ulugergerli., U.U., Kutlu, S., 2014. The assessment of geothermal potential of Turkey by means of heat flow estimation. *Bull. Min. Res. Exp.* 149: 201–210.
- Aktar, M., Karabulut, H., Ozalaybey, S., Childs, D.M., 2007. A conjugate strike-slip fault system within the extensional tectonics of western Turkey. *Geophys. J. Int.* 171 (3), 1363–1375.
- Aktug, B., Nocquet, J.M., Cingöz, A., Parsons, B., Erkan, Y., England, P., Lenk, O., Gürdal, M.A., Kilicoglu, A., Akdeniz, H., and Tekgül1, A., 2009. Deformation of western Turkey from a combination of permanent and campaign GPS data. *Journal of Geophysical Research*, 114.
- Alçıçek, M.C., 2007. Tectonic development of an orogen-top rift recorded by its terrestrial sedimentation pattern: the Neogene Eşen Basin of southwestern Anatolia, Turkey. *Sediment. Geol.* 200, 117–140.
- Alçıçek, M.C., ten Veen, J.H., Özkul, M., 2006. Neotectonic development of the Çameli Basin, southwestern Anatolia, Turkey. In: Robertson, A.H.F., Mountrakis, D. (Eds.), *Tectonic Development of the Eastern Mediterranean*. Geological Society, London, Special Publications, 260, 591–611.
- Altınok, Y., 1991. Assessment of the seismic risk of western Anatolia by Semi-Markov model. *Geophysics*, 5, 135–140.

Altunel, E., 1999. Geological and geomorphological observations in relation to 20 September 1899 Menderes earthquake, western Turkey: *Journal of Geological Society London*, 156, 241–246.

Altunel, E., Barka, A., and Akyüz, S., 1999. Paleoseismicity of the Dinar fault, SW Turkey. *Terra Nova*, 11 (6), 297–302.

Ambraseys, N.N., and Jackson, J.A., 1998. Faulting associated with historical and recent earthquakes in the eastern Mediterranean region. *Geophysical Journal International*, 133, 390–406.

Angelier, J., 1979. Determination of the mean principal directions of stresses for a given fault population. *Tectonophysics*, 56, 17–26.

Angelier, J., 1984. Tectonic analysis of fault slip data sets. *J. Geophys. Res.*, 89, 5835–5848.

Angelier, J., 2002. Inversion of earthquake focal mechanisms to obtain the seismotectonic stress -a new method free of choice among the nodal planes. *Geophys. J. Int.* 150, 58–609.

Arnold, R. and Townend, J., 2007. A Bayesian approach to estimating tectonic stress from seismological data. *Geophys. J. Int.* 170, 1336–1356.

Arpat, E., and Bingöl, E., 1969. The rift system in western Turkey: through on its developments. *MTA Bulletin*, 79, 1–9 [in Turkish with English Abstract].

Bağcı, G., 1996. Earthquake occurrences in western Anatolia by Markov model. *Geophysics* 10, 67–75.

Barka, A.A., Reilinger, R., Şaroğlu, F., Şengör, A.M.C., 1997. The Isparta Angle. Its importance in the neotectonics of the Eastern Mediterranean Region. In: Pişkin, Ö., Ergin, M., Savaşçın, M.Y., Tarcan, G. (Eds.). *Proceedings of International Earth Science Colloquium on the Aegean Region*, 9-14 October, 1995 İzmir-Güllük, Turkey, 1, 3–18.

Bayrak, Y., and Bayrak, E., 2012a. An Evaluation of Earthquake Hazard Potential for Different Regions in Western Anatolia using the Historical and Instrumental Earthquake Data. *Pure Appl. Geophys.* 169, 1859–1873.

Bayrak, Y., and Bayrak, E., 2012b. Regional variations and correlations of Gutenberg-Richter parameters and fractal dimension for the different seismogenic zones in Western Anatolia. *J. Asian Earth Sci.* 58, 98–107.

Bayrak, Y., Öztürk, S., Çınar, H., Kalafat, D., Tsapanos, T. M., Koravos, G.C., Leventakis, G.A., 2009. Estimating earthquake hazard parameters from instrumental data for different regions in and around Turkey. *Eng. Geol.* 105, 200–210.

Bayrak, Y., Öztürk, S., Koravos, G.C., Leventakis, G.A., Tsapanos, T.M., 2008. Seismicity assessment for the different regions in and around Turkey based on instrumental data: Gumbel first asymptotic distribution and Gutenberg-Richter cumulative frequency law. *Nat. Hazards Earth Syst. Sci.* 8, 109–122.

Bayrak, Y., Yılmaztürk, A., and Öztürk, S., 2005. Relationships between fundamental seismic hazard parameters for the different source regions in Turkey. *Natural Hazards*, 36, 445–462.

Beccaletto, L., and Steiner, C., 2005. Evidence of two-stage extensional tectonics from the northern edge of the Edremit Graben, NW Turkey. *Geodynamica Acta*, 18, 283–297.

Benetatos, C., A. Kiratzi, A. Ganas, M. Ziazia, A. Plessa, and G. Drakatos, 2006. Strike-slip motions in the Gulf of Sığaçık (western Turkey): Properties of the 17 October 2005 earthquake seismic sequence. *Tectonophysics*, 426, 263-279.

Bernardi, F., Braunmiller, J., Kradolfer, U., and Giardini, D., 2004. Automatic regional moment tensor inversion in the European-Mediterranean region. *Geophys. J. Int.*, 156, 1–14.

Bozkurt, E., 2000. Late Alpine evolution of central Menderes massif, western Anatolia, Turkey. *International Journal of Earth Sciences*, 89, 728–744.

Bozkurt, E., 2001. Neotectonics of Turkey - a synthesis. *Geodinamica Acta*, 14, 3–30.

- Bozkurt, E., 2002. Discussion on the extensional folding in the Alaşehir (Gediz) Graben, western Turkey. *Journal of Geological Society London*, 159, 105–109.
- Bozkurt, E., 2003. Origin of NE trending basins in western Turkey. *Geodinamica Acta*, 16, 61–81.
- Bozkurt, E., 2004. Granitoid rocks of the southern Menderes Massif (southwest Turkey): field evidence for Tertiary magmatism in an extensional shear zone. *International Journal of Earth Sciences*, 93, 52–71.
- Bozkurt, E., and Mittwede, S.K., 2005. Introduction: Evolution of Neogene extensional tectonics of western Turkey. *Geodinamica Acta*, 18, 153–165.
- Bozkurt, E., and Oberhänsli, R., 2001. Menderes Massif (western Turkey): structural, metamorphic and magmatic evolution- a synthesis. *International Journal of Earth Sciences*, 89, 679–708.
- Bozkurt, E., and Rojay, B., 2005. Episodic, two-stage Neogene extension and short-term intervening compression in western Anatolia: field evidence from the Kiraz basin and Bozdağ horst. *Geodinamica Acta*, 18, 299–316.
- Bozkurt, E., and Sözbilir, H., 2004. Tectonic evolution of the Gediz Graben: field evidence for an episodic, two-stage extension in western Turkey. *Geological Magazine*, 141, 63–79.
- Bozkurt, E., and Sözbilir, H., 2006. Evolution of the Large-scale Active Manisa Fault, Southwest Turkey: Implications on Fault Development and Regional Tectonics. *Geodinamica Acta*, 19, 427–453.
- Braunmiller, J. and Nabelek, J. 1996. Geometry of continental normal faults: Seismological constraints. *Journal of Geophysical Research*, 101(B2), 3045–3052.
- Braunmiller, J., Kradolfer, U., Baer, M., and Giardini, D., 2002. Regional moment tensor determination in the European-Mediterranean region-initial results. *Tectonophysics*, 356, 5–22.

Ceylan, S., 2006. Fractal properties of earthquakes in Marmara. *Journal of Istanbul Kültür University*, 4, 99–108.

Cihan, M., Saraç, G., and Gökçe, O., 2003. Insights into biaxial extensional tectonics: An example from the Sandıklı Graben, West Anatolia Turkey: *Geological Journal*, 38, 47–66.

Collins, A.S., and Robertson, A.H.F., 1998. Process of Late Cretaceous to Late Miocene episodic thrust sheet translation in the Lycian Taurides, SW Turkey. *Journal of Geological Society London*, 155, 759–772.

Çevikbilen, S.Y., Taymaz, T., and Helvacı, C., 2014. Earthquake mechanisms in the Gulfs of Gökova, Sığacık, Kuşadası, and the Simav Region (western Turkey): Neotectonics, seismotectonics and geodynamic implications. *Tectonophysics*, <http://dx.doi.org/10.1016/j.tecto.2014.05.001>. Last accessed December, 2014.

Çiftçi, N.B., 2007. Geological evolution of the Gediz Graben, SW Turkey: Temporal and Spatial variation of the graben. Middle East Technical University, Unpublished PhD Thesis, pp. 290.

Çiftçi, N.B., and Bozkurt, E., 2010. Structural evolution of the Gediz Graben, SW Turkey: temporal and spatial variation of the graben basin, *Basin Research*, 22, 846–873.

Çobanoğlu, İ., Alkaya, D., 2011. Seismic risk analysis of Denizli (Southwest Turkey) region using different statistical models. *Int. J. Phys. Sci.*, 6(11), 2662–2670.

Delvaux, D. and Barth, A., 2010. African stress pattern from formal inversion of focal mechanism data. *Tectonophysics*, 482(1-4), 105–128.

Delvaux, D., Moeys, R., Stapel, G., Petit, C., Levi, K., Miroshnichenko, A., Ruzhich, V., Sankov, V., 1997. Paleostress reconstructions and geodynamics of the Baikal region, Central Asia. Part II: Cenozoic rifting. In: Cloetingh, S., Fernandez, M., Munoz, J. A., Sassi, W., Horvath, F. (Eds.), (Editors), *Structural Controls on Sedimentary Basin Formation*. *Tectonophysics*, 282, 1–38.

Delvaux, D., Sperner, B., 2003. Stress tensor inversion from fault kinematic indicators and focal mechanism data: the TENSOR program. In: Nieuwland, D. (Ed.), *New Insights into Structural Interpretation and Modelling*. Geol. Soc. Lond. Spec. Publ. 212, 75–100.

Dewey, J.F., Şengör, A.M.C., 1979. Aegean and surrounding regions: Complex multiple and continuum tectonics in a convergent zone. *Geological Society of America Bulletin*, 90, 84–92.

Dewey, J.F., 1988. Extensional collapse of orogens. *Tectonics*, 7, 1123–1139.

Doğan, A. ve Emre, Ö., 2006. Ege Graben Sistemi'nin Kuzey Sınırı: Sındırgı-Sincanlı Fay Zonu. 59. Türkiye

Dogliani, C., Agostini, S., Crespi, M., Innocenti, F., Manetti, P., Riguzzi, F., and Savaşçın, Y., 2002. On the extension in western Anatolia and the Aegean Sea. *Journal of Virtual Explorer*, 8, 169–183.

Doğru, A., Gorgun, E., Ozener, H., and Aktug, B., 2014. Geodetic and seismological investigation of crustal deformation near Izmir (Western Anatolia). *Journal of Asian Earth Sciences*, 82, 21–31.

Dumont, J. F., Poisson, A., Şahinci, A., 1979. Sur l'existence de coulissements sénestres récents a l'extrémité orientale de l'arc Égéen (sud-ouest de la Turquie). *C. R. Acad. Sci. Paris*, 289, 261–264.

Dziewonski, A., Ekström, G., Franzen, J. and Woodhouse, J., 1987a. Global seismicity of 1977: centroid-moment tensor solutions for 471 earthquakes. *Physics of the Earth and Planetary Interiors*, 45(1), 11–36.

Dziewonski, A., Ekström, G., Franzen, J. and Woodhouse, J., 1987b. Global seismicity of 1978: centroid-moment tensor solutions for 512 earthquakes. *Physics of the Earth and Planetary Interiors*, 46 (4), 316–342.

El-Isa, Z.H. and Eaton, D.W., 2014. Spatiotemporal variations in the b-value of earthquake magnitude–frequency distributions: Classification and causes. *Tectonophysics*, 615-616, 1–11.

Elitez, İ., 2010. The Miocene-Quaternary Geodynamics of Çameli and Gölhisar Basins, Burdur-Fethiye Fault Zone. MSc Thesis, Istanbul Technical University, Institute of Eurasian Earth Sciences, SW Turkey, pp. 88.

Elitez, İ., Yaltrak, C., 2014. Burdur-Fethiye Shear Zone, Eastern Mediterranean, SW Turkey. *Proceedings of EGU General Assembly*, 04, 2014, Vienna, 16.

Elitez, İ., Yaltrak, C., Akkök, R., 2009. Morphotectonic evolution of the Middle of Fethiye-Burdur Fault Zone: Acıpayam, Gölhisar and Çameli Area, SW Turkey. *International Symposium on Historical Earthquakes and Conservation of Monuments and Sites in the Eastern Mediterranean Region, 500th Anniversary Year of the 1509 September 10, Marmara Earthquake, 10-12 September 2009, Istanbul*, 296–297.

Emre, Ö., Barka, A., 2000. Active Faults between Gediz Graben and Aegean Sea (Izmir Region). *BAD SEM 2000 Symposium*, Izmir.

Erdoğan, S., Şahin, M., Yavaşoğlu, H., Tiryakioğlu, İ., Erden, T., Karaman, H., Tarı, E., Bilgi, S., Tüysüz, O., Baybura, T., Taktak, F., Telli, A.K., Güllü, M., Yılmaz, İ., Gökalp, E., and Boz, Y., 2008. Monitoring of deformations along Burdur-Fethiye fault zone with GPS. *J. Earthquake Eng.*, 12(2), 109–118.

Erkül, F., Helvacı, C., and Sözbilir, H. 2005. Evidence for two episodes of volcanism in the Bigadic borate basin and tectonic implications for western Turkey. *Geological Journal*, 40, 1–16.

Ersoy, E.Y., Helvacı, C., and Palmer, R.M., 2011. Stratigraphic, structural and geochemical features of the NE–SW trending Neogene volcano-sedimentary basins in western Anatolia: Implications for associations of supra-detachment and transtensional strike-slip basin formation in extensional tectonic setting. *Journal of Asian Earth Sciences*, 41, 159–183.

Eyidoğan, H., and Jackson, J.A., 1985. A seismological study of normal faulting in the Demirci, Alaşehir and Gediz earthquake of 1960-1970 in western Turkey: implications for the nature and geometry of deformation in the continental crust. *Geophysical Journal of Royal Astronomy Society*, 81, 569–607.

Eyidoğan, H., Barka, A., 1996. The 1 October 1995 Dinar earthquake, SW Turkey. *Terra Nova*, 8, 479–485.

Firuzan, E., 2008. Statistical earthquake frequency analysis for Western Anatolia. *Turk. J. Earth Sci.* 17741–762.

Gardner, J. K., Knopoff, L., 1974. Is the sequence of earthquakes in Southern California, with aftershocks removed Poissonian? *Bull. Seismol. Soc. America*, 64, 1363–1367.

Gaulia, L., 2010. Detection of quarry and mine blast contamination in European regional catalogues. *Natural hazards*, 53, 229–249.

Genç, Ş.C., Altunkaynak, Ş., Karacık, Z., Yazman, M., Yılmaz, Y., 2001. The Çubukludağ graben, south of İzmir: its tectonic significance in the Neogene geological evolution of the western Anatolia. *Geodin. Acta*, 14, 45–55.

Gephart, J.W., 1990. FMSI: A FORTRAN program for inverting fault/slickenside and earthquake focal mechanism data to obtain the regional stress tensor. *Computer s & Geosciences*, 16, 953–989.

Gephart, J.W., Forsyth, D.W., 1984. An improved method for determining the regional stress tensor using earthquake focal mechanism data: application to the San Fernando earthquake sequence. *J. Geophys. Res.*, 89 (B11), 9305–9320.

GFZ: Deutsches GeoForschungsZentrum. <http://geofon.gfz-potsdam.de>. Last accessed February, 2014.

Görgün, E., Bohnhoff, M., Bulut, F., and Dresen, G., 2010. Seismotectonic setting of the Karadere-Duzce branch of the North Anatolian Fault Zone between the 1999 Izmit and Düzce ruptures from analysis of Izmit after- shock focal mechanisms. *Tectonophysics*, 482, 170–181.

Görür, N., Şengör, A.M.C., Sakıncı, M., Tüysüz, O., Akkök, R., Yiğitbaş, E., Oktay, F. Y., Barka, A., Sarıca, N., Ecevitöglu, B., Demirbağ, E., Ersoy, Ş., Algan, O., Güneysu, C., Aykol, A., 1995. Rift formation in the Gökova region, southwest Anatolia: implications for the opening of the Aegean Sea. *Geol. Mag.* 132, 637–650.

Grassberger, P., Procaccia, I., 1983. Measuring the strangeness of strange attractors. *Physica, D* 9, 189–208.

Gumbel, L.J., 1935. Les valeurs extremes des distribution statistiques. *Ann. Inst. Henri Poincare*, 5, 815–826.

Gumbel, L.J., 1958. *Statistics of extremes*. Columbia University, New York.

Gutenberg, B., and Richter, C., 1944. Frequency of earthquakes in California. *Bull. Seismol. Soc. Am.* 34 (4), 185.

Habermann, R.E., 1987. Man-made changes of seismicity rates. *Bull. Seism. Soc. Am.* 77 (1), 141–159.

Habermann, R.E., 1981. Precursory seismicity patterns: Stalking the mature seismic gap, in *Earthquake prediction - An international review*, edited by D. W. Simpson and P. G. Richards, 29–42, American Geophysical Union.

Habermann, R.E., 1983. Teleseismic detection in the Aleutian Island Arc. *J. Geophys. Res.* 88(B6), 5056–5064.

Hall, J., Aksu, A.E., Yaltrak, C., Winsor, J.D., 2009. Structural architecture of the Rhodes Basin: a deep depocentre that evolved since the Pliocene at the junction of Hellenic and Cyprus Arcs, eastern Mediterranean. *Marine Geology*, 258, 1–23.

Hall, J., Aksu, A.E., King, H., Gogacz, A., Yaltrak, C., and Çifçi, G., 2014. Miocene-Recent evolution of the western Antalya Basin and its linkage with the Isparta Angle, eastern Mediterranean. *Marine Geology*, 349, 1–23.

Heidbach, O., Tingay, M., Barth, A., Reinecker, J., Kurfeß, D., and Müller, B., 2008. The World Stress Map database release, doi:10.1594/GFZ.WSM. last Accessed September, 2014.

Hirata, T., 1989. Fractal dimension of fault system in Japan: Fractal structure in rock fracture geometry at various scales. *Pure and Applied Geophysics*.

Irmak, T.S., 2013. Focal mechanisms of small-moderate earthquakes in Denizli Graben (SW- Turkey). *Earth Planets Space*, 65, 943–955.

Jackson, J.A., and McKenzie, D.P., 1988. The relationship between plate motions and seismic moment tensors and rates of active deformation in the Mediterranean and Middle East. *Geophysical Journal*, 93, 45–73.

Jaume, S., and Sykes, L., 1999. Evolving towards a critical point: a review of accelerating seismic moment/energy release prior to large and great earthquakes. *Pure Appl. Geophys.* 155(2), 279–306.

Jenny, S., Goes, S., Giardini, D. and Kahle, H.G., 2004. Earthquake recurrence parameters from seismic and geodetic strain rates in the Eastern Mediterranean. *Geophysical Journal of International*, 157, 1331–1347.

Kagan, Y.Y., Knopoff, L., 1980. Spatial distribution of earthquakes: the two-point correlation function. *Geophysical Journal Royal Astronomical Society*, 62, 303–320.

Kahle, H.G., Straub, C., Reilinger, R., McClusky, S., King, R., Hurst, K., Veis, G., Kastens, K., Cross, P., 1998. The strain rate field in the eastern Mediterranean region, estimated by repeated GPS measurements. *Tectonophysics*, 294, 237–252.

Kaya, O., Ünay, E., Saraç, G., Eichhorn, S., Hassenrück, S., Knappe, A., Pekdeğer, A., and Mayda, S., 2004. Halitpaşa transpressive zone: implications for an Early Pliocene compressional phase in central western Anatolia, Turkey. *Turkish Journal of Earth Sciences*, 13, 1–13.

Khattari, K., 1973. Earthquake focal mechanism studies-A review, *Earth Sci. Rev.*, 9, 19–63.

Kiratzi, A., 2002. Stress tensor inversions along the westernmost north and central Aegean Sea. *Geophys. J. Int.* 106, 433–490.

Kiratzi, A., Louvari, E., 2003. Focal mechanisms of shallow earthquakes in the Aegean Sea and the surrounding lands determined by waveform modelling: a new database. *J. Geodyn.* 36, 251–274.

Kissel, C., and Laj, C., 1988, The Tertiary geodynamic evolution of the Aegean Arc: a palaeomagnetic reconstruction. *Tectonophysics*, 146, 183–201.

Kisslinger, C., and Jones, L.M., 1991. Properties of aftershocks in southern California. *J. Geophys. Res.* 96, 11947–11958.

Kisslinger, C., Bowman, J.R., and Koch, K., 1981. Procedures for computing focal mechanisms from local (SV/P) data. *Bull. Seism. Soc. Am.* 71, 1719–1729.

Koçyiğit, A., 2005. The Denizli graben-horst System and the eastern limit of western Anatolian continental extension: basin fill, structure, deformational mode, throw amount and episodic evolutionary history, SW Turkey. *Geodinamica Acta*, 18, 167–208.

Koçyiğit, A., and Özacar, A., 2003. Extensional neotectonic regime through the NE edge of the Outer Isparta Angle, SW Turkey: new evidence field and seismic data. *Turkish Journal of Earth Sciences*, 12, 67–90.

Koçyiğit, A., Ünay, E., Saraç, G., 2000. Episodic graben formation and extensional neotectonic regime in west Central Anatolia and the Isparta Angle: a case study in the Akşehir–Afyon Graben, Turkey. In: Bozkurt, E., Winchester, J.A., Piper, J.D.A. (Eds.), *Tectonics and Magmatism in Turkey and the Surrounding Area*. Geol. Soc. London, Spec. Publ., 173, 405–421.

Koçyiğit, A., Yusufoglu, H., and Bozkurt, E., 1999a. Evidence from the Gediz graben for episodic two-stage extension in western Turkey. *Journal of the Geological Society London*, 156, 605–616.

Koçyiğit, A., Yusufoglu, H., and Bozkurt, E., 1999b. Reply to ‘Discussion on evidence from the Gediz graben for episodic two-stage extension in western Turkey. *Journal of the Geological Society London*, 156, 1240–1242.

KOERI, 2005. Bogazici University Kandilli Observatory and Earthquake Research Institute: 17-21 October 2005 Sığacık Gulf-Seferihisar (İzmir) Earthquakes Report. <http://udim.koeri.boun.edu.tr/>. Last accessed February, 2104.

KOERI: Kandilli Observatory and Earthquake Research Institute, Boğaziçi University. <http://udim.koeri.boun.edu.tr/>. Last accessed February, 2014.

Kurt, H., Demirbağ , E., Kuşçu, İ., 1999. Investigation of the submarine active tectonism in the Gulf of Gökova, southwest Anatolia-southeast Aegean Sea, by multi-channel seismic reflection data. *Tectonophysics*, 305, 477–496.

Le Pichon, X., Angelier, J., 1979. The Hellenic arc and trench system: a key to the neotectonic evolution of the eastern Mediterranean area. *Tectonophysics*, 60, 1–42.

Le Pichon, X., Chamot-Rooke, C., Lallemand, S., Noomen, R., and Veis, G., 1995. Geodetic determination of the kinematics of central Greece with respect to Europe: implications for eastern Mediterranean tectonics. *Journal of Geophysical Research*, 100, 12675–12690.

Lund, B. and Townend, J., 2007. Calculating horizontal stress orientations with full or partial knowledge of the tectonic stress tensor. *Geophysical Journal International*, 170, 1328–1335.

McClusky, S., Balassanian, S., Barka, A.A., Demir, C., Ergintav, S., Georgiev, I., Gürkan, O., Hamburger, M., Hurst, K., Kahle, H.G., Kastens, K., Kekelidze, G., King, R., Kotzev, V., Lenk, O., Mahmoud, S., Mishin, A., Nadariya, M., Ouzounis, A., Paradissis, D., Peter, Y., Prilepin, M., Reilinger, R.E., Sanlı İ., Seeger, H., Tealeb, A., Toksöz, M.N., and Veis, G., 2000. Global Positioning System constraints on plate kinematics and dynamics in the Eastern Mediterranean and Caucasus. *Journal of Geophysical Research*, 105, 5695–5720.

- McClusky, S., Reilinger, R., Mahmoud, S., Sari, D.B., and Tealeb, A., 2003. GPS constraints on Africa (Nubia) and Arabia plate motions. *Geophys. J. Int.*, 155, 126–138.
- McKenzie, D.P., 1969. The relation between fault plane solutions for earthquakes and the directions of the principal stress. *Bull. Seism. Soc. Am.*, 59, 591–601.
- McKenzie, D.P., 1972. Active tectonics of the Mediterranean region. *Geophys. J. R. Astr. Soc.* 30, 109–185.
- McKenzie, D.P., 1978. Active tectonics of the Alpine-Himalayan belt: the Aegean Sea and surrounding regions. *Geophysical Journal of Royal Astronomy Society*, 55, 217–254.
- Meulenkamp, J.E., Van Der Zwan, G.J., and Van Wamel, W.A., 1994. On the late Miocene to recent vertical motions in the Cretan segment of the Hellenic arc. *Tectonophysics*, 234, 53–72.
- Meulenkamp, J.E., Wortel, M.J.R., Van Wamel, W.A., Spakman, W., and Hoogerduynstrating, E., 1988. On the Hellenic subduction zone and the geodynamic evolution of Crete since the late middle Miocene. *Tectonophysics*, 146, 203-215.
- Michael, A.J., 1984. Determination of stress from slip data: Faults and folds. *J. Geophys. Res.*, 89(11), 517-11,526.
- Michael, A.J., 1987. Use of Focal Mechanisms to Determine Stress: A Control Study. *J. Geophys. Res.*, 92, 357–368.
- Mogi, K., 1962. Study of elastic shocks caused by the fracture of heterogeneous materials and its relations to earthquake phenomena. *Bull Earthq. Res.* 40(1), 125–173.
- MTA: Maden Teknik ve Arama, Turkey. <http://www.mta.gov.tr/>. Last accessed February, 2015.
- Ocakoğlu, N., 2012. Investigation of Fethiye-Marmaris Bay (SW Anatolia): seismic and morphologic evidences from the missing link between the Pliny Trench and the Fethiye-Burdur Fault Zone. *Geo-Marine Letters*, 32, 17–28.

Ocakođlu, N., Demirbađ, E. and Kuşcu, İ., 2004. Neotectonic structures in the area offshore of Alaçatı, Dođanbey and Kuşadası (western Turkey): evidence of strike-slip faulting in the Aegean extensional province. *Tectonophysics*, 391, 67–83.

Ocakođlu, N., Demirbađ, E. and Kuşcu, İ., 2005. Neotectonic structures in İzmir Gulf and surrounding regions (western Turkey): evidences of strike-slip faulting with compression in the Aegean extensional regime. *Marine Geology*, 219, 155–171.

Okay, A.I., Satır, M., Maluski, H., Siyako, M., Monie, P., Metzger, R., Akyuz, H.S., 1996. Paleo- and Neo-Tethyan events in northwest Turkey: geological and geochronological constraints. In: Yin, A., Harrison, M. (Eds.), *Tectonics of Asia*. Cambridge University Press, Cambridge, 420–441.

Okay, A.I., Siyako, M., 1993. The revised location of the Izmir-Ankara Suture in the region between Balıkesir and Izmir. In: Turgut, S. (Ed.), *Tectonics and Hydrocarbon Potential of Anatolia and Surrounding Regions*. Ozan Sungurlu Symposium Proceedings. Ankara, 333–355 (in Turkish).

Oral, M.B., Reilinger, R.E., Toksöz, M.N., Kong, R.W., Barka, A.A., Kınık, İ., and Lenk, O., 1995. Global positioning system offers evidence of plate motions in Eastern Mediterranean. *EOS Transac.*, n.76 (9).

Öncel, A.O., Main, I., Alptekin, O., Cowie, P., 1996. Temporal variations in the fractal properties of seismicity in the north Anatolian fault zone between 31°E and 41°E. *Pure Applied Geophysics*, 147, 147–159.

Öncel, A.O., Wilson, T., 2002. Space-time correlations of seismotectonic parameters and examples from Japan and Turkey preceding the Izmit earthquake. *Bulletin Seismological Society of America*, 92, 339–350.

Öncel, A.O., 2004. Correlation of seismotectonic variables and GPS strain measurements in western Turkey. *Journal of Geophysical Research*, 109, 1–13.

Özener, H., Dogru, A., Acar, M., 2013. Determination of the displacements along the Tuzla Fault (Aegean region-Turkey): preliminary results from GPS and precise leveling techniques. *J. Geodyn.* 67, 13–20.

Özkaymak, Ç., Sözbilir, H., Uzel, B., Aküyuz, H. S., 2011. Geological and palaeoseismological evidence for late Pleistocene–Holocene activity on the Manisa Fault Zone, western Anatolia. *Turkish Journal of Earth Sciences*, 20 (4), 449–474.

Özmen, B., 2014. Assessment of the statistical earthquake hazard parameters for the Central Anatolia region, Turkey. *Arab J. Geosci.* doi 10.1007/s12517-014-1591-8. Last accessed December 2014.

Öztürk, S., 2012. Statistical correlation between b-value and fractal dimension regarding Turkish epicentre distribution. *Earth Sci. Res. J.* 16 (2), 103–108.

Papazachos, B.C., Papadimitriou, E.E., Kiratzi, A.A., Papazachos, C.B., Louvari, E.K., 1998. Fault plane solutions in the Aegean Sea and the surrounding area and their tectonic implication. *Boll. Geof. Teor. App.* 39, 199–218.

Papazachos, B., Kiratzi, A., Papadimitriou, E., 1991. Regional Focal Mechanism for Earthquakes in the Aegean area. *PAGEOPH*, 136, 407–420.

Papazachos, C.B., 1999. An alternative method for a reliable estimation of seismicity with an application in Greece and surrounding area. *Bulletin of Seismology Society of America*, 89, 111–119.

Pinar, A., 1998. Source inversion of the October 1 1995, Dinar earthquake Ms 6.1, a rupture model with implications for seismotectonics in SW Turkey. *Tectonophysics*, 292, 255–266.

Piper, J.D.A., Gürsoy, H., Tatar, O., İşseven, T., Koçyiğit, A., 2002. Palaeomagnetic evidence for the Gondwanic origin of the Taurides and rotation of the Isparta Agle, southern Turkey. *Geological Journal*, 37, 317–336.

Polat, O., Elcin, G., and Yilmaz, D., 2008. Earthquake Hazard of the Aegean Extension Region (West Turkey), *Turkish J. Earth Sci.* 17, 2008, 593–614.

- Pondrelli, S., A. Morelli, G. Ekström, S. Mazza, E. Boschi, and A.M. Dziewonski, 2002. European-Mediterranean regional centroid-moment tensors: 1997-2000. *Physics of the Earth and Planetary Interiors*, 130(1-2), 71–101.
- Pondrelli, S., Morelli, A. and Ekström, G., 2004. European-Mediterranean regional centroid-moment tensor catalog: solutions for years 2001 and 2002. *Physics of the Earth and Planetary Interiors*, 145(1-4), 127–147.
- Pondrelli, S., Salimbeni, S., Morelli, A., Ekström, G. and Boschi, E., 2007. European-Mediterranean Regional Centroid Moment Tensor catalog: Solutions for years 2003 and 2004. *Physics of the Earth and Planetary Interiors*, 164(1-2), 90–112.
- Price, S.P., Scott, B., 1994. Fault-block rotations at the edge of a zone of continental extension, southwest Turkey. *J. Struct. Geol.*, 16, 381–392.
- Purvis, M., and Robertson, A.H. F., 2004. A pulsed extension model for the Neogene-Recent E-W trending Alaşehir Graben and the NE-SW trending Selendi and Gördes basins, western Turkey. *Tectonophysics*, 391, 171–201.
- Purvis, M., and Robertson, A.H.F., 2005. Sedimentation of the Neogene-Recent Alaşehir (Gediz) continental graben system used to test alternative tectonic models for western (Aegean) Turkey. *Sedimentary Geology*, 173, 373–408.
- Reasenber, P., 1985. Second-order moment of Central California seismicity. *J. Geophys. Res.* 90, 5479–5495.
- Reilinger, R.E., McClusky, S.C., Oral, M.B., King, W., and Toksöz, M.N., 1997. GPS measurements of present day crustal movements in the Arabian-Africa-Eurasia plate collision zone. *Journal of Geophysical Research*, 102, 9983–9999.
- Reilinger, R., et al., 2006. GPS constraints on continental deformation in the Africa-Arabia-Eurasia continental collision zone and implications for the dynamics of plate interactions. *J. Geophys. Res.*, 111, B05411, doi:10.1029/2005JB004051. Last accessed December, 2014.

Ring, U., Gessner, K., Güngör, T., and Passchier, C.W., 1999. The Menderes Massif of western Turkey and the Cycladic Massif in the Aegean-do they really correlate. *Journal of Geological Society London*, 156, 3–6.

Rivera, L. and Cisternas, A., 1990. Stress tensor and fault plane solutions for a population of earthquakes. *Bull. Seism. Soc. Am.* 80, 600–614.

Robertson, A and Dixon, J., 1984. Introduction: aspects of geological evolution of eastern Mediterranean region. See Dixon and Robertson, 1–74.

Rojay, B., Toprak, V., Demirci, C., Süzen, L., 2005. Plio–Quaternary evolution of the Küçük Menderes Graben (Southwestern Anatolia, Turkey). *Geodinamica Acta*, 18, 317–331.

Rotstein, Y., 1984. Counter-clockwise rotation of Anatolian block. *Tectonophysics*, 108, 71–91.

Rydelek, P.A., and I.S. Sacks, 1989. Testing the completeness of earthquake catalogs and the hypothesis of self-similarity. *Nature*, 337, 251–253.

Rydelek, P.A., and I.S. Sacks, 1992. Comment on “Seismicity and detection/location threshold in the southern Great Basin seismic network” by Joan Gomberg, J. *Geophys. Res.* 97, 15361–15362.

Sadovsky, M.A., Golubeva, V.F., Pisarenko, and M.G., Shnirman 1984. Characteristic dimensions of rock and hierarchical properties of seismicity. *Izv. Ac. Sci. USSR Phys. Solid Earth*, 20, 87–96 (English Translation).

Sayıl, N., 2005. An application of the time- and magnitude-predictable model to long-term earthquake prediction in eastern Anatolia. *J. Seismol.* 9, 367–379.

Sayıl, N., and Osmañahin, I., 2004. An Application of the time- and magnitude-predictable model to long-term earthquake prediction in the Marmara region. The 16th International Geophysical Congress and Exhibition of Turkey, Cultural Center of Min Tech Res, Ankara, 107–111.

- Sayıl, N., and Osmañahin, I., 2005. An Application of the time- and magnitude-predictable model for the long term earthquake prediction in the Western Anatolia. International Symposium on the Geodynamics of Eastern Mediterranean: Active Tectonics of the Aegean Region, Kadir Has. Univ. Istanbul, 15-18 June 2005.
- Sayıl, N., and Osmañahin, İ., 2008. An investigation of seismicity for western Anatolia. *Nat. Hazards*, 44, 51–64.
- Scholz, C., 1968. Microfracturing and the inelastic deformation of rock in compression. *J. Geophys. Res.* 73(4), 1417–1432.
- Seyitođlu, G., 1997. Late Cenozoic tectono-sedimentary development of the Selendi and Uşak-Güre basins: a contribution to the discussion on the development of east-west and north trending basins in western Anatolia. *Geological Magazine*, 134, 163–175.
- Seyitođlu, G., and Scott, B.C., 1991. Late Cenozoic crustal extension and basin formation in west Turkey. *Geology Magazine*, 28, 155–166.
- Seyitođlu, G., and Scott, B.C., 1992. The age of the Büyük Menderes Graben (west Turkey) and its tectonic implications. *Geological Magazine*, 129, 239–42.
- Shanker, D., Yadav, R.B.S., Singh, H.N., 2007. On the seismic risk in the Hindukush-Pamir-Himalaya and their vicinity. *Curr. Sci. India*, 92(11), 1625–1630.
- Smith, W., 1981. The b-value as an earthquake precursor. *Nature*, 289, 136–139.
- Smith, W., 1986. Evidence for precursory changes in the frequency–magnitude b-value. *Geophys. J. R. Astron. Soc.* 86 (3), 815–838.
- Sözbilir, H., 2001. Geometry of macroscopic structures with their relations to the extensional tectonics: field evidence from the Gediz detachment, western Turkey. *Turkish Journal of Earth Sciences*, 10, 51–67.
- Sözbilir, H., 2002. Geometry and origin of folding in the Neogene sediments of the Gediz Graben, western Anatolia, Turkey. *Geodinamica Acta*, 15, 277–288.

Sözbilir, H., Erkül, F. and Sümer, Ö. 2003. Gümüldür (İzmir) ve Bigadiç (Balıkesir) arasında uzanan Miyosen sonrası yaşlı KD-Doğrultulu accommodation zonuna ait saha verileri, Batı Anadolu [Field evidence for post-Miocene NE-trending accommodation zone lying between Gümüldür (İzmir) and Bigadiç (Balıkesir), west Anatolia]. Geological Congress of Turkey, Ankara, Abstracts, 85–86.

Sözbilir, H., Uzel, B., Sümer, O., İnci, U., Ersoy, E.Y., Koçer, T., Demirtaş, R., Özkaymak, Ç., 2008. Evidence for a kinematically linked EW trending Izmir Fault and NE trending Seferihisar Fault: kinematic and paleo-seismological studies carried out on active faults forming the Izmir Bay, Western Anatolia. Geological Bulletin of Turkey, 51, 91–114.

Sözbilir, H., Sarı, B., Uzel, B., Sümer, O., Akkiraz, S., 2011. Tectonic implications of transtensional supra-detachment basin development in an extension-parallel transfer zone: the Kocaçay Basin, western Anatolia, Turkey. Basin Research, 23(4), 423-448.

Stein, S., Wysession, M., 2003. An introduction to seismology, earthquakes, and earth structure. Blackwell Publishing, Oxford.

Şaroğlu, F., Emre, Ö. and Kuşcu, İ., 1992. Active fault map of Turkey. MTA, Ankara.

Şaroglu F., Emre, Ö., Kuşcu I., 1995. Türkiye diri fay haritası. MTA Int. Report.

Şengör, A.M. C., 1979. The North Anatolian transform fault: its age, offset and tectonic significance. Journal of Geological Society London, 136, 269–282.

Şengör, A.M.C., 1987. Cross-faults and differential stretching of hanging walls in regions of low angle normal faulting: example from western Turkey. In: Coward, M.P., Dewey, J.F., Hancock, P.L. (Eds.), Continental extensional tectonics, Special Publication 28. Geological Society, London, pp. 575–589.

Şengör, A.M.C., Görür, N., and Şaroğlu, F., 1985. Strike slip faulting and related basin formation in zones of tectonic escape: Turkey as a case study, in K. Biddle, N. Christie-Blick, eds., Strike Slip Deformation, Basin Formation and Sedimentation: SEPM Special Publication, 37, 227–264.

Şengör, A.M.C., Satır, M., Akkök, R., 1984. Timing of tectonic events in the Menderes Massif, western Turkey: implications for tectonic evolution and evidence for Pan-African basement in Turkey. *Tectonics*, 3, 693–707.

Şengör, A.M.C., and Yılmaz, Y., 1981. Tethyan evolution of Turkey: A plate tectonic approach. *Tectonophysics*, 75, 181–241.

Tan, O., 2013. The dense micro-earthquake activity at the boundary between the Anatolian and South Aegean microplates. *J. Geodyn.* 65, 199–217.

Tan, O., and Taymaz, T., 2003. Seismotectonics of Karaburun Peninsula and Kuşadası Gulf: source parameters of April 2, 1996 Kuşadası Gulf and April 10, 2003 Seferihisar (Izmir) earthquakes. *International Workshop on the North Anatolian, East Anatolian and Dead Sea Fault Systems: Recent Progress in Tectonics and Paleoseismology and Field Training Course in Paleoseismology*, Middle East Technical University, Ankara, Abstracts, p. 147.

Taymaz, T., 1993. The source parameters of the Çubukdağ (W Turkey) earthquake of 1986 October 11. *Geophysical Journal International*, 113, 260–267.

Taymaz, T., Jackson, J., McKenzie, D., 1991. Active tectonics of the north and central Aegean Sea. *Geophys. J. Int.* 106, 433–490.

Taymaz, T., Tan, O. and Yolsal, S. 2004. Seismotectonics of western Turkey: a synthesis of source parameters and rupture histories of Recent earthquakes. *AGU Fall Meeting, Session T14, San Francisco-California, EOS Transactions*, 85 (47).

Taymaz, T., Yılmaz, Y., Dilek, Y., 2007. The geodynamics of the Aegean and Anatolia: introduction. *The Geological Society of London, Special Publications Book*. pp. 1–16.

ten Veen, J.H., 2004. Extension of Hellenic forearc shear zones in SW Turkey: the Pliocene-Quaternary deformation of the Eşen Çay Basin. *J. Geodyn.* 37, 181–204.

Tezcan, S., 1996. Probability analysis of earthquake magnitudes. *Turkish Earthquake Foundation, TDV/TR 96–001*, p26.

Taymaz, T., Price, S.P., 1992. The 12.05.1971 Burdur earthquake sequence: a synthesis of seismological and geological observations. *Geophys. J. Int.* 108, 589–603.

Tan, O., Taymaz, T., 2001. Source parameters of November 6, 1992 Doğanbey (Izmir) earthquake ($M_w=6.0$) obtained from inversion of teleseismic body-waveforms. 4th International Turkish Geology Symposium 24–28 September, 2001, Çukurova University, Adana, Turkey. Abstracts, p.171.

Uluğ, A., Duman, M., Avcı, M., Özel, E., Ecevitoglu, B., Demirbağ, E., Algan, O., Gökasan, E., 1996. Late Quaternary evolution of the Gulf of Gökova, southeastern Aegean Sea: Deltaic sedimentation and sea-level change (in Turkish). 11th Petroleum Congress and Exhibition of Turkey, Proceedings, 59–72.

Utsu, T., 1965. A method for determining the value of b in a formula $\log N=a - bM$ showing the magnitude-frequency relation for earthquakes. *Geophys. Bull. Hokkaido Univ.*, 13, 99-103.

Utsu, T., Ogata, Y., Matsu'ura, R.S., 1995. The centenary of the Omori formula for a decay law of aftershock activity. *J. Phys. Earth*, 43, 1–33.

Uzel, B. Sözbilir, H. 2008. A First Record of a Strike-slip Basin in Western Anatolia and its Tectonic Implication: The Cumaovası Basin. *Turkish J. Earth Sci.*, 17, 559-591.

Uzel, B., and Sözbilir, H., 2005. First record of Quaternary pull-apart basin in western Anatolia: the Cumaovası basin, İzmir-Turkey. *International Earth Sciences Colloquium on the Aegen Region, İzmir*, Abstracts, p. 119.

Uzel, B., and Sözbilir, H., 2006. Batı Anadolu'da normal faylar ve doğrultu atımlı fayların birlikte işlediği havzalara bir örnek: Cumaovası çekayır havzası, İzmir [An example of basins which developed under the control of normal faults and strike-slip faults: Cumaovası pull apart basin, İzmir]. 10th Meeting of Active Tectonics Research Group, Abstracts, p. 93.

Uzel, B., Sözbilir, H., Ozkaymak, Ç., 2012. Neotectonic evolution of an actively growing superimposed Basin in Western Anatolia: the inner Bay of Izmir, Turkey. *Turkish Journal of Earth Sciences*, 21, 439–471.

Vannucci, G., and Gasperini, P., 2004. The new release of the database of Earthquake Mechanisms of the Mediterranean Area (EMMA Version 2). *Annals of Geophysics*, Supplement to v. 47.

Wallace, R.E., 1951. Geometry of shearing stress and relation to faulting. *J. Geol.* 59: 118–130.

Warren, N.W., Latham, G. V., 1970. An experimental study of thermally induced microfracturing and its relation to volcanic seismicity, *J. Geophys. Res.*, 75, 4455–4464.

Westaway, R., 1990. Block rotations in western Turkey: Observational evidence. *J. Geophys. Res.* 95, 19857–19884.

Westaway, R., Guillou, H., Yurtmen, S., Demir, T., Scaillet, S., and Rowbotham, G., 2005. Constraints on the timing and regional conditions at the start of the present phase of crustal extension in western Turkey, from observations in and around the Denizli region. *Geodinamica Acta*, 18, 209–238.

Wiemer, S., 2001. A software package to analyze seismicity: ZMAP, *Seismological Research Letters*. 72, 373–382.

Wiemer, S., and Baer, M., 2000. Mapping and removing quarry blast events from seismicity catalogs, *Bull. Seism. Soc. Am.*, 90(2), 525-530.

Wiemer, S., Gerstenberger, M.C., Hauksson, E., 2002. Properties of the 1999, Mw 7.1, Hector Mine earthquake: implications for aftershock hazard. *Bull. Seismol. Soc. Am.* 92, 1227–1240.

Wiemer, S., McNutt, S., and Wyss, M., 1998. Temporal and three-dimensional spatial analyses of the frequency–magnitude distribution near Long Valley Caldera, California. *Geophys. J. Int.* 134 (2), 409–421.

Wiemer, S., Wyss, M., 1997. Mapping the frequency-magnitude distribution in asperities: an improved technique to calculate recurrence times. *J. Geophys. Res.* 102 (B7), 15115–15128.

Wiemer, S., and Wyss, M., 2002. Mapping spatial variability of the frequency-magnitude distribution of earthquakes. *Adv. Geophys.* 45, 259–302.

Woodside, J., Mascle, J., Huguen, C., Volkonskaia, A., 2000. The Rhodes Basin, a post-Miocene tectonic trough. *Mar. Geol.* 165, 1–12.

Wright, T.J., Parsons, B. E., Jackson, J.A., Haynes, M., Fielding, E.J., England, P.C., Clarke, P.J., 1999. Source parameters of the 1 October 1995 Dinar (Turkey) earthquake from SAR interferometry and seismic body modelling. *Earth Planet. Sci. Lett.* 172, 23–37.

WSM, CASMO: World Stress Map, Create A Stress Map Online. Available at www.world-stress-map.org. Last accessed September, 2014.

Wyss, M., K. Shimazaki, and Wiemer, S., 1997. Mapping active magma chambers by b-value beneath the off-Ito volcano, Japan, *J. Geophys. Res.*, 102, 20413–20422.

Yadav, R.B.S., Tripathi, J.N., Shanker, D., Rastogi, B.K., Das, M.C., Kumar, V., 2011. Probabilities for the occurrences of medium to large earthquakes in Northeast India and adjoining region. *Nat. Hazards*, 56, 145–167.

Yılmaz, Y., Genç, S.C., Gürer, Ö.F., Bozcu, M. Yılmaz, K., Karacık, Z., Altunkaynak, Ş., and Elmas, A., 2000, When did western Anatolian grabens begin to develop, in E. Bozkurt.

Yılmaztürk, A., Burton, P.W., 1999. Earthquake source parameters as inferred from body waveform modeling, southern Turkey. *J. Geodynamics* 27, 469–499.

Yolsal, Ç. S., Taymaz, T., and Cahit, H., 2014. Earthquake mechanisms in the Gulfs of Gökova, Sığacık, Kuşadası, and the Simav Region (western Turkey): Neotectonics, seismotectonics and geodynamic implications, *Tectonophysics*, <http://dx.doi.org/10.1016/j.tecto.2014.05.001>. Last accessed December, 2014.

Yolsal, S., Kilinc, H., and Taymaz, T., 2005. The Relationship between heat flow regime and active tectonics inferred from seismological data in western Anatolia. Proceedings World Geothermal Congress, 2005, Antalya, Turkey, 24–29 April 2005.

Zanchi, A., Angelier, J., 1993. Seismotectonics of western Anatolia: regional stress orientation from geophysical and geological data. *Tectonophysics* 222, 259–274.

Zhu, L., Akyol, N., Mitchell, B. J., and Sözbilir, H., 2006. Seismotectonics of western Turkey from high resolution earthquake relocations and moment tensor determinations. *Geophysical Research Letters*, 33, L07316, doi: 10.1029/2006GL025842. Last accessed September, 2014.

Zitter, T.A.C., Huguen, C., Woodside, J.M., 2005, Geology of mud volcanoes in the eastern Mediterranean from combined side scan sonar and submersible surveys: *Deep-Sea Research I*, 52, 457–475.

Zoback, M.L., 1992. Stress field constraints on intra-plate seismicity in eastern North America. *J. Geophys. Res.* 97 (B8), 11761-11782.

APPENDIX A

FOCAL MECHANISM SOLUTIONS

Table A. 1: Parameter list of earthquake focal mechanism solutions compiled in this study from various sources.

References are: 1, AFAD; 2, Benetatos *et al.*, 2006; 3, Braunmiller and Nabelek, 1996; 4, CMT; 5, EMMA; 6, ETH; 7, Eyidoğan and Jackson, 1985; 8, GFZ; 9, Kirtazi and Louvari, 2003; 10 McKenzie, 1972; 11, McKenzie, 1978; 12, Papazachos *et al.*, 1991; 13, RCMT; 14, Taymaz and Price, 1992; 15, Taymaz *et al.*, 1991; 16, Taymaz *et al.*, 2004; 17, Yılmaztürk and Burton, 1999; 18, Zanchi and Angelier, 1993.

Id	Longitude	Latitude	Y/M/D	M	Depth	H:M	Strike	Dip	Rake	Subset	Ref
1	26.9	38.7	1909.1.19	6	0.00	0:00	59	51	75	9	5
2	30.4	37.9	1914.10.3	6.9	0.00	0:00	222	42	-107	1	5
3	27.400	39.100	1919.11.18	6.8	0.00	21:54	270	45	-90	9	5
4	30.14	39.08	1924.11.20	6	0.00	0:00	308	35	-90	5	10
5	29.600	37.900	1925.8.7	6	0.00	6:46	64	50	-75	1	10
6	27.400	38.200	1928.3.31	6.4	0.00	0:29	90	45	-90	9	5
7	29.450	39.410	1928.5.2	6.1	0.00	21:54	300	45	-90	2	5
8	27.4	36.7	1933.4.23	6.4	0.00	0:00	60	45	-90	6	5
9	27.000	39.100	1939.9.22	6.4	0.00	0:36	56	52	-106	4	10
10	28.200	37.200	1941.5.23	6	0.00	22:34	65	45	-90	9	5
11	28.100	39.380	1941.11.15	6.1	0.00	0:00	288	51	-78	1	5
12	29.260	38.900	1944.6.25	6	0.00	4:16	308	35	-90	9	5
13	26.7	39.4	1944.10.6	6.7	20.00	2:34	260	70	-180	6	5
14	26.7	38.7	1949.7.23	6.7	0.00	15:03	262	41	-108	9	5
15	27.190	37.660	1955.7.16	6.7	10.00	7:07	292	55	-49	2	5
16	28.6	36.5	1957.4.25	7.2	1.00	2:25	58	85	19	10	5
17	27	36.5	1958.5.27	4.7	125.00	18:27	120	78	-21	1	17

Table A. 1 (continued)

18	27.4	36.5	1958.6.30	5.4	80.00	8:42	110	78	17	1	5
19	28.550	37.050	1959.4.25	6.2	1.00	0:26	65	76	-70	1	5
20	28.5	36.9	1959.4.25	5.3	0.00	1:05	39	70	-72	1	5
21	26.59	38.91	1959.11.19	5.4	10.00	14:00	240	60	-152	8	18
22	27.600	37.800	1960.4.10	4.9	0.00	22:05	46	70	146	7	5
23	28.3	36.6	1961.5.23	6.5	72.00	2:45	89	62	90	5	5
24	29.300	38.100	1963.3.11	5.3	0.00	7:27	331	67	163	9	7
25	29.900	37.300	1964.1.30	5.2	0.00	17:45	115	88	-25	1	18
26	28.330	38.470	1965.3.2	5.7	42.00	22:00	257	44	-134	9	7
27	29.320	37.850	1965.6.13	6	2.00	20:01	91	74	-103	8	5
28	27.800	37.700	1966.5.7	5.1	0.00	13:08	83	27	-90	8	3
29	29.3	36.8	1967.6.1	5.1	0.00	10:39	160	65	180	3	5
30	29.000	37.200	1967.10.26	4.9	0.00	4:55	151	64	-56	4	10
31	29.110	38.810	1968.3.11	5	23.00	18:40	46	60	144	1	5
32	27	36.6	1968.10.31	5.7	0.00	3:22	140	82	30	8	3
33	26.9	36.6	1968.12.5	6	7.00	7:52	57	46	-72	1	5
34	28.500	39.100	1969.3.23	6	8.00	21:08	112	34	-90	1	11
35	28.510	39.110	1969.3.24	5	30.00	1:59	165	45	-37	9	18
36	28.400	39.200	1969.3.25	6.1	8.00	13:21	288	51	-79	1	5
37	28.440	39.080	1969.3.25	4.9	42.00	16:13	240	52	116	1	5
38	28.460	38.550	1969.3.28	6.7	3.00	1:48	300	41	-97	9	18
39	28.450	39.130	1969.3.28	5	37.00	10:02	314	86	11	1	5
40	28.580	39.160	1969.4.30	5.4	8.00	20:20	288	55	-72	7	5
41	28.400	39.200	1969.10.7	5	13.00	5:09	52	70	5	1	5
42	29.500	39.200	1970.3.28	7.1	8.00	21:02	304	41	-97	10	5
43	29.460	39.280	1970.3.28	5	17.00	21:59	165	76	37	1	5
44	29.550	39.120	1970.3.28	5.5	33.00	23:11	74	32	-110	1	5
45	29.740	39.060	1970.3.29	5.3	39.00	6:56	275	59	-54	6	7
46	29.420	39.140	1970.3.29	4.9	22.00	19:11	162	76	37	10	7
47	29.400	39.430	1970.3.30	4.8	33.00	6:49	301	70	-90	1	5
48	29.260	39.340	1970.3.30	5	8.00	7:59	280	68	-90	1	5
49	29.410	39.330	1970.3.31	4.8	18.00	0:51	165	70	-27	1	5
50	29.790	39.030	1970.3.31	4.9	35.00	3:46	105	70	-90	1	11
51	29.270	39.320	1970.4.1	5	35.00	15:56	260	65	-119	1	5
52	29.320	39.340	1970.4.7	5.3	33.00	17:05	270	48	-120	1	5
53	29.410	39.110	1970.4.9	4.9	34.00	10:12	110	60	-90	1	5
54	29.300	39.340	1970.4.15	4.8	28.00	16:29	20	80	29	9	18
55	29.920	38.970	1970.4.16	5.6	8.00	10:42	112	60	-84	1	14
56	29.800	39.000	1970.4.19	6.1	9.00	13:29	104	43	-90	1	12
57	29.800	39.030	1970.4.19	5.8	24.00	13:47	114	24	-90	9	14

Table A. 1 (continued)

58	29.770	39.020	1970.4.22	5.3	37.00	5:24	95	85	-90	10	7
59	29.420	39.080	1970.4.22	4.8	48.00	18:38	135	51	-74	7	17
60	28.600	39.080	1970.4.23	5.6	28.00	9:01	77	50	-96	10	5
61	29.850	39.010	1970.4.24	4.9	32.00	0:40	293	69	-90	5	5
62	29.540	39.060	1970.4.27	4.9	11.00	22:24	75	90	90	9	17
63	29.240	39.400	1970.12.20	5.2	26.00	11:01	285	58	-82	10	5
64	29.890	39.030	1971.4.13	5.3	13.00	12:52	120	50	-90	9	15
65	29.700	37.570	1971.5.12	5.8	12.00	6:25	68	56	-80	8	4
66	29.700	37.600	1971.5.12	5.6	5.00	10:10	73	14	-90	8	4
67	29.600	37.600	1971.5.12	5.5	12.00	12:57	53	25	-92	5	5
68	29.670	39.070	1971.5.25	5.9	6.00	5:43	96	37	-108	8	4
69	30.240	37.300	1971.9.9	5.6	34.00	15:10	160	90	173	1	5
70	29.460	39.300	1972.3.14	5.6	18.00	14:05	101	35	-87	8	4
71	27.200	38.500	1974.2.1	5.2	0.00	0:01	250	66	-152	10	5
72	28.890	37.700	1976.8.19	6.1	4.00	1:12	276	69	-131	2	5
73	27.200	38.400	1977.12.16	5.2	0.00	7:37	303	70	-75	10	5
74	26.600	38.800	1979.6.14	5.9	8.00	11:44	262	41	-108	1	5
75	26.770	38.460	1979.6.16	5.8	15.00	18:42	255	58	-124	8	5
76	29.190	39.440	1979.7.18	5.3	15.00	13:12	111	34	-85	8	5
77	27.780	38.815	1980.1.1	6.6	16.00	16:42	58	90	180	5	5
78	27.700	36.970	1983.9.27	5.4	170.00	23:59	312	46	162	2	5
79	30.18	38.1	1985.10.1	6.2	8.00	17:57	312	56	-84	1	5
80	28.710	37.310	1986.10.11	5.6	15.00	9:00	320	57	-39	10	5
81	28.13	36.77	1987.6.19	5.3	59.50	18:45	316	54	137	9	5
82	26.8	37	1988.7.15	3	11.80	17:44	305	60	-137	8	4
83	26.89	37.77	1988.8.9	3.6	32.30	12:34	344	54	93	8	4
84	26.72	37.63	1988.8.9	3.6	21.50	13:09	10	49	107	5	9
85	26.88	37.27	1988.8.14	3.5	19.50	7:27	99	49	-76	5	9
86	26.89	37.26	1988.8.17	4.4	20.80	2:10	70	40	-89	8	4
87	26.81	36.99	1988.8.18	3.9	13.90	9:01	88	51	-69	8	4
88	26.8	36.99	1988.8.18	3.7	15.10	10:13	109	41	-70	9	9
89	26.87	37.25	1988.8.19	3.6	10.00	1:52	260	49	-98	5	9
90	26.79	37	1988.8.21	4	16.20	15:23	20	49	-41	1	16
91	26.81	36.98	1988.8.21	3.6	15.60	21:25	10	44	-81	8	4
92	28.320	37.010	1989.2.19	5.4	15.00	14:28	93	32	-85	8	4
93	29.440	37.760	1989.2.24	5.3	15.00	0:40	113	39	-77	5	9
94	28.200	37.100	1989.4.27	5.3	7.00	23:06	271	57	-103	8	4
95	28.010	37.060	1989.4.28	5.3	22.00	13:30	271	58	-103	10	5
96	29.640	37.000	1990.7.18	5.5	15.00	11:29	65	47	-114	8	4
97	26.980	37.840	1992.11.6	6	24.50	19:08	147	77	-5	8	5

Table A. 1 (continued)

98	26.97	38.02	1992.11.6	6	6.00	20:06	146	76	13	1	13
99	27.480	38.670	1994.1.28	5.4	45.00	14:15	114	60	-71	9	16
100	26.530	38.690	1994.5.24	5.2	10.00	2:05	119	54	-64	9	16
101	28.020	37.120	1994.11.13	5.4	15.00	6:56	139	36	-83	8	4
102	29.680	38.060	1995.10.1	6.4	15.00	15:57	125	30	-94	1	13
103	26.87	37.84	1996.4.2	5.3	9.00	7:59	261	53	-119	7	13
104	28.330	37.980	1997.1.21	5.2	18.10	20:47	316	72	-69	7	13
105	28.45	36.53	1998.2.24	4.5	33.00	15:11	323	45	92	7	13
106	30.160	38.100	1998.4.4	5.2	15.00	16:16	313	46	-105	1	13
107	29.330	37.220	1999.3.29	4.6	33.00	4:05	354	75	-16	1	13
108	27.890	39.290	1999.7.24	5	11.00	16:04	334	50	-27	1	13
109	27.980	39.330	1999.7.25	4.9	15.00	6:56	152	69	-32	1	13
110	28.240	36.750	1999.10.5	4.8	15.00	0:53	55	48	-75	1	13
111	29.390	37.78	2000.4.21	5.4	15.00	12:23	342	75	-72	9	13
112	27.700	39.360	2000.9.8	4.6	10.00	5:46	336	72	-28	8	4
113	29.050	37.920	2000.10.4	5	8.00	2:34	135	28	-93	8	4
114	26.810	37.840	2001.3.1	4.4	10.00	13:31	145	56	-53	1	13
115	27.920	39.300	2001.5.24	4.5	15.00	3:18	323	20	-14	8	4
116	27.740	39.350	2001.6.22	5.1	5.00	11:54	342	52	-25	6	13
117	27.880	39.470	2001.6.23	4.8	10.00	12:18	347	52	-4	7	4
118	27.880	38.660	2002.1.21	4.7	10.00	14:34	130	56	-70	9	13
119	29.180	37.700	2002.7.30	4.7	8.00	12:20	153	41	-41	9	13
120	28.030	36.670	2002.9.26	4.3	5.00	20:44	239	28	-105	9	13
121	26.860	38.050	2003.4.10	5.7	15.00	0:40	250	76	-160	10	13
122	26.750	37.920	2003.4.17	5.2	15.00	22:34	156	50	-15	1	13
123	28.040	39.030	2003.6.22	4.6	7.00	23:46	135	46	-68	8	4
124	28.770	37.880	2003.7.23	5.3	15.00	4:56	97	31	-111	8	4
125	28.890	38.110	2003.7.26	4.7	10.00	1:00	56	69	-158	8	4
126	29.050	38.030	2003.7.26	5.4	15.00	8:36	60	57	-147	8	4
127	28.920	38.120	2003.7.26	4.8	10.00	13:31	101	22	-110	1	6
128	26.920	36.630	2003.09.13	4.9	155.00	13:46	92	71	8	1	13
129	26.830	38.970	2003.12.16	4.5	15.00	10:41	76	57	-122	9	13
130	30.280	38.380	2004.6.9	4.3	38.00	3:15	207	67	-89	9	6
131	27.700	36.880	2004.8.3	4.7	10.00	5:33	266	56	-74	8	4
132	27.930	36.770	2004.8.3	5.2	12.00	13:11	74	38	-97	1	6
133	27.880	36.800	2004.8.4	5.5	12.00	3:01	75	40	-95	3	13
134	27.970	36.820	2004.8.4	5.2	12.00	4:19	71	42	-111	8	4
135	27.910	36.810	2004.8.4	5.3	12.00	14:18	75	41	-94	1	6
136	27.790	36.730	2004.8.4	5.3	10.00	15:48	255	84	-6	8	4
137	27.880	36.540	2004.08.20	4.5	77.00	11:12	345	62	172	1	6

Table A. 1 (continued)

138	27.760	39.180	2004.11.5	4.6	10.00	17:30	138	41	-90	3	13
139	27.963	39.256	2004.12.2	4.6	15.00	15:51	69	80	-156	1	6
140	28.330	36.880	2004.12.20	5.3	12.00	23:02	105	45	-69	3	13
141	28.210	37.060	2004.12.21	4.2	9.00	0:23	266	52	-93	8	2
142	28.340	37.010	2004.12.28	4.4	10.00	20:34	276	41	-56	5	2
143	27.870	36.840	2005.1.10	5.4	15.10	23:48	255	51	-114	none	2
144	27.919	37.018	2005.1.10	5.2	9.00	23:50	93	53	-89	4	2
145	27.840	36.840	2005.1.11	5	12.20	4:35	255	60	-103	10	2
146	27.714	39.177	2005.1.13	4.3	15.00	13:39	257	86	169	6	2
147	26.870	38.110	2005.01.29	4.8	10.00	18:52	241	66	-164	6	2
148	26.700	37.800	2005.6.23	4.7	18.00	22:44	232	37	-175	9	2
149	26.780	36.570	2005.08.01	4.7	133.00	13:35	306	39	-172	2	2
150	26.632	38.15	2005.10.17	3.9	10.00	4:31	157	70	-25	6	2
151	26.62	38.153	2005.10.17	5.4	15.00	5:45	247	82	-175	8	4
152	26.66	38.168	2005.10.17	3.9	12.00	6:16	156	74	-31	2	2
153	26.629	38.158	2005.10.17	4.1	18.00	7:05	172	80	-17	8	2
154	26.615	38.164	2005.10.17	3.6	6.00	7:49	166	58	-95	6	2
155	26.653	38.166	2005.10.17	3.8	16.00	8:07	175	80	-12	6	2
156	26.654	38.177	2005.10.17	4.3	18.00	8:28	255	67	-170	6	2
157	26.632	38.138	2005.10.17	4.2	11.00	8:34	152	85	-43	3	2
158	26.64	38.166	2005.10.17	3.4	5.00	8:50	221	85	-165	2	2
159	26.663	38.178	2005.10.17	5.8	7.00	9:46	136	81	-11	9	2
160	26.660	38.150	2005.10.17	5.8	12.00	9:47	231	76	-177	8	2
161	26.635	38.147	2005.10.17	5.2	21.00	9:55	255	73	-175	8	2
162	26.64	38.14	2005.10.17	3.7	5.00	10:57	327	83	-10	6	2
163	26.684	38.18	2005.10.17	3.9	6.00	11:20	145	82	-16	2	2
164	26.705	38.187	2005.10.17	3.7	16.00	11:48	351	82	71	2	2
165	26.753	38.152	2005.10.17	3.4	5.00	12:02	141	86	18	2	2
166	26.673	38.132	2005.10.17	3.2	7.00	12:05	47	79	-24	2	2
167	26.681	38.175	2005.10.17	3.5	4.00	12:09	153	81	-37	9	2
168	26.674	38.136	2005.10.17	3.7	7.00	12:22	239	85	164	7	2
169	26.657	38.146	2005.10.17	3.2	6.00	12:32	251	72	-143	4	2
170	27.011	38.392	2005.10.17	3.6	10.00	12:34	239	52	-169	9	2
171	26.65	38.146	2005.10.17	4	8.00	12:43	319	83	10	9	2
172	26.657	38.179	2005.10.17	3.9	5.00	13:16	151	85	-29	9	2
173	26.638	38.173	2005.10.17	3.8	11.00	13:22	155	83	-8	9	2
174	26.689	38.126	2005.10.17	3.4	17.00	14:53	38	90	12	9	2
175	26.642	38.154	2005.10.17	3.9	10.00	23:13	249	88	174	9	2
176	26.664	38.134	2005.10.18	3.5	5.00	5:04	52	74	-164	9	2
177	26.635	38.174	2005.10.18	4.2	22.00	16:00	167	82	35	6	2

Table A. 1 (continued)

178	26.705	38.159	2005.10.18	3.9	19.00	22:49	77	81	171	6	2
179	26.612	38.129	2005.10.19	3.6	17.00	5:51	176	88	-19	9	2
180	26.67	38.181	2005.10.19	4.6	15.00	10:11	244	89	178	9	2
181	26.632	38.168	2005.10.19	3.7	7.00	10:22	332	86	36	9	2
182	26.717	38.157	2005.10.20	4	19.00	9:10	71	89	-179	9	2
183	26.694	38.183	2005.10.20	5.8	7.00	21:40	231	66	-162	9	2
184	26.608	38.112	2005.10.21	3.8	20.00	0:34	353	90	19	9	2
185	26.599	38.178	2005.10.21	4.3	10.00	11:47	244	88	-175	6	2
186	26.839	38.2	2005.10.21	3.7	13.00	16:34	44	81	162	8	2
187	26.765	38.157	2005.10.22	3.7	12.00	7:21	151	87	-17	8	2
188	26.628	38.184	2005.10.22	3.7	19.00	15:35	80	89	179	9	2
189	26.56	38.185	2005.10.22	3.6	20.00	18:00	338	82	46	8	2
190	26.715	38.149	2005.10.22	3.5	18.00	19:05	341	86	-10	8	2
191	26.594	38.11	2005.10.23	4	17.00	14:59	79	88	171	3	13
192	26.573	38.155	2005.10.24	3.6	12.00	16:55	169	87	17	3	13
193	26.525	38.092	2005.10.24	3.6	18.00	17:03	239	81	142	8	4
194	26.607	38.174	2005.10.24	3.9	18.00	21:15	155	89	-4	8	4
195	26.702	38.178	2005.10.25	3.8	20.00	8:58	163	86	23	8	4
196	26.578	38.127	2005.10.26	3.8	13.00	17:48	349	89	-17	6	13
197	26.61	38.128	2005.10.29	4.2	14.00	14:48	261	67	-158	8	4
198	26.644	38.138	2005.10.31	4.9	16.00	5:26	231	75	156	1	13
199	26.65	38.127	2005.10.31	4.2	12.00	6:48	340	88	-3	9	13
200	27.780	38.800	2005.12.24	4.6	14.00	3:56	355	49	-15	8	4
201	26.940	36.670	2006.04.19	4.6	131.00	5:40	337	57	169	9	13
202	28.650	37.800	2006.6.5	4.8	21.70	4:23	295	34	-88	9	13
203	28.900	38.190	2007.1.23	4.9	13.20	21:22	301	28	-103	8	4
204	29.210	36.890	2007.10.29	5.3	12.00	9:23	275	37	-107	7	1
205	29.410	36.960	2007.10.29	4.7	13.00	19:41	76	41	-117	8	4
206	29.270	36.990	2007.10.31	4.8	5.00	17:58	73	39	-126	8	4
207	29.340	36.830	2007.11.16	5.1	13.00	9:08	263	38	-108	1	6
208	26.950	38.610	2008.01.05	4.3	11.00	5:11	240	85	148	4	1
209	28.940	37.840	2008.4.25	5	12.20	4:48	160	77	-65	8	4
210	29.1508	37.0192	2009.1.1	3.7	22.52	19:01	300	72	173	6	1
211	28.980	39.150	2009.2.17	5.2	16.80	5:28	131	55	-57	1	1
212	26.960	37.580	2009.6.20	5.1	12.00	8:11	105	36	-90	4	1
213	27.040	37.650	2009.6.20	5.1	10.00	8:28	291	41	-73	5	1
214	27.5892	37.8568	2009.8.1	4.1	7.03	15:43	100	51	-97	1	1
215	28.690	37.900	2009.12.4	4.9	13.60	6:02	128	58	-67	9	1
216	29.1245	39.0568	2010.3.2	4.2	24.36	0:43	193	77	-50	7	1
217	29.6883	36.7312	2010.5.26	4.5	20.66	14:22	12	39	-142	9	13

Table A. 1 (continued)

218	27.5943	36.9763	2010.7.9	4.1	26.31	14:17	280	56	-83	9	1
219	27.4003	36.8	2010.7.15	4.3	22.42	5:35	118	79	-26	6	1
220	26.840	36.790	2010.07.16	5.2	168.00	8:11	78	54	-9	1	1
221	30.3463	36.9807	2010.7.25	4.3	7.32	17:06	92	45	-28	8	4
222	27.0433	37.4865	2010.8.4	4.2	12.66	20:38	36	44	161	7	1
223	27.952	38.0022	2010.10.5	4.1	17.11	23:43	281	54	-115	7	1
224	27.340	37.690	2010.11.11	5	17.10	20:08	114	44	-63	5	1
225	27.3385	37.8558	2010.11.14	4.1	18.66	5:21	78	26	-84	8	4
226	27.9827	36.7845	2010.12.14	4.2	55.00	23:02	5	89	144	10	1
227	28.0227	39.0602	2011.5.1	4.1	24.88	15:04	165	46	-65	8	4
228	27.360	36.570	2011.5.8	5.2	12.90	6:50	60	30	-97	9	1
229	27.2632	36.8552	2011.5.8	4.9	18.22	6:51	78	33	-70	9	13
230	29.110	39.080	2011.5.19	5.9	12.10	20:15	98	44	-96	9	1
231	29.040	39.120	2011.5.19	4.6	8.00	21:12	319	60	-63	9	1
232	29.1078	39.1442	2011.5.19	4.6	7.00	20:25	89	47	-83	9	1
233	29.0317	39.1128	2011.5.19	4.3	6.99	21:21	127	44	-68	7	1
234	29.1235	39.131	2011.5.19	4.3	20.83	21:33	98	28	-106	5	1
235	29.1065	39.1413	2011.5.20	4.1	16.92	0:13	81	35	-89	none	1
236	29.0837	39.1147	2011.5.20	4.3	17.38	0:58	252	64	-95	2	1
237	29.0023	39.1443	2011.5.20	4	6.97	4:00	123	53	-59	10	1
238	29.0872	39.1202	2011.5.20	4.2	7.09	5:00	79	46	-79	3	1
239	29.0513	39.1037	2011.5.21	4	7.00	21:43	124	47	-89	1	8
240	27.1522	39.0988	2011.5.23	4	26.37	10:06	88	80	-171	8	4
241	29.0217	39.1013	2011.5.24	4.2	16.80	2:55	44	58	-87	2	1
242	29.199	39.111	2011.5.27	4.4	16.00	7:43	118	57	-57	5	1
243	29.040	39.090	2011.5.28	5.1	14.10	5:47	314	45	-65	10	1
244	29.0278	39.1123	2011.5.28	4	16.62	18:06	99	45	-78	10	1
245	29.0853	39.1425	2011.5.29	4.5	5.04	1:31	129	37	-50	1	1
246	29.0112	39.1567	2011.5.30	4	15.29	22:03	148	87	-40	9	1
247	29.1018	39.1122	2011.6.4	4.1	15.63	13:51	307	45	-73	9	1
248	29.095	39.143	2011.6.5	4	6.98	21:29	60	42	-99	8	4
249	28.3405	39.0975	2011.6.10	4.7	34.38	22:47	154	70	46	6	1
250	28.7742	36.5967	2011.6.15	4	25.98	18:23	96	68	165	6	1
251	29.130	39.070	2011.6.27	5	19.30	21:14	313	55	-66	10	8
252	29.0443	39.1217	2011.6.27	4.4	12.15	21:28	326	56	-76	6	1
253	29.0032	39.1232	2011.6.29	4	9.28	11:40	139	84	-50	6	1
254	26.620	36.500	2011.7.2	4.5	128.00	21:30	344	59	-175	3	1
255	29.0147	39.1037	2011.7.3	4.1	10.78	14:16	275	64	-131	6	1
256	29.0328	39.123	2011.7.13	4.3	14.70	1:31	329	45	-72	6	1
257	29.1243	39.0638	2011.7.17	4	13.84	19:51	105	57	-97	10	13

Table A. 1 (continued)

258	29.093	39.1048	2011.7.19	4.1	17.66	21:16	299	69	-119	9	13
259	29.0957	39.139	2011.8.25	4.3	22.54	4:19	77	26	-98	6	1
260	26.580	36.870	2011.09.10	4.5	9.00	2:22	37	20	-104	1	1
261	26.580	36.890	2011.09.10	4.3	3.00	6:06	31	33	-164	1	1
262	28.057	39.0052	2011.10.8	4	25.38	22:10	114	53	-70	8	4
263	28.6738	36.534	2011.10.24	4	25.83	10:06	167	52	-28	1	1
264	28.7075	36.5233	2011.10.24	4.2	23.32	10:14	76	57	121	1	1
265	30.1883	38.8625	2011.12.10	4.2	13.44	5:15	119	53	-63	1	1
266	30.2932	37.0073	2011.12.15	4.3	77.60	6:38	101	87	157	1	1
267	27.1748	37.9908	2011.12.27	4.1	26.44	5:59	286	52	-60	1	1
268	27.1802	37.9685	2011.12.27	4.4	6.85	7:51	289	49	-62	1	1
269	27.1508	37.4838	2012.1.27	4.2	13.51	17:43	123	31	-83	1	1
270	27.1838	37.5073	2012.1.27	4	7.06	19:06	113	51	-72	1	1
271	27.3343	36.7952	2012.2.12	4.2	21.18	19:17	42	53	-91	1	1
272	27.4768	38.1458	2012.2.20	4.1	10.41	6:34	285	47	-70	1	1
273	30.004	38.6035	2012.3.29	4.2	12.77	10:13	315	54	-74	1	1
274	29.4537	37.921	2012.4.4	4.3	23.39	0:33	40	51	81	1	1
275	29.1222	39.1227	2012.4.16	4.7	6.90	10:10	73	51	-134	1	1
276	29.1142	39.1468	2012.4.17	4.5	6.99	20:45	305	59	-52	1	1
277	29.120	39.110	2012.4.19	4	7.00	19:52	299	66	-58	3	13
278	29.0975	39.1525	2012.4.20	4.4	20.59	16:39	53	73	-163	1	1
279	29.1438	39.124	2012.4.23	4.3	6.31	16:14	279	53	-104	1	1
280	29.250	39.090	2012.4.26	4.8	13.60	22:05	296	55	-66	8	4
281	27.000	38.550	2012.5.1	4.8	12.00	14:48	294	41	-47	8	4
282	26.6412	38.663	2012.5.2	4.3	26.01	0:02	139	84	-25	6	1
283	26.6305	38.655	2012.5.3	4	26.18	1:57	132	68	-5	1	1
284	29.100	39.130	2012.5.3	5.2	12.00	15:20	98	39	-89	8	4
285	29.039	39.1018	2012.5.3	4.5	25.41	16:16	153	48	-60	1	1
286	29.0968	39.136	2012.5.3	4.4	23.70	17:10	265	70	-110	1	1
287	29.1057	39.1352	2012.5.3	4.7	14.22	21:45	127	40	-60	1	1
288	29.1023	39.1195	2012.5.4	4.5	23.94	2:00	311	35	-66	4	1
289	28.5287	37.0355	2012.5.8	4.3	23.36	7:31	298	70	-50	4	1
290	29.1497	39.0978	2012.5.9	4.2	7.01	17:49	293	69	-73	4	1
291	27.9018	39.4612	2012.5.18	4	7.01	1:47	46	81	-175	1	1
292	27.5747	36.9345	2012.5.19	4.2	18.38	12:21	291	44	-41	10	1
293	28.160	36.940	2012.06.04	4.5	6.00	14:19	241	44	-122	2	13
294	28.4823	37.0387	2012.6.9	4.2	20.92	14:33	284	38	-59	1	1
295	28.9073	36.5302	2012.6.10	6	33.77	12:44	10	81	14	7	1
296	29.1483	39.107	2012.6.13	4.3	21.58	6:40	122	34	-66	2	1
297	29.1593	39.1168	2012.6.19	4.9	25.91	1:46	100	60	-108	7	1

Table A. 1 (continued)

298	28.2912	37.1728	2012.7.18	4	25.40	17:46	156	47	-24	7	1
299	28.030	38.710	2012.8.3	4.6	5.00	10:18	81	89	-152	8	13
300	28.069	38.7178	2012.8.4	4.2	22.94	2:23	357	84	3	7	1
301	28.053	38.7327	2012.8.7	4	18.05	23:17	275	67	-153	1	1
302	28.0463	38.7242	2012.8.7	4.2	22.21	23:57	169	49	-28	3	1
303	28.033	38.7117	2012.8.25	4.1	17.40	7:24	171	71	-26	9	1
304	27.6217	38.974	2012.9.5	4.1	20.71	15:49	172	68	-20	4	1
305	29.1787	39.1385	2012.10.30	4.1	21.35	0:12	40	67	-129	10	1
306	27.9387	36.6002	2012.11.24	4.3	11.66	21:04	215	46	-80	9	1
307	27.9277	36.5883	2012.11.24	4.2	20.59	21:31	219	58	-70	9	1
308	27.9445	36.6172	2012.11.24	4.1	4.45	21:35	1	41	-114	8	1
309	27.922	36.5958	2012.11.25	4	10.77	8:51	227	49	-75	8	1
310	27.940	36.610	2012.11.26	4.8	19.40	17:35	35	31	-94	8	4
311	28.6405	37.2087	2012.11.30	4.2	20.27	2:32	294	50	-98	8	1
312	27.9543	36.6298	2012.12.2	4	4.05	19:02	245	62	-53	8	1
313	27.5205	38.7153	2013.1.7	4	24.74	11:40	288	53	-134	9	1
314	29.3203	37.9095	2013.2.20	4.1	22.78	6:59	107	71	-20	9	1
315	26.920	37.410	2013.2.21	4.8	11.00	10:18	31	89	170	8	1
316	26.5115	36.7298	2013.2.27	4.1	140.27	22:05	240	88	10	9	13
317	29.0583	39.1203	2013.3.12	4.1	12.81	20:47	228	65	176	9	1
318	27.7677	36.9433	2013.4.28	4.2	21.74	16:30	261	47	-69	9	1
319	28.410	36.890	2013.5.16	5	13.50	3:02	293	38	-97	9	1
320	28.41	37.0053	2013.5.16	4.4	20.87	21:21	113	45	-88	8	4
321	28.3715	37.0218	2013.5.16	4.2	16.61	21:26	122	41	-92	2	1
322	29.0983	39.1362	2013.5.29	4	7.00	14:43	296	55	-65	9	1
323	29.022	39.1392	2013.6.9	4.1	15.61	14:18	225	74	-172	9	1
324	26.784	38.8048	2013.6.9	4	26.69	15:15	117	57	-65	10	1
325	27.9318	36.6242	2013.6.21	4.2	83.41	18:26	229	83	-8	8	1
326	26.8428	37.3902	2013.7.25	4.1	25.43	23:05	215	72	-153	8	1
327	29.416	39.2092	2013.8.7	4.4	20.86	5:20	286	62	-105	3	1
328	27.3967	36.7517	2013.10.18	4.3	113.45	1:26	20	82	-15	7	1
329	27.5083	36.8848	2013.10.30	4	21.97	3:17	268	51	-72	9	1
330	27.5615	36.7778	2013.11.4	4	104.47	15:41	18	70	11	4	1

Table A. 2: P- T-, S_{Hmax} , S_{Hmin} axes and stress regimes computed from focal mechanism solutions listed in Table A. 1.

NF = normal faulting; NS = predominately normal faulting with strike-slip component; SS = strike-slip faulting; TS = predominately thrust faulting with strike-slip component; TF = thrust faulting; UF = undefined.

Id	Longitude	Latitude	P-az	P-dip	T-az	T-Dip	SHmax Az.	SHmin Az.	Regime
1	26.9	38.7	159.3	5.3	273.3	77.1	160	70	TF
2	30.4	37.9	33.9	78.0	144	4.2	53	143	NF
3	27.400	39.100	270.0	90.0	360	0.0	90	0	NF
4	30.14	39.08	38.0	80.0	218	10.0	128	38	NF
5	29.600	37.900	34.7	77.9	143.4	3.9	52	142	NF
6	27.400	38.200	90.0	90.0	180	0.0	90	0	NF
7	29.450	39.410	300.0	90.0	30	0.0	120	30	NF
8	27.4	36.7	60.0	90.0	150	0.0	60	150	NF
9	27.000	39.100	270.8	75.8	157.9	5.6	69	159	NF
10	28.200	37.200	65.0	90.0	155	0.0	65	155	NF
11	28.100	39.380	250.2	79.3	9.509	5.3	99	9	NF
12	29.260	38.900	38.0	80.0	218	10.0	128	38	NF
13	26.7	39.4	123.4	14.7	217	13.3	125	35	SS
14	26.7	38.7	71.8	77.4	184.4	4.9	93	3	NF
15	27.190	37.660	261.5	57.4	354.3	1.8	84	174	NF
16	28.6	36.5	190.7	9.7	283.7	16.9	12	102	SS
17	27	36.5	75.9	23.3	168.4	5.8	77	167	SS
18	27.4	36.5	242.6	3.2	333.8	20.4	64	154	SS
19	28.550	37.050	359.7	54.7	139.1	28.3	37	127	NF
20	28.5	36.9	335.7	60.9	115.3	23.0	17	107	NF
21	26.59	38.91	95.5	39.8	188.5	3.7	97	7	NS
22	27.600	37.800	99.8	7.5	3.925	37.8	98	8	SS
23	28.3	36.6	179.0	17.0	359	73.0	179	89	TF
24	29.300	38.100	198.3	4.9	290.9	27.8	19	109	SS
25	29.900	37.300	67.6	18.9	163.2	15.9	71	161	SS
26	28.330	38.470	91.3	59.5	196.8	8.9	104	14	NF
27	29.320	37.850	343.0	59.0	191.4	27.9	111	21	NF
28	27.800	37.700	173.0	72.0	353	18.0	83	173	NF
29	29.3	36.8	22.2	17.4	117.8	17.4	25	115	SS
30	29.000	37.200	107.3	56.8	217.1	12.5	123	33	NF

Table A. 2 (continued)

31	29.110	38.810	101.1	0.4	10.73	45.5	101	11	TS
32	27	36.6	269.3	14.6	6.752	26.6	93	3	SS
33	26.9	36.6	46.3	77.2	314.4	0.4	44	134	NF
34	28.500	39.100	202.0	79.0	22	11.0	112	22	NF
35	28.510	39.110	145.6	52.8	40.01	11.5	135	45	NF
36	28.400	39.200	248.1	79.9	10.21	5.4	99	9	NF
37	28.440	39.080	311.9	3.8	211.8	69.4	131	41	TF
38	28.460	38.550	82.6	83.8	215	4.2	125	35	NF
39	28.450	39.130	88.2	4.9	179.1	10.6	88	178	SS
40	28.580	39.160	246.5	73.0	5.241	8.4	93	3	NF
41	28.400	39.200	7.8	10.6	274.4	17.4	6	96	SS
42	29.500	39.200	86.6	83.8	219	4.2	129	39	NF
43	29.460	39.280	290.6	14.0	30.92	35.7	115	25	SS
44	29.550	39.120	216.0	72.1	358.5	14.3	85	175	NF
45	29.740	39.060	238.2	58.7	340.2	7.2	67	157	NF
46	29.420	39.140	287.6	14.0	27.92	35.7	112	22	SS
47	29.400	39.430	211.0	65.0	31	25.0	121	31	NF
48	29.260	39.340	190.0	67.0	10	23.0	100	10	NF
49	29.410	39.330	123.6	32.9	215.9	3.4	125	35	SS
50	29.790	39.030	15.0	65.0	195	25.0	105	15	NF
51	29.270	39.320	127.9	59.2	10.8	15.2	107	17	NF
52	29.320	39.340	108.1	68.2	200.7	1.0	111	21	NF
53	29.410	39.110	20.0	75.0	200	15.0	110	20	NF
54	29.300	39.340	149.3	12.4	245.8	27.4	152	62	SS
55	29.920	38.970	37.8	74.3	197.6	14.8	106	16	NF
56	29.800	39.000	194.0	88.0	14	2.0	104	14	NF
57	29.800	39.030	204.0	69.0	24	21.0	114	24	NF
58	29.770	39.020	5.0	50.0	185	40.0	95	5	UF
59	29.420	39.080	103.0	76.7	213.7	4.8	123	33	NF
60	28.600	39.080	307.5	83.3	171.3	4.8	81	171	NF
61	29.850	39.010	203.0	66.0	23	24.0	113	23	NF
62	29.540	39.060	165.0	45.0	345	45.0	165	75	UF
63	29.240	39.400	218.3	75.6	9.211	12.7	98	8	NF
64	29.890	39.030	30.0	85.0	210	5.0	120	30	NF
65	29.700	37.570	10.0	76.6	150.8	10.5	60	150	NF
66	29.700	37.600	163.0	59.0	343	31.0	73	163	NF
67	29.600	37.600	147.1	70.0	324.5	20.0	55	145	NF
68	29.670	39.070	249.0	75.8	18.79	9.2	107	17	NF
69	30.240	37.300	205.2	4.9	114.8	4.9	25	115	SS
70	29.460	39.300	178.9	79.8	8.846	10.0	99	9	NF

Table A. 2 (continued)

71	27.200	38.500	109.8	36.1	18.52	1.8	109	19	SS
72	28.890	37.700	141.3	48.7	34.59	14.2	130	40	NS
73	27.200	38.400	234.5	61.5	21.16	24.4	103	13	NF
74	26.600	38.800	71.8	77.4	184.4	4.9	93	3	NF
75	26.770	38.460	111.8	60.6	8.504	7.4	102	12	NF
76	29.190	39.440	182.9	78.6	17.4	11.1	108	18	NF
77	27.780	38.815	103.0	0.0	193	0.0	103	13	SS
78	27.700	36.970	176.5	19.5	284.1	40.4	3	93	UF
79	30.18	38.1	243.0	78.1	37.68	10.8	127	37	NF
80	28.710	37.310	287.5	49.3	196.7	0.7	107	17	NS
81	28.13	36.77	194.9	1.5	286.8	53.7	15	105	TF
82	26.8	37	160.7	50.5	66.21	3.7	158	68	NS
83	26.89	37.77	71.9	9.0	267.3	80.7	72	162	TF
84	26.72	37.63	88.1	2.7	346.5	77.0	87	177	TF
85	26.88	37.27	73.0	79.0	179.1	3.1	88	178	NF
86	26.89	37.26	151.9	85.0	339.3	5.0	69	159	NF
87	26.81	36.99	60.1	73.3	163.3	3.9	72	162	NF
88	26.8	36.99	117.8	75.8	4.936	5.6	96	6	NF
89	26.87	37.25	117.0	82.9	355.7	3.7	86	176	NF
90	26.79	37	356.8	54.5	257.5	6.5	170	80	NF
91	26.81	36.98	15.8	83.6	273.6	1.3	4	94	NF
92	28.320	37.010	167.5	76.6	359.4	13.1	90	0	NF
93	29.440	37.760	142.6	79.5	13.79	6.7	105	15	NF
94	28.200	37.100	144.9	74.4	10.33	11.1	102	12	NF
95	28.010	37.060	146.9	73.5	10.36	12.1	102	12	NF
96	29.640	37.000	259.9	72.7	351.7	0.6	82	172	NF
97	26.980	37.840	103.2	12.7	11.94	5.7	102	12	SS
98	26.97	38.02	99.6	1.0	9.228	19.0	100	10	SS
99	27.480	38.670	63.6	68.8	190.3	13.0	97	7	NF
100	26.530	38.690	85.1	68.5	190.5	6.0	98	8	NF
101	28.020	37.120	199.5	79.9	43.99	9.2	135	45	NF
102	29.680	38.060	225.9	74.8	37.93	15.1	127	37	NF
103	26.87	37.84	110.3	66.9	11.1	3.9	102	12	NF
104	28.330	37.980	255.7	57.8	30.03	23.7	111	21	NF
105	28.45	36.53	231.6	0.0	322.3	88.6	52	142	TF
106	30.160	38.100	143.6	79.3	53.55	0.0	144	54	NF
107	29.330	37.220	311.1	21.8	41.18	0.3	131	41	SS
108	27.890	39.290	306.0	44.5	203.9	12.0	118	28	NS
109	27.980	39.330	110.8	37.1	205	5.5	114	24	SS
110	28.240	36.750	34.5	78.7	134.4	2.0	44	134	NF

Table A. 2 (continued)

111	29.390	37.78	275.2	56.4	57.7	27.8	136	46	NF
112	27.700	39.360	293.6	32.3	27.15	5.6	116	26	SS
113	29.050	37.920	232.2	72.9	47.22	17.0	136	46	NF
114	26.810	37.840	112.6	59.7	209.7	4.2	119	29	NF
115	27.920	39.300	316.3	46.3	173.4	37.3	105	15	UF
116	27.740	39.350	311.8	42.1	211.2	11.5	125	35	NS
117	27.880	39.470	310.2	28.3	206.8	23.4	123	33	UF
118	27.880	38.660	88.4	71.1	205.8	8.9	114	24	NF
119	29.180	37.700	141.0	56.9	29.75	13.3	125	35	NF
120	28.030	36.670	3.0	70.9	160.1	17.7	68	158	NF
121	26.860	38.050	113.4	23.9	21.75	3.6	112	22	SS
122	26.750	37.920	124.2	36.5	19.99	18.3	116	26	SS
123	28.040	39.030	123.6	74.3	29.64	1.1	120	30	NF
124	28.770	37.880	238.5	71.1	22.24	15.4	109	19	NF
125	28.890	38.110	276.8	30.1	6.968	0.4	97	7	SS
126	29.050	38.030	272.9	45.1	6.454	3.6	95	5	NS
127	28.920	38.120	225.6	64.8	26.35	24.0	111	21	NF
128	26.920	36.630	47.0	7.9	314.3	18.9	46	136	SS
129	26.830	38.970	289.9	62.7	187.4	6.4	99	9	NF
130	30.280	38.380	118.9	68.0	296.2	22.0	25	115	NF
131	27.700	36.880	219.4	73.5	344.6	9.7	73	163	NF
132	27.930	36.770	200.2	81.6	349	7.2	78	168	NF
133	27.880	36.800	200.9	84.0	348.5	5.1	79	169	NF
134	27.970	36.820	247.1	75.3	355.7	4.8	85	175	NF
135	27.910	36.810	200.8	85.2	347.8	4.1	78	168	NF
136	27.790	36.730	210.3	8.5	120.3	0.0	30	120	SS
137	27.880	36.540	208.8	14.2	305.5	24.8	32	122	SS
138	27.760	39.180	228.0	86.0	48	4.0	138	48	NF
139	27.963	39.256	294.0	24.0	199.9	9.2	112	22	SS
140	28.330	36.880	97.5	75.2	0.313	1.9	90	0	NF
141	28.210	37.060	159.2	82.7	358.1	7.0	88	178	NF
142	28.340	37.010	272.9	66.7	162.4	8.6	75	165	NF
143	27.870	36.840	101.4	71.3	1.743	3.3	93	3	NF
144	27.919	37.018	8.1	82.0	182.3	8.0	92	2	NF
145	27.840	36.840	134.3	71.9	354.4	14.1	87	177	NF
146	27.714	39.177	302.8	4.9	211.9	10.6	122	32	SS
147	26.870	38.110	100.8	27.8	194.1	6.3	103	13	SS
148	26.700	37.800	80.1	37.0	198	31.9	95	5	UF
149	26.780	36.570	153.8	37.7	269.3	29.2	168	78	UF
150	26.632	38.15	115.7	31.5	207.1	2.2	117	27	SS

Table A. 2 (continued)

151	26.62	38.153	111.5	9.2	201.8	2.1	111	21	SS
152	26.66	38.168	112.3	33.0	208.2	8.9	115	25	SS
153	26.629	38.158	127.7	19.1	219.3	4.6	129	39	SS
154	26.615	38.164	60.8	76.4	259.6	12.9	171	81	NF
155	26.653	38.166	130.9	15.5	221.2	1.3	131	41	SS
156	26.654	38.177	115.9	22.9	209.9	9.4	118	28	SS
157	26.632	38.138	100.0	32.8	207.3	24.8	109	19	UF
158	26.64	38.166	86.2	14.1	354.5	6.9	85	175	SS
159	26.663	38.178	91.7	14.1	182	1.3	92	2	SS
160	26.660	38.150	94.8	11.9	186.5	7.8	96	6	SS
161	26.635	38.147	118.1	15.4	210.4	8.5	119	29	SS
162	26.64	38.14	282.4	12.0	12.83	2.0	102	12	SS
163	26.684	38.18	100.3	16.9	191.9	5.4	101	11	SS
164	26.705	38.187	97.2	34.3	240.2	49.5	114	24	UF
165	26.753	38.152	274.0	9.7	6.742	15.5	95	5	SS
166	26.673	38.132	2.3	24.7	96.22	8.5	4	94	SS
167	26.681	38.175	104.8	32.1	206.6	18.0	112	22	SS
168	26.674	38.136	285.7	7.6	193.7	14.8	105	15	SS
169	26.657	38.146	114.8	38.6	16.08	10.7	109	19	SS
170	27.011	38.392	93.2	33.4	196.4	19.2	100	10	SS
171	26.65	38.146	93.2	2.0	183.6	12.0	93	3	SS
172	26.657	38.179	103.5	23.8	200.9	16.3	108	18	SS
173	26.638	38.173	110.4	10.6	200.6	0.7	110	20	SS
174	26.689	38.126	172.4	8.5	263.6	8.5	173	83	SS
175	26.642	38.154	294.2	2.8	204	5.7	114	24	SS
176	26.664	38.134	274.6	22.5	4.823	0.4	95	5	SS
177	26.635	38.174	294.4	17.7	35.02	30.0	119	29	SS
178	26.705	38.159	302.7	0.1	32.72	12.7	123	33	SS
179	26.612	38.129	129.7	14.8	222.9	11.9	132	42	SS
180	26.67	38.181	289.0	0.7	199	2.1	109	19	SS
181	26.632	38.168	99.9	21.4	201.8	27.6	106	16	UF
182	26.717	38.157	296.0	1.4	26	0.0	116	26	SS
183	26.694	38.183	90.6	29.2	183.5	5.0	92	2	SS
184	26.608	38.112	126.4	13.3	219.6	13.3	128	38	SS
185	26.599	38.178	109.0	4.9	18.82	2.1	109	19	SS
186	26.839	38.2	91.4	6.0	359.4	19.1	90	0	SS
187	26.765	38.157	105.2	14.1	197.7	9.8	106	16	SS
188	26.628	38.184	305.0	0.0	35.01	1.4	125	35	SS
189	26.56	38.185	100.5	23.9	210	37.0	109	19	UF
190	26.715	38.149	296.0	9.9	26.71	4.2	116	26	SS

Table A. 2 (continued)

191	26.594	38.11	124.5	4.9	33.82	7.8	124	34	SS
192	26.573	38.155	302.3	9.8	34.8	14.1	123	33	SS
193	26.525	38.092	293.0	18.6	190.5	32.7	107	17	SS
194	26.607	38.174	110.0	3.5	200.1	2.1	110	20	SS
195	26.702	38.178	294.9	13.1	29.51	19.0	117	27	SS
196	26.578	38.127	302.9	12.7	35.42	11.2	124	34	SS
197	26.61	38.128	120.9	31.3	212	1.9	122	32	SS
198	26.644	38.138	280.5	5.4	187.7	27.4	100	10	SS
199	26.65	38.127	295.0	3.5	25.07	0.7	115	25	SS
200	27.780	38.800	323.8	37.0	218.7	19.0	135	45	SS
201	26.940	36.670	200.8	15.8	300.2	29.9	25	115	SS
202	28.650	37.800	17.6	78.9	203.6	11.0	114	24	NF
203	28.900	38.190	60.9	71.4	220.6	17.5	129	39	NF
204	29.210	36.890	66.0	76.3	197.1	9.1	105	15	NF
205	29.410	36.960	253.9	71.3	4.867	6.9	93	3	NF
206	29.270	36.990	253.1	65.4	8.043	10.9	94	4	NF
207	29.340	36.830	59.6	76.2	185.8	8.2	94	4	NF
208	26.950	38.610	290.1	18.8	190.8	25.3	106	16	SS
209	28.940	37.840	98.7	51.8	230.3	27.6	128	38	UF
210	29.1508	37.0192	164.9	7.8	257.4	17.5	166	76	SS
211	28.980	39.150	99.2	63.0	198.3	4.6	107	17	NF
212	26.960	37.580	195.0	81.0	15	9.0	105	15	NF
213	27.040	37.650	303.7	77.8	189	5.2	100	10	NF
214	27.5892	37.8568	331.4	82.1	195	5.8	106	16	NF
215	28.690	37.900	86.6	67.3	202	10.2	109	19	NF
216	29.1245	39.0568	141.8	43.4	253.5	21.3	155	65	UF
217	29.6883	36.7312	202.8	55.4	317.4	16.0	41	131	NF
218	27.5943	36.9763	214.0	77.8	4.968	10.7	94	4	NF
219	27.4003	36.8	73.0	26.1	167.8	9.8	76	166	SS
220	26.840	36.790	42.0	30.3	300.4	19.0	36	126	SS
221	30.3463	36.9807	69.0	47.3	321.6	15.4	58	148	NS
222	27.0433	37.4865	260.5	20.4	10.03	42.0	87	177	UF
223	27.952	38.0022	134.2	69.1	28.48	5.9	120	30	NF
224	27.340	37.690	107.3	71.1	5.226	4.1	96	6	NF
225	27.3385	37.8558	155.1	70.7	343.5	19.1	75	165	NF
226	27.9827	36.7845	56.3	23.8	314.3	25.3	50	140	UF
227	28.0227	39.0602	154.7	71.7	57.73	2.3	149	59	NF
228	27.360	36.570	168.7	74.4	335.1	15.2	64	154	NF
229	27.2632	36.8552	113.4	72.7	333.6	13.4	67	157	NF
230	29.110	39.080	266.8	85.7	12.24	1.2	102	12	NF

Table A. 2 (continued)

231	29.040	39.120	277.3	63.5	29.94	10.9	116	26	NF
232	29.1078	39.1442	64.9	84.6	174.1	1.8	84	174	NF
233	29.0317	39.1128	122.8	74.6	21.62	3.1	113	23	NF
234	29.1235	39.131	224.0	70.6	19.81	17.8	107	17	NF
235	29.1065	39.1413	166.9	80.0	350.3	10.0	80	170	NF
236	29.0837	39.1147	151.3	70.6	345.7	18.9	78	168	NF
237	29.0023	39.1443	94.2	65.5	191.6	3.4	101	11	NF
238	29.0872	39.1202	67.9	82.1	161.2	0.5	71	161	NF
239	29.0513	39.1037	53.4	87.9	213.3	2.0	123	33	NF
240	27.1522	39.0988	312.7	13.4	42.86	0.6	133	43	SS
241	29.0217	39.1013	323.3	76.8	131.8	13.0	41	131	NF
242	29.199	39.111	83.0	61.9	185.2	6.4	93	3	NF
243	29.040	39.090	305.1	72.4	206.6	2.7	118	28	NF
244	29.0278	39.1123	94.8	81.5	0.546	0.6	91	1	NF
245	29.0853	39.1425	129.9	63.0	11.09	13.8	106	16	NF
246	29.0112	39.1567	96.4	29.4	201.4	24.6	104	14	UF
247	29.1018	39.1122	299.4	78.3	205.2	0.9	115	25	NF
248	29.095	39.143	217.5	83.1	336.4	3.3	66	156	NF
249	28.3405	39.0975	274.4	13.7	18.96	46.0	99	9	TS
250	28.7742	36.5967	322.7	5.5	55.32	25.8	144	54	SS
251	29.130	39.070	277.9	69.3	25.85	6.6	114	24	NF
252	29.0443	39.1217	276.2	74.6	46	10.0	134	44	NF
253	29.0032	39.1232	84.1	37.8	198.1	27.7	98	8	UF
254	26.620	36.500	203.2	24.7	301.8	18.1	28	118	SS
255	29.0147	39.1037	135.9	52.2	33.08	9.8	127	37	NS
256	29.0328	39.123	322.6	77.3	226.4	1.4	136	46	NF
257	29.1243	39.0638	352.8	76.8	200.1	11.7	111	21	NF
258	29.093	39.1048	171.0	56.2	50.24	18.9	148	58	NF
259	29.0957	39.139	184.1	70.5	353	19.2	81	171	NF
260	26.580	36.870	150.0	64.0	317.9	25.5	44	134	NF
261	26.580	36.890	229.1	44.4	352.1	29.1	69	159	UF
262	28.057	39.0052	79.7	73.0	189.9	6.0	98	8	NF
263	28.6738	36.534	137.5	44.2	37.66	10.0	132	42	NS
264	28.7075	36.5233	144.5	7.1	40.17	63.3	142	52	TF
265	30.1883	38.8625	87.6	68.4	190.4	5.0	99	9	NF
266	30.2932	37.0073	148.9	13.8	54.26	18.2	147	57	SS
267	27.1748	37.9908	259.0	66.6	355.3	2.7	84	174	NF
268	27.1802	37.9685	268.5	69.2	359.6	0.4	90	0	NF
269	27.1508	37.4838	193.1	75.4	27.9	14.2	119	29	NF
270	27.1838	37.5073	83.0	75.4	190.3	4.5	99	9	NF

Table A. 2 (continued)

271	27.3343	36.7952	306.9	82.0	132.7	8.0	43	133	NF
272	27.4768	38.1458	270.2	75.5	1.005	0.2	91	1	NF
273	30.004	38.6035	273.5	74.9	33.66	7.7	122	32	NF
274	29.4537	37.921	136.4	5.6	264.8	81.0	137	47	TF
275	29.1222	39.1227	278.0	57.2	12.46	2.8	101	11	NF
276	29.1142	39.1468	267.7	57.3	8.833	7.1	96	6	NF
277	29.120	39.110	341.6	56.7	96.16	15.3	1	91	NF
278	29.0975	39.1525	275.3	23.9	5.55	0.5	95	5	SS
279	29.1438	39.124	140.6	76.8	18.93	7.0	110	20	NF
280	29.250	39.090	261.9	69.3	9.851	6.6	98	8	NF
281	27.000	38.550	285.3	61.5	174.1	11.1	88	178	NF
282	26.6412	38.663	91.7	22.1	187	12.8	95	5	SS
283	26.6305	38.655	90.1	19.0	356	11.7	88	178	SS
284	29.100	39.130	181.3	84.0	7.289	6.0	97	7	NF
285	29.039	39.1018	134.9	68.2	42.29	1.0	132	42	NF
286	29.0968	39.136	146.1	60.0	10.17	22.5	108	18	NF
287	29.1057	39.1352	129.4	69.3	16.05	8.5	108	18	NF
288	29.1023	39.1195	334.3	71.8	203.9	12.1	117	27	NF
289	28.5287	37.0355	251.5	48.7	359.9	15.5	84	174	NS
290	29.1497	39.0978	229.3	62.2	10.1	22.2	92	2	NF
291	27.9018	39.4612	270.4	9.9	0.853	2.9	90	0	SS
292	27.5747	36.9345	274.6	56.2	168.1	10.7	82	172	NF
293	28.160	36.940	70.1	67.7	173.1	5.3	81	171	NF
294	28.4823	37.0387	290.6	68.5	172.3	10.6	85	175	NF
295	28.9073	36.5302	143.4	3.3	234.4	16.2	143	53	SS
296	29.1483	39.107	148.0	71.3	14.83	13.0	108	18	NF
297	29.1593	39.1168	331.6	69.4	203	13.2	117	27	NF
298	28.2912	37.1728	129.6	43.8	23.84	15.8	120	30	NS
299	28.030	38.710	309.3	20.1	212.2	18.6	125	35	SS
300	28.069	38.7178	312.0	2.1	221.7	6.4	132	42	SS
301	28.053	38.7327	134.8	34.9	44.06	1.1	134	44	SS
302	28.0463	38.7242	142.2	45.6	39.28	12.3	133	43	NS
303	28.033	38.7117	129.2	31.6	221.4	3.6	130	40	SS
304	27.6217	38.974	131.6	29.3	40.32	2.3	131	41	SS
305	29.1787	39.1385	264.4	51.5	157.2	13.3	72	162	NS
306	27.9387	36.6002	203.5	82.8	297.9	0.6	28	118	NF
307	27.9277	36.5883	173.3	69.8	294.7	10.9	22	112	NF
308	27.9445	36.6172	176.3	73.2	287.8	6.3	16	106	NF
309	27.922	36.5958	201.9	78.3	306.4	3.0	35	125	NF
310	27.940	36.610	136.6	75.8	307.9	14.1	37	127	NF

Table A. 2 (continued)

311	28.6405	37.2087	156.9	82.3	29.67	4.7	120	30	NF
312	27.9543	36.6298	204.8	56.2	309.4	9.6	36	126	NF
313	27.5205	38.7153	135.8	56.3	227.4	1.1	137	47	NF
314	29.3203	37.9095	65.4	27.3	335.4	0.1	65	155	SS
315	26.920	37.410	76.5	6.3	345.7	7.8	77	167	SS
316	26.5115	36.7298	14.4	5.6	105.2	8.5	14	104	SS
317	29.0583	39.1203	91.2	14.7	186.7	20.1	94	4	SS
318	27.7677	36.9433	246.2	74.8	336.3	0.0	66	156	NF
319	28.410	36.890	59.2	81.6	208	7.2	118	28	NF
320	28.41	37.0053	112.3	88.6	21.59	0.0	112	22	NF
321	28.3715	37.0218	231.6	85.8	33.42	4.0	123	33	NF
322	29.0983	39.1362	260.2	67.9	8.187	7.1	96	6	NF
323	29.022	39.1392	88.0	16.8	179.7	5.8	89	179	SS
324	26.784	38.8048	78.4	67.3	188.9	8.3	96	6	NF
325	27.9318	36.6242	184.4	10.6	274.6	0.7	4	94	SS
326	26.8428	37.3902	77.3	31.6	344.2	5.0	75	165	SS
327	29.416	39.2092	164.9	69.2	26.96	15.7	121	31	NF
328	27.3967	36.7517	335.4	16.2	66.74	4.8	156	66	SS
329	27.5083	36.8848	238.0	75.4	345.3	4.5	74	164	NF
330	27.5615	36.7778	332.3	6.6	239.7	21.6	151	61	SS